Studies of Structure and Water Vapor Transport Properties of Shape Memory Segmented Polyurethanes for Breathable Textiles

A thesis submitted in partial fulfillment of
the requirements for the Degree of
Doctor of Philosophy

By
SUBRATA MONDAL

Institute of Textiles and Clothing
The Hong Kong Polytechnic University
August, 2005

CERTIFICATE OF ORGINALITY

I hereby declare that the thesis entitled "**Studies of Structure and Water Vapor Transport Properties of Shape Memory Segmented Polyurethanes for Breathable Textiles**" which is submitted to the Hong Kong Polytechnic University, Hong Kong for the award of Doctor of Philosophy is my original work, to the best of my knowledge and belief, it reproduces no material previously published or written, except where due acknowledgement has been made in the text. The matter embodied in this dissertation has not been submitted for the award of any other degree or diploma.

_____Signature

Subrata MONDAL _____(Name of student)

TO MY PARENTS FOR THEIR CONSTANT SUPPORT

ABSTRACT

Shape memory polyurethanes (SMPU) have segmented structure which is capable of changing their shape upon application of heat. Large change of thermomechinical properties would occur across the glass transition temperature (T_g) or soft segment crystal melting temperature (T_{ms}) of SMPU. In addition to the change of thermomechanical properties of SMPU, it also has large change in moisture vapor permeability above and below the T_g/T_{ms}. From the literature review it was found that the transition temperature for water vapor permeability is above 40 °C, which would not be suitable for breathable textile applications. Therefore the key objective of this study is to investigate the role of segmental structure and soft segment crystal melting on water vapor permeability of shape memory segmented polyurethane (SPU) for breathable textiles.

In this study, six unique factors on structure, shape memory and water vapor transport properties of segmented polyurethanes (SPU) have been investigated. These factors are hard segment, hydrophilic block length, hydrophilic segment content, hydrophilic and/or carboxylic unit content, mixed polyol block and multi wall carbon nano tube (MWNT). For this purpose, three different kinds of polyols such as polycaprolactone diol (PCL), polytetramethylene glycol (PTMG) and polypropylene glycol (PPG) with different molecular weight were used as soft segment, on the other hand 4,4'-methhylene (bisphenyl) diisocyanate (MDI) and 1,4-butane diol (1,4-BDO) were used as hard segment. SPUs were modified by hydrophilic segment such as polyethylene glycol (PEG) with different molecular weight, and/or carboxylic group containing unit such as

dimethyl amino propionic acid (DMPA). In addition SPUs were reinforced with different quantity of functionalized multi wall carbon nano tube. Polymers were synthesized by two or three steps polymerization techniques. SPUs were characterized by Fourier transform infra red (FTIR) spectroscopy, Raman spectroscopy, wide angle X-ray diffraction (WAXD), differential scanning calorimetry (DSC), scanning electron microscopy (SEM), transmission electron microscopy (TEM), dynamic mechanical thermal analysis (DMTA), positron annihilation lifetime spectrometry (PALS), thermogravimetry analysis (TGA), Instron, and shape memory behavior which was measured by Instron having temperature control chamber. Water vapor transport properties were measured by equilibrium sorption, dynamic sorption and water vapor permeability measurements (ASTM 96 E).

Experimental results revealed significant variations in macromolecular structure, shape memory effect and water vapor transport properties of SPUs depending on segmental architecture. There is evidence that the microcrystalline structure formation in SPU would depend on the selection of soft segment. SPUs are completely amorphous, when the polyol is non-crystalline at room temperature. Furthermore the introduction of little amount of MWNT slightly increases the soft segment crystallinity. These micro crystal melting point temperatures are in the room temperature range (15 – 23 °C) which enhances the water vapor permeability (WVP) above room temperature through the nonporous membrane structure. The membranes with completely amorphous structure have no such abrupt changes of WVP in the experimental temperature range. The behavior of water vapor transport of SPU membranes were not only influenced by soft segment crystal melting point but also interpreted on the basis of chemical nature of soft

segment in the SPU backbone, hydrophilicity, hard/soft segment content and free volume. TEM images show two phase micro-phase separated structure which was depended on the type of polyol used. Experimental result shows that the shape recovery effect was improved by increasing the percent crystallinity or physical cross-linking between the polymer chains.

Selected SPUs were applied to the cotton fabrics by coating method. Water pressure resistance value of 24.5 mbar was achieved for the coated fabric with PTMG (M_n 2900) based SPU containing 15 wt% of PEG (M_n 3400). Coated fabrics also maintained good water vapor permeability, therefore confirmed the physiological comfort to the wearer. MWNT reinforced SPU coated fabrics show excellent UV blocking properties. With only 1 wt% of MWNT in the SPU, the UV protection factor (UPF) was about 125 (rated as excellent, >+50) achieved as compared to the uncoated fabric having UPF of 5.6 which is non rate able.

This study stated development of temperature stimulating shape memory segmented polyurethanes membrane with improved water vapor permeability and soft segment crystal melting temperature in the room temperature range. Such nonporous membrane would be applicable to develop smart breathable textiles by laminating solid nonporous membrane instead of microporous membrane on a suitable base fabric which would have lower water vapors permeability at low temperature and significant increase of water vapor permeability with increasing temperature. This "flexible barrier function" would enable the garment to intelligently adjust its insulating properties in response to temperature changes which will assure optimum comfort regardless of temperature.

Systematic study on structure and water vapor transport properties presented in this thesis throws light to the polymer chemist to develop smart polyurethane membrane through molecular design from wide range of raw materials available for polyurethane synthesis.

PUBLICATIONS

PATENTS

1. J. L. Hu and S. Mondal, *Methods of producing di-block polymer,* **U. S. Patent** Application, US10/459,587, Filed on December, 2003.
2. J. L. Hu, Z. Yang, K. W. Yeung and S. Mondal, *A method of manufacturing shape memory polyurethane*, **U. S. Patent** Application, US10/715,552, Filed on November, 2003.

BOOK CHAPTERS

3. J. L. Hu and S. Mondal, Chapter 8: *Temperature sensitive shape memory polymers for smart textile applications*, Editor: Professor Heikki Mattila, in Intelligent Textiles and Clothing, Woodhead Publishing Ltd., Accepted (will be publish in summer, 2006).
4. J. L. Hu and S. Mondal, Chapter 10: *Study of shape memory polymer films for breathable textiles*, Editor: Professor Heikki Mattila, in Intelligent Textiles and Clothing, Woodhead Publishing Ltd., Accepted (will be publish in summer, 2006).

CONFERENCE PAPERS

5. Mondal S, and Hu JL, *Mass transfer through non-porous segmented polyurethane membrane for textile lamination: Confluence of soft segment crystal melting and block length of hydrophilic segment*, The Textile Institute 84th World Conference, 22-25, March, 2005, Raleigh, North Carolina, USA, Presented.
6. Hu JL, and Mondal S, *Water vapor permeable thermoplastic polyurethane for textile application*, 8th Asian Textile Conference, ATC 8, 9 – 11 May, 2005, Teheran, Iran, Accepted.
7. Mondal S, and Hu JL, *Influence of soft segment crystal melting in the room temperature range on water vapor permeability of nonporous hydrophilic PU membrane for textile application*, Fiber Society Spring 2005, Conference, 24 – 27th May, 2005, St. Gallen, Switzerland, Presented.
8. Mondal S, and Hu JL, *Water vapor transport through nonporous polyurethane membrane for waterproof breathable fabric: combined influence of hydrophilicity and room temperature range soft segment crystal melting*, 'The Future of the 20th Century: Collecting, Interpreting and Conserving Modern Materials, Conference in Winchester, UK, 26th - 28th, July, 2005, Accepted.

REFERRED JOURNAL PAPERS

9. J. L. Hu and S. Mondal, *Structural characterization and mass transfer properties of segmented polyurethane: Influence of hydrophilic block length*, **Polymer International**, 2005, **54** (5), 764-771, (SCI, IF – 1.125).

10. S. Mondal and J. L. Hu, *Structural characterization and mass transfer properties of nonporous segmented polyurethane membrane: Influence of the hydrophilic segment content and soft segment melting temperature*, **Journal of Membrane Science,** Status: in Press, (SCI, IF – 2.108).
11. S. Mondal and J. L. Hu, *Structural characterization and mass transfer properties of nonporous segmented polyurethane membrane: Influence of hydrophilic and carboxylic group*, **Journal of Membrane Science**, Status: in Press, (SCI, IF – 2.108).
12. S. Mondal and J. L. Hu, *Structural characterization and mass transfer properties of polyurethane block copolymer: Influence of mixed soft segment block*, **Polymer International**, Status: Accepted, (SCI, IF – 1.125).
13. S. Mondal and J. L. Hu, *Thermal degradation study of functionalized MWNT reinforced segmented polyurethane membrane*, **Journal of Elastomers and Plastics**, Status: Accepted, (SCI, IF – 0.317).
14. S. Mondal, J. L. Hu, Z. Yang, L. Yan and Y. S. Szeto, *Shape memory polyurethane for smart garment*, **Research Journal of Textile and Apparel, 6**(2), Nov 2002, 75-83.
15. S. Mondal and J. L. Hu, *Temperature stimulating shape memory polyurethane for smart clothing*, **Indian Journal of Fibre and Textile Research**, Invited paper, Status: Accepted, (SCI, IF – 0.112).
16. S. Mondal and J. L. Hu, *Shape Memory Study of Functionalized MWNT-reinforced Polyurethane Copolymer,* **Iranian Polymer Journal**, Status: Provisionally Accepted, (SCI, IF – 0.326).

17. S. Mondal and J. L. Hu, *Influence of hard segment on thermal stability of segmented polyurethane for coating applications*, **Polymer Plastics Technology and Engineering**, Status: Submitted, (SCI, IF – 0.352).
18. S. Mondal and J. L. Hu, *Structural Characterization and Mass Transfer Properties of Dense Segmented Polyurethane Membrane: Influence of Hard Segment and Soft Segment Crystal Melting Temperature*, **Journal of Membrane Science**, Status: Submitted, (SCI, IF – 2.108).
19. S. Mondal, J. L. Hu and Y. Zhu, *Free volume and water vapor permeability of dense segmented polyurethane membrane*, **Journal of Membrane Science**, Status: Accepted, (SCI, IF – 2.108).
20. S. Mondal and J. L. Hu, *A study on soft segment crystallization in microphase separated polyurethane block copolymer*, **Polymer**, Status: Submitted, (SCI, IF – 2.433).
21. S. Mondal and J. L. Hu, *A Novel approach to excellent UV protecting cotton fabric with functionalized MWNT containing water vapor permeable PU coating*, **Journal of Applied Polymer Science**, Status: Submitted, (SCI, IF – 1.021).
22. S. Mondal and J. L. Hu, *Studies of shape memory property on thermoplastic segmented polyurethanes: Influence of PEG 3400*, **Journal of Elastomers and Plastics**, Status: Submitted, (SCI, IF – 0.317).
23. S. Mondal and J. L. Hu, *Influence of film casting condition and thermal treatment on order structure of polyurethane block copolymer*, **Iranian Polymer Journal**, Status: Submitted, (SCI, IF – 0.326).

24. S. Mondal and J. L. Hu, *Microstructure and Water Vapor Transport Properties of Functionalized Carbon Nanotube Reinforced Segmented Polyurethane Composite Film*, **Polymer International**, Status: Submitted, (SCI, IF – 3.30).

IF – Impact Factor for 2004

ACKNOWLEDGEMENT

First and foremost, I would like to express my sincere gratitude to my chief supervisor, Prof. JinLian HU. Without her genuine help, it would be impossible for me to join this interesting project. Her continual support and encouragement have kept me going over the last three years. Working under her supervision has been a rich experience and shall always be a pleasant memory.

My thanks are given to Mr. J. YEUNG of Material Research Centre, The Hong Kong Polytechnic University for his help to characterizing polymer by using wide angle X-ray diffraction (WAXD), scanning electron microscopy (SEM), and differential scanning calorimetry (DSC).

I would like to express my sincere thanks to, Ms. M. N. SUN of fabric objective measurements lab for helping me with Instron and UV visible spectrophotometer, Mr. W. K. HO of Chemical lab for guiding safety issues during synthesis and helping with UV-vis spectroscopy, Mr. K. O. CHOI of physical testing lab for his help to measure water penetration pressure of coated fabric, and Mr. W. K. TAM of chemical workshop for his help during fabric coating.

Thanks are also due to Ms. Z. YAN, Material Science Department, Hong Kong University of Science and Technology, for measuring the Transmission Electron Microscopy (TEM) image of polymer, and Dr. S. R. SHI for measuring Raman spectra of the samples.

My sincere thanks are given to my colleagues Mr. JI Fenglong for his unselfish help for shape memory testing and data analysis, Mr. ZHU Yong for his help to measure and analysis free volume of polymers, and Mr. YEUNG Lap-Yan for his help to prepare samples for TEM, and dynamic mechanical thermal analysis (DMTA) testing.

Next, I would like to thank to all the friends I have made here, the list is too long to mentioned but their friendship helped to make my stay in Hong Kong a really happy one.

I would like to acknowledge the International Postgraduate Scholarship of the Hong Kong Polytechnic University for providing resources and funding for my research studentship throughout this PhD study.

Next, I would also like to thank, Prof. David Tomanek of Theoretical Condensed Matter of Physics, Michigan State University for his permission to reproduce Figure 2.13, and the following publishers for their kind permission to use their copyright materials:

1. Vilar Polyurethanes, http://www.poliuretanos.com.br/, Av. Epitácio Pessoa, 3930/803 – Lagoa, Rio de Janeiro – RJ, Brazil, ZIP CODE 22471 000.
2. Technomic Publishing Co. Inc

Finally, I am taking this opportunity to thank, all individually those who have assisted me in one way or the other in this endeavor.

TABLE OF CONTENTS

LIST OF FIGURES

Figures

Figures

Figures

Figures

LIST OF TABLES

CHAPTER 1

INTRODUCTION

1.1 RESEARCH BACKGROUND

1.1.1 Shape Memory Polymers

Shape memory materials are one kind of smart material which has the ability to remember its original shape that is the material deformed into a temporary shape and returns to its original shape by external stimuli. This feature is known as shape memory effect which was first observed in samples of gold-cadmium in 1932 and 1951, and in brass (copper-zinc) in 1938. It was not until 1962, however, that William J. Buehler and coworkers at the Naval Ordnance Laboratory (NOL) discovered that the nickel-titanium shows this shape memory effect [1]. Shape memory polymers (SMPs) are one type of shape memory material defined as the polymeric materials with the ability to sense and respond to external stimuli in a predetermined shape. Polymers such as polynorbornene, trans-polyisoprene, styrene-butadiene copolymer, crystalline polyethylene, some block copolymers, ethylene-vinyl acetate copolymer and segmented polyurethane etc. have been discovered with shape memory effect [2]. Organic shape memory polymers have lower recovery force than do shape memory alloys but offer easier processability, light weight, lower production costs, biocompatibility, color variation etc [3]. Compared with shape memory alloys, SMPs have better potentiality for textile and clothing applications. In case of SMAs, mechanical properties can be adjusted only within a limited range, and maximum deformation that could undergo is about 8 %. In contrast shape memory polymers (SMPs) have easy shaping, high shape stability, and adjustable transition

temperature. Both the shape memory effect and the elasticity memory effect of shape memory polymers make them a useful candidate for today's intelligent material system and structures [4].

1.1.2 Waterproof Breathable Textiles

The discussion of water vapor transfer will by nature focus on the ability of breathable textiles to reduce both heat stress and uncomfortable sensation of wetness [5-6] whilst maintaining protection from wind and rain in comparison to totally impermeable fabrics [7]. In order to provide wearing comfort to the wearer, the garment should have high capacity of water vapor transmission so that the forming perspiration can evaporate and be transmitted from the body surface to the environment. Earlier fabrics coated/laminated with rubber or synthetic materials, such as PVC, or acrylate were used as waterproof clothing. These materials were watertight; however, their water vapor transmission was very low [8].

1.1.3 Waterproof breathable textiles with nonporous membrane

Today's modern technologies offer various possibilities for making waterproof and breathable textile constructions [9]. A well known method to produce water proof breathable textiles is to coat/laminate breathable nonporous membranes (films) or laminate microporous films on a suitable base fabric surface. Microporous film laminates "breaths" due to their permanent, air-permeable pore structures. The basic principle consists of large number of micropores with size sufficiently large to allow the penetration of perspiration molecules, but small enough to prevent water droplet going through the fabric [10]. Water vapor could easily escape from the body surface to the

environment, however prevents the water droplet penetration. However, with the use of a porous film, deformations of film causes breaking of films or increase the size of pores that causes the delimitation of polymer films from the fabric surface and the water resistance becomes too poor. From the wearing comfort point [11] of view high water vapor permeability is required as per physiological comfort is concerned. Such moisture vapor permeability can not be obtained with a general nonporous polymer films. As the coated and laminated fabrics composed of thin layer of film and fabrics, therefore the film permeability would play important role in order to make successful breathable textiles. The option may be the shape memory polymer (SMP) films as the large change of thermomechinical properties would occur across the glass transition temperature (T_g) or soft segment crystal melting point temperature (T_{ms}) [12]. In addition to the change of thermomechanical properties of SMP, it was found that SMP also has large change in moisture permeability above and below the T_g/T_{ms}. Based on the T_g/T_{ms} set at room temperature, the SMP has low moisture permeability below the T_g/T_{ms}, during the glassy state, and has high moisture permeability above T_g/T_{ms}, during the rubbery state. This behavior would be useful with SMP-laminated textiles that could provide thermal insulation at cold temperature and high permeability at room temperature or above.

1.2 BREATHABLE TEXTILES

1.2.1 Breathability and Clothing Comfort

The movement of water vapor through a textile is an important factor in garment comfort. The human body would attempt to maintain core body temperature around 98.6 °F. The balance between perspiration and heat productions by the body and loss of the same is the comfort factor. The body would be in a state of comfort when the body

temperature is about 35 °C and there is no moisture on the skin [7]. In order to maintain the comfort, the primary functions of breathable textiles are:

1 To keep the wearer dry (from external water ingress and from internally generated condensation).

2 To provide protection against the cold.

3 To protect from wind chill factors, which is perhaps the bonus features that the waterproof breathable textiles have due to their wind passage resistant nature.

The total heat transfer through the clothing from the body to the environment, considering the thermal and evaporation resistance of the clothing has been given by Woodcock [8]:

$$H = (T_s - T_a)/I + (P_s - P_a)/E \quad \text{----------(1.1)}$$

Where H = total heat transfer, $T_s - T_a$ = temperature differences between skin and ambient, $P_s - P_a$ = water vapor pressure difference between skin and ambient, I= insulation of the clothing, and E= evaporation resistance of the clothing.

By incorporating thermal insulation products with the waterproof and breathable textiles in the garment assembly, the effect of wind chill is greatly reduced. Through a combination of selected materials in the garment construction and suitable lining material, it is possible to either delay the formation of condensation by sweating and/or wick the condensed perspiration away during the period of activity in the inclement climates, thus increasing the wearer's comfort. It should be remembered that the body perspires to cool down during and after periods of strenuous activity and the fact

perspiring aids the return of body temperature to a comfortable balance. The perspiration rates of different activity are given in Table 1.1[9].

Table 1.1: Approximate work and perspiration rates associated with various activities [9]

Activity	Work rate (Watt)	Perspiration rate ($g.day^{-1}$)	Limit of Use		
Sleeping	60	2280			
Sitting	100	3800			
Gentle walking	200	7600	●		
Active walking	300	11500	●		▶
with light pack	400	15200	▲	■	▶
with heavy pack	500	19000	▲	■	□
in mountain	600-800	22800-38400	▲	■	□
Very heavy work	1000-1200	38000-45600			

Note: ● = coated; ▲= hydrophilic membrane, ■ = microporous membrane; ▶ = woven cotton; □ = woven microfibres (Adapted with permission from Holmes D A, *J. Coated Fabrics*, 29 (4), (April 2000), 306 © Technomic Publishing Co. Inc. [9])

The heat loss by evaporation is the only way to dissipate heat from the body when environment temperature is greater than skin temperature. Liquid sweat is transformed into vapor at the skin surface, and it is passed into the environment. Evaporation of the moisture from the skin surface is tremendously effective in disposing of body heat. The loss of heat through perspiration and heat flux through fabrics are very important. Part of this heat loss is by moisture evaporation. The greater the rate of moisture evaporation, the greater will be the comfort. Mass diffusion may also result from a temperature gradient in a system; this is called thermal diffusion. Similarly, a concentration gradient can give rise to a temperature gradient and a consequent heat transfer. In sum, cold

weather clothing, besides insulating, should ideally have three main features, including water vapor permeable, windproof and waterproof. Two types of fabrics are in use for foul weather clothings which are impermeable fabrics and the breathable fabrics. An impermeable fabric is both wind and waterproof but not water vapor permeable. A breathable fabric, on the other hand, meets all the features of foul weather clothing and is water vapor permeable [8].

Table 1.2: Basic requirements for BWF [11]

Water proof breathable should, as indicated by the name, provide both waterproofness and "brethability".
Windproofness
Abrasion resistance (wet and dry conditions)
Tear resistance
Strength of the coating/good adhesion of the membrane/film to the textile surface.
Easy care, wash resistance and washability
Lightness and packability (becoming increasingly popular for all outdoor activities)
Durability
Flexibility
Stretchability including stretch fabrics with thermal properties
Quietness
Handle, look, etc.
Other characteristics according to specific end uses: flame retardancy, chemical protection, high visibility, stain resistance and oil resistant

Note: besides these "traditional" requirements the trend is clearly towards new functions and properties, such as "clever fabrics", solar (UV) protection, sweat and moisture control (Adapted with permission from Kramar L, *J. Coated Fabrics*, 28(October), 1998, 107, © Technomic Publishing Co. Inc. [11])

1.2.2 Breathable Fabrics

Textiles with good breathing properties have been become indispensable. They protect from rain, snow and wind but allow water vapor (perspiration) to penetrate. This guarantees a high level of comfort, especially when the article is worn during the physical effort in sports and during work [10]. Many textile products are waterproof but only a few provides "breathability". On the other hand, standard fabrics are "breathable" but not waterproof. Some basic requirements of water proof breathable textiles are summarized in Table 1.2 [11].

Breathable textiles can be categorized into four main types [8]:

(1) Closely woven fabric with water repellent treatment

(2) Microporous film laminates and coatings

(3) Hydrophilic film laminates and coatings

(4) A combination of microporous coating with a hydrophilic top coat

1.2.2.1 High-Density-Fabrics (HDF)

The fabrics can be woven with microfibres so densely that no interstices can be seen between the yarns. The microfibres are fibers that have linear density less than 1 decitex per fiber. The fabrics made of microfibers are extremely soft which have a fine touch [13]. Water vapor permeability of such kind of fabric is high – a certain water resistance will be given by post treatment with water repellent agents such as flurocarbons and silicones. They provide for higher water tightness as compared to the traditional textiles, but they do not give permanent protection in rain. Their water vapor permeability is excellent [14].

Examples are [13]:

1 HOECHST with its microfibre TREVIRA-FINENESS (0.65 dpf) (polyester), which is used, for example, by ROTOFIL AG to weave their "CLIMAGUARD".

2 ICI with TACTEL MICRO/24 CARAT (0.4 dpf) (polyamide) used, for example, by FINLAYSON in "MICROSPIRIT".

3 du PONT de NEMOURS fibre: "SUPPLEX" (0.9 dpf) (polyamide).

4 BURLINGTON'S : VERSATECH microfibre based fabric.

5 TORAY Ind. Inc. with "DYNA-BRIGHT" to weave their "H_2OFF"

6 KURARAY with "WRAMP" to weave "ARCUS".

1.2.2.2 Microporous Film Laminates and Coatings

In the lamination technique, a functional (water-resistant/breathable) barrier film is "glued" to a suitable base fabric. Lamination of the film on a fabric uses special adhesives, sometimes even breathable ones. If non-breathable adhesive are used, care has to be taken not to cover the whole surface in the coating process. Microporous laminates/coatings breathe due to their permanent, air-permeable pore structures. The basic principle consists of large number of micropores with a size sufficiently large to allow the penetration of perspiration molecules, but small enough to prevent water droplets from going through the fabrics [11].

1 To render a film breathable, holes can be made in it: Teflon renders itself perfectly to this in a biaxial-stretching process, such as: GORE-TEX (W.L. GORE/U.S.A) and MICROTEX (NITTO Elec. Ind./Japan).

2 Polyurethane/polyacrylate microporous film is also available, such as: PORELLE film made by PORVAIR/GB in a coagulation process or REPEL film

(polyacrylate) made by GELMAN SCIENCE/U.S.A. in a photopolymerization process.

1.2.2.3 Hydrophilic Film Laminates and Coatings

The solid or compact structure of the product would prevent penetration of water droplet whereas transmission of water vapor is provided by molecular mechanism (absorption-diffusion-desorption) [9]. From the hydrophilic group containing polyurethane solution the solvent will be evaporated leaving a compact film behind [14]. Hydrophilic groups built in the polymer chains can absorb, diffuse, and desorbs water vapor molecules through the film [10], examples are [13]:

1 SYMPATEX film (polyester), a product of ENKA GLANZSTOFF (D)

2 BION II film (polyurethane), a product of TOYO CLOTH C°/J

3 EXCEPOR-U (polyamioacid/PU), a product of MITSUBISHI-KASEI.

1.2.2.4 A Combination of Microporous Coatings with Hydrophilic Top Coat

The combination of microporous and hydrophilic layers is also possible [11]. A microporous coating or film, for example, can be further coated with a hydrophilic layer in order to increase the waterproofness, and to seal the surface pores, reducing the possibility of contamination of microporous layer by dust particles, detergents, pesticides etc. A hydrophilic finish on a microporous structure is used to upgrade the water-resistancy of microporus coatings. Care has to be taken to select a hydrophilic finish that does not impart an unacceptable effect in brethability. Ucecoat NPU2307 finish on top of Ucecoat 2000 (S) microporous coating is an example [13].

1.2.3 Polymeric Membranes

Membranes include a formidable array of materials that are widely used in a range of applications. Membranes are used for separations, controlled release, coating and packaging barriers, lamination, and so on. For these purpose the membrane must allow certain constituents to pass through. They must have a high permeability to certain type of molecule. In most general sense, a synthetic membrane is a barrier which separates two phases and restricts the transport of various chemical species in rather specific manner [15]. A membrane can be homogeneous or heterogeneous, symmetric or asymmetric in structure; it may be solid or liquid; it may be neutral, may carry positive or negative charges, or may be bipolar. Its thickness may vary between less than 100 nm to more than a centimeter and may be porous or nonporous (dense). Mass transport through a membrane may be caused by convection or by diffusion of individual molecules which is induced by an electrical field, or a concentration, pressure or temperature gradient [16].

1.2.3.1 Porous Membrane

The dimensions of the pore (0.1~10μm) [16] is larger than the perspiration molecules and much smaller than the water droplet. Therefore, the fabric laminated/coated with porous membrane would be able to prevent penetration of water droplet, and therefore could provide good overall balance between breathability and waterproofness. The fine structure of porous membranes is closely related to the properties of the polymer and the solvent that interacts with each other during the casting process. The dispersity of polymer molecule in solution depends on its species, concentration, molecular weight, temperature, solvent species, storing period in solution and so on [17]. These membranes

consist of a solid matrix with defined holes or pores. Their structure may be symmetric, i.e. the pore diameters do not vary over the membrane cross section, or they may be asymmetrically structured, i.e. the pore diameters would increase from one side to the other by a factor of 10 to 1000.

1.2.3.2 Non-porous Membrane

Nonporous/dense membrane consists of a dense film through which permeants are transported by diffusion under the driving force of a pressure, concentration, temperature, or electrical potential gradient [16]. The membrane structure of a dense membrane is considered to be a rubbery state or a glassy state, depending on its glass transition temperature, except in the case of a crystalline dense membrane. A dynamic free volume in the rubbery state and static frozen free volume (microvoid) in the glassy states are readily available for permeation through the dense membrane [15]. These membranes are capable of transporting water vapor molecules, gases as well as liquids. Non-porous membrane does not contain any macroscopic pores. The transport is determined by the diffusion mechanism which means the components first dissolved in the membrane due to a driving force. Permeation is occurred due to the diffusivity and/or solubility. Transport rate of a species through a membrane is inversely proportional to the membrane thickness.

1.2.4 Merits of Non-porous Membranes over Porous one for Breathable Laminates

Waterproof breathable textiles could be made by coating or laminating micro porous film on a suitable base fabric. The water droplet penetration is effected via micro-fine

pores which are produced by special process during the production of the film or during coating. The perspiration can be easily escapes from the body surface to the environment very quickly. Small drops of rain or spray cannot penetrate this breathable system, despite its pore structure, as the diameter of water vapor molecules is 0.35 nm and same of water droplet is about ≥ 1 μm [5].

Besides the famous PTFE membranes (Gore-Tex, Gore) where the pores are achieved during production by stretching the membranes, there are also microporous hydrophobic polyurethane membrane on the market. The pores of these membranes were produced by special coagulation process [10]. The advantages of microporous membranes over hydrophilic one are [11]:

1 Better breathability: hydrophilic coatings/lamination is influenced by the thickness of the coating/laminates and number of hydrophilic groups present in the film structure.
2 Better handle: Hydrophilic coating has stiffer handle.
3 Hydrophilic coating tends to wrinkle in wet conditions.

Despite of better breathability, the microporous films have several disadvantages, such as:

1 Pore sealing of micropore of coating or laminates would occur during usage which will affect the brethability. The pore-sealing micropores likelihood of contamination by a number of agencies which includes particulate and air-borne dirt, pesticide residues, insect repellents, sun tan lotions, salts (marine environment), skin exudates, and detergents and surfactants used for laundering

or drycleaning. All of these contaminants have been suspected of lowering the brethability [18].

2 During the use of microporous film laminates/coatings, deformation of film would cause breaking of films or increasing of the size of pores so that the water proofness become too poor to practical use. Numerous little degraded loose segments can be easily mixes with human sweat, becoming an ideal culture medium in which bacteria and mold can grow. If the latter happens, the fabric can easily be affected by all kinds microorganisms (e.g. bacteria and mildew) and deteriorate the films which will affect the waterproofness as well as fabric appearance.

3 Microporous film has poor tearing strength as compared to solid structure of nonporous one.

As compared to the microporus films, the advantages of nonporous breathable films are as follow:

1 The film making procedure is simple and the production speed is higher.

2 Having solid structure and no holes the nonporous films are less sensitive to possible degradation.

The Table 1.3 shows some features of nonporous and microporous films for textile lamination.

Having solid structure, nonporous films would possess several advantages as compared to microporous films. Since certain amount water vapor permeability is required in order to fulfilling the wearer comfort, therefore, how to improve the permeability of

nonporous membrane is really a challenge for polymer chemist. Permeability of nonporous membrane could be enhanced by introducing hydrophilic groups in the polymer backbone, as the permeability occurs through the nonporous films by molecular mechanism (sorption – diffusion – desorption). However, too much hydrophilic groups causes swelling of films, and weight loss of film increases during washing due to increasing solubility, and the waterproofness would continue to decreases after each wash [11].

Table 1.3: Features of Microporous and Nonporous Films [19]

Nonporous	Microporous
Windproof	Windproof (arguments)
Water proof and liquid proof	Water proof and liquid resistance
Selective permeability	Non selective permeability
High water entry pressure	Low water entry pressure
Good tearing strength	Low tearing strength
High water vapor transmission	High water vapor transmission

(Adapted with permission from Johnson L., and Samms, J., *J. Coated Fabrics*, 27 (July), (1997), 48 © Technolmic Publishing Co. Inc [19])

1.2.5 Designing of Breathable Textiles with Nonporous Membranes

Technical discussion of water proof breathable fabrics is usually the highly contentious subject of water vapor transmission properties. In this context, breathability refers to the capacity of a fabric layer, garment or clothing assembly to transmit water vapor which is emitted from the body as perspiration to the outside atmosphere. A discussion on the mechanism of water vapor permeability is useful in understanding the principle of

designing of breathable fabrics. Mass transfer through porous film would occur through the permanent pore structure of porous film (Figure 1.1). However, the non-porous films are dense, pinhole free polymer membranes. These polymer films are also usually hydrophilic and absorb water very quickly. This is important property that produces a "wicking" action which will actively attracts water vapor molecules. Non-porous film allows the transmission of water vapors through a process which is called active diffusion. This is the same transport mechanism by which helium escapes from a toy balloon. The permeant would dissolve on the surface of the film on the side of the higher concentration, and then diffuses across the film. When the vapor arrives at the opposite surface, it would desorbed and typically enter the surrounding airspace as gas or vapor. Water vapor transfer through nonporous membrane occurs in molecular mechanism i.e. sorption-diffusion-desorption. A discussion of the mechanism of water vapor transfer through nonporous films is given below.

Since in nonporous films, there are no micropores, and mass transfer can result from different phenomena [21]. There is a mass transfer associated with convection in that mass is transported from one place to another in the flow system. This type of mass transfer occurs on a macroscopic level which is usually treated in the subject of fluid mechanics. There will be a mass transfer on a microscopic level as the result of diffusion from regions of high concentration to regions of low concentration due to the concentration gradient. Higher concentration means there are more molecules per unit volume. Mass diffusion may also result from a temperature gradient in a system; this is called thermal diffusion. Similarly, a concentration gradient can give rise to a temperature gradient and a consequent heat transfer. The permeability is a collective

process of diffusion and sorption and hence, the permeability of mass molecules in polymer would depend on both the diffusion and solubility [21]. Chemical structure and film thickness are the main determinants of the permeability in a non-porous membrane [22]. However the selection of polymer from wide range of availability is important in order to make successful breathable textiles.

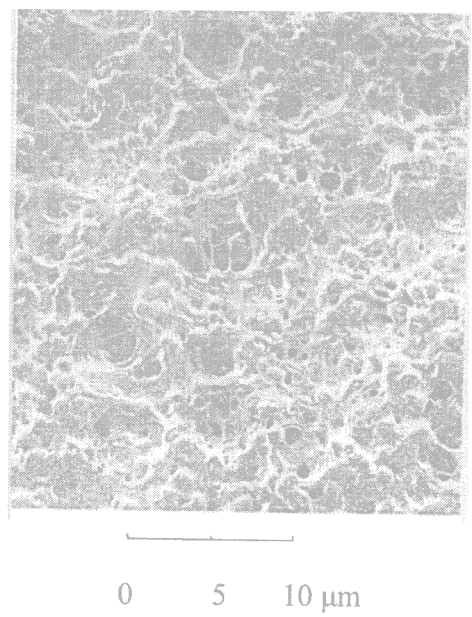

Figure 1.1: Schematic presentation of porous polyurethane topcoat (Adapted with permission from Lomax G R, *J Coated Fabric*, 15(Jul.), 1985, 40 © Technomic Publishing Co. Inc. [20])

Several characteristics make the segmented and shape polyurethane would be suitable for use in breathable textile, such as their flexibility which yields a soft hand and material maintain good barrier properties while providing high brethability. Since there are wide ranges of raw material available for polyurethane preparation, therefore the knowledge of their morphology and factors influencing permeability is extremely useful.

1.3 SATEMENT OF PROBLEMS AND OBJECTIVES

Having solid structure, nonporous film laminates would possess several advantages as compared to microporous films. However, the condensation problem is acute in nonporous film laminates due to the lower water vapor permeability because of solid and compact structure. Introducing polyethylene oxide segment in hydrophobic polymer chains may be the good option for improving the permeability. Polyethylene oxide (PEO) segment has a low binding energy for water vapor molecules which will permit rapid diffusion of water vapor molecules. The PEO segment is flexible therefore the end products would have better tactile properties. However, too much PEO makes the polymer water soluble or causes swelling of membrane which will increase the weight of garment due to the absorption of water. Therefore, it is necessary to make hydrophilicity balance. The good option may be the temperature stimulating shape memory segmented polyurethane which has capability of changing their shape upon application of heat. Large change of thermomechinical properties would occur across the glass transition temperature (T_g) or soft segment crystal melting temperature (T_{ms}) of shape memory segmented polyurethane (SMPU). In addition to the change of thermomechanical properties of SMPU, it may have large change in moisture vapor permeability above and below the T_g/T_{ms} because of morphological structure changes.

Segmented polyurethanes (SPU) are linear $[(\text{soft segment})(\text{hard segment})]_n$ block copolymers. Their versatile physical and functional properties are usually engineered by tailoring the soft and hard segment. From the literature review it was found that the water vapor permeability through the shape memory segmented polyurethane membrane has been studied rarely. Some researcher studied water vapor permeability of the shape

memory segmented polyurethane having soft segment crystal melting temperature about 50 °C which would not be suitable for breathable textiles applications.

CNTs including MWNTs or SWNTs are potentially excellent nano filler for polymer matrix due to their unique physical, mechanical, and chemical properties, including high Young's modulus and strength, thermal and electrical conductivity, thermal stability, high specific surface area, and many others. Several properties could be improve by reinforcing little amount of CNT nano fillers in polymer membrane matrix. Generally, permeability would decrease with filler content. Therefore, it would be interesting to investigate how nano filler influences the permeability of nonporous membrane.

Based on the literature review and substantial research gap between the lower water vapor permeability and higher T_{ms} of shape memory segmented polyurethane, we think following studies would be interesting and challenging:

- To investigate the role of segmental architecture on the macromolecular structure, shape memory effect and water vapor permeability of segmented polyurethanes.
- To investigate the soft segment crystallization, therefore design the polymer structure to achieve soft segment crystal melting point temperature in the room temperature range for breathable textile applications.
- To investigate the influence of carbon nano tubes (CNT) on macromolecular structure, shape memory, water vapor permeability and UV-blocking properties of SPU.
- To investigate the water vapor permeability of SPU and CNT-SPU coated fabrics.

1.4 SIGNIFICANCE OF WORK

Low water vapor permeability at lower temperature and significant increase of the water vapor permeability with increasing temperature is required for breathable textiles. When the temperature within the garment is low, the membrane would act to reduce permeability which will prevent the escape of body heat to passing through it. This will help to retain body heat. However, there are no such systematic study on micro structure and water vapor permeability of shape memory segmented polyurethane for breathable textile applications. It is therefore necessary for tailoring the molecular structure from wide range of raw materials available for polyurethane synthesis.

In the direct response to the above statement, this thesis has attempted the challenges of developing shape memory segmented polyurethane with improved water vapor permeability with an integrated approach including the following significances:

- Crystal melting causes discontinuous density change inside the membranes which enhances the water vapor permeability of polymer membrane. However, the higher crystal melting point temperature would not be useful for textile and apparel application. In this study, molecular structures were designed in order to achieve soft segment crystal melting temperature in the room temperature range.
- Microstructure and water vapor permeability of shape memory segmented polyurethanes were investigated systematically in this project in order to tailoring the polymer structure for higher water vapor permeability.
- In addition, this is the first time carbon nano tubes were introduced in the segmented polyurethane (SPU) matrix. Influences of carbon nano tube (CNT) on

microstructures, shape memory effect and water vapor transport properties of SPUs were investigated accordingly.

- A novel approaches for the excellent UV blocking properties of CNT-SPU coated fabrics were adopted in this study.

1.5 METHODOLOGY

We synthesized the polymers by two or three steps polymerization techniques. Dispersion of carbon nano tubes were done by functionalization techniques. After the synthesis of polymers, membranes were casted on Teflon coated steel plate.

Microstructure, morphology and thermal properties of SPU were studied systematically by FTIR, Raman, SEM, WAXD, DSC and TG measurements. Thermomechanical and tensile properties of polymers were measured by DMTA and Instron respectively. Shape memory properties of SPU were measured by Instron having temperature control unit. PALS was used to measure the free volume of the polymers.

Water vapor transport properties of SPUs were measured by dynamic sorption, equilibrium sorption and water vapor permeability measurements. Finally free volume data were correlated with water vapor permeability results.

1.6 OUTLINE OF THE THESIS

This thesis stated the development of temperature stimulating shape memory segmented polyurethanes with improved water vapor permeability and soft segment crystal melting temperature in the room temperature range. It comprises 8 chapters.

Chapter 1 stated general background of the investigations, breathable textiles, merits of nonporous membrane over porous one for breathable textiles. Statements of problems, significance of the studies and brief methodologies have been included in this chapter.

Chapter 2 includes comprehensive literatures on phase separation and properties of segmented polyurethane, macromolecular structure of shape memory polyurethane, structural factors influencing the water vapor permeability of shape memory segmented polyurethane, properties of carbon nano tube (CNT), dispersion of CNTs in the polymer matrix.

Material selections and purifications, synthesis process, membrane preparations and polymer characterizations have been reported in chapter 3. The characterization techniques used in this study includes: Fourier transform infra red (FTIR) spectra, Raman spectroscopy, wide angle X-ray diffraction (WAXD), differential scanning calorimetry (DSC), thermogravimetry analysis (TG), dynamic mechanical thermal analysis (DMTA), scanning electron microscopy (SEM), transmission electron microscopy (TEM), Instron, and water vapor transport properties which was measured by water vapor permeability measurements, equilibrium sorption and dynamic sorption measurements. Finally, coating of cotton fabrics by selected synthesized shape memory polyurethane and their characterizations are also described in this chapter.

In chapter 4, microstructures and thermal properties of SPUs are included. This chapter describes the studies of H-bonded/non H-bonded structures by FTIR, studies of microcrystalline structures by WAXD, thermal properties by DSC, phase separation by

TEM, surface structures observations by SEM and finally thermal degradation properties of the SPU which was measured by TG techniques.

Thermo-mechanical properties, uni-axial tensile testing properties and shape memory properties of SPUs have been presented in chapter 5. Storage modulus, loss modulus and tan (delta) value have been presented as function of temperature. Un-axial tensile testing results of SPU at room temperature and cyclic tensile testing results are included in this chapter.

Chapter 6 discusses the structural factors influencing the water vapor transport properties of SPU. Water vapor transport properties of SPUs have been reported in the form of dynamic sorption, equilibrium sorption and water vapor permeability. Finally, free volumes of selected polyurethane and their relation with water vapor permeability have been reported in this chapter.

Chapter 7 is concerned with coating of fabrics by selected polymers. This chapter includes evaluation of coated fabrics by scanning electron microscopy (SEM), water pressure head measurements, tensile strength measurements and water vapor permeability measurements. Finally, UV blocking of multi wall carbon nano tube containing SPU coated fabrics have been investigated.

Chapter 8 presents the summary of conclusions; finally some future works have been suggested in this chapter.

CHAPTER 2

LITERATURE REVIEW

Comprehensive literatures pertaining to phase separation and properties of segmented polyurethane, macromolecular structure of shape memory polyurethane, structural factors influencing the permeability of shape memory segmented polyurethane, properties of carbon nano tube (CNT), dispersion of CNTs in the polymer matrix are reviewed here.

2.1 SHAPE MEMORY SEGMENTED POLYURETHANE

2.1.1 About Polyurethane

Polyurethane (PU) is frequently referred to the "most versatile polymer." It is the diversity of the materials used to synthesize polyurethanes that give them their "versatility." Because of this versatility, polyurethanes are useful in four major types of products such as foams, fibers, coatings/laminations and elastomers [23]. Polyurethane is the reaction product of polyisocyanates and polyols. They are a family of heterogeneous polymers which contain the urethane linkage (-NH-CO-) within the polymer chains which is analogous to the carbamate group in organic chemistry [24]. Urethane groups usually do not constitute the majority of the functional groups within polyurethane. Therefore, it has the ability to incorporate other functional groups in the polymer backbone that contributes to the range of properties exhibited by polyurethane polymers [25]. Consequently, the properties of polyurethanes are ranged from rigid hard thermosetting materials to those of much softer elastomers. Generally, thermoplastic polyurethanes have very high tensile strength, toughness, abrasion resistance, and

resistance to degradation. The domain structure of polyurethanes and their scope for structural diversity creates a wide variety of uses and applications for these materials.

2.1.2 Ordinary Polyurethane, and Segmented and Shape Memory Polyurethane

The properties of ordinary polyurethanes (e.g., from 1,6-hexane diisocyanate and 1,4-butane diol) are similar to polyamides. It is composed of two starting materials [24] such as a) diisocyanate and b) either short chain glycol or long chain polyethers or polyester glycol. The PU made by short chain glycol and diisocyanate has multiple hydrogen bonding between –NH- and –OC- groups which results in highly cross-linked (Figure 2.1), high hardness and strength, and low degree of solubility [26]. On the other hand, the PU obtained by reaction of long chain, non-crystalline, unbranched, OH-functional polyethers or polyesters with stoichiometric amounts of diisocyanates which contain about 4 to 7 % urethane groups [23]. The intermolecular forces for polyethers and polyesters PUs are weak van der Waal force, as a result of hardness and strength are comparatively low and the product exhibit rubber-like properties. All these products have single phase and they don't presents segmented structure. The technical importance of ordinary PU is cross-linked hard products (PU rigid foams, non-textile coatings).

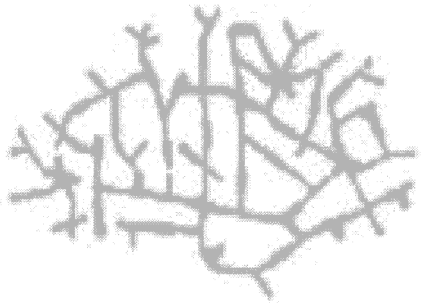

- = diurethane linkage

T= triurethane linkage

+ = tetraurethane linkage

* = polyurethane linkage

Figure 2.1: Ordinary Polyurethane (Rigid, Highly Cross-linked), (Adapted with permission from Vilar Polyurethanes, http://www.poliuretanos.com.br/[26])

On the other hand segmented polyurethanes are alternating block copolymers consisting of flexible soft segments and rigid hard segments [26-28] (Figure 2.2). Segmented polyurethanes are composed of three basic starting materials these are a) long chain polyether or polyester polyol, b) diisocyanate and c) glycol chain extender. These types of polyurethane are characterized by segmented structure (Figure 2.3) and their morphology depends on chemical composition and the length of the segment (block). The hard blocks are formed by the reaction of a diisocyanate with a low molecular weight glycol (chain extender) which is generally semicrystalline and imparts stiffness and reinforcement to the polymer matrix. Hard block usually constitute 30-50% by weight of the total volume. On the other hand soft -segments-rich microphase is formed by polyol which is responsible for the elastic behavior of polyurethanes. The soft segment is usually amorphous with a T_g below room temperature. The microphase separation of these two dissimilar blocks produces regions of hard block concentration (domains) which will act as cross-link points for the soft blocks, thus giving rise to the rubbery nature of these polymers. These types of segmented structure could show shape

memory effect depending on the composition. The segmented polyurethane has micro phase separated structure due to the thermodynamic incompatibility between the hard and soft segment. Hard segments can bind themselves via hydrogen bonding and crystallization which makes the PU very solid below melting temperature. Reversible phase transformation of soft segment is reported to be responsible for the shape memory effect. Therefore, the shape memory effect could be controlled via molecular weight of soft segment, mole ratio between hard and soft segment, and polymerisation process [29].

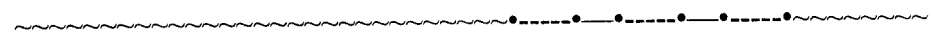

| ← soft segment → | ← hard segment → |

~~~~~~~ = long chain diol, — = short chain diol, ----- = diisocyanate, • = urethane group.

Figure 2.2: Segmented Polyurethane

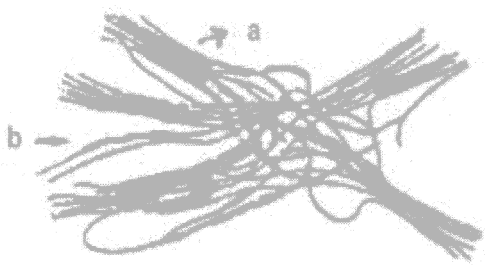

a - hard block domain

b - soft block domain

Figure 2.3: Polyurethane with Segmented Domain Structure (Adapted with permission from Vilar Polyurethanes, http://www.poliuretanos.com.br/[26])
~~~~~~~

The physical and mechanical properties of segmented polyurethane and their shape memory behavior would depend on hard and soft segment compositions, and their segregation.

2.1.3 Hard and Soft Segment of Segmented Polyurethane

A PU prepared with one mole of long chain linear polyol [poly(1,4-butane diol adipate)], two moles of diisocyanate (MDI) and one mole of chain extender (1,4-butane diol) presents the structure which is shown in Figure 2.4. Soft segments which are quite mobile and are normally present in a coiled shape.

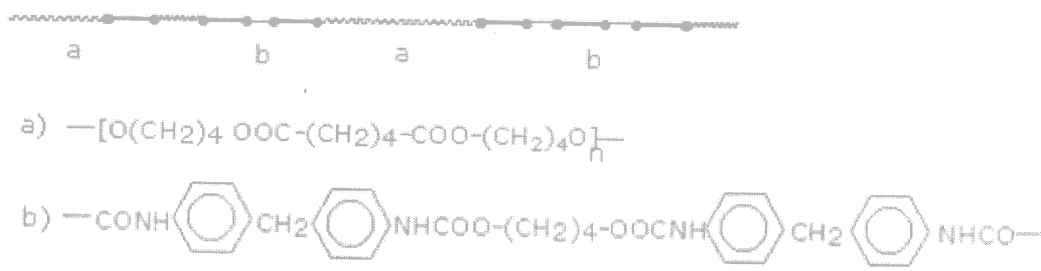

Figure 2.4: a) soft segments, b) hard segments (Adapted with permission from Vilar Polyurethanes, http://www.poliuretanos.com.br/[26])

Morphology of segmented polyurethane would depend on composition and content of hard and soft segments. Due to the extreme contrariety in physical properties between the constituent components, copolymers might be expected to show phase separations in solution and domain structure in the solid state [30-35]. Phase separation takes place in segmented polyurethanes due to the thermodynamic incompatibility between the hard

and soft segments. The phase separation influences the physical properties of PU as well its functional properties such as permeability. The microphase separation of segmented polyurethane and its influence on PU properties are discussed in the following paragraphs.

2.1.4 Phase Separation

Polyurethanes are segmented block copolymers [25] with an A_nB_m type structure, where A represents the hard block, B represents the soft block, and m and n represents the corresponding degree of polymerization. Generally, the hard and soft segments of polyurethane have positive heat of mixing, therefore incompatible. Therefore, there is a tendency toward phase separation of the two components; however, the topology of the block copolymer molecules imposes the restrictions on segregation, leading to microdomain formation [30]. As a consequences, phase separation (segregation) occurs and covalently linked microphase structures are formed. The coherent matrix which consists of flexible soft segments, results in high deformability of the resulting material. In contrast, within the hard segment domains, molecules are fixed by physical interaction. Because of covalent coupling to the soft segments, they inhibit plastic flow of the chains, thus creating elastomeric resiliency. Hard segment domain can act as multifunctional spacious crosslinked areas. The larger the phase segregation, the lower the polarity of the flexible segments. Therefore, segregation is less pronounced in polyester urethanes compared to polyether urethanes, and is most pronounced in polybutadiene urethanes. Formation of hydrogen bonds, crystallization of hard segments, chain folding, free volume effect, and kinetic arguments have all been proposed as

possible explanations for this phase separation behavior of segmented polyurethanes. Due to the high polarity difference between the hard and soft segments three-dimensional hydrogen bonding network structure would be formed. The microphase separation of these two chemically distinct compounds gives rise the useful physical, mechanical and functional properties of the segmented polyurethanes [25].

2.1.4.1 Hard Domain Segregation and SPU Properties

The degree of phase separation between the hard and soft segments (Figure 2.5) depends on the interaction (affinity) between hard segments to each other or towards the soft segment respectively [36-41]. The phase structure is directly responsible for many of the unique mechanical properties in this class of materials. The property would depend on the size and perfection of the phase separated morphology. The mechanical properties of segmented polyurethanes (SPU) can be optimized by carefully choosing the types of hard and soft segments, molecular weight, molecular weight distribution of the two components, stoichiometric ratio between them and sample fabrication. In general, modulus is increased almost linearly with hard segment content which is due to the stiffness to the polymer chain. The glass transition temperature (T_g) is increased with hard segment content due to the strong allophanate interaction by excess hard segment in the polymer. T_g could be also increased with the number of benzene rings in hard segment at a constant mole ratio of hard segment/soft segment. Increase of hard segment would increase the cross-link point, thus it is expected that the polyurethane membrane with greater cross-link densities needs more thermal energy to initiate chain movement. The cross-linked formed due to hard segment domains would impart elasticity to the polymer which are reversible to heat and solvation.

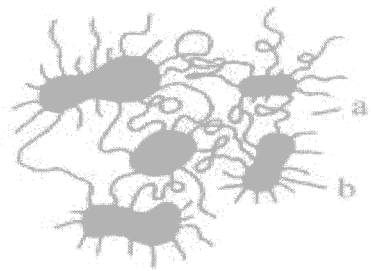

a - soft block domain

b - hard block domain

Figure 2.5: Segregated Structure of Segmented Polyurethane (Adapted with permission from Vilar Polyurethanes, http://www.poliuretanos.com.br/[26])

Depending upon the amount of hard segment in the segmented polyurethane, different microdomain structure would be formed [42-44]. Polyurethane with low hard segment content has morphology of dispersed, short, hard segment cylinders embedded in a matrix of soft segment [42]. An alternating hard- and soft- segment rod like or lamellar microdomain structure was characteristic of materials with higher hard segment contents. The length of lamellae or rod like microdomains remained constant. At very high hard segment contents, a morphology having a dispersed soft segment phase was observed. Presence of three-dimensional hydrogen bonding within hard domains leads to the unusually strong hard domain cohesion [42]. Upon decrease of hard segment content, a change of morphology from interconnecting to more isolated hard domains took place. In increasing hard segment the mechanical properties of the materials have been improved [45-47], because there are increases in the degree of inter chain hydrogen bonding which will lead to the formation of more rigid film. The looser packing of the rigid segments is responsible for the somewhat greater dissolution of the segments in the flexible phase while fewer of them remain in the rigid domains. As a result, the modulus

is reduced and the elongation at break increases. At greater elongations, however, more pronounced crystallization may occur in the flexible segments, with a resultant higher tensile strength.

2.1.4.2 Soft Domain Segregation and SPU Properties

The degree of phase separation, and hence the polyurethane properties would depend on the type of flexible segment as well. Due to strong interactions of the ester function of the oligoester chains with the urethane group of the rigid segments than with the ether functions of oligoether chain, microphase separation takes place to greater extent in polyetherurethanes than in polyesterurethanes [41]. The degree of microphase separation is increased with increasing the block length of polyol, with the shortest block length the resulted SPU being almost single-phase [27, 48]. The polyurethane properties would be improved with more complete phase separation and greater ordering of the segments in the hard phase. The more distinct the separation of the soft, flexible segments phase from the hard phase, the lower is the T_g of the polymer and greater the ability to withstand low temperatures. The property of the elastomers depends on the type and molecular weight of polyol, and the ratio of hard to soft segments [49]. Oligoetherols with weaker molecular interactions give the polyurethanes greater flexibility, a lower modulus of elasticity, and a greater elongation at break as compared with oligoesterols. Polyetherurethane with a regular structure of flexible segments would possess a mechanical strength similar to polyesterurethanes. The oligoetherols such as PTMG with a symmetrical structure give polyurethanes with superior characteristics and the property of stress-induced reversible crystallization. The side chains (such as methyl

groups) in oligo-oxypropylenols prevent crystallization of the flexible segment which will reduce the mechanical properties of the resulting polyurethanes. This is because of the higher cohesive energy of the polyester chains. Increasing the molecular weight of polymer by increasing the soft segment molecular weight would result in lowering of the mechanical property which will make the polymer softer and more extensible. By selecting the type and molecular weight of soft segments, the properties such as physical, shape memory and water vapor permeability of segmented polyurethane could be tailored. The shape memory effect of polyurethane with segmented structures has been reviewed in the following paragraphs:

2.1.5 Shape Memory Polyurethane

Shape memory materials are stimuli responsive materials. They have the capability of changing their shape upon application of an external stimulus. Shape memory may be triggered by heat, light, electric filed, magnetic field, chemical, moisture, pH and other external stimuli [3-4]. Change in shape caused by change in temperature is called thermally induced shape memory effect. These materials are stable at two or more temperature states. While in these different temperature states, they have the potential to be different shapes once their 'transformation temperatures' (T_x) have been reached. Shape Memory Alloys (SMA) and Shape Memory Polymers (SMP) are the materials with very different shape changing characteristics. While exposed to their T_x, devices made from SMAs have the potential to provide force such as in the case of actuators. Devices made from SMPs in contrast, while exposed to their T_x, provide mechanical property loss as in the case with releasable fasteners. Shape memory polyurethane

(SMPU) is a class of polyurethane that is different from conventional polyurethane in that these have segmented structure with wide range of glass transition temperature (T_g) or soft segment crystal melting point temperature (T_{ms}). SMPUs are able to remember their original shape; the material would be deformed into a temporary shape and return to its original shape by external stimuli. Their morphology depends on chemical composition and the chain length of the soft segment (block). The shape memory polyurethane has micro phase separated structure due to the thermodynamic incompatibility between the hard and soft segment. Hard segments can bind themselves via hydrogen bonding and crystallization, making the polymer solid below melting point temperature. Reverse phase transformation of soft segment is reported to be responsible for the shape memory effect. The shape memory effect can be controlled via molecular weight of the soft segment, mole ratio between soft and hard segment, and polymerization process [50]. Shape memory properties could be triggered by various external stimuli [51-52] such as temperature, pH, electric field, magnetic field etc. Our concern is temperature stimulating shape memory polyurethane. The principle of temperature stimulating shape memory effects have been reviewed in the following paragraphs.

2.1.5.1 Principle of Temperature Stimulating Shape Memory Effect

Temperature sensitive shape memory polymers are a special class of adaptive materials which can convert thermal energy directly into mechanical work. This phenomenon known as shape memory effect (SME) occurs when one of these special polymers is mechanically stretched at high temperature, fixed the deformed shape at low temperatures, and then heated above a critical transition temperature which would be

result in the restoration of the original shorter "memory" shape of the specimen [53]. The proposed theories would express well the thermomechanical properties of thermoplastic polymer, such as shape fixity, shape recovery, and recovery stress [54]. The mechanism of shape memory behavior with temperature stimuli can be schemed briefly as outlined in Figure 2.6. These materials have two phase structure, namely, the fixing phase which will remember the initial shape and the reversible phase shows a reversible soft and rigid phase transition with temperature.

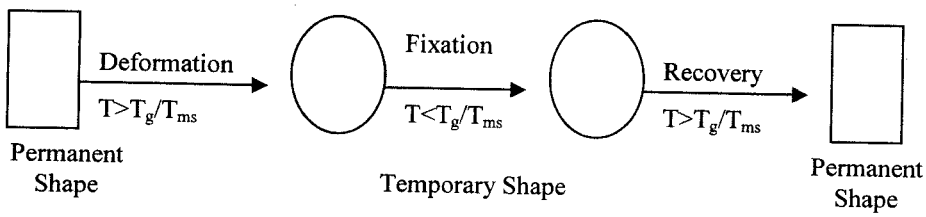

Figure 2.6: Typical temperature stimulating shape memory behaviors

At temperature above the glass transition temperature (T_g), the polymer would be changed into a rubbery elastic state (Figure 2.7) where it can be easily deformed without stress relaxation by applying external forces over a time frame $t<\tau$, where τ is a characteristic relaxation time. When the material is cooled below its T_g/T_{ms}, the deformation is fixed and the deformed shape remains stable. The pre deformation shape can be easily recovered by reheating the material to a temperature higher than the T_g/T_{ms} [55]. Therefore, admirable shape memory behavior requires a sharp transition from glassy state to the rubbery state, a long relaxation time, and a high ratio of glassy modulus to rubbery modulus. The micro morphology of SMPs strongly affects its mechanical properties. There are many factors which can influences these shape

memory behavior such as chemical structure, composition, and sequence-length distribution of the hard and soft segment in segmented polymer, overall molecular weight and its distribution.

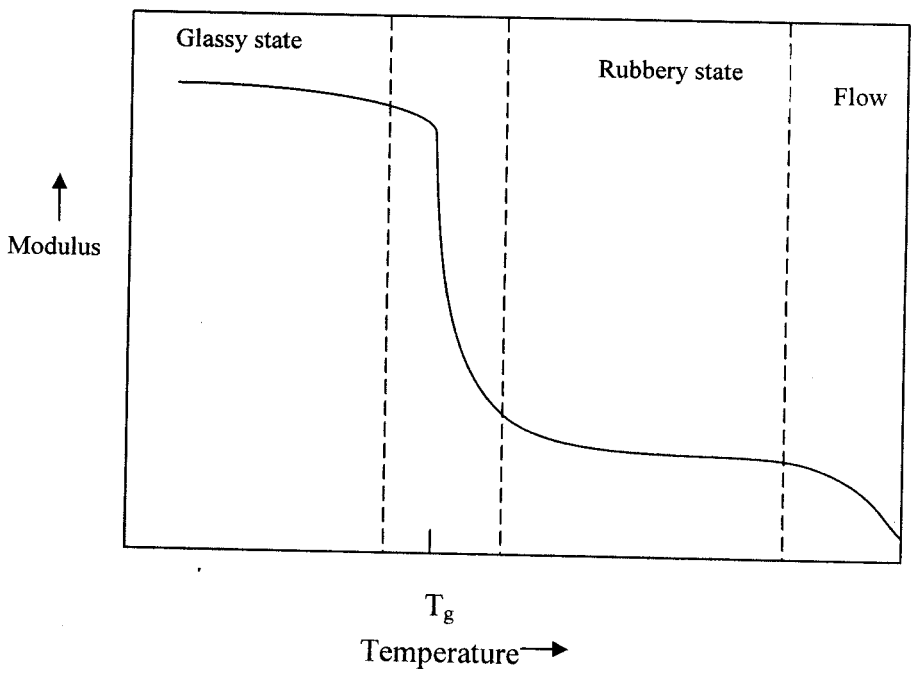

Figure 2.7: Temperature dependency elasticity of thermoplastic polymer

An elastomer might exhibit shape memory functionality if the material can be stabilized in the deformed state in a temperature range that is relevant for the particular application. The shape is deformed under stress at a temperature near or above T_g or the soft segment crystal melting temperature, T_{ms}. The deformed shape is fixed by cooling below T_g or T_{ms}. The deformed shape reverts to the original shape by heating the sample above T_g or T_{ms}.

2.1.5.2 Macromolecular Structure of Shape Memory Polyurethane

In shape memory polyurethane micro-crystal are used for memorizing the original shape and glassy state is used for maintaining the transient shape. In general, interpolymer chain interactions are so weak that one-dimensional polymer chains cannot keep a certain shape above T_g/T_{ms}. To maintain a stable shape, polymer chains should have a three dimensional network structure. Inter-polymer chain interactions are useful for constructing the polymer network crystal aggregate or glassy state formation, chemical cross-linking, and chain entanglement. The latter two are permanent and used for constructing the original shape. The other interactions are thermally reversible which are used for maintaining the transient shapes. Li et al. [56-57] stated that the crystallinity of the soft segment regions at room temperature and the formation of stable hard segment domains acting as physical crosslinks in the temperature range above the melting temperature of the soft segment crystals are the two necessary conditions for a segmented polyurethane copolymer with shape memory behavior. The response temperature of shape memory is dependent on the melting temperature of the soft segment crystals. The final recovery rate and the recovery speed are mainly related to the stability of the hard segment domains under stretching and are dependent on the hard segment content of the copolymers.

Phase transition temperature of the shape memory polyurethane is little higher than the glass transition/soft segment crystal melting temperature. Phase transition would accompany a great change in thermomechanical properties of polyurethane. A large drop of modulus and an enhanced micro-Brownian motion on heating through the glass transition or melting temperature can be used in the molecular design of shape memory

behavior [56-58]. Shape memory characteristics of the segmented polyurethane having crystallizable soft segment are closely related with the temperature dependent dynamic mechanical properties of the materials [56, 59]. A large glassy state modulus would lead to large shape recovery upon heating and standing at high temperature. Deformed shape of the shape memory polyurethane would be recovered if the reversible phase was heated to a soften state. When the reversible phase was cooled to a hardened state, it could keep the deformation. However, the fixed phase consists of a high transition temperature or a crosslinking point.

Few researchers studied the structure and dynamic mechanical thermal properties of segmented polyurethane with shape memory behavior. High T_g or T_m of hard segment would be considered as fixed phase. On the other hand low T_g or T_m of soft segment is the reversible phase. Chemical composition of hard and soft segment is important for shape memory behavior. The amount of the hard-segment-rich phase would affect the ratio of recovery, that is, the low hard segment content would lead to the recovery of the deformed specimen being incomplete [60]. The recovery rate would influence by the modulus ratio and the size of the dispersed phase in the micromorphology. Lee, et al. [60] shows that the polyurethane with 20 or 25 wt% of hard segment could not have shape recovery due to weak interaction or physical cross-link. On the other hand polyurethane with 50 wt% of hard segment did not show shape recovery due to the excess interaction among the hard segments and the resulting rigid structure. The maximum stress, tensile modulus, and elongation at break was increased significantly at 30 wt% of hard segment content, and the highest loss tangent was observed at the same composition. Finally, they obtained 80-95 % of shape recovery at 30-45 wt% of hard segment. Kim et al. [50]

and Lee et al. [61] have studied the effect of crystallization of polycaprolactone diol, as the reversible phase on shape memory behavior. Lin et al. [62-63] studied the morphology, viscoelastic properties and shape memory behavior of segmented polyurethane having trimethylol propane (TMP). The fixed phase in this case is the chemical crosslinking points by TMP and the reversible phase is soft segment (polyol) with different length of molecular chain.

From the above discussion we found that large change of mechanical and thermomechinical properties would occur across the phase transition temperature of shape memory segmented polyurethane (SMPU). In addition to the change of mechanical properties of SMPU, it may also have large change in moisture vapor permeability of nonporous membrane, above and below the T_g/T_{ms} because of morphological structure changes.

2.2 WATER VAPOR PERMEABILITY THROUGH DENSE POLYMER MEMBRANE

Non-porous membranes are dense polymer membranes. These polymer membranes are usually hydrophilic which produces a "wicking" action that will actively attract water vapor molecules. Non-porous membrane allows the transmission of vapors through a process called activated diffusion. The permeant would be dissolved on the surface of the membrane on the side of the highest concentration, and then diffuses across the film. When the vapor arrives at the opposite surface, the permeant desorbs and typically enters the surrounding airspace as a gas or vapor. Chemical structure and film thickness are the main determinants of permeability in a non-porous membrane [21].

Permeation through dense membrane is a collective process of diffusion and sorption, hence, the permeability of mass molecules through the dense polymer membrane depends on both the diffusion and solubility [22]. Mass transfer can result from different phenomena [21]. There is a mass transfer associated with convection in that mass is transported from one place to another in the flow system. This type of mass transfer would occur on a macroscopic level which is usually treated in the subject of fluid mechanics. There will be a mass transfer on a microscopic level as the result of diffusion from regions of high concentration to the regions of low concentration due to the concentration gradient. Higher concentration means there are more molecules per unit volume. Mass diffusion may also result from a temperature gradient in a system; this is called thermal diffusion. Diffusion of mass and the conduction of heat will obey very similar equations. In particular, diffusion in one dimension is described by the following form of Fick's law:

$J = -D*dc/dx$ ----------(2.1)

Where D is diffusion coefficient and dc/dx is the concentration gradient.

2.2.1 Fundamental Theory

2.2.1.1 Solubility-Diffusion Model

The effect of concentration and pressure gradient driving forces on permeation through membranes can be described in terms of the solution-diffusion model [Figure 2.8] and Fick's law. The membrane permeability can be divided into two parts as the permeability is the product of the diffusion coefficient and the sorption coefficient [64-65]:

$P = DK$ ----------(2.2)

The sorption coefficient K in equation (2.2) is the term linking the concentration of a component in the fluid phase with its concentration in the membrane polymer phase. Sorption is an equilibrium term; conventional thermodynamics can be used to calculate sorption of water vapors in polymers to within a factor of 2 or 3. However, diffusion coefficient D is kinetics term that reflects the effect of the surrounding environment on the molecular motion of permeating components. Calculation of diffusion coefficients in liquids and gases is possible, but calculation of diffusion coefficients in polymers is much more difficult.

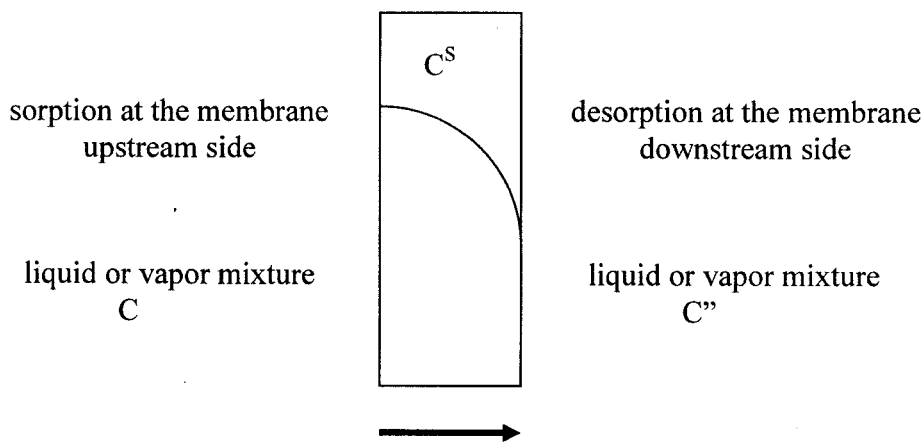

Figure 2.8: Permeation through non-porous membrane according to the sorption-diffusion-desorption model. C, C^S and C' are the composition of the feed, absorbed and permeated mixture, respectively.

As a general rule, membrane material property changes will affect the diffusion coefficient of a permeant much more than the sorption coefficient. Diffusion of vapors or liquids through polymeric materials is a complex process whose quantitative analysis

is not trivial which are still remaining subject to debate [66-67]. Diffusion behavior can be classified into three categories [68]: (i) Fickian diffusion, in which the rate of diffusion is much less than that of sorption and the sorption equilibrium is rapidly established. (ii) Sorption-controlled process, in which the diffusion rate is very rapid compared with the sorption rate, therefore, sorption is the key step for the mass transfer process. (iii) Non-Fickian diffusion or anomalous diffusion, which occurs when the diffusion rate and the sorption are comparable. Among these three kinds of diffusion behaviors, the non-Fickian diffusion which commonly occurs in the case of liquid penetrants and glassy polymer membranes is the most complicated one.

2.2.1.2 Diffusion Coefficient, Sorptivity, and Permeability

The diffusion coefficient is a kinetic parameter which depends on the mobility of polymer chain segments. To get diffusion coefficient Da, $[(M_t/M_\alpha)*h]$ would plot against $\sqrt{t}$. Where M_t and M_α are the fractional weight gains of sample at time t and at equilibrium, respectively, and h is the initial sample thickness [69-70]. The near actual diffusion coefficient value (Da) would be obtained through multiplying Dm by an average edge correction factor (Rac) which depends upon the time average thickness. Hence,

$$Da = Dm \times Rac \quad \text{----------(2.3)}$$

Sorptivity (S), the measure of fractional solvent absorption by the polymer at equilibrium, is expressed as the gram of solvent absorbed per gram of polymer. On the other hand permeability (P) is calculated from the product of near actual diffusion coefficient and sorptivity.

2.2.1.3 Concentration Dependent Diffusion

Two types of laws have been proposed to describe the concentration dependency of the diffusion coefficient of a unique penetrant through the polymeric materials. The first law is purely empirical which has been applied to systems that do not involve strong specific interactions (i.e. polar systems). Aitken and Barrer in 1995 [71] proposed the most ancient law which was suggested a linear increase with the penetrant concentration in the polymer C_s according to:

$$D = D_0(1 + kC_s) \text{ ----------} (2.4)$$

The second type of law has been derived from theoretical consideration based on free volume theories [72-73] whose main aspects have been briefly reviewed by Mears [74]. Derived on the basis of a statistical calculation and assuming the additivity of free volume contributions for polymer and solvent, the Long's model certainly provides the most used equation to describe the concentration dependence of diffusion coefficient [75]:

$$D = D_o \exp(\gamma C_s) \text{ ----------} (2.5)$$

Where D_o is the diffusion coefficient at infinite dilution (also called intrinsic diffusivity) and γ the plasticizing constant. The latter parameter characterizes the solvent ability to plasticize the polymer which increases its own diffusion through the swollen material.

2.2.1.4 Activation Parameter of Diffusion

As the diffusion increases with the temperature which is indicating that the diffusion process is temperature dependent. The diffusion and permeation follows the Arrhenius relationships:

$Da = D_o \exp^{-E_D/RT}$ and $P = P_o \exp^{-Ep/RT}$ ----------(2.6)

Where, E_D is the activation energy required to create opening between the polymer chains to permit penetrant molecules to pass. E_D is the function of inter- and intrachain forces [76].

2.2.1.5 Film Thickness

Fick's law governs the rate of transport of the permeant through the membrane under the existing concentration gradient. If diffusion coefficient (D) is not a function of concentration, integration across the film thickness h, gives [21]:

$J = D(c_1 - c_2)/h$ ----------(2.7)

Where c_1 and c_2 are the concentrations of permeant at high and low pressure faces of the membrane surface, and h is the thickness of membrane.

Substituting values of c_1 and c_2 from Henry's law ($c = Sp$) equation 2.7 becomes:

$J = DS(p_1 - p_2)/h$ ----------(2.8)

Where, p_1 and p_2 are the external partial pressure of the vapor on the high and low pressure sides of the membrane. (D.S) is termed as the permeability (P). From equation

2.8, it is clear that for ideal systems, permeation rate of permeant is directly proportional with the pressure gradient and inversely proportional with membrane thickness.

2.2.1.6 Free Volume and Diffusion

Generally speaking, dense polymer membranes have no pores; however there exists the thermally agitated motion of chain segments which will generate penetrant-scale transient gaps in the matrix allowing penetrants to diffuse from one side of membrane to the other side [77]. Accordingly, it is reasonable that a dense polymer membrane can be regarded as a "porous medium", where pores are gaps among the polymer matrix. According to the free-volume theory

1. It is possible to associate a local volume, v of molecular-scale with each chain segment.
2. When v is greater than a certain critical value v_c, the excess $v - v_c$ can be regarded as the free-volume which is defined as the local free-volume and marked as v_f.
3. The minimum free-volume of penetrant molecule with volume v_m for a diffusive step is v_p, defined as its equivalent molecular volume.
4. Molecular transport only occurs when $v_f > v_p$.
5. Local free volume v_f of each chain segment can be redistributed continually without any local free energy.

The total free-volume V_f of a given polymer can be calculated as follows:

$$V_f = A + BT \quad \text{----------(2.9)}$$

Where A and B are specific constants of the polymer and T is the absolute temperature. The transport of penetrants through a dense polymer membrane is similar to the fluid transport through a "porous medium". The difference in these two cases is that the size and position of "pores" within the dense polymer membrane are changing with time, i.e. a penetrant passes through a "pore" with a certain probability.

Polymer chains do not pack perfectly; some unoccupied space –free volume – exists between the polymer chains (Figure 2.9). Fractional free volume v_f (cm^3/cm^3), is usually defined as

$v_f = (v - v_0)/v$ ----------(2.10)

where, v is the specific volume of the polymer (cm^3/g) and v_0 volume occupied by the molecules themselves (cm^3/g). The free volume of a polymer is the sum of the many small spaces between the polymer chains in the amorphous, noncrystalline structures. Although these free volume is only a few percent of the total volume which is sufficient to allow some rotation of segments of the polymer backbone. As the temperature increases, the free volume of polymer also increases. At glass transition temperature, T_g, the free volume is reduced to a point at which the polymer chains can no longer rotate freely.

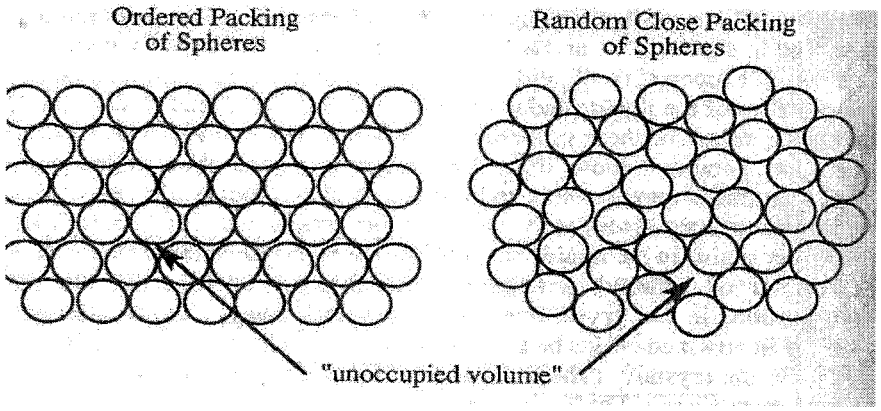

Figure 2.9: Concept of free volume

2.2.2 Permeability through Dense SPU Membrane

Dense SPU membranes are pin hole free. The permeability occurs through the nonporous membranes in molecular mechanism which is defined by sorption-diffusion-desorption. Therefore, the structural factors are the main determinants for nonporous membranes permeability.

2.2.2.1 Structural Factors Influencing SPU Membrane Permeability

2.2.2.1.1 Effect of Structure of Polymer on Permeability

Not only the polymer-penetrant interactions but also the primary structures of the polymer itself are very important for understanding of membrane functions such as sorption, diffusivity, and permeability of small molecule [15]. High permeability coefficient which is reflecting a low cohesive energy and enhances the segmental motion: in other words, low glass transition temperature (T_g). The cohesive energy of polymer membranes is determined by such factors as chain flexibility (internal rotation of repeating unit), coulombic interaction, van der Waals interaction, hydrogen bonding, and so on. A high permeability coefficient is generally attained when each factor except

flexibility is low and is not affected by the penetrant. Therefore, the polymer, which contains a monomer unit with a high charge density, dipole moment, and capability for hydrogen bonding, will give a low permeability coefficient. Permanent flux increases with the increasing value of the prepolymers molecular weight [78]. This means that longer molecular chains originate larger polymer network holes and therefore higher fluxes.

Permeation behaviors are slightly complicated when polymer membranes are influenced by penetrant; in other words, the polymer-penetrant interaction is not weak. A strong polymer-penetrant interaction would depress the cohesive energy of the polymer, therefore, permeation and diffusion becomes easy which is indicating a tendency towards the increases of permeability. However, when the polymer-polymer interaction relative to the polymer-penetrant is strong, the penetrant is not able to enhance permeation through the polymer membrane. The permeability behavior is qualitatively interpreted by the balance of the cohesive energy of polymer membranes and the – penetrant interaction. The permeability of water vapor through hydrophilic polymer capable of forming hydrogen bonding is one example of a strong polymer-penetrant interaction.

2.2.2.1.2 Effect of Hard Segment on Permeability

Interactions between SPU chains (Figure 2.10), mainly hydrogen bonding between hard segments, contribute the distinguishing physical properties of SPUs. However, systematic investigations of the influence of hard block chemical structure on water sorption or permeation has been reported very rarely [79]. Water sorption and diffusion

for polyurethane obtained from different diisocyanates (MDI or different isomers of H12MDI), 1,4-BDO and polyether (PPO) or polyester (PBA) soft segments has been investigated by Kanapitsas et al. [80]. They observed that for all polymers, the water sorption was very low (typically, G<3%) and the small differences observed for the different polymers could reasonably not be ascribed to any change in the hard block chemical structure. In the same way, the diffusion coefficient did not vary significantly with the hard block composition.

Yen et al. studied the water vapor permeability of cast polyurethane films using H_{12}MDI-1, 1,4-BDO as hard segment, and PTMG (M_w 650, 1000, 2000, 2900) and PBA (M_w 1000, 2000, 3000) as soft segments. The films with higher hard segment ratios had highest breaking strength but the water vapor permeability, on the other hand became lower [78]. In another study a strange phenomena was observed [81], in that the permeation was increased with increase of hard segment content of PU membranes, while the permeability ratio was decreased.

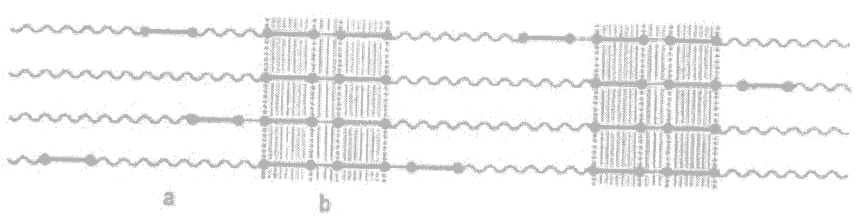

Figure 2.10: Interchain interaction between hard and soft segments: a) soft segments, b) hard segments (Adapted with permission from Vilar Polyurethanes, http://www.poliuretanos.com.br/[26])

Mutual diffusion coefficients of penetrant-polymer systems of the same polyether soft segment domains, but different in their hard segment content were studied by Ponangi et al. [82]. The diffusion coefficient was decreased with increasing hard segment at all temperature. They correlated the mutual diffusion coefficient as a function of permeant concentration and temperature with Fujita's free volume theory, corrected for the presence of hard segment in polyurethanes.

2.2.2.1.3 Effect of Soft Segment on Permeability

Very strong influence of the soft block chemical nature on water sorption and permeability has been reported in the literatures. Schneider et al. [83] studied the water sorption and permeability for four SPU, X/MDI/1,4-BDO with different type of soft segment (PEO 2000, PTMG 2000, PPO 2000, PBA 2000). For soft segments of PTMG 2000, PPO 2000 and PBA 2000, extremely low water sorption were obtained at 21°C (typically G<3 wt%). As expected from these very low sorption values, these SPU were poorly permeable to water (normalize water fluxes less than 1.5 kg μm/m^2 h at 21°C). On the other hand PEO 2000 based SPU shows much higher water sorption (G = 113%) and permeability (normalized water flux J = 165 kg μm/m^2 h) at the same operating temperature. Hsieh et al. [84] had obtained very low water sorption and permeability at ambient temperature for SPU X/MDI/1,4-BDO with soft segment of PTMG 2000, PBA 2000 and PCL 2000. For these SPU, water permeability was shown to increase in the following order of the soft segment X = PBA<PCL<PTMG. An ester group has much stronger interaction with water vapor molecules than an ether group. The large decrease in water vapor permeability (almost –100%) were observed with the polyurethane with the soft segment of PBA and PCL, which may be related with the combined action of an

increase of glass transition temperature and an accumulation of methylene groups in the soft segment block structure.

The effect of structure (composition and length) of soft segments on water vapor permeability of polyurethane based on low molecular weight homopolymer or tri block (PEP) copolymers of ethylene and propylene oxides and 4,4'- diphenylmethane diisocyanate with hydrazine as chain extender, were studied by Petrik et al. [85]. Sorption values were found to be lower than the reference values computed under the assumptions. This finding was assigned to the shielding effect of hard segment domains on the interaction of water molecules with hydrophilic (ethoxamer) groups of soft segments. Tsunoda et al. [86] had studied the water vapor permeability of polyurethane with soft segment derived from tetrahydrofuran and ethylene oxide, bis (4-isocyanatocyclohexyl) methane and isophorone diamine as hard segment. They observed that the high polyol moiety shows the highest water vapor-permeability.

2.2.2.1.4 Effect of Functional Groups on Permeability

Jeong et al. [87] had investigated the water vapor permeability of polyurethanes based on poly(caprolactone) diol (M_n 4000, PCL 4000), hexamethylene diisocyanate, 4,4'-diphenylmethane diisocyanate and hexamethylene diamine which was modified with hydrophilic segments, and dimethylol propionic acid (DMPA) as functional unit. Their result shows that the DMPA segment enhances the crystallization of PCL segments by reducing the miscibility between hard and PCL segments. DMPA units play their role as a water vapor barrier at temperature below crystal melting temperature (T_{ms}) by increasing the crysllinity of PCL segments which would create path for water vapor

transfer at temperatures above T_{ms} (Figure 2.11). Jeong et al. [88] had reported the thermoplastic polyurethane on amorphous soft segments from the reaction of hexamethylene diisocyanate and 1,2-butane diol, and the crystalline hard segment from 4,4'-methylenediphenyl diisocyanate and 1,6-hexane diol modified with DMPA. The neutralized DMPA unit was found to increase the sensitivity of the thermoresponsive water vapor permeability (WVP) by amplifying the increase of WVP at the temperature range above the glass transition temperature. Similar results were obtained by Hsieh et al. [89] from polyurethanes having tertiary amine and carboxyl groups. They observed that, when the content of the functional groups is increased, the crystallinity of the membrane also increases, and the vapor permeability at room temperature decreases. This increase in the crystallinity of the polyurethane soft segment is possibly due to increasing intermolecular forces [90-91] through increasing the polarity of the SPU hard segment or strengthening hydrogen-bonding by the –COOH group between the SPU hard and soft segment.

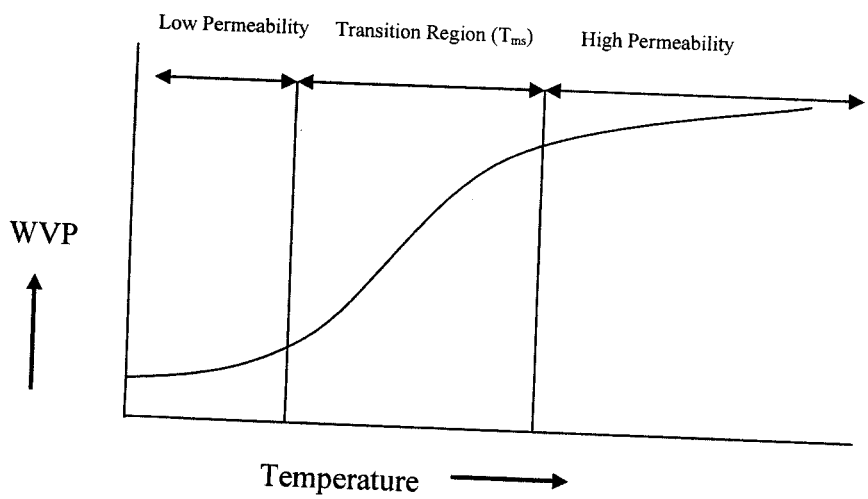

Figure 2.11: Influence of soft segment crystal melting on WVP

2.2.2.1.5 Effect of Hydrophilic Segment on Permeability

According to the sorption-diffusion model for non-porous membranes, permeability is a function of sorption of the penetrant in the polymer membrane. The high chain mobility of the breathable thermoplastic segmented polyurethanes is evidenced by glass-transition temperatures well below 0°C for all the ether (PEO) soft segments will allow for the high diffusion coefficients that are found for water vapor molecules. It is generally assumed that the high water vapor permeabilities are related to the continuous soft-segment phase observed within the thermoplastic polyurethanes. Valentová et al. [92] studied the structure and sorption behavior of two component and three component polyurethane. Two components PUs were made by using two diisocyanate and mesogenic diol. On the other hand three components PU were made by two diisocyanate, mesogenic diol and a polybutadiene diol with stoichiometric ratios of reactive hydroxyl and isocyanate groups. They found nematic and smectic mesophase structure in two component polymer. On the other hand, two phase structure were observed in three components PUs. Isothermal equilibrium and dynamic water sorption measurements revealed that the three-component polymers are more hydrophilic than two components.

Water absorption is highly dependent on the PEO content as well as on the molecular weight. The increase in water absorption with increasing molecular weight of the PEO soft segment is believed to reflect the extent of phase separation between hard and soft segments. A lower-molecular-weight of soft segment usually results in mechanically tougher films which will reduce the mass transfer. Yilgor et al. [64] studied the water vapor permeability (WVP) of hydrophilic polyurethane having constant hard segment

content, whereas the polyethylene oxide (PEO) contents were varied between 0% and 50% by weight. The relationship between PEO content and WVP follows an S-shaped curve. For copolymer containing up to about 15% by weight of PEO, WVP was fairly low. This is followed by a region where WVP increases continuously for membrane containing between 15% and 30% of PEO. Further increase in PEO content above 30% does not influence the WVP. Low molecular weight PEG (200) decreases the degree of crystallinity of PCL 4000 soft segments [87] by reducing the miscibility of hard and PCL segments, and WVP of polyurethane film was triggered at temperatures around 50°C. The chain mobility of the PCL segment and closely linked hydrophilic segment is enhanced by phase transition. Effect of chain lengths of polyethylene glycol on the membrane permeability have been investigated by Bharadwaj et al. [93]. The diffusion coefficient and sorption of polyurethane elastomer, from castor oil based polyol, polyethylene glycol (PEG) of various molecular weight (200, 400, and 600) and toluene diisocyanate, were found to decrease with an increase in chain length of PEG. Different results were obtained by Chen et al. [94] from the PU containing PEG of molecular weight 600, 1000 and 1540. They observed that as the molecular weight of PEG increases the weight percentage of urethane and urea groups is reduced, with a trend of lower strength and higher water absorption which creates more favorable pathways through the film for water vapor molecules.

Sorption of water by polyurethane-ureas based on triblock copolymers of ethylene and propylene oxides depends not only on the content of ethoxamer units but also on the overall length of the soft blocks and on the position of ethoxamer units with respect to

the hard segments [85]. The latter appears to "shield" the neighboring soft segment units from the interaction with water.

The effect of higher-molecular-weight hydrophilic segments on sorption and permeability were investigated by several authors [94-96]. With higher molecular weight PEG will form more distinct—but hard-segment-poor-PEO domains that are able to absorb larger amount of water. The increase in water absorption with PEO content basically shows an exponential increase in the plotted range which can be explained by a decreasing amount of "physical" cross-links formed by the hard-segment domains. These cross-links would impose a swelling limit on the hydrophilic PEO regions. With low PEO content, the absorbed water is bound to the PEO chains through hydrogen bonding. Above certain PEO content, freezing water is increasingly present. This freezing water can be revealed with a technique known as thermoporometry which measures the freezing/melting point depression of water clusters in polymers through DSC analysis. Pore sizes varying from 2 to 7 nm can be determined with this technique. With increasing the block length of PEG components in the polymer, the WVP would be also increased (Figure 2.12) due the increase of flexibility of the polymer chains and increase of hydrophilicity. Increasing hydrophilicity would increase the interactions between water vapor molecules and polymer chain segments. On the other hand, longer polymer chains of PEG originate larger polymer network holes that will also enhance the water vapor flux. Analyzing the properties of very closely related SPU (PEO 1450/PTMG 2000/H12MDI/1,4-BDO) with a much higher hard block content (W_{HB} ≈0.6), Schneider et al. [96] reported interesting results on water sorption which varies linearly (rather than exponentially) with the PEG content in the polymer backbone. This

rather unexpected trend might be related to the particularly strong rigidity of these copolymers containing almost 60 wt% of hard blocks.

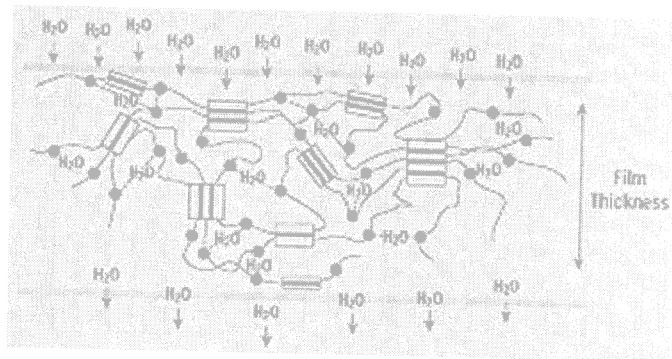

Figure 2.12: Schematic representation for water transport through a non-porous hydrophilic membrane (Adapted with permission from Johnson L, and Samms J, *J. Coated Fabrics*, 27 (July), (1997), 48 © Technolmic Publishing Co. Inc [19]).

Hayashi et al. [97] studied the high moisture permeability polyurethane for textile applications. They prepared a series of hydrophilic polyurethane with different M_w of polyols and measured their water vapor permeability according to ASTM E 96 (Method A-1). The water vapor permeability of the PU depends mainly upon the ethylene oxide concentration of the system due to an increase in the water molecule's solubility. The T_g of the materials was controlled by the flexibility of the polymer chain, which is dependent on the molecule weight of the polyol, the fraction of the hard segment, and the type of the chain extender.

2.2.2.2 Water Vapor Permeability through Shape Memory Polyurethane

Thermal-responsive shape-memory polyurethanes are segmented polymer which consists of two phases, a thermally reversible phase for maintaining a transient shape and a fixed phase structure for recovering the original shape. Micro-crystal, glassy states, chain entanglements can be used as fixed phase structures for memorizing the original shape. The thermally reversible phase is designed to have a large drop in the elastic modulus with heating above the shape-recovery temperature. Therefore, the melting temperature of the crystalline segment or the glass-transition temperature (T_g) of the amorphous segment can be used as a shape recovery temperature. The large change of mechanical and thermomechinical properties occurs across glass transition temperature (T_g) or soft segment crystal melting point temperature (T_{ms}) of shape memory polyurethane (SMPU) [97]. In addition to the change of thermo-mechanical properties of SMPU, it was found that SMPU also has large change in moisture permeability above and below the T_g/T_{ms}. The SMPU has low moisture permeability below the T_g/T_{ms}, during the glassy state, and has high moisture permeability above T_g/T_{ms}, during the rubbery state.

Water vapor permeability in shape memory polyurethanes have been hardly investigated by the researchers. Jeong [88] et al. studied the water vapor permeability of shape memory thermoplastic polyurethane, based on amorphous soft segment from the reaction of hexamethylene diisocyanate and 1,2-butane diol, and the crystalline hard segment from 4,4'-methylenediphenyl diisocyanate and 1,6-hexanediol. PUs were modified by hydrophilic segments, diol-terminated poly(ethylene oxide) or dimethylol propionic acid (DMPA). They observed that as the hydrophilic segment content was

increased the hysterisis in shape memory effect increases by reducing the crystallinity of the hard segment. The neutralized DMPA unit enhances the sensitivity of the thermoresponsive water vapor permeability (WVP) by amplifying the increase of WVP at the temperature range above the glass transition temperature. Jeong [87] et al. investigated the WVP of polyurethane based on poly(caprolactone) diol (Mw 4000), hexamethylene diisocyanate, 4,4'-diphenylmethane diisocyanate and hexamethylene diamine which were modified by hydrophilic segments, diol-terminated poly(ethylene oxide) (Mw 200) or DMPA. The polymers showed temperature sensitive water vapor permeability at the melting temperature of the PCL phase which was enhanced by modification with hydrophilic segments. On the other hand fatigue in shape memory effects was minimized by introducing some amount of DMPA units in the polyurethane chains. Chen [98] et al. studied the water-swollen and shape memory properties of a series of shape memory polyurethane with different component ratio of PEG (Mw 400, 780 and 1870), MDI, BDO and cross-linker, diethanolamine (DEA). The water-swollen ratio was increased with both increasing molecular weight of PEG soft segments and decreasing density of the chemical cross-bonding. They also reported some interesting observations, when the mole ratio of soft segment to hard segment is close, the shape recovery time reduces along with the increasing density of the chemical cross-bonding. When the densities of the chemical cross-bonding are similar, the shape recovery time reduces with the increasing molecular weight of the PEG soft segments.

2.3 ABOUT CARBON NANO TUBE (CNT)

We wanted to reinforce carbon nano tube in the SPU matrix, and investigate the structure, shape memory and water vapor transport properties of CNT-SPU, therefore, here we reviewed the properties CNT, their dispersion and polymer properties improvements with nano particles.

Carbon nano tubes (CNT) are attracting considerable attention due to their unique physical, mechanical, and chemical properties, including high Young's modulus and strength, thermal and electrical conductivity, thermal stability, high specific surface area, and many others [99-109]. CNTs are closely related to carbon nano fibre [110]. The diameter of carbon nanofibre is 50-200 nm [111] and that of single wall carbon nanotubes (SWNT) is about 1 nm and multiwall carbon nanotube (MWNT) is 2-50 nm. According to the number of walls, carbon nanotubes (CNT) are classified into single-wall nano tubes (SWNTs) and multi-walle nano tubes (MWNTs). SWNTs are single cylindrical structures. MWNTs (Figure 2.13) can be considered as the form of SWNTs covered with more of this kind of cylindrical structures. CNTs can be synthesized with arc-discharge, pyrolysis, laser vaporization, plasma chemical vapor deposition, thermochemical vapor deposition, electrolysis and so on. Some properties of typical multi wall carbon nano tube are given in Table 2.1.

Table 2.1: Properties of multi wall carbon nano tube [112]

Diameter:	2-50 nm.
Compressive strength:	150 GPa
Buckling strain:	5%
Fracture strain:	>18%
Tensile strength:	1.72 GPa
Tensile modulus:	450 GPa

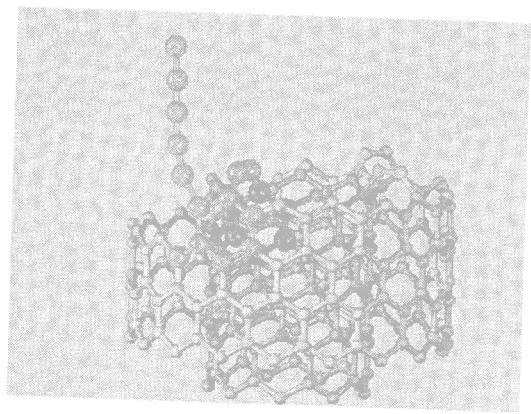

Figure 2.13: Typical picture of multi-wall carbon nanotube, MWNT (Adapted with permission from Rinzler et. al., Science, **269** (5230), 1550-1553, (1995) [99])

2.3.1 Dispersion of CNT in Polymer Matrix

CNTs, including MWNTs and SWNTs, are potentially excellent nano filler for polymer matrix due to their unique mechanical properties. However, to develop high performance polymers with CNT, the challenges often lie in the achievement of homogeneous dispersion of CNTs in the polymer matrices and strong interfacial interactions. Being hydrophobic nature, it is very difficult to disperse the CNTs in the polymer matrix. The

research is going on rapidly in the field of modification of CNTs by functionalization without affecting the large bulk properties of parent CNTs.

Amino groups of aniline would readily react with carbon nano tube. Dissolution of nano tube in aniline can be observed by the color change of the solution after reflux for short time [113]. With continuous heating, the original colorless aniline solutions first became to brownish and then turned to dark red. The solubility of SWNT in aniline is up to 8 mg/mL. This aniline-nanotube solution can be readily diluted with other organic solvents such as acetone, THF, and DMF.

2.3.2 Property Improvements with Nano Particles

We could not found any literatures on CNT/SPU. However improvements of polymer properties by nano particles have been currently become a very significant topic of research. Safadi et al. [114] studied the electrical conductivity of polystyrene with MWNTs. The research revealed that the presence of 2.5 vol % of MWNT transforms the films from insulating to conductive (surface resistivity, ρ, approaching 10^3 Ω from ≥ 10^{12}Ω). Electron transport in nano tubes is unique, and the tubes are highly conducting in the axial direction [115]. Their highly conductive graphite structure, establishes an efficient conducting network inside the matrix at much lower concentration compared to the traditional carbon black fillers or graphite fibres. Zhou et al. [116] and Chen et al. [117] investigated the UV absorbancy of polyurethane nano-silica composites; they observed that the absorbance and reflection of UV light by the polyurethane film was increased as the nano-SiO_2 content increased, especially at wavelength 290-400 nm. Tien et al. [118] revealed that with 1% of tethered nano-sized layered silicates from

morillonite, 40 °C increase in the degradation temperature and 14% increase in the degradation activation energy as compared to that of parent polyurethane. Gall et al. [119] reported the influence of SiC nanoparticulate on shape memory properties of commercially available resins. The constraint bending recovery force in the nanocomposites was shown to increase by 50 % with the addition of 20 wt% of SiC.

Textile technology would not escape from the applications of nanoparticles. Researchers all over the world are investigating the possible applications of nanotechnology in the textile fields. Commercial products already came to the market. Here we reviewed some of the application of nano particle in the textile fields. A new anti-static fabric for outdoor workwear was developed by W. L. Gore [120-121]. The fabric consists of anti-static Gore-Tex membrane made from polytetrafluroethane (PTFE) containing conductive microscopic nano-carbon particles sandwiched between an outer fabric of modacrylic/cotton and an inner lining. Any charge, which is formed, was discharged harmlessly. The membrane is protected from mechanical stress by inner and outer layers. In addition the binding of conductive nano-carbon particles to the PTFE would prevent loss of effectiveness during the use or after washing. The wind and water proof properties of the membrane makes the fabric especially suitable for outdoor work-wear, particularly in the chemical, petrochemical and energy supply industries. Researcher had developed bi-component polypropylene fiber [122] containing spherical silver nanoparticles as an antibacterial agent.

CHAPTER 3

EXPERIMENTAL

This chapter includes material selection and purification, synthesis process and characterization techniques of polymers. Different characterization techniques were used to characterize the polymer such as Fourier transform infra red spectra (FTIR), Raman spectroscopy, wide angle X-ray diffraction (WAXD), differential scanning calorimetry (DSC), thermogravimetry analysis (TG), dynamic mechanical thermal analysis (DMTA), scanning electron microscopy (SEM), transmission electron microscopy (TEM), Instron. On the other hand, water vapor transport properties were measured by water vapor permeability measurement, equilibrium sorption and dynamic sorption measurement. The cotton fabrics were coated with selected synthesized segmented polyurethanes and their evaluations process are also described in this chapter.

3.1 Material Selection and Synthesis

3.1.1 Material Selection

The versatility of the chemistry and wide choice of raw materials available for the urethane chemist [123-124] enable a variety of polymers with specific properties to be "tailor made". Due to the wide choices available, selection of the right type of raw materials is important for the specific application. The selection of the building blocks (polyols and isocyanates) is critical in producing the right polyurethane for final end applications.

3.1.1.1 Polyol Selection

In theory, any di- or poly-functional polyol can be used to prepare polyurethane; however, the most common raw materials include polyester diols, polyether diols, and polycarbonate diols. The selection of molecular weight would determine the wide range of physical properties of polymer. The lower the molecular weight, the shorter would be the polymer chains as a result of harder the polymer. Conversely, the higher the molecular weight, the longer would be the polymer chain length as a result of the softer and more flexible of polymer. With the above in mind, the followings are the selection possibility for building blocks of polyol (Table 3.1 – 3.3) in making the right polyurethanes for each end use.

Table 3.1: Advantages and Disadvantages of Polyether diols [25,124]

Polyethylene glycol, Polypropylene glycol, Polytetramethylene glycol	
Advantages	Disadvantages
• Excellent softness and flexibility. • Excellent moisture vapor transmission rate (MVTR). • Good hydrolytic stability. • Cheaper in most cases than polyester. • Low to high molecular weight available.	• Lower adhesion to low energy surfaces. • UV and weather stability is not as good as polyester polyol. • Not as tough as polyester or polycarbonate. • Lower physical properties than polyester.

Table 3.2: Advantages and disadvantages of Polyester Adipate and Polycaprolactone diols [25, 124]

Polyester Adipate, Polycaprolactone	
Advantages	Disadvantages
• Highly polar, has excellent adhesion to low energy surfaces. • Low to high molecular weights are available. • Excellent toughness and abrasion resistance. • Better exterior stability. • Better physical properties than the polyether.	• Less solvent resistance. • Hydrolytic stability is not as good as other diols. • Reduced MVTR figures. • Higher raw material cost than polyethers.

Table 3.3: Advantage and disadvantages of Polycarbonate diol [25, 124]

Polycarbonates	
Advantages	Disadvantages
• Good hydrolytic stability. • Good flexibility. • Good abrasion resistance.	• High cost. • Availability.

3.1.1.2 Isocyanate Selection

The selection of isocyanate is also critical in determining what type of polyurethane is to be made. As with the polyols selection, the same holds true concerning the hardness factor; the lower the molecular weight, the harder would be the polymer and the higher

the molecular weight, softer, more flexible the polymer will be. The advantages and disadvantages of different isocyanates are given in Table 3.4.

Table 3.4: Benefits of Isocyanates [25, 124]

Isocyanates	
Aromatic (TDI and MDI)	Aliphatic (HDI, TMXDI, IPDI and H-MDI)
• Inexpensive. • Harder.	• Light and heat stable. • Better flexibility.

TDI: Tolune Diisocyanates, MDI: 4, 4'-diphenylmethane Diisocyanate, HDI: Hydrogeneted Methylene Diisocyanate, TMXDI: Tetramethyl Xylene Diisocyanate, IPDI: Isophorane Diisocyanate and H-MDI: Hydrogeneted Diphenylmethane Diisocyanate.

3.1.1.3 Chain Extender Selection

Chain extender can be categorized into two general classes such as aromatic diols and diamines, and corresponding aliphatic dilos and diamines. In general, aliphatic chain extenders would yield softer materials than aromatic chain extenders. Diamine chain extenders would react rapidly and vigorously with isocyanates to produce urea groups, and the resultant urea groups can produce a polymer cross-linking with biuret links. On the other hand, glycol extended polyurethanes are more flexible and weaker than the amine-extended analogs.

Based on the literature review and selection criteria, we have selected the following raw materials: Polypropylene glycol (number average molecular weight 1000 and 3000 g mol^{-1}, PPG 1000 and PPG 3000) was obtained from International laboratory, USA and all the other chemicals such as Polycaprolactone diol (number average molecular weight 2000 and 3000 g mol^{-1}, PCL 2000 and PCL 3000), polytetra methylene glycol (number average molecular weight 2000 and 2900 g mol^{-1}, PTMG 2000 and PTMG 2900), polyethylene glycol (number average molecular weight 200, 2000 and 3400 g mol^{-1}, PEG 200, PEG 2000 and PEG 3400), hexamethylene diisocyanate (HDI), 1,4-butane diol (1,4-BDO), 4,4'-diphenylmethane diisocyanate (MDI), dimethylol propionic acid (DMPA) were obtained from Aldrich. The chemical structure of raw materials are given in Figure 3.1. Multi wall carbon nano tube (MWNT) used in this research was also obtained from Aldrich. Six unique factors have been studied in this project; their compositions are given in Table 3.5 – 3.10.

Table 3.5: Composition of SPU (Influence of hard segment)

	Feed (x 10^{-3} mol)					
Sample Code	PCL 2000	PEG200	HDI	MDI	1,4-BDO	HS (wt %)
S_1	10	25	5	80.25	50.25	58.7
S_2	12.25	25	6.25	63.99	32.74	47.9
S_3	15	25	7.5	49	16.5	37.5
S_4	17.50	25	8.75	42.50	8.75	31
S_5	14	-	4	35	25	30
HS	-	12.50	5	65.50	58	100

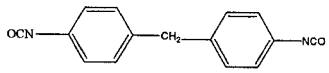

methylene bis(p-phenyl isocyanate) (MDI)

HO—$CH_2CH_2CH_2CH_2$—OH

1,4 – butanediol (1,4 – BDO)

HO—$[(CH_2)_5—CO—O]_n(CH_2)_6[O—CO—(CH_2)_5]_n$—OH

Polycaprolactone diol (PCL)

HO—$[CH_2—CH_2—CH_2—CH_2—O]_n$—H

Poly (tetramethylene) glycol (PTMG)

HO—$[CH_2—CH(CH_3)—O]$—H

Polypropylene glycol (PPG)

HO—$[CH_2—CH_2—O]_n$—H

Polyethylene glycol (PEG)

Figure 3.1: Chemical structure of raw materials

Table 3.6: Composition of SPU (Influence of hydrophilic block length)

Sample Code	Feed (x 10^{-3} mol)				
	PTMG2000	PEG	MDI	1,4-BDO	PEG (wt %)
S_6	14.75	22.5 (PEG-200)	44	7.15	9.86
S_7	14.75	2.25 (PEG-2000)	37	20	9.98
S_8	14.75	1.33 (PEG-3400)	36.08	20	10.03
S_9	9	-	38	28.79	-

Table 3.7: Composition of SPU (Influence of hydrophilic segment content)

	Feed (x 10^{-3} mol)				
Sample	PTMG 2900	PEG 3400	MDI	1,4-BDO	Wt% of PEG 3400 content
S_{10}	9.65	0.59	32.064	21.82	5
S_{11}	8.9	1.176	32.03	21.89	10
S_{12}	10	1.77	17.77	6.0	15
S_{13}	12.06	0	18.06	6	0

Table 3.8: Composition of SPU (Influence of hydroxyl and/or carboxyl unit)

	Feed (x 10^{-3})					
Sample	PPG 1000	PEG 3400	DMPA	MDI	1,4-BDO	Wt% of PEG 3400 and/or DMPA content
S_{14}	32.5	1.471	0	45.72	11.76	10 (PEG 3400)
S_{15}	22	0	30	56	4	10 (DMPA)
S_{16}	24	0.6	15	48	8.4	10 (PEG 3400 and DMPA)
S_{17}	26	0	0	48	22	0

Table 3.9: Composition of SPU (Influence of mixed polyol block)

	Feed (x 10^{-3})					
Sample	Polyol-I	Polyol-II	PEG 3400	MDI	1,4-BDO	Wt% of PEG
S_{18}	5(PCL3000)	5(PPG3000)	1.2	18	7	10
S_{19}	5(PCL3000)	5.17(PTMG2900)	1.2	18	7	10
S_{20}	5(PPG3000)	5.17(PTMG2900)	1.2	18	7	10
S_{21}	10(PCL3000)	0	1.2	18	7	10

Table 3.10: Composition of SPU (Influence of MWNT content)

	Feed (x 10^{-3} mol)				
Sample	PTMG 2900	PEG 3400	MDI	1,4-BDO	Wt% of MWNT
S_{11}	8.9	1.176	32.03	21.89	0
S_{22}	8.9	1.176	32.03	21.89	0.25
S_{23}	8.9	1.176	32.03	21.89	0.50
S_{24}	8.9	1.176	32.03	21.89	1.0
S_{25}	8.9	1.176	32.03	21.89	2.5

3.1.2 Material Purifications

Purification of the polyols, chain extenders and solvents are very important, as the isocyanates would react readily with water [25]. The presence of water in the reaction medium during synthesis could lead to the production of unstable carbamic acids which would be decomposed to amines, and carbon dioxide gas would be liberated that will produce foam in the reaction mixture. The amine can then react with an isocyanate group (Figure 3.1) to form urea group. The above side reaction will lead to lower molecular weight of the polyurethane, finally poor mechanical and other properties. The water from the polyol was removed by vacuum drying. On the other hand water from the chain extender and solvent was removed by molecular sieve (4 Å). Moreover, in order to eliminate the influences of the atmospheric moisture, polymerization was carried out in nitrogen atmosphere.

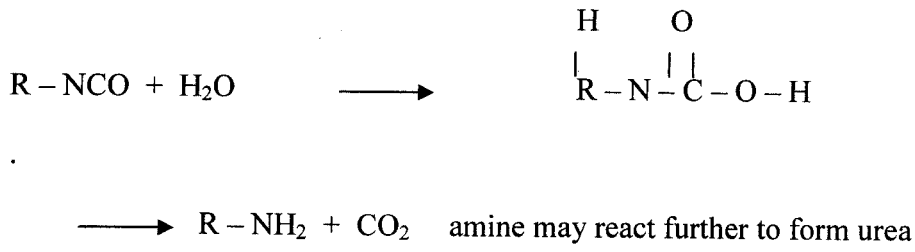

Figure 3.2: Side reactions of isocyanates with water commonly used in polyurethane synthesis.

PPG 3000, PTMG 2000, PTMG 2900, PCL 2000, and PCL 3000 were vacuum oven dried at 80 °C for 12 h prior to use. On the other hand, PEG 200, PEG 3400 and PPG 1000 were vacuum oven dried at 80 °C for 4 h prior to use. N,N' -dimethyl formamide (DMF), 1,4-BDO were dried by 4 Å molecular sieve, and DMPA was dried at vacuum oven at 80 °C for 2 h prior to use. MDI and HDI were used as received.

3.1.3 Synthesis

SPUs were synthesized from bifunctional diisocyanate (OCN-R-NCO), polyol [H-(-O-R'-)$_m$-OH] and chain extender [H-(-O-R"-)$_p$-OH]. The polymers were modified with polyethylene glycol [H-(-O-R"-)$_n$-OH] and/or DMPA. Three steps (S_1 –S_4, S_{18} – S_{20}) and two steps (S_5 – S_{17}) polymerization techniques were employed for synthesis. In order to get the linear polymer, the mole ratio of NCO to OH was kept at 1.0:1.0. The general structure of the polymer is given in Figure 3.3.

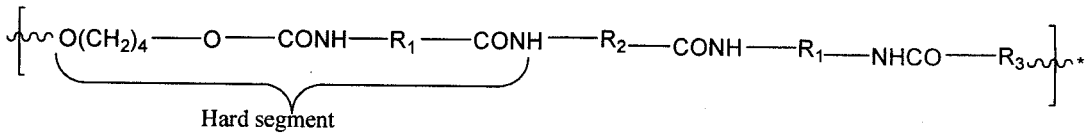

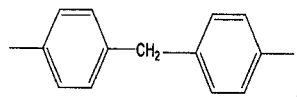

R_1=

Soft segment ⟶ Polyol = HO – R_2 – OH, PEG = HO – R_3 – OH

Figure 3.3: General structure of segmented polyurethane (SPU)

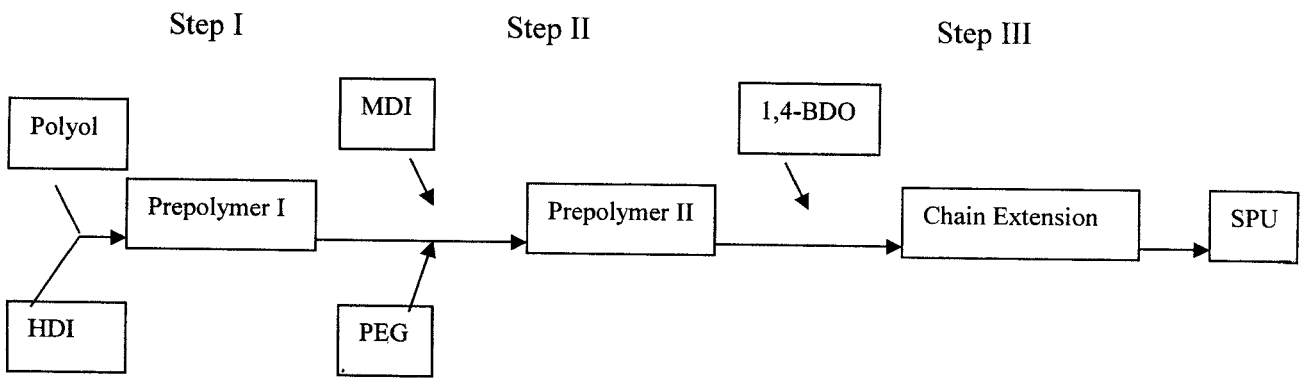

Figure 3.4: Three steps synthesis process

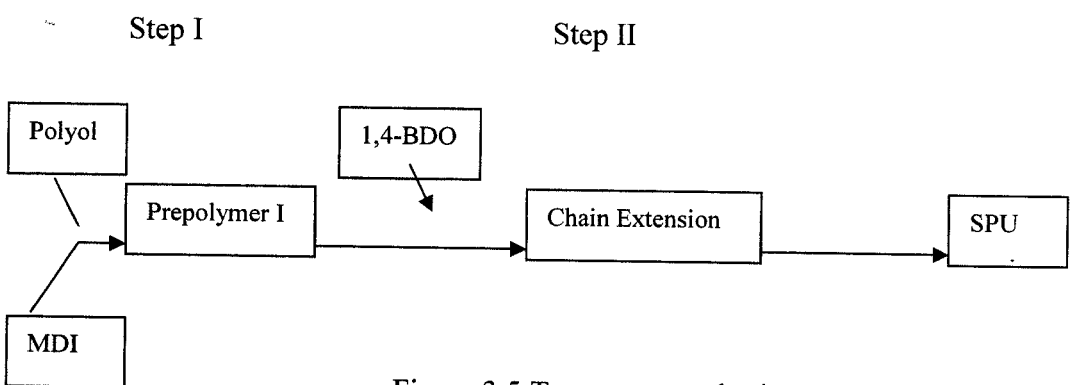

Figure 3.5:Two steps synthesis process

Typical three steps (Figure 3.2) procedure for the preparation of SPU with 58.7 % of hard segment (sample code S_1) was as follows: a 500 mL round-bottom, three-necked

flask equipped with a mechanical stirrer, nitrogen inlet, and thermometer was charged with 0.84 gm of HDI (5 x 10^{-3} mol), 20 gm of PCL 2000 (10 x 10^{-3} mol) and 50 mL of DMF. The system was heated up to 85 °C in an oil bath, and stirred for 1 hour in order to prepare prepolymer I. In the second step, 5 gm of PEG 200 (25 x 10^{-3} mol) and 20.063 gm of MDI (80.25 x 10^{-3} mol) were added in the reactor sequentially, and reacted for another 1 hour to prepare prepolymer II. For chain extension, diluted 4.529 gm of 1,4-BDO (50.25 x 10^{-3} mol) with DMF was added in the reactor drop wise and the prepolymer was subsequently chain extended with 1,4-BDO for 4 hours at 85 °C. DMF was added in the reactor occasionally when the viscosity of the reaction mixture was too high. The final polymer concentration was about 20 % (w/w).

A typical two steps synthesis procedure (Figure 3.3) for the preparation of SPU of sample code S_5, was as follow: a 500 mL round-bottom, three-necked flask equipped with a mechanical stirrer, nitrogen inlet, and thermometer was charged with 0.648 gm of HDI (4 x 10^{-3} mol), 26 gm of PCL 2000 (13 x 10^{-3} mol) and 50 mL of DMF. The system was heated up to 85 °C in an oil bath and stirred for 1 hour to prepare prepolymer. After one hour, 9 gm of MDI (36 x 10^{-3} mol) was added in the reactor sequentially, and reacted for another 1 hour to prepare the final prepolymer. For chain extension, diluted 2.457 gm of 1,4-BDO (27 x 10^{-3} mol) with DMF was added in the reactor drop wise and the prepolymer was subsequently chain extended with 1,4-BDO for 4 hours at 85 °C. DMF was added in the reactor occasionally when the viscosity of the reaction mixture was too high. The final polymer concentration was about 20 % (w/w).

3.1.4 Synthesis Route of MWNT Dispersed SPU

Being the hydrophobic nature and nano particle size of MWNTs, this is a big challenge for dispersion of the carbon nano tubes in hydrophilic polyurethane. Although some efforts have been made in the direction of dispersion of nano tubes, most studies to date have involved cutting and chemical functionalization of nano tubes, or attachment of polymers with solubilizing features. This approach has two disadvantages: on one hand, tedious chemical derivitazation is often required, while on the other hand, cut carbon nano tubes derivatives may have significantly different properties than those of parent one. In this work, the MWNTs have been functionalized with aniline before the dispersion in SPU solution. Theoretical studies suggested that the functionalization of carbon nanotubes would not greatly decrease its strength. Hence, we seek to explore the possibility of using the physical interactions between the chemically functionalized MWNTs and the polymer matrix to produce strong interfacial interactions. The dispersion of MWNT in SPU solutions are presented schematically in the Figure 3.4

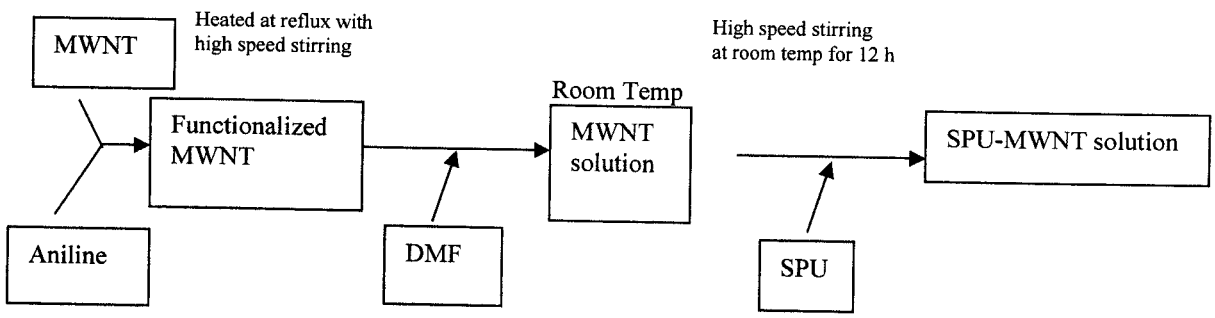

Figure 3.6: Flow chart for the dispersion of MWNT in SPU solution

3.1.4.1 Functionalization of MWNT

MWNT beads were crushed by hand grinding before functionalization. As the literature reported, the solubility of nanotube in aniline is up to 8 mg/mL [113], therefore the MWNT : aniline was kept 8 mg : 1 mL in all cases. In a typical functionalization process, 80 mg of accurately weighed MWNT was added to 10 mL of aniline, and the mixture was heated at reflux with a high-speed shearing stirring by magnetic stirrer for 4 h in dark. After being cooled down to room temperature, aniline-nanotube solution was diluted with 40 mL of DMF.

3.1.4.2 Preparation of Functionalized MWNT-SPU Solution

SPU nanotube solutions were prepared with 5 different contents of MWNTs such as 0, 0.25, 0.50, 1.0 and 2.5 wt/wt% (weight percent with respect to polymer solid content). Functionalized and the diluted MWNT solution was added with previously synthesized SPU, and then the mixture was stirred by high-speed stirring at room temperature for 12 h. The final SPU-MWNT solution concentration was about 15 % (w/w).

3.2 MEMBRANE PREPARATION

Thin films were casted from the polymer solution where the thickness of the film was controlled by the polymer concentration. Membranes were casted from the diluted SPU solution (concentration about 5 % w/v) in N,N-dimethyl formamide (DMF) on the Teflon coated steel plate. Solvent evaporation and the film quality have been studied by the researcher widely [125-134]. Rapid solvent evaporation causes thermocapilary instability on the film surface which will give rough film surface. Based on the literature review and in order to get defect free nonporous membrane, the solvent was evaporated

slowly at 60 °C for 12 h. The final residual solvent was removed under vacuum at 80 °C for another 12 h. Then the Teflon plates were taken out from the vacuum oven and kept at room temperature for 2 h. After 2 h, membranes were taken out from the Teflon plate. The thickness of the membrane for mechanical testing was about 0.2 mm and about 90 μm for water vapor transport properties. On the other hand, 10-15 μm of films were casted for FTIR and Raman spectra measurements.

3.3 CHARACTERIZATION OF POLYMERS

After synthesis and membrane preparation, different moieties in the polymer were identified by FTIR. Interaction between MWNT and SPUs were identified by Raman spectroscopy. Surface structures were characterized by the scanning electron microscopy (SEM). Polyurethane morphology was characterized by the transmission electron microscopy (TEM). Order structures were measured by the wide angle X-ray diffraction (WAXD) and differential scanning calorimitry (DSC). Thermogravimetry (TG) technique was used to measure thermal stability of the SPU. Mechanical and shape memory effects were measured by Instron. On the other hand thermo-mechanical property was evaluated by the dynamic mechanical thermal analysis (DMTA). Positron annihilation lifetime spectroscopy (PALS) was used to measure the free volume. Water vapor transport properties were measured by water vapor permeability measurements, equilibrium sorption and dynamic sorption measurements. The details of the methodologies adopted for this project are described in the following paragraphs:

3.3.1 Determination of Solid Content

The known weight of polymer was taken in a petridsh. Then the patridsih was put in the oven at 160 °C (above the boiling point of DMF). The amount of residue was weighed till its constant weight was obtained. The solid content of the polymer was then determined as follows:

Solid content % = (constant weight of residue/original weight of sample)*100 ---(3.1)

3.3.2 Fourier Transform Infra Red (FTIR) Measurements

Infrared spectroscopy could be used to identify the chemical groups within a compound. Chemical bonds within materials would vibrate at characteristic frequencies. Therefore, when the infrared radiation passes through the material at certain frequencies, the molecule would absorb the energy and vibrate [25]. Emission or absorption spectra arise when molecules undergo transitions between quantum states corresponding to two different internal energies. The energy difference ΔE between the states is related to the frequency of the radiation emitted or absorbed by the quantum relation, $\Delta E = h\nu$. Infrared frequencies in the wavelength range of 1-50 μm (10000 cm^{-1} – 200 cm^{-1}) are associated with molecular vibration and vibration-rotation spectra. Each group is capable of a number of different modes of vibration, such as stretching and bending, therefore a number of peaks could often be attributed to the presence of a particular chemical structure.

The IR data at room temperature were collected by using the Nicolet 5DXC Fourier Transform Infrared (FTIR) machine. Each sample was scanned from 400 – 4000 cm^{-1} at room temperature.

3.3.3 Raman Spectroscopy

Raman spectra data were taken with a Renishaw RM 3000 Micro-Raman system at room temperature. The laser excitation was a He-Ne laser (wave length = 633 nm) and the power output was 25 mW, the laser power on sample was 5mW. The spectral resolution was maintained at approximately 1 cm^{-1}. The total time of the measurement for each specimen was 120 s. Each sample was scanned from 400 to 2000 cm^{-1}.

3.3.4 Wide Angle X-ray Diffraction (WAXD)

The X-ray diffraction method is a powerful tool for investigating the orderly arrangements of atoms or molecules through the interaction of electromagnetic radiation which will give interference effects with structures comparable in size to the wavelength of the radiation. If the structures are arranged in an orderly array or lattice, the interferences are sharpened that the radiation is scattered or diffracted only under specific experimental conditions. Knowledge of these conditions will give information regarding the geometry of the scattering structure.

WAXD data could be used to calculate the degree of crystallinity (χ). The crystallinity % is given by the following equation:

$\chi = [\int s^2 I_c(s)ds]/[\int s^2 I(s)ds]$ ----------(3.2)

where, $s = (2 \sin\theta)/\lambda$, $I_c(s)$ is the intensity of crystal component, I (s) is the intensity of total component.

The distance between the parallel planes in the crystallites was calculated by the Bragg's equation

$d = n\lambda / 2 \sin\theta$ ----------(3.3)

Where, θ is incident angle, λ is the wavelength of the radiation and n is an integer indicating the order of diffraction.

The X-ray data were taken by X-ray Diffractometer (Philips Xpert XRD System) at 40 kV power, 40 mA current and a radiation of wavelength 1.542 Å. Diffraction patterns were obtained in the range of Bragg's angle, $2\theta = 10 - 50°$. The scanning speed was 0.03 sec/step.

3.3.5 Transmission Electron Microscopy (TEM)

As its name indicates, TEM works by forming an image with those electrons that have been transmitted through a sample. It is a technique, therefore, which can only be used for thin film samples. Staining is also required to differentiate between hard and soft segment of segmented polyurethane. The thin films of thickness about 50 nm would be exposed to the RuO_4 at room temperature for one hour. TEM could be used to determine the morphology of segmented polyurethane by providing sufficient contrast between the phases. The transmission electron micrographs of stained specimens were obtained

under transmission electron microscope instrument. TEM of SPU and MWNT-SPU films were obtained with Phillips CM 120. Samples were prepared by dispersing the SPU or MWNT-SPU solution on the deionized water and put the copper grid on the thin polymer layer on water at room temperature. Taken out the grid with film carefully and dried. RuO_4 was used for staining the samples. Image of pure MWNT were obtained without staining. All the experiments were carried out at an accelerating voltage of 120 kV.

3.3.6 Differential Scanning Calorimetry (DSC)

Differential scanning calorimetry (DSC) is a thermal characterization technique which is used to characterize the glass transition temperature (T_g) and melting temperature (T_m) of a material, the degree of crystallinity and degree of phase separation. A sample of the material is placed inside calorimeter and heated at a fixed heating rate [25]. The amount of energy needed to maintain a fixed rate of temperature increase is measured. Changes in the specific heat would denote the changes in the mobility of the polymer chains. Characterization of the thermal properties of segmented polyurethanes indicates that there are multiple thermal transitions in these materials. The glass transition temperature is identified by a change in heat capacity which will appear as a baseline shift. An endo-thermal or exothermal peak in the DSC thermogram denotes the melting temperature or crystallization temperature of the polymer. In differential scanning calorimetry (DSC) technique, the heat flux of the sample is monitored against time or temperature. In the present study Perkin-Elmer DSC 7 was used to measure the heat of fusion (ΔH), T_{ms}, T_g etc. Each samples having weight from 10 to 15 mg was scanned from –50 to 120°C at a scanning rate of 10 °C/min under the dry nitrogen.

3.3.7 Thermogravimetry (TG) Analysis

In thermogravimetric analysis, a sensitive balance is used to follow the weight change of the sample as a function of temperature. Typical applications include the assessment of the thermal stability, decomposition temperature and maximum degradation temperature. Thermogravimetry (TG) and deravative thermogravimetry (DTG) data were taken using Mattler TG analyzer. The samples were heated from 25 to 700°C in nitrogen atmosphere at nitrogen flow rate of 50 mL/min and static air at differential heating rate (5, 10, and 20 °C/min). The samples weights were 5-10 mg in all cases. During the heating period, the weight loss and temperature difference data were reported as a function of temperature.

3.3.8 Tensile Strength and Shape Memory Testing

The tensile properties of polymers were measured to provide information on the mechanical strength of polymeric material. Test involves the application of a constant rate of uniaxial extension to the sample. The engineering stress, defined as the force normal to the initial cross-section of the test sample is measured as a function of extension, under a constant rate of extension [25]. The tensile properties of the polyurethane membranes were measured at room temperature with rectangular strip of samples of dimension 40 × 10 × 0.15~0.2 mm, using Instron 4466 according to ASTM D-638. The crosshead speed was set at 10 mm/min. An average of 5 tests results were reported for each sample. On the other hand, shape memory effects of the materials were measured by Instron with a temperature controlled temperature chamber. Thermomechanical (shape memory) tests were carried out in the following manner: (a) apply deformation (ε_m) to the sample with a constant crosshead speed of 10mm/min at

T_k, (b) cool down the sample to T_l with the same ε_m, (c) maintain at T_l for 5 min with removal of the load, and (d) raise the temperature from T_l to T_k and keep at T_k for 5 min. Under the conditions, shape retention (fixity) and shape recovery are defined as follows:

$$\text{Shape retention (\%)} = \varepsilon_u * 100/\varepsilon_m \quad \text{----------(3.4)}$$

$$\text{Shape recovery (\%)} = (\varepsilon_m - \varepsilon_p) * 100/\varepsilon_m \quad \text{----------(3.5)}$$

where, $T_k = T_{ms} + 20°C$, $T_l = T_{ms} - 15°C$, ε_m = strain at 50% elongation, ε_u = retention at $T_{ms} - 15°C$, ε_p = recovery strain at $T_{ms} + 15°C$ and T_{ms} = soft segment crystal melting temperature.

The experimental equipment for shape memory testing is a tensile machine with temperature chamber and temperature control unit. Heating and cooling of the specimens were carried out by spraying it with heated compressed air and cooled compressed air by passing cold water-propanol mixture through a heat exchanger. The temperature was measured by a thermocouple. The tip of the thermocouple was placed near the specimen. The elongation of specimen was measured by displacement of crosshead.

3.3.9 Dynamic Mechanical Thermal Analysis (DMTA)

Dynamic mechanical thermal analysis (DMTA) is an important technique capable of providing considerable information on the position of transitions and the mechanical properties of the polymer. DMTA will measure the storage modulus (E') and the loss modulus (E") as a function of temperature. A sinusoidal mode of deformation is applied to the sample. The sample is scanned from well below the glass transition temperature to

the point when the sample becomes too soft to test in a given apparatus. DMTA data provide information on first and second-order transition (T_m and T_g), the degree of phase separation, and the mechanical properties such as the glassy state and the rubbery plateau modulus [25]. The sample was deformed cyclically in dynamic mechanical thermal analysis under forced vibration conditions. Modulus was recorded as a function of the temperature. The dynamic mechanical properties of polymer are described in terms of complex dynamic modulus:

$$E^* = (E'^2 + E''^2)^{1/2} = E' + E'' \text{ ----------(3.6)}$$

Where E' is the storage modulus and E" is the loss modulus. The phase angle (δ) is given by: $\tan \delta = E'' / E'$. The different modulus would allow for the better characterization of the materials, therefore, could examine the ability of the material to return or store energy (E'), to its ability to lose energy (E"), and the ratio of these effects ($\tan \delta$), which is called damping.

Dynamic mechanical measurements were performed in a tension mode by dynamic mechanical thermal analyzer (Perkin Elmer Diamond DMA Lab System) over the temperature from –150 or -100 to 120 °C at a frequency of 2 Hz under N_2 purging and a heating rate of 2 °C min^{-1}. A rectangular film specimen (15 × 10 × 0.15~0.2 mm) was cleanly mounted on grips so that the sample length was 7 mm. A length-to-thickness ratio was larger than 10 in orders to neglect the DMA's dependence on the Poisson ratio. Tension was applied at a loading rate of 10 mm/min. Results were reported in the form

of storage modulus, loss modulus, and loss tangent (tan δ) as a function of the temperature.

3.3.10 Scanning Electron Microscopy (SEM)

In the present study, SEM photographs were taken in order to study the surface of SPU and MWNT-SPU films. Scanning Electron Microscopy (SEM) studies have primarily been used to study the surface topography of polymeric materials. SEM techniques are used to examine the morphological structure of the materials, and assess the gross uniformity of the sample surface. The sample preparation of the polymer for SEM is specimen-specific and usually involves the coating of polymer sample with a thin conducting layer of gold [25]. SEM photographs were taken by a Leica Stereoscan 440 equipped with an Oxford energy dispersive X-ray system, operating at 20 kV.

3.3.11 Free Volume Measurements

In polymers, diffusion of mass molecules would occur through the voids (free volume) between polymer chains. Therefore, the rate of diffusion depends to a large extent on size of the penetrant molecules and size of the gaps available [135]. From the basic principle of the free volume theory, the mobility of polymer segments and the diffusion coefficient of a penetrant vapor in a polymer-diluents system are determined primarily by the free volume of the polymer-penetrant system. The mobility (m_d) of a penetrant organic molecule relative to the polymer is given by:

$$m_d = D_T/RT = A_d \exp\{-B_d/f(T,\Phi_1)\} \quad \text{----------(3.7)}$$

where f(T, Φ_1} is the average fractional free volume of the polymer-penetrant system and A_d and B_d are parameters that are characteristic of a given polymer-penetrant pair which are independent of the temperature and penetrant concentration. D_T is the thermodynamic diffusion coefficient of the organic molecule relative to the polymer, which is related to the mutual diffusion coefficients (D):

$D_T = [D/(1 - \Phi_1)]*d \ln \Phi_1/d \ln a_1$ ----------(3.8)

In equation 3.8, a_1 is the activity of the penetrant in the polymer and Φ_1 is the penetrant (organic) volume fraction in the polymer at a given activity.

Fractional free volume could be determined by positron annihilation lifetime spectroscopy (PALS). The attributions of three resolved lifetime components to various states of positron annihilation are: (1) the first short-lived component τ_1 with intensity I_1 is attributed to the p-Ps and free positron annihilations. (2) The intermediate lifetime component, τ_2 with intensity of I_2 is considered to be caused mainly by the annihilation of positrons trapped at the defects present in the crystalline regions or trapped at the crystalline-amorphous (c-a) interface. And (3) the longest lived component τ_3 with intensity of I_3 is due to the pick-off annihilation of the o-Ps in the free-volume sites present in amorphous regions of the polymer matrix.

In polymers, the o-Ps pick-off lifetime (τ_3) with intensity of I_3 is important, since τ_3 is related to the average free-volume size and I_3 is related to the combination of number density of free-volume holes and the probability of o-Ps formation, therefore, we focused the above two factors in this investigation. Since the diffusion in polymers has a

direct relation to the free-volume content of the polymer (equation 3.8), for better understanding of the diffusion kinetics in terms of free-volume, we need to look at τ_3 and I_3 only. These two parameters are independent of the first two lifetime components. Therefore, we presented only τ_3 and I_3 results and the discussion related to them. The o-Ps lifetime (τ_3) is related to the free-volume hole size by a simple relation given by Nakanishi et al. [136]. As in this model, the o-Ps resides in a spherical potential wall of radius R_0 having an infinite potential. It is further assumed that the o-Ps annihilates in a homogeneous electron layer of thickness ΔR inside the wall. The final relation according to this model between o-Ps lifetime (τ_3) and free-volume radius (R) is as follow:

$$\tau_3^{-1} = 2\left[1-(R/R_0)+(1/2\pi)\sin(2\pi R/R_0)\right]ns^{-1} \quad \text{----------(3.9)}$$

where, $R_0 = R + \Delta R$. The parameter ΔR has been determined by fitting the experimental values of τ_3 obtained for materials of known hole sizes such as zeolites. The value of ΔR =0.1656 nm was obtained in this way. The above equation is used to calculate the free-volume radius of the polymer samples at each sorption level. Then the average free-volume size was evaluated by $V_{f3} = (4/3)\pi R^3$. From this average free-volume size, the fractional free-volume (F_v) would be calculated by using the following equation:

$$F_v = CV_{f3}I_3 \quad \text{----------(3.10)}$$

where C is the structural constant and can be obtained from the measurement of the thermal expansion coefficient of free-volume.

Positron lifetime data were obtained with ORTEC (US) fast-fast lifetime spectrometer. The time resolution was about 280 ps (FWHM). ^{22}Na with 30 μCi was used as radioactive positron sources. About one million counts were collected for each spectrum. The source sample assembly was mounted on a liquid nitrogen cryostat. PATFIT-88 software was used to evaluate the data.

3.3.12 Measurements of Equilibrium Sorption

The equilibrium sorption of the membranes with dimension of 5.0 × 5.0 × 0.006~0.01 cm were measured by immersion in de-ionized water at five different temperature such as 10, 15, 25, 35, and 45 °C. Vacuum dried the samples at 60 °C until constant weight was reached before immersed in the water. Periodically (every 4 hours) the samples were removed and the surface water was quickly wiped out with filter paper, and weighted, until the constant weight was achieved. The equilibrium sorption was expressed as the percentage of membrane weight gain, and determined by using the following equation:

$$D_w = (W_s - W_d)/W_d \times 100\% \text{ ----------} (3.11)$$

where, W_d and W_s are the weight of membranes before immersion and after equilibrium weight gained respectively.

3.3.13 Dynamic Sorption Measurements

Diffusion coefficients of small molecules through polymeric materials are usually derived from the gravimetric measurements. Mass uptake of a polymer film of thickness δ is usually obtained as a function of time during the transient regime of vapor or liquid sorption at constant solvent activity a_s. Analysis of experimental data is based on solving the Fick's second equation according to several methods that have been reviewed by Crank [69] and recently briefly summarized by Balik [66]. As way of very typical examples, an average value for the penetrant diffusion coefficients, D, can be obtained from a plot giving the ratio of the swollen polymer mass at time t and $t = \alpha$ (corresponding to sorption equilibrium), M_t/M_α, as a function of the square root of time $t^{1/2}$ (Figure 3.5) and the diffusion coefficients can be calculated from the initial slope (s_0) of the curve, when $t \longrightarrow 0$:

$$M_t/M_\alpha = (4/\delta)*(D/\pi)^{1/2}*t^{1/2} \quad \text{----------(3.12)}$$

Therefore,

$$D = (\pi/16)*(\delta s_0)^2 \quad \text{----------(3.13)}$$

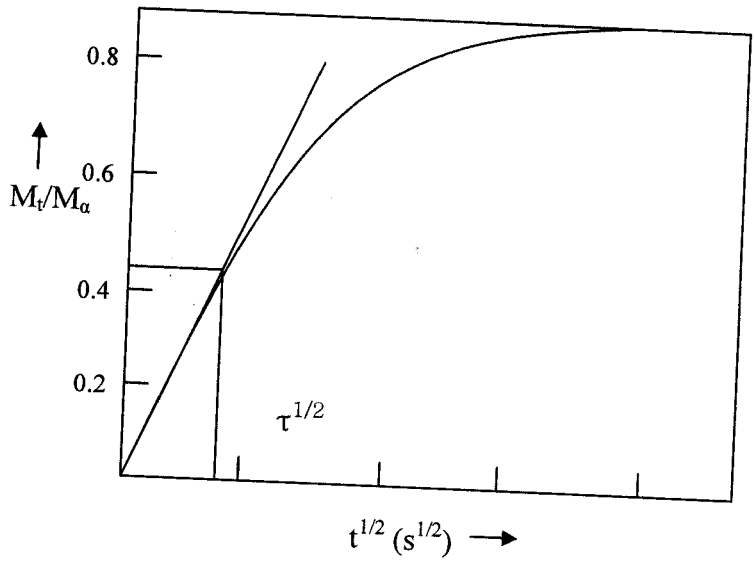

Figure 3.7: Determination of average diffusion coefficient from a transient sorption experiment: key parameters s_0 and τ.

In our study, we obtained the trend of the dynamic sorption by plotting the M_t/M_∞ as function of square root of time in sec.

3.3.14 Measurements of Water Vapor Permeability (WVP)

WVP was measured according to the ASTM (E 96-80B) method. Round bottom plastic cups with diameter of 65 mm and a height of 90 mm were filled with deionized water. Membranes were placed over the top of the cups and secure the perfect sealing between cup and membranes. The gap between the membrane and water surface was about 3 mm. During all the WVP measurements, air surrounding the membranes had a constant temperature and 70 % of relative humidity. Samples thickness for all measurement was about 90 micron. The cups were placed in a constant temperature chamber at the desired temperature (12, 18, 25, 35 or 45 °C). The weight losses after 24 h were measured. On the average, three different samples were used for each WVP measurements, which are

expressed in units of ($g/m^2/24$ h). The result of water vapor permeability (WVP) was calculated as follow:

$$WVP = G / tA = (G/ t) / A \quad \text{----------(3.14)}$$

Where,

G = weight change in gm.

t = duration test in hour

A = test area in m^2

3.4 COATING OF COTTON FABRIC WITH SPU AND EVALUATION OF COATED FABRICS

Selected SPUs and MWNT containing SPUs were applied to the cotton fabric by coating method. A thin film was formed (thickness about 20 μm) and the quality of the coated fabric would depend on the properties of the thin film and adhesion of the polymer on the fabric surface. The control of penetration of the viscous material on the porous substrate is absolutely essential. Too little penetration can result in an inadequate bond formation; too much in excessive stiffening, reduced tearing strength, and an unacceptable appearance and poor hand feeling.

3.4.1 Coating of Fabrics

SPU with different concentrations (0, 0.25, 1.00 and 2.50 % w/w) of MWNT was further dissolved homogeneously in N,N'-dimethyl formamide (DMF) in ultra sound bath. Scoured and bleached white cotton fabrics of weight 118 g m^{-2} was coated by knife over

roller machine (Weamer Mathis AG). The coated substrates were dried at 90 °C for 20 min to remove the N,N-dimethylformamide and then cured at 120 °C for 10 min. The thickness of the uncoated and that of the coated fabrics were 0.21-0.22 mm and 0.23-0.25 mm respectively which was measured by Mitutoyo thickness gauge (accuracy 0.001 mm). In order to easily identify the coated and uncoated fabrics throughout the discussions, the samples are coded and tabulated in Table 3.11.

The add-on % on the coated fabric was about 30% and calculated by using the formula:

$$\text{Add-on} = [(X - Y)/Y] \times 100 \text{----------} (3.15)$$

where, Y is the conditioned weight of the control fabric and X is the conditioned weight of the coated fabric.

Table 3.11: Coding of coated and uncoated fabrics

Sample code	Descriptions
F_0	Uncoated fabrics
F-PTMG-PEG10	Coated fabrics with SPU sample of S_{10}
F-PTMG-PEG15	Coated fabrics with SPU sample of S_{12}
F-PCL-PEG10	Coated fabric with PSU sample of S_{19}
F-PU	Coated fabrics with SPU solution containing no MWNT
F-0.25CNT	Coated fabrics with SPU solution containing 0.25 w/w% MWNT
F-1.00CNT	Coated fabrics with SPU solution containing 1.00 w/w% MWNT
F-2.50CNT	Coated fabrics with SPU solution containing 2.50 w/w% MWNT

3.4.2 Equipment and Measurements

The surface of the coated and uncoated fabrics were observed by scanning electron micrographs (SEM) made with a Leica Stereoscan 440 equipped with an Oxford energy dispersive X-ray system, operating at 20 kV.

Water vapor permeability of coated and uncoated fabrics was measured by following the same procedure as described in section 3.3.12.

Tensile properties of the coated and uncoated fabrics were measured according to the ASTM standard, 1 inch strip and 75 mm of gauge length by Instron 4411.

Water proofness of the coated and uncoated fabrics were measured by hydrostatic head tester (Textest, AG, FX 3000, Zurich, Switzerland), according to the AATCC 127 standard.

UV blocking properties of the coated and uncoated fabrics were measured according to the Australian/New Zealand AS/NZS 4399:1996 with a Varian Cary 300 Conc UV visible spectrophotometer. The UV spectrophotometer was used to measures the UV properties in terms of UV protection factor (UPF). With a UPF of 50+ which defines excellent protection according to Australian/New Zealand standards. The so-called UV-protection factor (UPF) is defined [137] as:

$$UPF = \frac{\int_{290}^{400} E_\lambda S_\lambda d\lambda}{\int_{290}^{400} E_\lambda S_\lambda . \tau_\lambda d_\lambda} \quad \text{----------(4.16)}$$

where λ represents the wavelength in nm, E_λ is the relative erythemal effectiveness, S_λ is the solar UV spectral irradiance in W m^{-2} nm^{-1} (data from Albuquerque, NM are used in this study), and $d\lambda$ is the wavelength increment in nm.

A Perkin Elmer UV-vis spectrophotometer (Lamda 18) was used to measure the absorbance spectra of the polymer solution (concentration 0.5 % w/v) in the range of 200-700 nm.

3.5 SUMMARY OF EXPERIMENTAL

In summary, based on the literature review and selections criteria, we have selected PTMG, PPG and PCL with molecular weight of 1000, 2000, 3000 g mol^{-1} as soft segment. 4,4'-MDI, HDI and 1,4-BDO were used as hard segment. Polyurethanes were modified with PEG (M_w 200, 2000, 3400 g mol^{-1}) or DMPA. Two or three steps polymerization techniques were employed to synthesize the polymers. SPUs were characterized by several techniques such as: FTIR, RAMAN, SEM, TEM, DSC, WAXD, DMTA, and Instron.

FTIR studies were carried out to investigate the hydrogen bonding between the hard and soft segments. Surface of nonporous membranes were observed by SEM. Raman and SEM studies were carried out to investigate the entrapment of MWNT by SPU. Phase separation and MWNT dispersions were observed by TEM techniques. Semicrystalline and amorphous structures were investigated by WAXD and DSC measurements. Viscoelastic properties and glass transition temperatures were observed by dynamic mechanical thermal analysis (DMTA). Tensile properties of the SPUs were investigated

by Instron. On the other hand shape memory effects of segmented polyurethanes were observed by Instron with temperature controlled chamber.

Water vapor transport properties of polymers were measured by the dynamic sorption, equilibrium sorption and water vapor permeability measurements. Cotton fabrics were coated by knife over roller machine. The coated or uncoated fabrics were evaluated by tensile strength measurements, waterproofness and water vapor permeability measurements. UV blocking properties of the coated fabrics with MWNT containing SPUs were measured by UV-vis spectroscopy. On the other hand, UV absorption properties of MWNT-SPU solution were measured by UV visible spectrophotometers.

CHAPTER 4

MICROSTRUCTURE AND THERMAL PROPERTIES OF SPU

This chapter describes the micro structure and thermal properties of SPU. Fourier transform infrared analysis was used to characterize the hydrogen and non-hydrogen bonded structure in SPU. Raman spectroscopy was used to investigate the entrapment of MWNT in SPU matrix. Non-porous surface structure was observed by scanning electron microscopy (SEM). Phase separated morphology and dispersion of MWNT was observed under transmission electron microscopy (TEM). Wide angle X-ray diffraction (WAXD) and differential scanning calorimetry (DSC) were employed to characterize the semicrystalline structure of SPU, and thermogravimetry (TG) analysis was used to measure thermal degradation properties of SPUs.

4.1 H-BONDED STRUCTURE OF SPU

Polyurethanes are segmented copolymers containing flexible soft segment (polyol) and rigid hard segment which contains urethane moieties. SPUs are extensively hydrogen-bonded [138-142] between the hard and soft segments. The presence of hydrogen bond will increase the overall cohesion of the materials, as these bonds are stronger and more directional than other intermolecular force in SPU. Hydrogen bonding would involve the N-H group in urethane and urea groups as doner, and urethane carbonyl, the ester carbonyl (in polyesterurethanes), or the ether oxygen (in polyetherurethanes) as the acceptor. Chemical bonds within a material would vibrate at a characteristic frequency;

the molecule will absorb the energy and vibrate. Each group possesses a number of normal modes of vibration, such as stretching and bending, therefore, a number of peaks could be attributed in the presence of a particular chemical structure. Identification of these peaks and their relative magnitude will help to predict the molecular structure [25].

4.1.1 Influence of Block Length of Hydrophilic Segment on H-bonded Structure

FTIR results for the influence of hydrophilic segmental block length on microstructure of SPU are shown in Figure 4.1. It can be observed that the band at free C=O (1730 cm^{-1}) groups would become sharper when PEG segment was introduced in the SPU backbone. Sample S_6 (PEG-200) has very sharp band at free C=O groups absorbance. It may be due to the plasticization effect of low molecular weight PEG which breaks hydrogen bonding of the SPU systems. On the other hand SPU without PEG block (S_9) has exhibited very weak C=O free absorbance bands, which signifies most of the C=O groups in the samples were H-bonded.

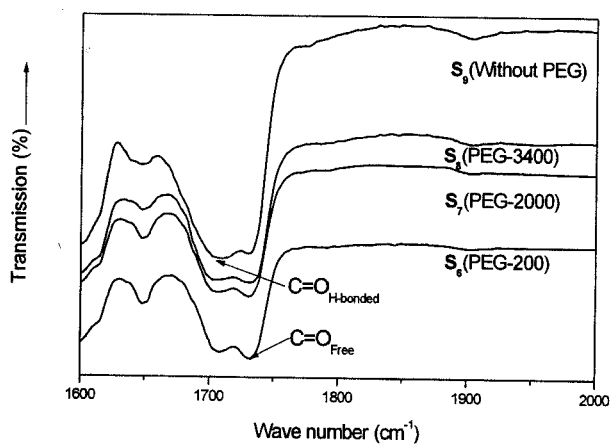

Figure 4.1: FTIR spectra of PU (S_6-S_9)

4.1.2 Influence of Hydrophilic Segment Content on H-bonded Structure

Figure 4.2 shows the FTIR results for the influence of hydrophilic segment content on SPUs samples. As PEG 3400 was introduced in the polymer backbone (5 and 10 wt% PEG 3400 content), $C=O_{H\text{-bonded}}$ peaks grows up which signifies the fact that the interactions among the hard segment (composed of MDI and 1,4-BDO) and soft segment increases through hydrogen bonding between C=O groups and –O- groups, and dipole-dipole interaction of phenyl ring. The $C=O_{Free}$ peak was again grown up with 15 wt% of PEG 3400 content (S_{12}) that may be due to the unstable and distorted interactions. This implies that the original inter- and intra-molecular hydrogen bonds involved in SPU films were destroyed due to the interpenetration and entanglement between SPU chains and long chain PEG 3400. If the intervened segment was long and flexible enough (S_{10}) it will allow perfect topographical position of hard and soft segment for interaction [143]. The urethane carbonyl groups residing in the hard segments of relatively short chain length are more likely to be solubilized by long PEG 3400 segment as the content of PEG 3400 is increased which will break the hydrogen bonding.

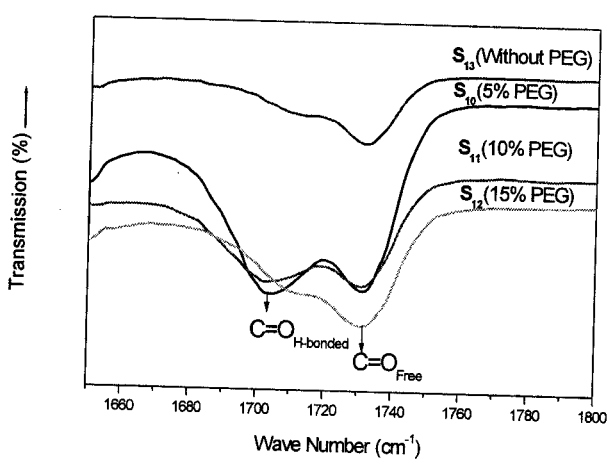

Figure 4.2: FTIR spectra of PU samples (S_{10}-S_{13})

4.1.3 Influence of Hydrophilic and/or Carboxylic Unit on H-bonded Structure

The FTIR spectra for the influence of hydrophilic and/or carboxylic group on SPUs are shown in Figure 4.3. Interesting differences were observed in comparing the free and hydrogen bonded carbonyl groups which would depend on the amount of hydrophilic or acid group in the polymer backbone. For SPU (S_{17}) without hydrophilic and acid groups, the carbonyl stretching (both hydrogen bonded and free, C=O) is barely detectable. However, the peak at $C{=}O_{H\text{-}bonded}$ stretching was grown up for the sample containing 10 wt% of DMPA unit (S_{15}) which suggests that the interaction between the polymer chains increases due to the hydrogen bonding and dipole-dipole interactions [61]. Alternately, free C=O group arises and H-bonded C=O was demised when 10 wt% of hydrophilic segment (PEG 3400 g mol^{-1}) was introduced in the polymer (S_{14}) backbone. This implies that the original inter- and intra-molecular hydrogen bonds in SPU films were destroyed due to the interpenetration and entanglement by PEG 3400 segment. Since the block length of PEG 3400 segment is higher than that of PPG 1000, therefore, small quantity of PEG 3400 will cause chain entanglement in the resulted SPU. A combination of hydrophilic and acid groups, the effect could produce the orientation level of hard and soft segment or alternately the hydrogen bonding, intermediate between S_{14} and S_{15} as shown in Figure 4.3.

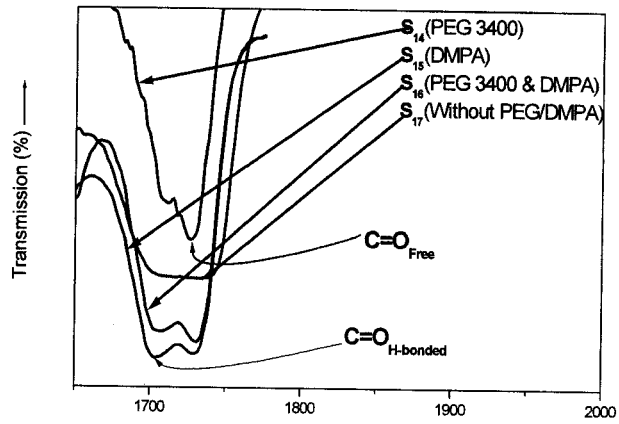

Figure 4.3: FTIR spectra in the C=O stretching region (S_{14}-S_{17})

4.1.4 Influence of Mixed Polyol Block on H-bonded Structure

Figure 4.4 shows the FTIR spectra of NH groups stretching for the effect of mixed block on the hydrogen bonded structure. The free NH ($NH_{H\text{-}Free}$) group has an IR absorption band at 3510-3530 cm^{-1}, whereas the signal for hydrogen bonded ($NH_{H\text{-}bonded}$) group was appeared at 3300-3347 cm^{-1}. The position and shape of the peaks have been changed with composition of soft segment. An ester group has much stronger interaction than an ether group, which may be the reason of having lower absorption spectra of $NH_{H\text{-}Free}$ for S_{21}. On the other hand broad peak of $NH_{H\text{-}Free}$ was obtained for sample S_{20} due to the soft-soft segment phase mixing which breaks the inter-chain interactions. It is interesting to note that, a small peak near 3450 cm^{-1} has been grown between $NH_{H\text{-}Free}$ and $NH_{H\text{-}bonded}$ for the SPU containing PCL 3000. The new peak is significant for sample S_{21} which suggests that the presence of ester group may increase the interaction between the polymer chains.

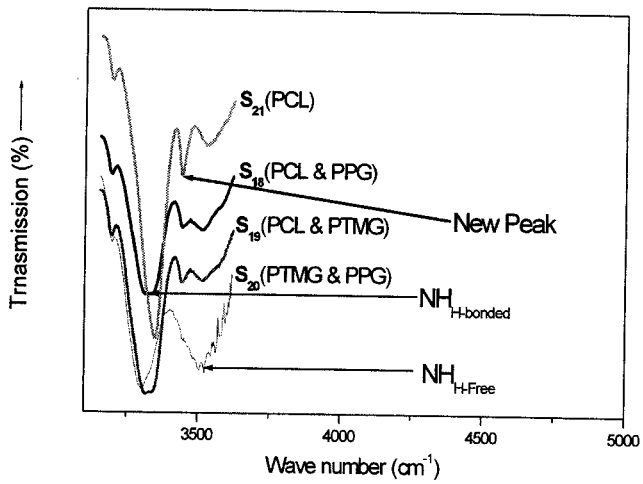

Figure 4.4: NH stretching of PUs (S_{18}-S_{20})

4.1.5 Influence of MWNT on H-bonded Structure

The influences of MWNT on SPU structures are shown in Figure 4.5. The interaction between chemical groups on either the same or different molecules can cause a shift of the IR peak position of the participating groups. The intensity of the hydrogen bonded C=O stretching peak at 1704 cm^{-1} was decreased for SPU-MWNT containing 0.25% of MWNT (S_{22}) with respect to the SPU without MWNT (S_{11}) which is implying the breaking of hydrogen bond. The variation in peak intensity with further increase of MWNT is not significant. Compared with the spectrum of SPU without MWNT the intensity of peak at about 1648 cm^{-1} for MWNT-SPU was increased which signifies the interaction of MWNT and SPU. The increase intensity is more pronounced for sample with 0.25% of MWNT (S_{22}) as compared with sample without MWNT. From the IR figure we can see that the absorbency of SPU with MWNT content increases owing to the MWNTs having very high absorbency.

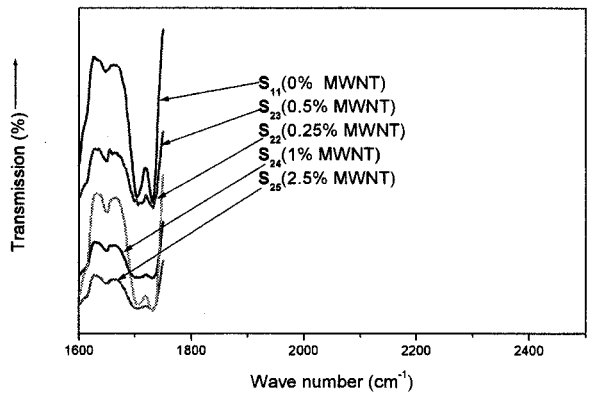

Figure 4.5: FTIR spectra of SPUs (S_{11}, S_{22}-S_{25})

4.2 ENCAPSULATION OF MWNT IN SPU

Raman spectroscopy was used to characterize encapsulation of MWNT by polymer matrix. The Raman spectra of pure MWNT and MWNT containing films are shown in Figure 4.6. The two main features in the Raman spectra are the D and G peaks at approximately 1350 and 1600 cm^{-1}, respectively. The G-band (due to strain in the C-C bonds) corresponds to the symmetric E_{2g} vibration mode in graphite-like materials, while the appearance of the strong D line can be associated with the turbostratic structure of the carbon sheets in the tubes, namely the finite size (nanometer order) of the crystalline domains [144]. D and G bands of MWNTs were diminished for the samples of S_{22} (0.25% MWNT content) and S_{23} (0.50% MWNT content) which indicates that the MWNTs were entrapped by the polymer with low percentage of MWNTs. When the content of MWNTs were increased to 1.0% or 2.5% the peaks (D and G modes) again appeared due to some MWNTs migrated on the surface with increasing content of nano tubes in the polymer. No MWNTs were observed on the surface of the SEM (Figure 4.8) picture of polymer membrane with low MWNT content, however some MWNTs can be observed from the film with 2.5% of MWNT (Fig 4.9).

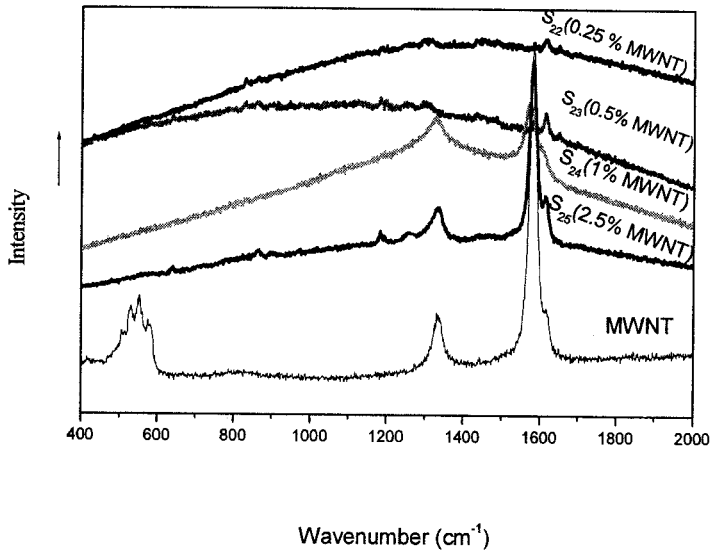

Figure 4.6: RAMAN spectra of SPUs

4.3 SURFACE STRUCTURE OF SPU FILM

The nonporous SPU surface structures are shown in Figure 4.7 – 4.9. All the SEM figures show nonporous defect free surface structure of SPU. SPU with 0.50 % (w/w) of MWNT content, no MWNTs were observed on the film surface. When the MWNT content was increased to 2.5 % (w/w), some MWNT migrate to the surface of SPU films.

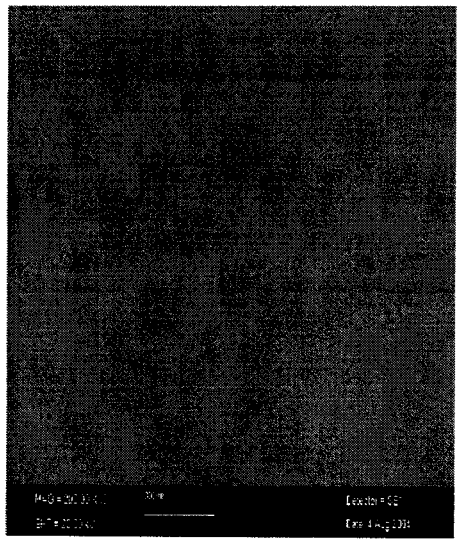

Figure 4.7: SEM photograph of S_{11} (Without MWNT)

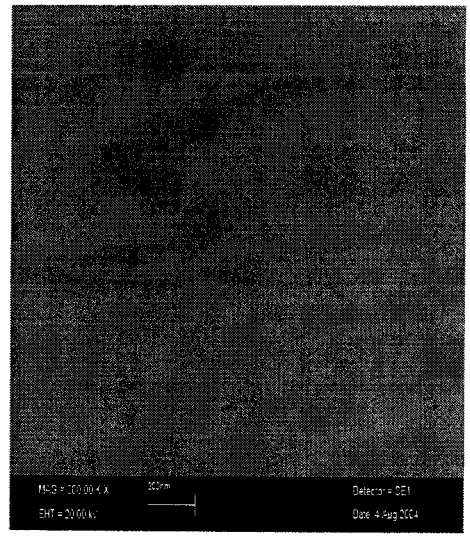

Figure 4.8: SEM photograph of S_{23} (0.5% MWNT)

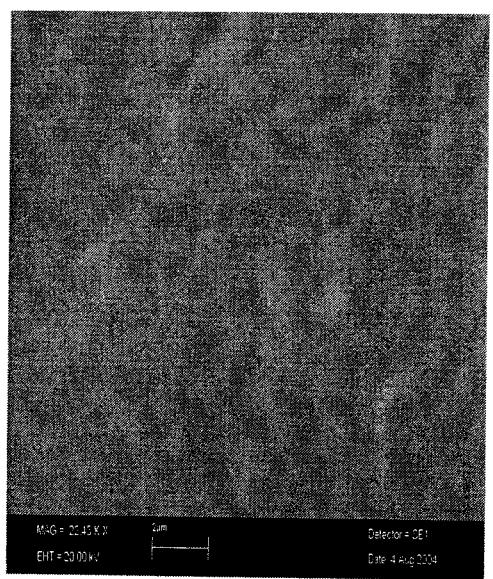

Figure 4.9: SEM photograph of S_{25} (2.5% MWNT)

4.4 PHASE SEPARATION OF SPU

Microphase separation can be more easily detected under TEM image. The ease of backbone rotation of soft segment would cause a higher degree of microphase separation. The darker lines in the micrographs are the soft segment crystal phase, and the lighter lines are rest of the soft segment and soft-hard mixed phase region. The boundary

between two phases appears to be rough, because RuO_4 induces stain in both soft and hard segment phases and also particularly soft segment crystalline phase. The staining procedure is short duration, thus may causes non-uniformity of the samples which would creates the roughness of the phase boundaries.

TEM images of the S_{13} (Figure 4.10) shows a morphology that is phase segregated on a macroscopic level. On the other hand, introduction of PEG 3400 in the SPU (S_{11}) (Figure 4.11) would cause phase separation in microscopic level due to some extent phase mixing by PEG chain and hard segment. Order morphology of soft segment rich domain could not be formed due to the presence of hard segments. Hard segment will strongly hinder the diffusion of chains and disrupted the formation of an order structure. These will prevent the system from arranging freely by effectively locking random portions of the chain by chain entanglement. When both segments are crystallizabe in a mixed block SPU, more regular and distinct phase separation was observed (Figure 4.12). Interesting TEM image (Figure 4.13) was observed from the sample contain mixed block having one crystallizable (PTMG 2900) and another noncrystallizable (PPG 3000) block, in this case, PPG 3000 caused phase mixing of PTMG 2900 segment, and PTMG 2900 crystal would be dispersed on the phase mixed soft-soft segment and soft - hard segment matrix. Hard segment content in SPU is 13% in S_{19}; therefore, they do not aggregate mutually and can not form separated domain. Though the formations of the hard segments are not observed in the TEM images, this does not imply that the copolymers are homogeneous. It might be that the hard segment does not crystallize and they are too small to be observed by TEM in those conditions. To understand more thoroughly the morphological behavior of SPUs, the kinetic effects should be considered.

Soft segment viscosity, hard segment mobility and interaction between the hard segments can be used to determine the kinetic effects [145]. Increases in the phase separations rate are expected with either increasing the hard segment mobility or decreasing in soft segment viscosity. The mixed block of PTMG 2900 – PPG 3000 soft segment reduces the soft segment viscosity which would increase the incompatibility between hard and soft segments. Therefore, more distinguish phase separations were observed between hard-soft segment matrix and soft segment crystal (Figure 4.13).

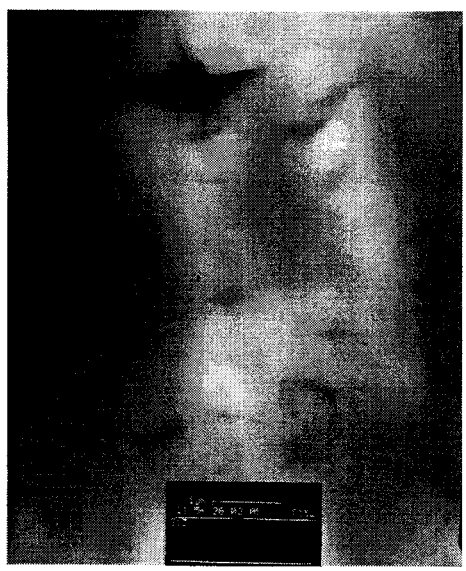

Figure 4.10: TEM image of S_{13} (Without PEG)

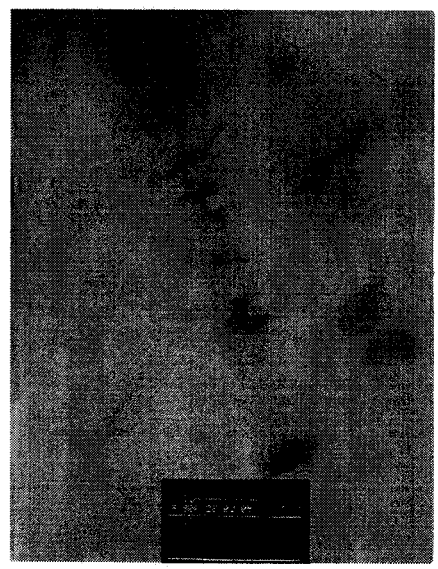

Figure 4.11: TEM image of S_{11} (10 % PEG)

Figure 4.12: TEM image of S_{19} (PTMG and PCL)

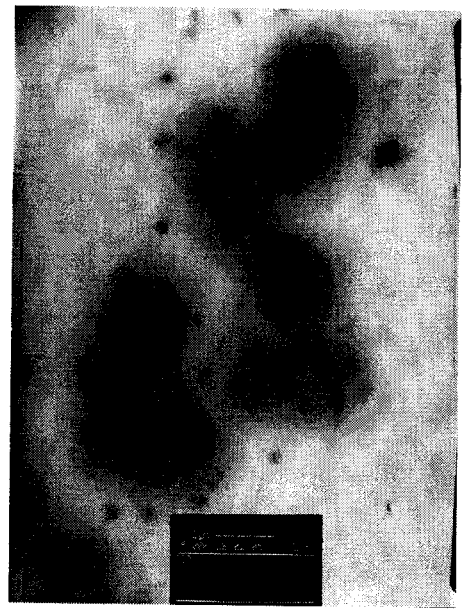

Figure 4.13: TEM image of S_{20} (PTMG and PPG)

Figure 4.14 – 4.16 shows the pristine MWNT and MWNT-SPU films. The dispersion of functionalized carbon nano tubes with 1 wt% of MWNT is clearly shown in Figure 4.16. There is no agglomeration present in the specimen. The dark lines are interactions of the nano tubes layers and polymer. It can be seen that nano tubes layers are effectively intercalated or exfoliated in the SPU matrix [146]. The average diameter of the pristine nano tube is about 20 nm (Figure 4.14). In the images of crude MWNTs (Figure 4.14), we can see that the individual tubes separated each other clearly. For the samples of MWNT-SPU (Figure 4.15), it can be observed that some parts of the tubes are coated with polymer layers [147]. These MWNTs have diameter of about 110 nm which are thicker than pristine MWNTs. The difference in diameter was suggested that some SPU chains interact with the amino groups of the MWNT-aniline [148]. This observation implies that the functionalization is likely occurred along the MWNT length, although it is believed that a higher degree of functionalization occurs at the end of the MWNTs

where reactivity is higher. From the Figure 4.16, we can see that MWNTs are well dispersed in the SPU matrix.

Figure 4.14: TEM image of pure MWNT

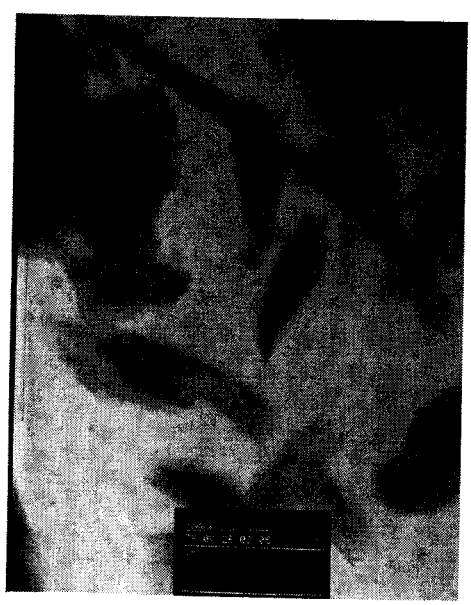

Figure 4.15: TEM image of S_{24} (0.5% MWNT)

Figure 4.16: TEM image of S_{24} (0.5% MWNT)

4.5 CRYSTAL/AMORPHOUS STRUCTURE OF SPU

4.5.1 Influence of Hard Segment on Crystal Structure of SPU

WAXD results for the influence of hard segment on crystal structure are shown in Figure 4.17 and data are presented in Table 4.1. The X-ray pattern of semi-crystalline polymer shows both sharp features associated with region of three dimensional orders, and more diffused features characteristic of molecular disordered region.

Table 4.1: WAXD data's of polyol and related SPU

Samples	d_{Bragg} (nm)		Crystallinity (%)	
	1	2	From WAXD	Calculated from wt fraction of polyol
PCL2000	0.412(21.55)	0.374(23.795)	40.4	--
S_1	0.414(21.45)[a]	0.375(23.73)	10.2	16.2
S_2	0.417(21.31)	0.376(23.65)	11.3	20.2
S_3	0.415(21.4)	0.373(23.81)	18.2	24.3
S_4	0.415(21.40)	0.375(23.71)	19.9	28.3
S_5	0.414(21.47)	0.374(23.76)	13.6	24.3
HS	0.761(11.63)	--	6.3	--
PTMG2000	0.441(20.11)	0.362(24.57)	26.3	--
S_6	0.452(19.63)	--	0.95*	17.0
S_7	0.445(19.95)	--	8.9*	17.2
S_8	0.436(20.38)	--	5.2*	17.3
S_9	0.464(19.11)	--	0	15.7

[a]The value inside the bracket indicates the Bragg's angle (2θ) and *value calculated by equation 4.1

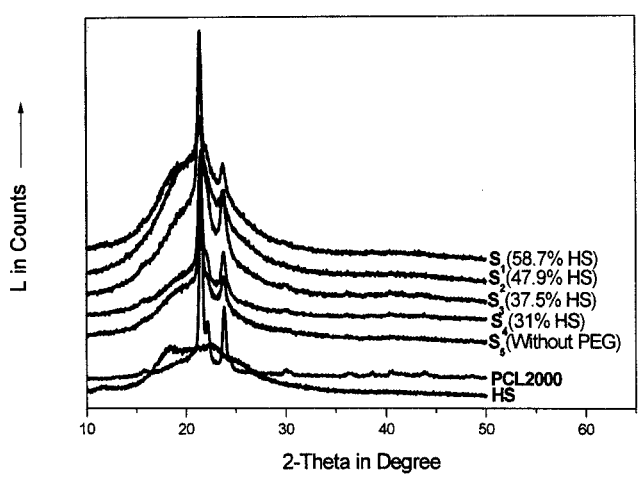

Figure 4.17: WAXD pattern of SPU and HS

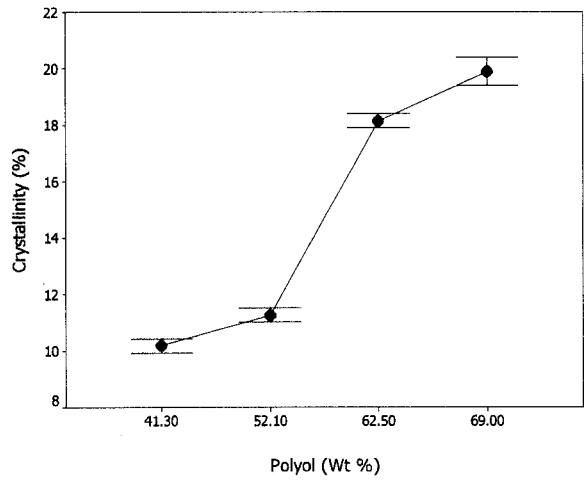

Figure 4.18: Relationship between percentage crystallinity and amount of PCL in the SPUs

From Figure 4.17 we can see that, pure PCL 2000 and SPU spectra displayed two broad halos at 2θ of 23.705-23.795 ° and 21.545-21.4 ° respectively that can be attributed to a short range order of two crystalline peaks and broad amorphous peak. The occurrence of both types of features was suggested that the ordered and disordered region coexists in semicrystalline polyol and SPUs. The X-ray data indicates that the soft segment (polyol) can form crystalline structure in the segmented polyurethane. In all cases the actual crystalline structure in the polymer is lower than that the calculated value from the weight fraction of polyol (Table 4.1), may be due to the reinforcing effect of hard segment into the soft domain matrix which hinders the crystallization process of soft domain. Percentage crystallinity was increased (Figure 4.18) with increasing polyol content in the SPUs or in other ways decreased with increasing hard segment. From the WAXD spectra of 100 % hard segment (HS), we can see that there is little crystalline structure. However in the polyurethane, these hard segments probably act as reinforcing filler to the soft matrix, moreover these are scattered and their chain length is shorter than soft segments. This may be the reason why the hard segment can not form

crystalline structure in the segmented polyurethane. From the WAXD results we can see that, S_1, contain 58.7 % of HS, the percentage crystallinity of S_1 is comparable to that of S_2 (47.9 % HS), that may be the little aggregation of hard segment in S_1 is possible as it contain highest soft segment among five samples.

4.5.2 Influence of Block Length of Hydrophilic Segment on Crystal Structure of SPU

X-ray diffraction patterns for the influence of hydrophilic block length on SPU's microstructures are shown in Figure 4.19 and data are tabulated in Table 4.1. From the Figure 4.19, we can see that, pure PTMG 2000 polyol has two prominent diffraction peaks at Bragg's angle of 20.11 ° and 24.565 °. However, the related SPU has one broad halo at 19.11 – 20.38 ° which signifies the amorphous structure. Interestingly, the DSC data shows the endothermic peaks of S_6, S_7 and S_8 samples. Therefore, the broadening of the diffraction maxima may be due to the presence of small crystallite size. The quantitative measurements of the disorder are difficult because broadening of diffraction maxima due to the presence of small crystal size, amorphous region or by the diffraction within large crystal [149-150]. The percentage of crystallinity of S_6 – S_8 can be roughly estimated from the WAXD data and DSC results which can be calculated by the following formula:

$$(\chi_{PU}\ \%)/\Delta H_{PU} = (\chi_{Polyol}\ \%)/\Delta H_{Polyol} \text{ ----------(4.1)}$$

Where, χ_{PU} % and χ_{Polyol} % are percentage crystallinity of SPU and polyol respectively. On the other hand, ΔH_{PU} and ΔH_{Polyol} are heat of fusion of SPU and polyol respectively.

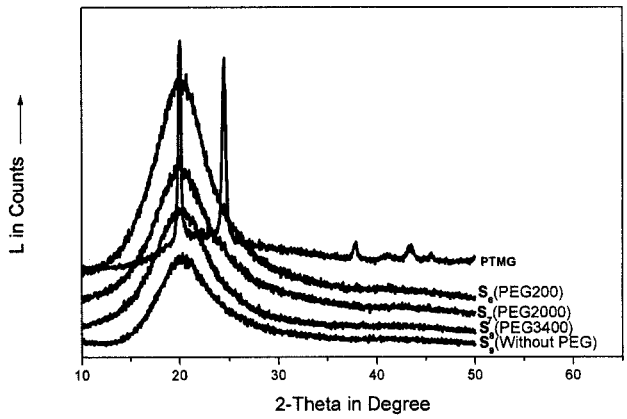

Figure 4.19: WAXD patterns of PTMG 2000 and corresponding SPU ($S_6 - S_9$)

4.5.3 Influence of Hydrophilic Segment Content on Crystal Structure of SPU

The X-ray data of pure PTMG 2900 and SPUs for studying the effect of hydrophilic block content on crystalline structure formation is shown in Figure 4.20. Soft segment would form crystalline structure in the segmented polyurethane due to their long ordered structure [149]. Therefore, in our study we carried out WAXD study of pure PTMG 2900 in order to understand the influence of PTMG 2900 on SPU structure. Pure PTMG 2900 shows typical diffraction peaks at $2\theta = 20°$ & 24.5°. However, the resulted SPUs shows a broad haloes at $2\theta = 20°$ which may be due to the amorphous structure or presence of small crystalline structure or diffraction from large crystal [150]. DSC results confirmed the endothermic peak, therefore the broad haloes is due to the presence of small crystallite which may be scattered in the polymer matrix, and could not be detected by WAXD. The percent crystallinity of the SPUs could be roughly estimated from the WAXD data and DSC results, and can be calculated by using equation 4.1. The percent crystallinity calculated from equation 4.1, are in the following order, S_{10} (8.83

%)>S_{11} (10.32 %)>S_{13} (12.79 %)>S_{12} (14.77 %). Little amount (5 wt %) of PEG 3400 hinders the crystallization process. The arrangements of soft segment during crystallization are restricted by the chain entanglement of PEG 3400. S_{12} has highest amount of order structure. With increasing PEG 3400 content some aggregation of crystalline PEG 3400 segment may be possible in the phase separated structure which will increase the total order structure in the resulted SPU.

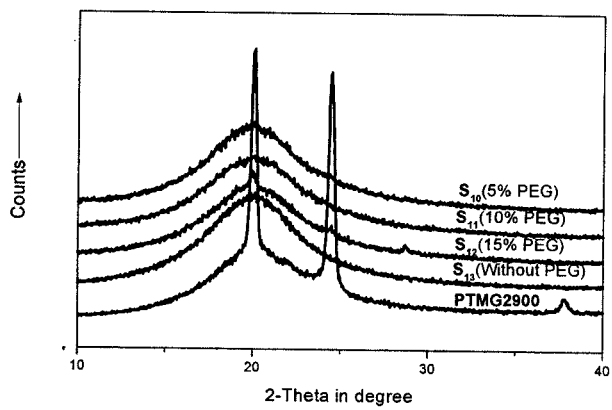

Figure 4.20: WAXD results of SPU (S_{10}-S_{13})

4.5.4 Influence of Hydrophilic and/or Carboxylic Unit on Amorphous Structure of SPU

WXRD of all samples for the influence of hydrophilic and/or carboxylic unit on micro structure at room temperature was exhibited a broad halos at 2θ ~ 19.37 ° (Figure 4.21), corresponding to the inter-shell spacing (d ~ 4.5Å). The broad halos may be due to the scattering from large crystal, or the presence of small crystalline structure or from amorphous region [150]. From the DSC heating results no endothermic peaks were observed, therefore, the broad halos are due to the amorphous region. This suggests that the chain length of soft segments (M_n 1000) used in this study is relatively short, and the

interaction between soft and hard segments is relatively strong which makes the microphase separation of soft and hard segments difficult. The soft segment in this study is liquid at room temperature therefore, it could not be able to form crystalline structure in the resulted SPU. On the other hand hard segment content is about 25 wt% which acts as reinforcing filler. The hard segments are scattered in the polymer matrix, therefore do not aggregate mutually and arrange orderly, and finally cannot form crystal structure [151].

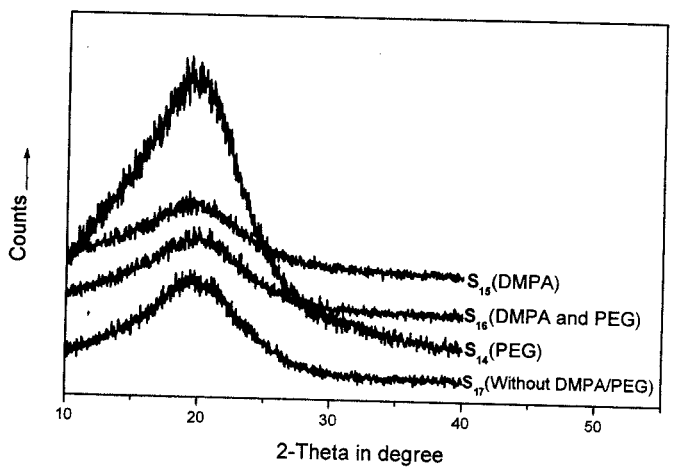

Figure 4.21: WAXD pattern of SPU (S_{14} –S_{17})

4.5.5 Influence of Mixed Polyol on Crystal Structure of SPU

WAXD results at room temperature for the influence of mixed block soft segment on micro crystalline structure are shown in Figure 4.22 – 4.23. Polyurethanes for this study composed of about 80 wt% of long polyol (soft segment). Because of their long polymer chains and ordered structures, soft segment could form crystalline structure in the segmented polyurethane copolymer. Therefore, for better understanding, the WAXD measurement of pure PTMG 2900 and PCL 3000 were carried out, and the results are

shown in the Figure 4.23. However, PPG 3000 is liquid at room temperature and its WAXD can not be performed. From Figure 4.23, we can see that pure PCL 3000 has two sharp diffraction peaks and the resulted SPUs (Figure 4.22) based on PCL 3000 also shows two diffraction peaks which indicates the presence of order structure. The percent crystallinity of resulted SPUs is lower than that of crystallinity calculated from the weight fraction of pure polyol due to the presence of hard segment which would act as reinforcing filler and hinder the crystallization process of polyol.

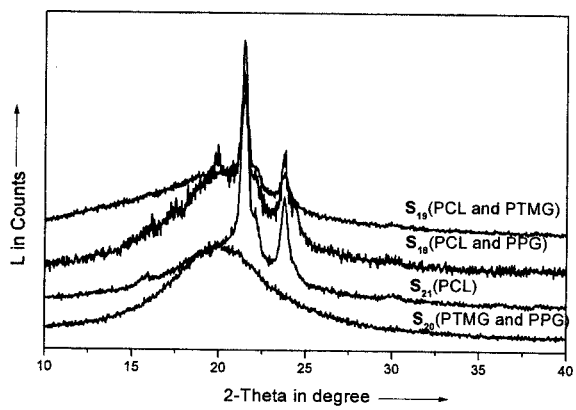

Figure 4.22: WAXD pattern of SPU ($S_{19} - S_{21}$)

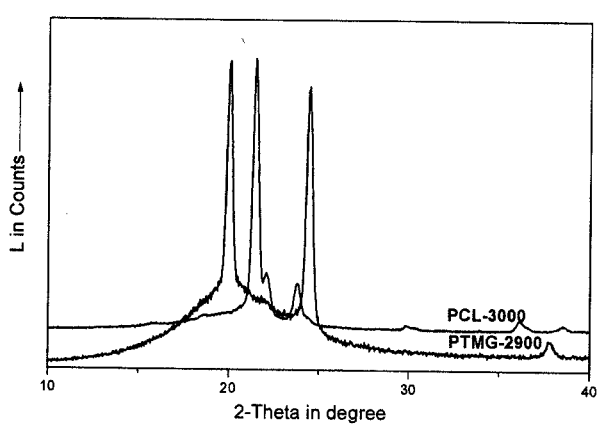

Figure 4.23: WAXD of pure PTMG 2900 and PCL 3000

Sample with only PCL 3000 (S_{21}) has the highest percentage of crystallinity among the four samples, due to their phase separated structure. The introduction of another soft segment block (PPG 3000 or PTMG 2900) would hinder the crystallization of PCL 3000 segment due to the soft-soft segment phase mixing which makes the situation difficult for ordering of soft segment. The percent crystallinity of PCL 3000 based SPUs, detected by WAXD and calculated by Young's equation [152], were in the following order S_{21} (28.8 %)>S_{19} (23.2 %)>S_{18} (20 %). From the Figure 4.22, we can see that, SPU based on PTMG 2900 and PPG 3000 has broad halos at $2\theta \sim 20$ which may be due to the amorphous structure or presence of small crystalline structure or reflection from large crystal [150]. DSC result confirms the endothermic peak, therefore the broad halos is due to the presence of small crystallites which are scattered and could not be detected by WAXD. The percentage crystallinity of S_{20} is 7.3 % which could be roughly estimated from equation 4.1.

4.5.6 Influence of MWNT on Crystal Structure of SPU

WAXD results for the influence of MWNT on SPU structure are shown in Figure 4.24. All samples show broad halo at 19.11 – 20.38 ° which may be due to the small crystallite size, amorphous region or by diffraction within the large crystal [150]. Interestingly DSC heating curve showed endothermic peak. Therefore, the broadening of diffraction maxima may be due to the presence of small crystallite size which is scattered in the sample. A new peak was appeared from the films with MWNT near 26.4 °. The peak at 2θ= 26.4 ° is absent in SPU without MWNT, and in all MWNT containing SPU the same visible at θ=26.4 °. The WXRD pattern of the parent nano tubes exhibits a intense (002) Bragg reflection at 2θ= 26.1, corresponding to the inter

shell spacing (d= 3.4 Å) of the concentric cylinders of graphite carbon [153]. The presence of these peaks in MWNT containing SPU samples suggests that the layer structure was formed in the MWNT reinforced SPU.

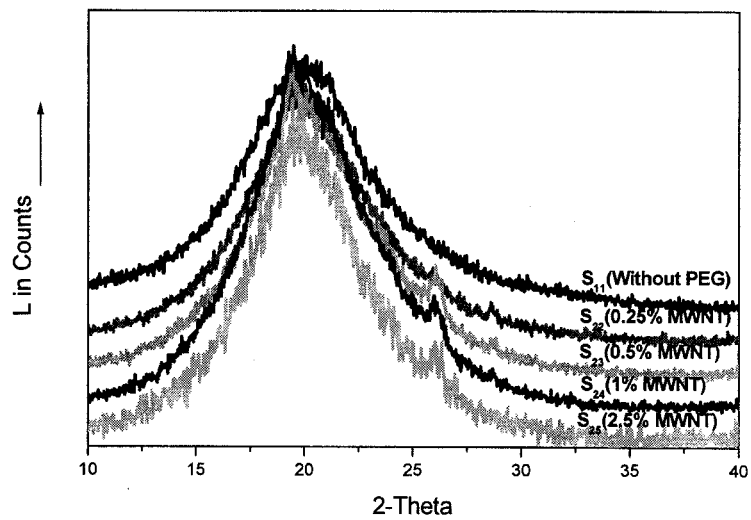

Figure 4.24: WAXD pattern of SPUs (S_{11}, S_{22} –S_{25})

4.6 THERMAL TRANSITION OF SPU

4.6.1 Influence of Hard Segment on Thermal Transition of SPU

Typical DSC thermograms for the influence of hard segment on SPU micro-crystalline structure are presented in Figure 4.25 – 4.27 and the relevant data are shown in Table 4.2. In order to understand the role of hard segment in the segmented polyurethane, hard segment was scanned from –50 to 200 °C and pure polyol (PCL 2000) was scanned from –50 to 120 °C.

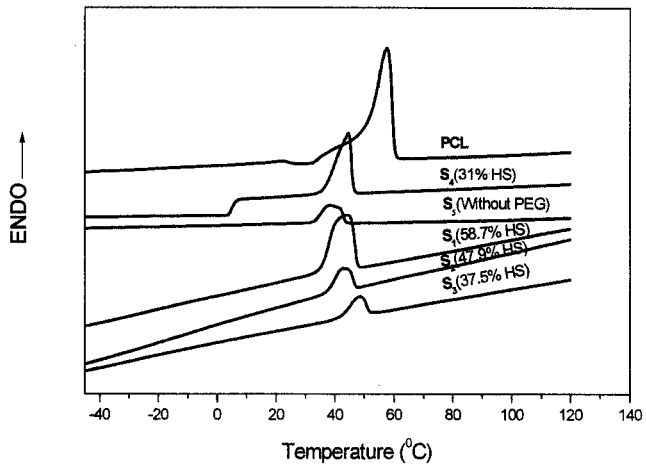

Figure 4.25: DSC heating thermograms of PCL 2000 and resulted SPU

Table 4.2: DSC data of SPU (S_1 –S_5)

Samples	ΔH_1 [a]	T_{ms1} [b]	ΔH_2 [a]	T_{ms2} [b]	ΔH_{c1} [a]	T_{cs1} [b]	T_g [b]
S_1	15.1	42.2	--	--	--	--	--
S_2	9.3	44.2	--	--	--	--	--
S_3	30.8	43.2	--	--	--	--	--
S_4	35.4	44.3	--	--	--	--	7.3
S_5	22.8	38.3	--	--	--	--	--
PCL	72.7	57.5	--	--	72.8	19.3	--
HS	12.5	71.2	63.8	177.7	15.4	180.6	--

ΔH is heat of fusion, T_{ms} crystal melting temperature, ΔH_c heat of crystallization, T_{cs} crystallization temperature, T_g glass transition temperature, [a] data are in g J^{-1}, on the other hand [b] are in °C

T_{ms} and heat of fusion for pure PCL 2000 is higher than that of the corresponding polyurethane. The decrease of heat of fusion and equilibrium melting temperature in the resulted SPU is due to the change of the free energy by miscible hard segment. In general, heat of fusion was increased with increasing the soft segment content in the polyurethane (Table 4.2), however S_1 (58.7 % HS) has a higher heat of fusion than

sample S_2 (47.9 % HS). In fact, 100% of HS can also form crystalline structure which is observed in DSC thermogram (Figure 4.26) and WAXD, however when these are present in the polyurethane, they cannot form the regular structure due to their short chain length as compared to the polyol chain length which will cause lack of organization. Therefore, in sample S_1 where hard segment content is higher than that of the other samples, some organization may occur which would enhance the hard segment aggregation as a result of increase of overall heat of fusion.

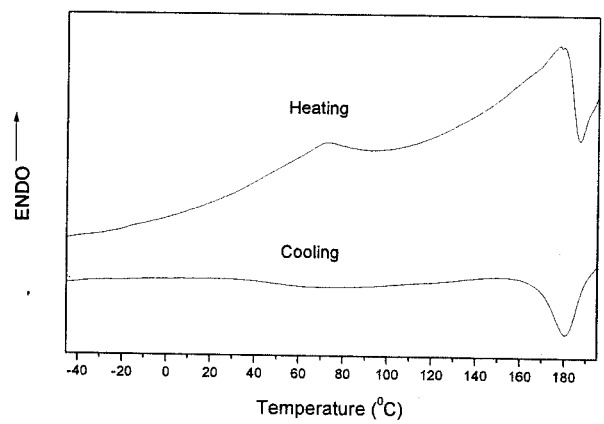

Figure 4.26: Heating and cooling thermograms of hard segment

Sample S_4 and sample S_5 (without PEG) have the same quantity of HS (30 %), however the percent crystallinity (Table 4.2) and heat of fusion of sample S_5 is lower than that of S_4. The increase of the component may create more favorable condition for crystallization in case of S_4.

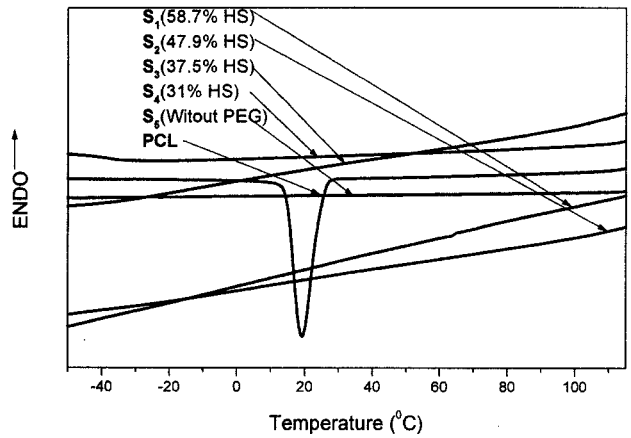

Figure 4.27: Cooling thermogram of PCL 2000 and SPU

From the DSC cooling curve (Figure 4.27), we cannot observe any exothermic peak in SPU samples except for pure PCL 2000 and pure hard segment (Figure 4.26). That may be due to the phase mixing of the hard and soft segment domain of this kind of polyurethane. However, when they are in pure form, they will favor the crystallization.

4.6.2 Influence of Hydrophilic Block Length on Thermal Transitions of SPU

DSC results for the influence of hydrophilic block length on microstructure are shown in Figure 4.28 – 4.29 and data are presented in Table 4.3. Figure 4.28 shows no endothermic peak for the sample S_9 containing no hydrophilic segments. That may be due to the flexible nature of PTMG 2000 soft matrix, where hard segment acts as reinforcing filler which would prevent the crystallization of soft matrix. On the other hand introduction of the hydrophilic segment to the SPU can enhance the crystallization of soft matrix. PEG segment increases the mobility of the polymer chains which will facilitate the crystallization process. With low molecular weight of PEG - 200, the actual

percentage crystallinity is very low compared to the calculated percentage crystallinity from polyol weight fraction. The plasticization effect of PEG – 200 created unfavorable condition for soft segment crystallization. The percentage crystallinity of SPU is highest with the PEG - 2000 as compared with PEG - 200 or PEG - 3400. This result from the fact that, crystallization in polymers is involved the steps of (primary) nucleation and relatively rapid spherulitic growth, followed by a slow, kinetically difficult improvement in crystal perfection [150]. The molecule must undergo a considerable degree of motion during crystallization. The motion may be optimum with PEG – 2000 as this molecular weight is comparable with polyol (PTMG 2000) molecular weight which would enhance the intermolecular packing of small crystalline domains. The percentage of crystallinity was decreased with PEG – 3400 due to the chain entanglement which will hinder the crystallization process of soft domain.

Table 4.3: DSC data of SPU ($S_6 - S_9$)

Samples	ΔH_1[a]	T_{ms1}[b]	ΔH_2[a]	T_{ms2}[b]	ΔH_{c1}[a]	T_{cs1}[b]	ΔH_{c2}[a]	T_{cs2}[b]	T_g[b]
S_6	0.7	15.5	0.3	42.8	--	--	--	--	--
S_7	28.4	15.7	--	--	12.5	34.4	--	--	-40.3
S_8	22.5	12.8	--	--	13.0	-13.0	3.3	-35.2	--
S_9	--	--	--	--	--	--	--	--	--
PTMG	32.3	24.5	81.1	39.0	94.2	2.3	--	--	--

ΔH is heat of fusion, T_{ms} crystal melting temperature, ΔH_c heat of crystallization, T_{cs} crystallization temperature, T_g glass transition temperature, [a] data are in g J^{-1} or [b] are in °C

The cooling thermogram (Figure 4.29) indicates that the heat of crystallization of sample S_7 was higher than that for sample S_8. Chain entanglement hinders the crystallization

process which may be reason of decrease of heat of crystallization of sample S_8. No exothermic peak was observed for sample S_6 and S_9 possibly due to the increasing phase mixing. On the other hand phase separation of sample S_7 is better than the sample S_8, which can be seen from the DSC cooling results and Tanδ spectra of DMTA results. The distance between the two peaks of S_7 is larger than the S_8 (from Figure 5.5) which signifies better phase separation as a result of more regular structure.

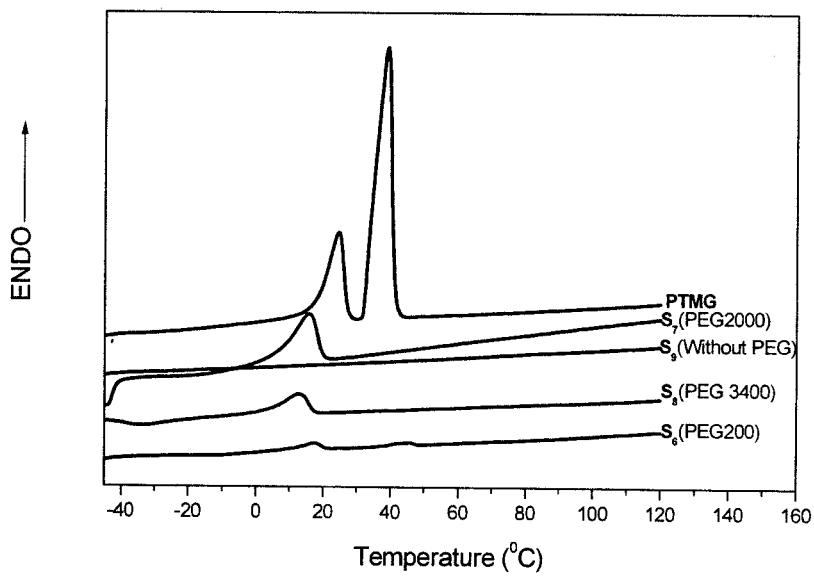

Figure 4.28: Heating thermogram of PTMG 2000 and related SPU (S_6 – S_9)

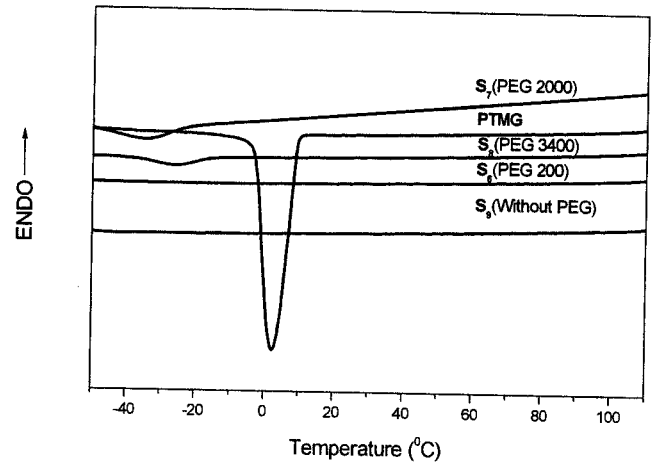

Figure 4.29: Cooling thermogram of PTMG 2000 and related SPU

4.6.3 Influence of Hydrophilic Segment Content on Thermal Transitions of SPU

Soft segment crystal meting temperature (T_{ms}) and heat of fusion (ΔH) obtained from the DSC data for the influence of hydrophilic block content on micro structure are summarized in Table 4.4 and are shown in Figure 4.30 – 4.31. Pure PTMG 2900 has two sharp peaks at 27.8 (T_{ms1}) and 36.67 (T_{ms2}) °C (Figure 4.38). All the resulted SPU has lower T_{ms} as well as ΔH than that of pure PTMG 2900 due the presence of hard segment which would hinder the crystallization process of PTMG 2900. The T_{ms} and ΔH was further decreased with 5 wt% of PEG 3400 content, may be due to the little amount of linear PEG 3400 molecules enhance the flexibility and mobility of polymer chains which plasticizes the soft segment phase of SPU as a result of reduction of the order structure of soft segment [150]. SPU without PEG 3400 has higher heat of fusion than that of SPUs with PEG 3400 which signifies more crystalline structure in S_{13}.

Table 4.4: DSC data of SPU ($S_{10} - S_{13}$)

Samples	ΔH (Jg^{-1})	T_{ms} (°C)	ΔH_c (Jg^{-1})	T_c (°C)
S_{10}	22.2	19.8	29.6	-15.0
S_{11}	23.7, 2.3	22.2, 38.5	29.2	-15.5
S_{12}	5.2, 31.9	19.0, 38.6	34.7	-8.4
S_{13}	32.2	20.9	40.1	-10.9
PTMG 2900	42.8, 32.6	27.8, 36.7	70.8	7.5

ΔH heat of fusion, T_{ms} soft segment crystal melting, ΔH_c heat of crystallization, T_c crystallization temperature.

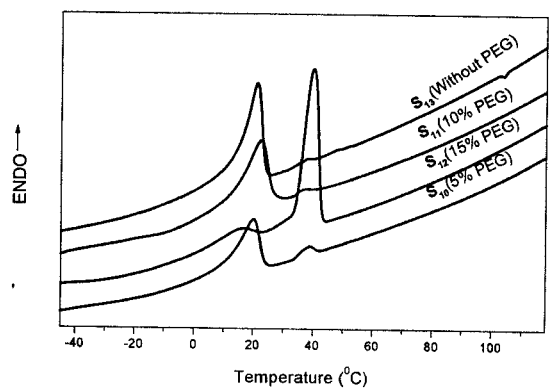

Figure 4.30: DSC heating thermogram of SPU ($S_{10} - S_{13}$)

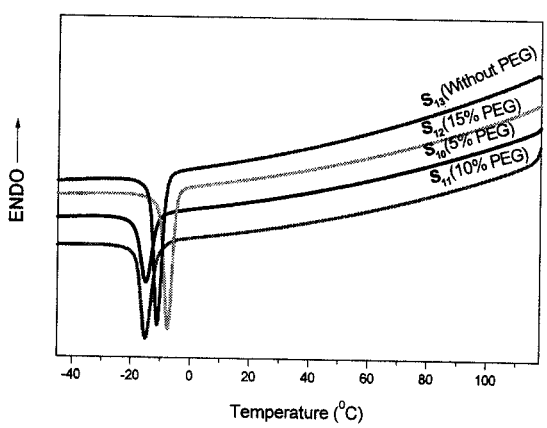

Figure 4.31: DSC cooling thermogram of SPU ($S_{10} - S_{13}$)

It is interesting to note that, for SPUs with 10 wt% (S_{11}) and 15 wt% (S_{12}) of PEG 3400 content, the T_{ms} shifted to the higher values which is close to secondary crystal melting peak of pure PTMG 2900. The increase of PEG 3400 content would increase the tendency of phase separation imposed by long flexible PEG 3400 segment as a result of more order structure in SPU.

4.6.4 Influence of Hydrophilic and/or Carboxylic Unit on Thermal Transitions of SPU

Thermal transitions of the SPUs for influence of hydrophilic and/or carboxylic group content on SPU structure are shown in Figure 4.32 – 4.34. Figure 4.32 – 4.34 shows no endo or exo-thermic peaks which signifies that all the SPU samples are amorphous in nature. These results are supported by the measurements of WAXD data as well. Soft segments form crystalline structure in the segmented polyurethane due to their longer chain length and order structure. In this study, we used PPG 1000 as soft segment which is liquid in room temperature, therefore, PPG 1000 could not form order structure in the resulted SPU. No distinct melting or crystallization peak of hard segment was observed by DSC as well. Lower percentage of hard segments do not provide well order structure, therefore proper ratio of hard to soft segment is necessary for ordering of hard segment. These hard segments are rather scattered throughout the polymer matrix which would act as reinforcing filler. Glass transition temperature (T_g) of sample with DMPA unit is much higher than that of the other samples due to the presence of ionic groups which will provide more interaction due to: (1) hydrogen bonding between carbamoyl group and carbonyl groups, (2) dipole-dipole interaction between carbonyl group, (3) induced dipole-dipole interaction between the aromatic rings [61]. These interactions increase the

number of physical cross-links in the polymer matrix which will hinder the chain mobility as a result of higher T_g. In contrast, the T_g was decreased with PEG 3400 by increasing the chain mobility. However the study of glass transition temperature would be better performed by dynamic mechanical thermal analysis, and will be presented and discussed in the next chapter.

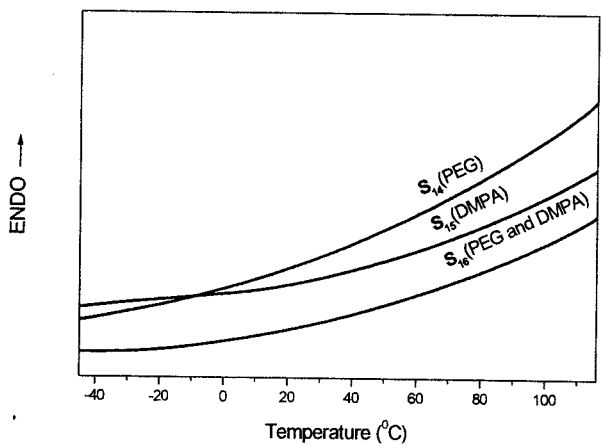

Figure 4.32: DSC heating thermogram of SPU ($S_{14} - S_{16}$)

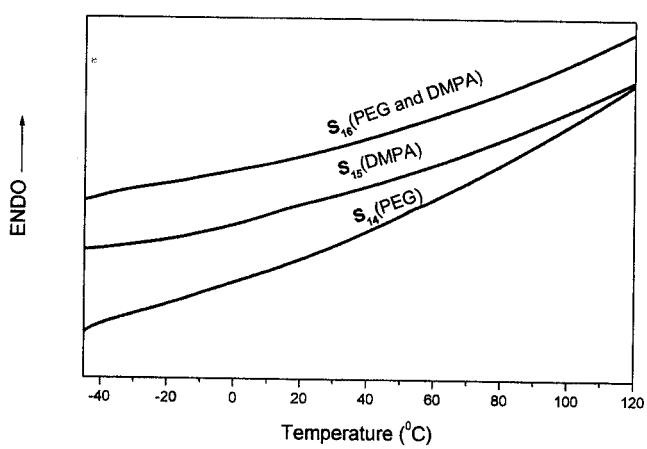

Figure 4.33: DSC cooling thermogram SPUs ($S_{14} - S_{16}$)

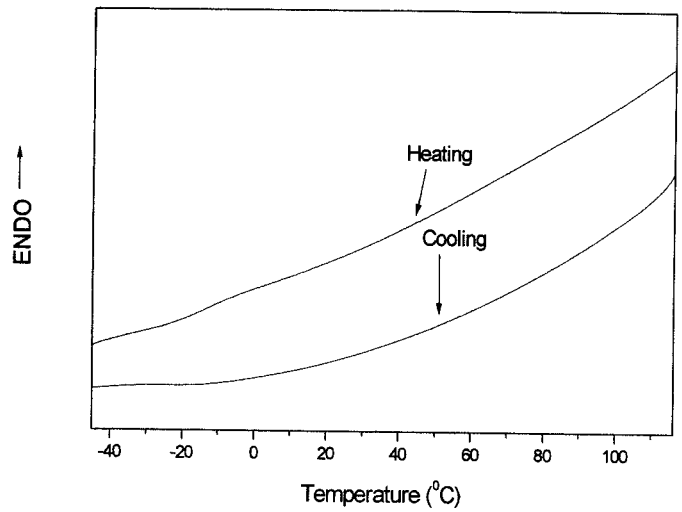

Figure 4.34: DSC heating and cooling thermogram of S_{17} (Without PEG and DMPA)

4.6.5 Influence of Mixed Soft Segment on Thermal Transition of SPU

Soft segment crystal meting temperature (T_{ms}) and heat of fusion (ΔH) were obtained from the DSC data for the mixed soft blocks, and are summarized in Table 4.5. The DSC results are shown in Figure 4.35 – 4.37. Pure PTMG 2900 has two sharp endothermic peaks (Figure 4.38), at 27.8 and 36.7 °. On the other hand, pure PCL 3000 has single sharp endothermic peak, at 63.6 °C (Figure 4.38). Each transition has been attributed to a specific phenomenon. In DSC, the amount of energy needed to maintain a fixed rate of temperature is measured. Change in heat of fusion denoted the changes in the mobility of polymer chains [25].

Table 4.5: DSC data of SPU (S_{18} –S_{21})

Samples	ΔH (Jg^{-1})	T_{ms} (°C)	ΔH_c (Jg^{-1})	T_c (°C)
S_{18}	29.4	51.2	3.2	-9.6
S_{19}	9.3, 30.4	19.2, 46.8	1.7, 28.2	-7.7, 7.7
S_{20}	18.3, -7.8	20.3	--	--
S_{21}	52.5	55.5	33.8	-3.5
PTMG 2900	42.8, 32.6	27.8, 36.7	70.8	7.5
PCL 3000	92.5	63.6	77.9	25

ΔH heat of fusion, T_{ms} soft segment crystal melting, ΔH_c heat of crystallization, T_c crystallization temperature and T_g glass transition temperature.

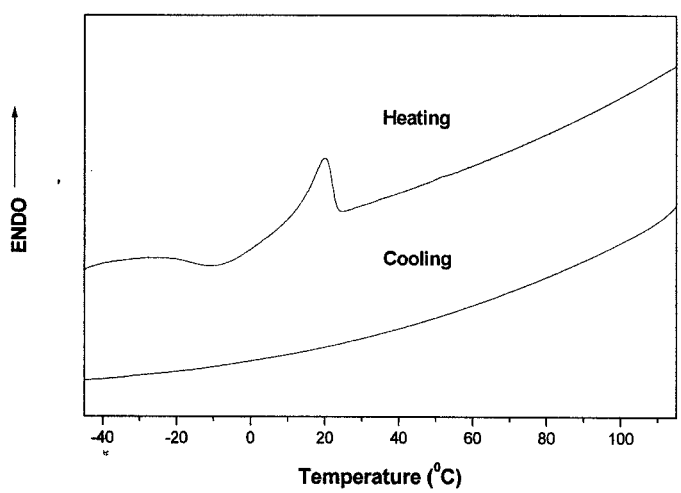

Figure 4.35: DSC thermogram of S_{20} (PTMG and PPG)

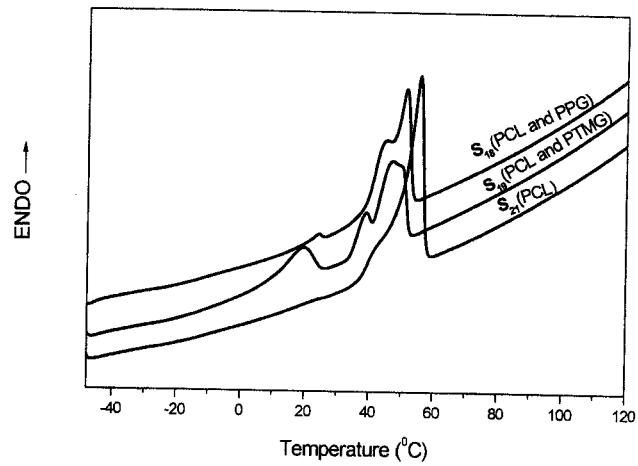

Figure 4.36: Heating thermogram of SPU (S_{18}, S_{19}, S_{21})

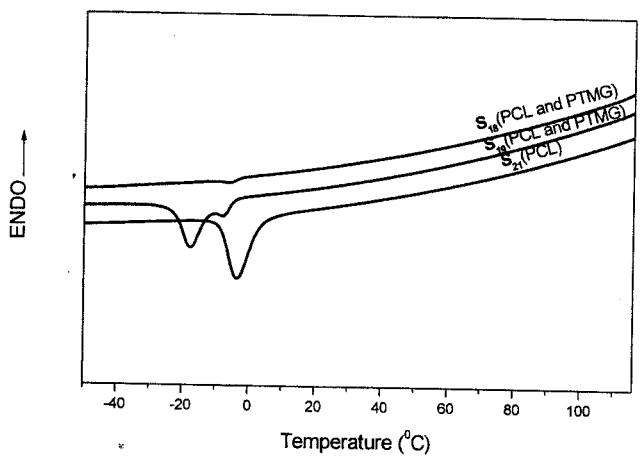

Figure 4.37: Cooling thermogram of SPU (S_{18}, S_{19}, S_{21})

All the resulted SPUs have lower heat of fusion than the calculated heat of fusion from weight fraction of pure soft segment due to the phase mixing by hard and soft segment and soft-soft segment which would hinder the crystallization process of soft segment.

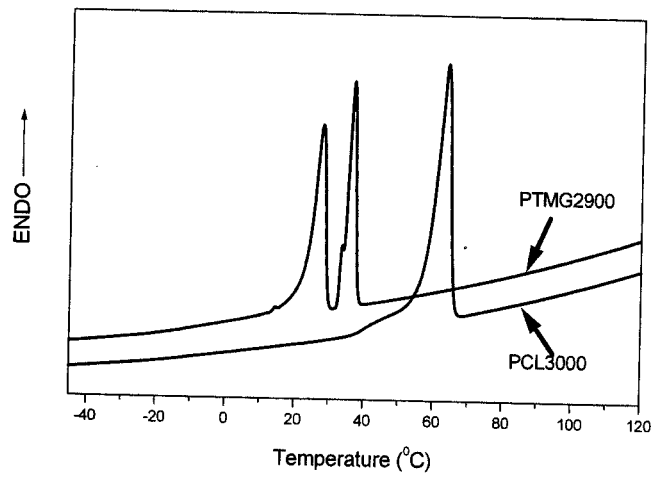

Figure 4.38: Heating thermogram of pure PTMG 2900 and PCL 3000

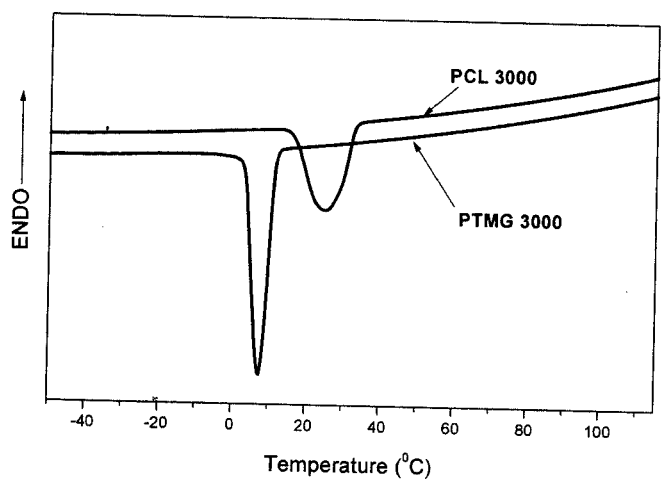

Figure 4.39: DSC cooling thermogram pure PTMG 2900 and PCL 3000

PCL 3000 based SPU samples have heat of fusion in the following orders: $S_{21}>S_{19}>S_{18}$. The reduction in crystallinity by the miscibility of PCL 3000 and PPG 3000 segments seems to be the cause of the decreases of the heat of fusion for sample S_{18}. A sharp peak in S_{19} for PTMG 2900 phase was appeared at 19.2 °C. The shape of endo-thermic peak

(S_{18} and S_{19}) as well as exothermic peak (S_{19}) of the mixed blocks SPUs are different from that of single soft block SPU (S_{21}) due to the phase mixing which would alter the shape and position of transition. The heat of fusion of S_{20} (PPG 3000-PTMG 2900) is lowest among the all four samples due to the phase mixing of PTMG 2900 phase by PPG 3000, and these phase mixing finally will decrease the order structure of PTMG 2900 phase. PPG 3000 itself could not form the crystalline structure, that's the reason of lower percent crystallinity as a result of decrease of heat of fusion.

From the DSC cooling results, pure PTMG 2900 as well as pure PCL 3000 shows the prominent exothermic peak (Figure 4.39). Resulted SPUs containing only PCL 3000 and PCL 3000-PTMG 2900 soft block shows the sharp exothermic peak which signifies crystallization during cooling cycle. The exothermic peak was divided in two parts in case of sample S_{19} which contains same quantity of PCL 3000 and PTMG 2900 blocks that may be due to the fact that both phases separately formed crystalline structure in the resulted SPU. Presence of PPG 3000 prevents the crystallization of PCL 3000 (S_{18}) phase as well as PTMG 2900 (S_{20}) phase in DSC cooling cycle due to phase mixing by PPG 3000 segment.

4.6.6 Influence of MWNT on Thermal Transition of SPU

Influences of the MWNT on DSC results are shown Figure 4.40 – 4.41 and data are presented in Table 4.6. The DSC results of pure PTMG 2900 (soft segment) is shown in Fig 4.38 – 4.39. From the Figure 4.40, we can see that, all samples show sharp endothermic peak which signifies the presence of crystalline structure in the SPU. The soft segment (polyol) can form crystalline structure in the segmented polyurethane [149].

In all samples percent of PTMG 2900 is 65 wt%. The heat of fusion of resulted SPU due to the melting of soft segment crystal is lower than that of

Table 4.6: DSC data of SPU (S_{11}, $S_{22} - S_{25}$)

Samples	ΔH (Jg^{-1})	T_{ms} (°C)	ΔH_c (Jg^{-1})	T_c (°C)
S_{11}	23.7	22.2	29.2	-15.5
S_{22}	25.5	22.4	29.0	-14.9
S_{23}	24.3	22.7	26.7	-16.4
S_{24}	22.2	21.5	24.9	-15.0
S_{25}	21.9	20.7	24.3	-17.4
PTMG 2900	42.8 ,32.6	27.8, 36.7	70.8	7.5

ΔH heat of fusion, T_{ms} soft segment crystal melting, ΔH_c heat of crystallization, T_c crystallization temperature.

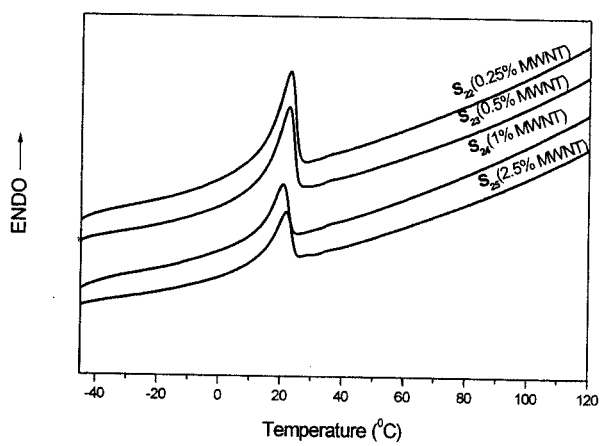

Figure 4.40: DSC heating thermogram of SPU ($S_{22} - S_{25}$)

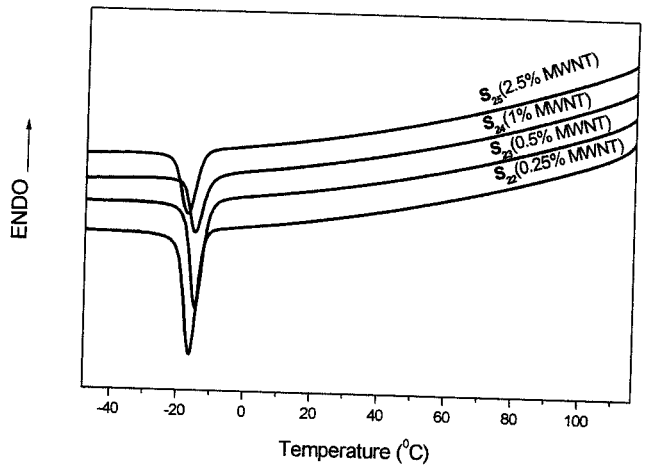

Figure 4.41: DSC cooling thermogram of SPUs (S_{22} –S_{25})

heat of fusion of pure PTMG 2900 that may be due to the presence of hard segment (1,4-BDO and MDI) which would act as reinforcing filler and hinder the crystallization process of soft segment. The heat of fusion of S_{22} having low content of MWNT (0.25%) is slightly higher than that of sample without MWNT which is suggested that slightly more order polymer chain packing were obtained at 0.25 wt% of MWNT. That may be due to the presence of little amount of MWNT which would enhance the crystallization process. In fact crystallization in polymer involves three steps of primary nucleation and relatively rapid spherulitic growth, followed by a slow kinetically difficult improvement in crystal perfection [150]. Little amount of nano particles may act as nucleus for nucleation of crystal which will enhance the crystallization process. The slightly decrease of crystallization temperature (the temperature corresponding to the maximum of the crystallization exotherm) with 0.25 wt% of MWNT indicates that the crystallization by nano tube became easier. There is a much lower impact of additional nano tubes, suggesting that almost enough nanotubes are present at 0.25 wt% MWNT to

provide sufficient surface area for the crystallite nucleation [110]. Further increase of MWNT decreases the heat of fusion which is related with the degree of crystallinity. The further increased MWNT acts as filler which would suppress the mobility of soft segment as a result of decreases of the crystallinity of soft segments. From the DSC cooling curve (Figure 4.39 and Figure 4.41), we can see that the pure PTMG 2900 as well as all samples shows sharp exothermic peaks which was signifies the crystallization of soft segment. However, T_g of all samples could not be detected by DSC. Study of the glass transition temperature would be better performed by dynamic-mechanical thermal analysis, and will be presented and discussed in DMTA analysis section of chapter 5.

4.7 THERMAL DEGRADATION PROPERTIES OF SPU

In the application of breathable coating or laminating fabrics the polyurethane film has become an important element [154-159]. However, these materials are generally not very thermally stable [160]. Thermal stability is a problem for segmented polyurethane film particularly above their softening point temperature. Degradation can lead to significant changes in the polyurethane mechanical properties and surface chemistry. Therefore, the knowledge of their behavior during thermal decomposition is very important. When the SPU would apply on the fabric surface by coating method, we need to cure the polymer at certain temperature; therefore the polymer should be thermally stable at that temperature.

The TG experiments were carried out at different heating rate (5, 10 and 20 °C min^{-1}) and the results are presented in Figure 4.42. From the Figure 4.42, it can be seen that as the heating rate was increased, the thermal stability also increased which is actually due

to the temperature gap between the samples and system. At higher heating rate, the temperature gap between the machine and samples is also higher, that's why the curve shifted to the higher values. The influences of hard segment (HS) on thermal stability of SPUs are presented in Figure 4.43 – 4.45 and data are tabulated in Table 4.7. Pure hard and soft segment degradations are shown in Figure 4.46 and Figure 4.47 respectively. Figure 4.43 shows TG results of typical sigmoidal form for all samples. From the results we can see that as the HS content in the polymer was increased the thermal stability was decreased. It has been indicated that the initial degradation would occur in the hard segments [160].

Table 4.7: Characteristic temperature of PCL 2000 series SPU at heating rate of 10 °C/min

Sample	$T_{10\%}$ (° C)		$T_{d,1/2}$ (° C)		$T_{d,max}$ (° C)	
	Air	N_2	Air	N_2	Air	N_2
S_1	283.8	294.2	333.2	339.5	343.2, 442.4, 542.7	347.3, 452.9
S_2	286.6	303.1	344.7	362.2	341.4, 443.7, 548.6	348.7, 448.9
S_3	300.1	312.4	351.5	366.3	339.4, 446.3, 566.5	365.1, 454.4
S_4	304.5	317.3	363.5	369.6	360.4, 455.6, 582.0	307.0, 414.2
S_5	315.2	325.6	389.0	375.8	349.2, 446.7, 582.3	389.5, 452.8
HS	273.2	280.0	316.5	328.3	290.5, -- 534.8	299.8, 475.4
PCL (2000)	277.0	316.3	361.5	395.2	320.4, 400.5, 509.8	405.3, 555.8

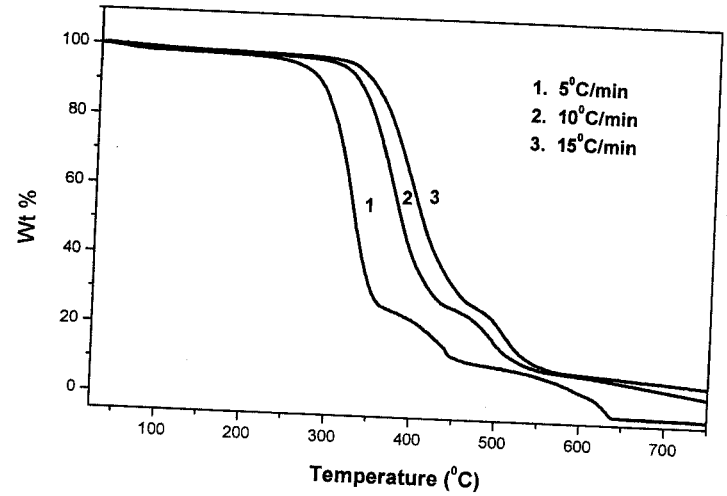

Figure 4.42: TG results of S_2 at different heating rate

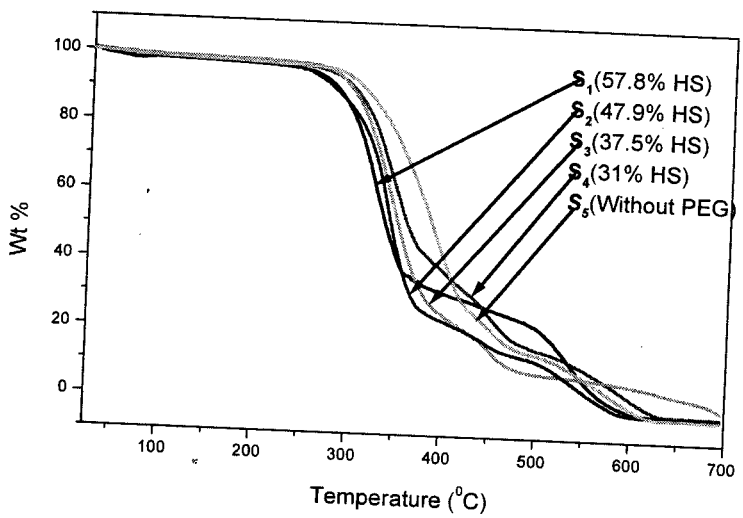

Figure 4.43: TG curves of SPU at 10 °C min^{-1} under air

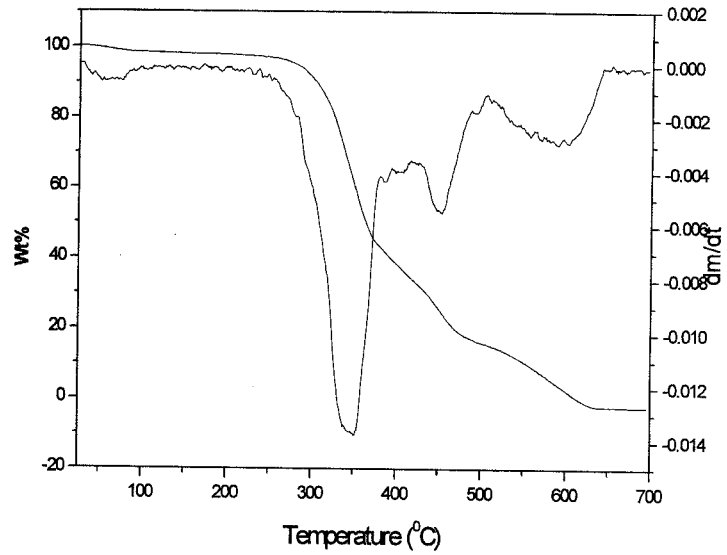

Figure 4.44: TG and DTG curves of S_2 at 10 °C min^{-1} under air

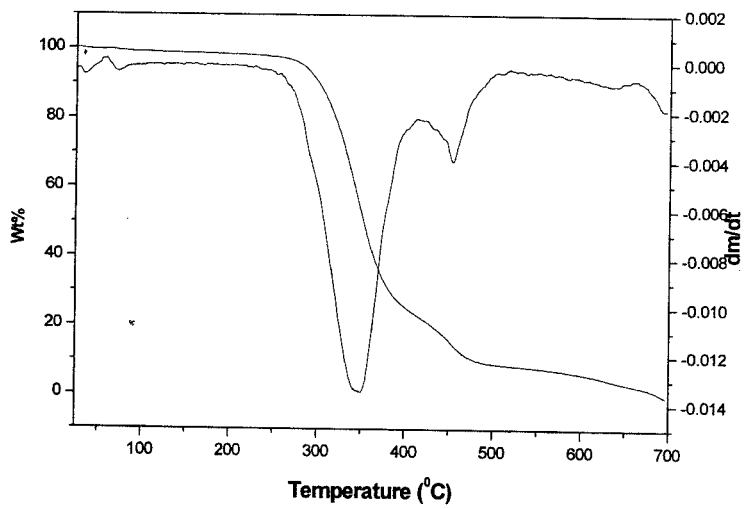

Figure 4.45: TG and DTG curves of S_3 at 10 °C min^{-1} under nitrogen

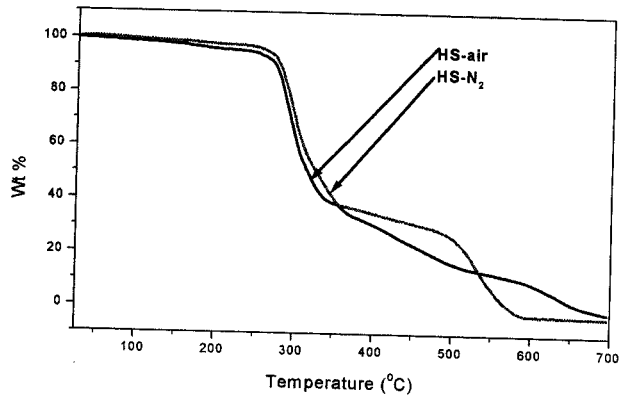

Figure 4.46: TG graphs of hard segment at 10 °C min^{-1} under air and nitrogen

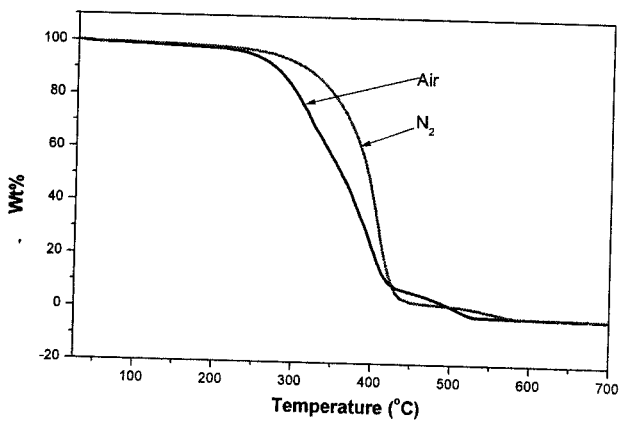

Figure 4.47: TG graphs of pure PCL 2000 at 10 °C min^{-1} under air and N_2

In the discussion of the degradation mechanism of SPU, the DTG curves in the air are rather more complex as compared to the curves in nitrogen. In all cases for polyurethane, the degradation in air is three stages process; on the other hand in nitrogen, it is two-stage process. Since the additional exothermic peak was not observed when TG carried out under nitrogen, it is apparent that the lower stability in air, and the multiphase process must be related to the oxidation reactions between the soft and hard segments. All polyurethane samples in air exhibited one degradation step more in comparison to

the degradation in nitrogen. As reported in other studies of thermal degradation on polymers, it is possible to assume that during the degradation in air the last step (in the temperature range between 509 and 583 °C) is correspond to the advanced fragmentation of the chain formed in the first and second stages of decomposition, as well as the secondary reaction of dehydrogenation and gasification, and decomposition of the char formed in the previous steps [161-162]. From the Table 4.7, we can see that during the degradation of pure hard segment, there are only two peaks in DTG curves in air as well as in nitrogen. From the degradation spectra of HS, we can see that, there is peak near 290 °C. Therefore, the degradation of first stage at about 350 °C is probably related to the hard segment degradation. On the other hand the second stage of degradation from 442 – 447 °C may be related to the degradation of soft segment i.e. PCL segments. The actual DTG peaks are higher than the corresponding pure hard and soft segment peaks due to the variation of molecular weight of polymer, morphology (phase separation) or different bond viz. urethane, allophanate presence in SPU.

4.8 SUMMARY OF MICROSTRUCTURE AND THERMAL PROPERTIES OF SPU

The polymer chain interaction would depend on topographical position of hard and soft segments which was detected by FTIR measurements. H-bonded structures of SPU depend on types of polyol, and block length and content of hydrophilic segment. Low molecular weight of PEG 200 would break the hydrogen bonding due to the plasticization effect of PEG 200. In contrast, presence of DMPA unit causes strong interactions between the polymers chains of PPG 1000 based SPUs. The original inter and intra-molecular hydrogen bonds involved in the PPG 1000 based SPUs were

destroyed by PEG 3400. This phenomenon may be due to the entanglement of polymer chains by PEG 3400 chains. The position and shape of FTIR peaks have been changed with composition of soft segment in the mixed block SPU. Single block SPU with PCL 3000 polyol has strong H-bonded structures. In contrast introduction of PPG 3000 or PTMG 2900 segment along with PCL 3000 would loosen the intra chain interaction due to the phase mixing. The presence of MWNTs in SPU matrix would alter the interaction between the polymer chains. The FTIR results shows that absorbency of MWNT containing SPU were increases with increasing MWNT content in the polymer backbone due to the high absorbance capability of MWNT particles.

SEM studies revealed the defect free surface structure of SPU. Two phase polymer morphology was detected by TEM measurements. Phase separation would depend on the type of polyol used in SPU. Extent of the microphase segregation was increased and regular when both blocks are crystallizable in mixed block soft segment polyurethane copolymer. However, presence of non-crystalizable block would cause phase mixing as a result of lower order structure. PTMG based SPU shows a morphology that is phase segregated in a macroscopic level and regular way. On the other hand, introduction of PEG 3400 in the PTMG based SPU causes phase separation in microscopic level due to some extent phase mixing by PEG segment. Raman spectroscopy results revealed that the MWNT particles were encapsulated by polymer membranes at low content. The well dispersion of hydrophobic carbon nano particles were observed by TEM image. The diameters of MWNT in SPUs are higher than that of MWNT in pure form. Therefore the functionalization was occurred along the nano tube which would help to coat the nano tubes by polymer molecules.

WAXD and DSC results revealed the semicrystalline polymer structure when pure polyols have crystal structure. SPU based on liquid polyol such as PPG 1000 has completely amorphous structure. With the increase of soft segment in SPU, the percent crystallinity was also increased which signifies the crystallization of soft segment. In contrast, the increase of hard segment hinders the percent crystallinity of resulted SPU due to their reinforcing filler effect. The hard segments are scattered through out the polymer matrix and their shorter chain length do not provides order structures in the resulted SPU. All the PTMG based SPUs show micro-crystalline structure. In contrast, all the PPG 1000 based SPUs were amorphous in nature. Soft segment forms crystalline structure separately in the resulted mixed block SPU when both polyol blocks are crystallizable in pure state. Little amount of MWNTs increases the percent crystallinity of soft segment, may be due to the nucleation by nano particles. The MWNT containing SPU shows a new peak at 2θ =26.4° due to the concentric cylinders of graphite layers. The presence of this peak has proven the functionalization of MWNT.

The heat of fusion increases with increasing soft segment content in the PCL 2000 based SPU due to the increases of crystalline structures. PTMG 2000 based SPU without hydrophilic segment did not show endothermic peaks due to their amorphous structure. Microcrystal structures would be formed with the introduction of PEG segment. Higher heat of fusion was observed with SPU having PEG 2000 block. The presence of PEG 200 segment decreases the heat of fusion due to the plasticization effect of low molecular weight of PEG molecules. The heat of fusion was also decreased with PEG 3400 due to the chain entanglement posses by long chain PEG molecules in soft domain which hinders the soft segment crystallization. The PTMG 2900 based SPU with 15

wt% of PEG 3400 has higher soft segment crystal melting point temperature than the SPU with 5 or 10 wt% of PEG 3400. The shifting of T_{ms} is due to the phase separation imposed by longer PEG 3400 segments in PTMG 2900 based SPU. No exothermic or endothermic peaks were observed for the SPUs with PPG 1000 due to their amorphous structure. However, the glass transition temperature of PPG 1000 based SPU was increased in the presence of DMPA unit in the polymer matrix due to the ionic interactions. The shape and position of endothermic and exothermic peaks have been altered with the presence of mixed polyol blocks, when both blocks are crystallizable in pure state. The heat of fusion of PCL 3000 based SPUs decreases when PPG 3000 or PTMG 2900 was used as mixed block along with PCL 3000. The decrease of heat of fusion is due to the soft-soft segment phase mixing which would hinder the crystallization of PCL 3000 phase. The heat of fusion was little bit increased with little quantity (0.25 wt%) of MWNT due to the crystallization by nano particles. Further increase of MWNTs content decreases the heat of fusion due to the decrease of crystal structures.

Thermal degradation property of SPU depends on the amount of soft segment in the polymer. Higher the soft segment contents in SPU the better would be the thermal degradation properties. DTG results revealed that two stage degradation of SPU in air as compared to three stages in nitrogen. The multi phase process of SPU degradation in air is related with the oxidation reaction between the soft and hard segments.

CHAPTER 5

MECHANICAL AND THERMOMECHANICAL PROPERTIES OF SPU

This chapter presented the influences of six factors on dynamic mechanical thermal (DMTA) property, tensile testing property and shape memory effects of SPUs. Storage modulus, loss modulus and tan (delta) value have been presented as function of temperature. Un-axial tensile testing results of SPU at room temperature and cyclic tensile testing results are included in this chapter.

5.1 THERMO-MECHANICAL PROPERTIES OF SPUs

5.1.1 Influence of Hard Segment on Thermo-mechanical Properties of SPU

DMTA is an important technique capable of providing considerable information on the position of transitions and the thermo-mechanical properties of polymers [25]. Typical dynamic mechanical thermal analysis (DMTA) results for the effect of hard segment on SPUs are shown in Figure 5.1 – 5.3. In Figure 5.1, we can see that the sharp fall of tensile storage modulus occurs at the temperature of T_g. The storage modulus was increased sharply with increasing hard segment content in the SPUs which is due to the increases of cohesion between hard and soft segment. T_g (Table 5.1) was also increased with increasing hard segment due the strong allophanate interaction by excess of hard segments.

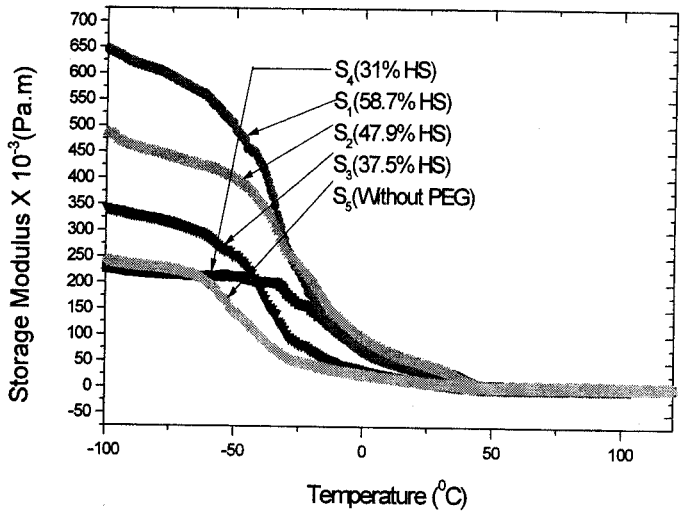

Figure 5.1: Storage modulus of SPU ($S_1 - S_5$)

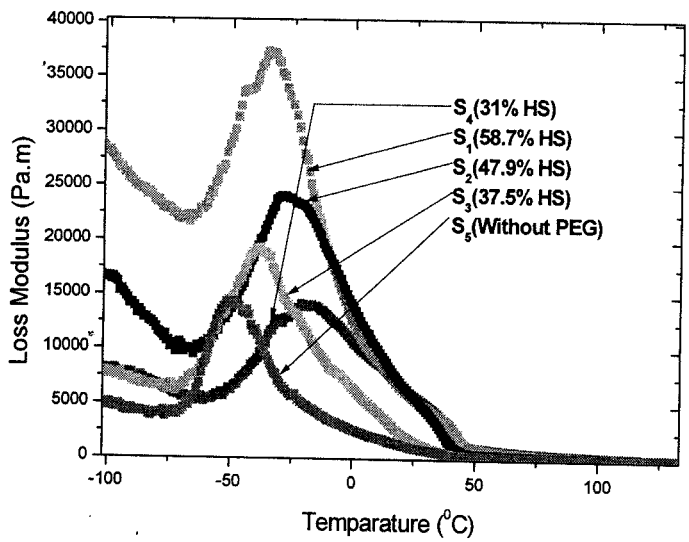

Figure 5.2: Loss modulus of SPU ($S_1 - S_5$)

Tanδ value indicated the amount of energy dissipated in the form of heat during deformation. Tanδ value of SPUs was increased with increasing soft segment (polyol) content in the polymer which signifies the increase of the flexibility of polymer chains.

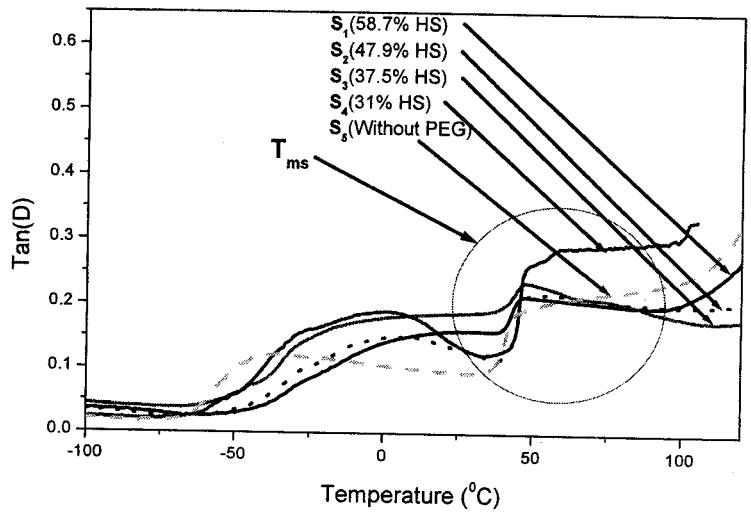

Figure 5.3: Tanδ spectra of SPUs (S_1 –S_5)

5.1.2 Influence of Block Length of Hydrophilic Segment on Thermo-mechanical Properties of SPU

The dissipation factor spectra for the influences of block length of hydrophilic segment (Figure 5.5), shows two peaks for S_7 and S_8 : a broad peak which is correspond to the soft segment T_g, and a secondary transition at about (0.5 T_g). With increase of PEG block length, the T_g of the soft segment was decreased due to the increasing of flexibility of the polymer chains. The low temperature transition is related to the T_g of the soft-segment phase. However, the T_g (Table 5.1) of S_7 (PEG - 2000) is lower than that of the S_8 (PEG - 3400), that may be due to the increase of crystallinity results in a deceases of T_g. This is due to the fact that the crystallization brought about by longer segment

lengths would promote greater purity in the microphase separated soft segment phase. For SPU without PEG (S_9) or small block length of hydrophilic segment such as PEG-200 (S_6), the α transition peak was become unclear. Tanδ values were increased with increasing PEG block lengths which signifies increasing softness or improved tactile properties. The glass transition temperatures of SPUs obtained from loss modulus graphs (Figure 5.4) are tabulated in Table 5.1.

Table 5.1: Glass transition temperature of SPU from DMTA results

Samples	T_g (°C) (Approximate value)
S_1	-33[a]
S_2	-27[a]
S_3	-38[a]
S_4	-19[a]
S_5	-49.5[a]
S_6	-63[a]
S_7	-75[a]
S_8	-72[a]
S_9	-67[a]
S_{14}	-42[b]
S_{15}	38[b]
S_{16}	1.5[b]
S_{17}	-25[b]

[a] value obtained from loss modulus spectra and [b] values obtained from Tanδ spectra.

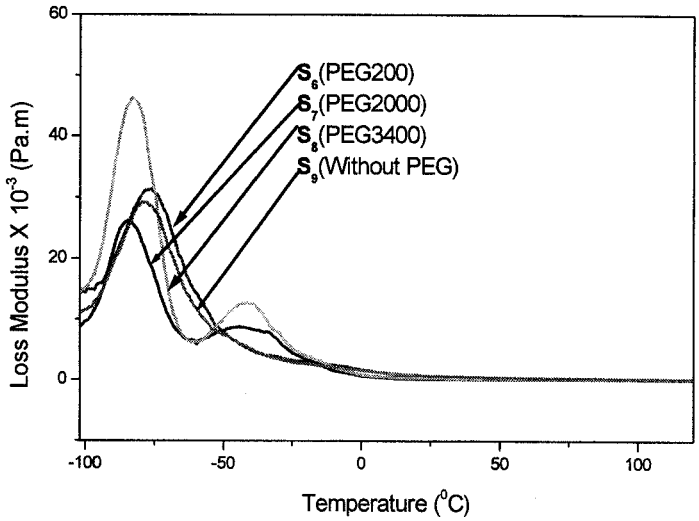

Figure 5.4: Loss modulus of SPU (S_6 – S_9)

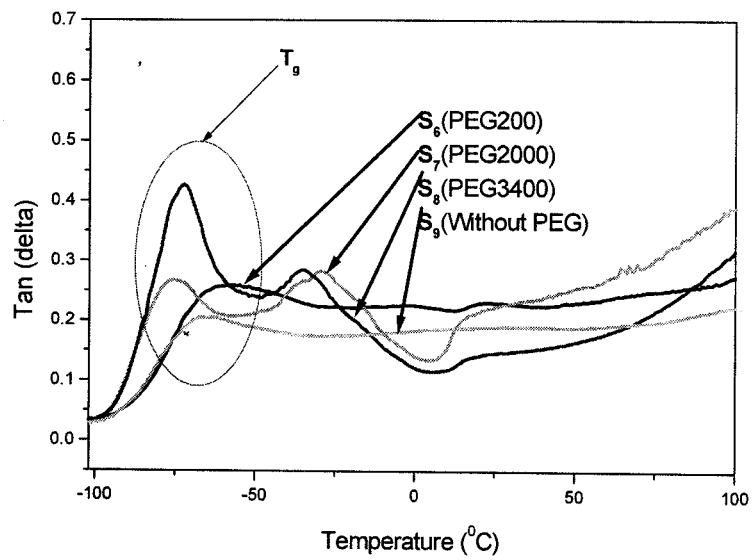

Figure 5.5: Tanδ spectra of SPU (S_6 – S_9)

5.1.3 Influence of Hydrophilic Segment Content on Thermo-mechanical Properties of SPU

DMTA results of SPUs for the influence of hydrophilic segment contents are shown in Figure 5.6-5.7. Figure 5.6 show that the SPU containing 5 wt% of PEG has highest storage modulus. As the content of PEG was decreased with accompanying of increase of hard segment, the interaction between the polymer chains (in S_{10}) was increased and consequently the storage modulus was increased. In all other cases storage modulus are almost same, however S_{12} which contains 15 wt% of PEG has higher tensile storage modulus below the glass transition temperature due to their increasing chain flexibility. The glassy state modulus was increased for SPUs having PEG segment in polymer backbone. The temperature associated with the peak magnitude of tan (δ) is defined as the glass transition temperature (T_g), and its height and shape can provide information about the degree of order and freedom of molecular mobility of soft segment [163]. In addition, the crystallization behavior of the polymers can be described by the shape of the tan (δ) peak [145]. Since tan (delta) peaks are not sharp, therefore it is difficult to measure the exact T_g of corresponding samples. However we could get rough idea about the T_g from tan (delta) peaks. The SPU without PEG 3400 shows a T_g lower than that of SPUs with PEG 3400. Possibly, this is due to an increase in soft segment crystallites (DSC results). The increasing crystalline domain would probably restrict the solubilization of the hard segments in the soft segment domain which causes the T_g to decrease [145]. The thermodynamic incompatibility between the soft and hard segments becomes more distinct in this case. This implies that S_{13} is more phase separated, TEM image supported the fact. Tan (δ) peak is unclear for the sample with 5 wt% of PEG

3400 content which strongly suggested that a notable increase in interaction between the polymers chains (FTIR results). Analysis of the transition in SPUs with different PEG 3400 content suggested that it could arise from the disruption of the associations between the hard and soft segments. Tan (δ) value of the sample with 15 wt% of PEG 3400 content is highest among four samples which indicate greater mobility of the polymer chains due to the presence of flexible PEG 3400. More mobile polymer chains are associated with higher energy when the polymer is subjected to deformation [145].

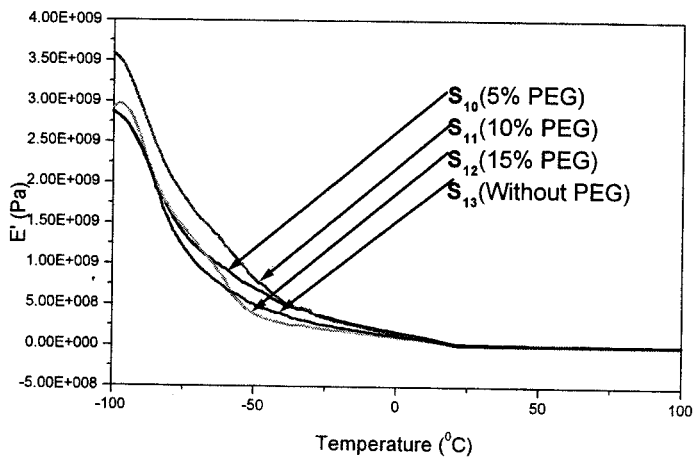

Figure 5.6: Storage modulus of SPU ($S_{10} - S_{13}$)

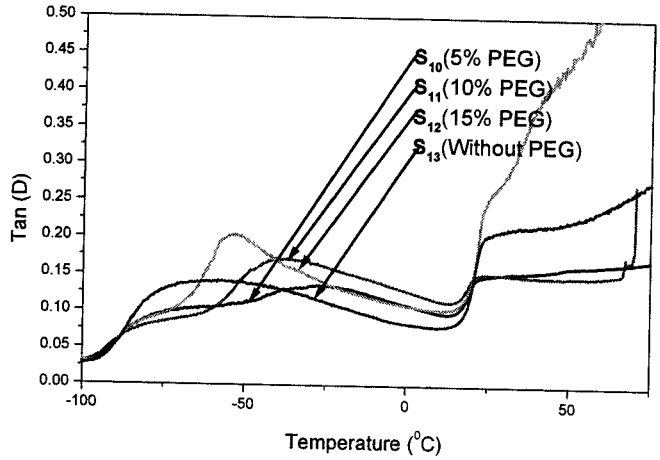

Figure 5.7: Tan (delta) results of SPU ($S_{10} - S_{13}$)

5.1.4 Influence of Hydrophilic and/or Carboxylic Unit on Thermo-mechanical Properties of SPU

The changes in tensile modulus (E') of polyurethanes on heating for the influence of hydrophilic and/or carboxylic unit content are shown in Figure 5.8. The moduli will change with temperature as the molecular motions within the polymer chains was changed. The second order transitions are indicated by the dramatic drop in storage modulus. The glassy state modulus of S_{15} is much higher than the other SPUs regardless of the temperature. The strong interaction between the polymer chains due to the presence of ionic (-COOH) groups is the reason. The storage modulus of sample (S_{16}) which contains both PEG 3400 and DMPA is higher than that of SPU without hydrophilic/carboxylic group. Presence of small quantity of DMPA increases the interaction between the polymer chains, as a result of increase of the modulus.

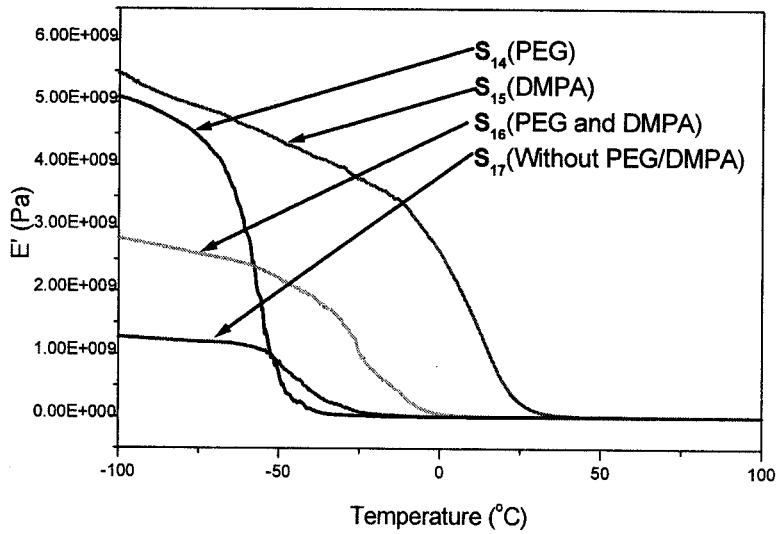

Figure 5.8: Storage modulus of SPU ($S_{14} - S_{17}$)

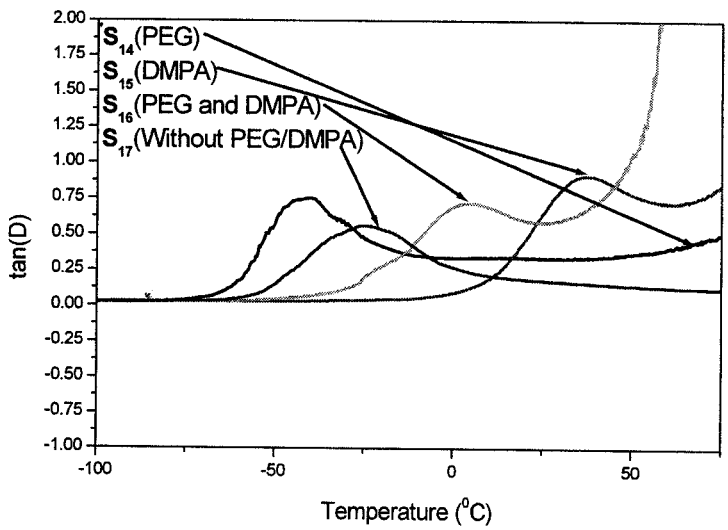

Figure 5.9: Tan (delta) of SPU ($S_{14} - S_{17}$)

The ratio of E"/E' is the loss tangent (tanδ). The peak of either storage modulus curve or the peak of the tanδ curves are often employed to define the glass transition temperature

(T_g). Here we defined T_g from the peak of the tan (δ) curve (Figure 5.9). Glass transition temperatures of SPUs were decreased with the introduction of PEG 3400 segment in the SPU as compared with the sample without any hydrophilic group (S_{17}). The possible explanation for this difference is that the kinetics of the glass transitions are altered with the presence of flexible PEG 3400 segment which increases the mobility of polymer chains as s result of more rapid overall transition. Glass transition temperature of the SPU with DMPA (S_{15}) was increased significantly due to the strong ionic interaction (discussed in 4.1 section) by carboxylic groups which will reduce the polymer backbone mobility due to the formation of ionic cross-links. T_g of S_{16} is lower than the S_{17}, and in between the S_{14} and S_{15}. The presence of DMPA increases the interaction between the polymer chains, and PEG 3400 on the other hand increases the chain flexibility. The tan (delta) value of SPU containing 10 wt% of DMPA is highest among the all SPUs: this phenomenon could be explained by breaking of physical cross-linking imposed by carboxylic group at glass transition temperature which enhances the flow. Since the T_g for SPU without DMPA is -25 °C, therefore, at 38 °C polymer would flow significantly which will increase the tan delta value.

5.1.5 Influence of Mixed Polyol on Thermo-mechanical Properties of SPU

Figure 5.10 and 5.11 shows the tensile storage modulus (E') and dissipation factor (tan δ) respectively as a function of temperature for the influence of mixed polyol block. The glassy state modulus of S_{20} is higher than that of other SPUs. The presence of flexible soft segment (PTMG 2900 and PPG 3000) in the polymer backbone and nearly amorphous structure which would increase the glassy state modulus. There are dramatic

fall of storage modulus of S_{20} at T_g which is quite obvious as compared to the other sample because of the presence of flexible backbone that will increase chain mobility at and above T_g. The order of storage modulus of PCL 3000 based SPUs are as follow: $E'_{S21}>E'_{S18}>E'_{S19}$. Increase amount of crystallinity by reduced phase mixing and stronger inter-chain interaction of ester group will cause higher glassy state modulus of S_{21}. Introduction of flexible PPG 3000 or PTMG 2900 segment in PCL 3000 phase decreases the storage modulus. Storage modulus of S_{18} was slightly higher than the S_{19}, linear and flexible PTMG 2900 segment increases the chain mobility as a result of lower glassy state modulus. However in case of S_{18}, the chain mobility would become a bit tougher due to the presence of methylene group in PPG 3000.

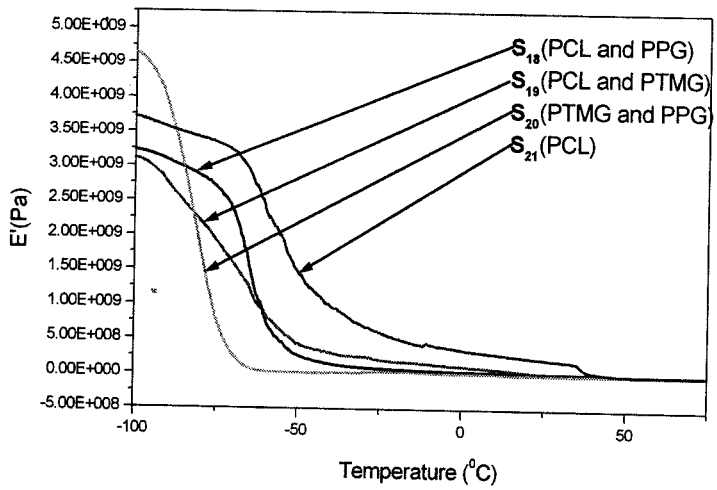

Figure 5.10: Storage modulus of SPU ($S_{18} - S_{21}$)

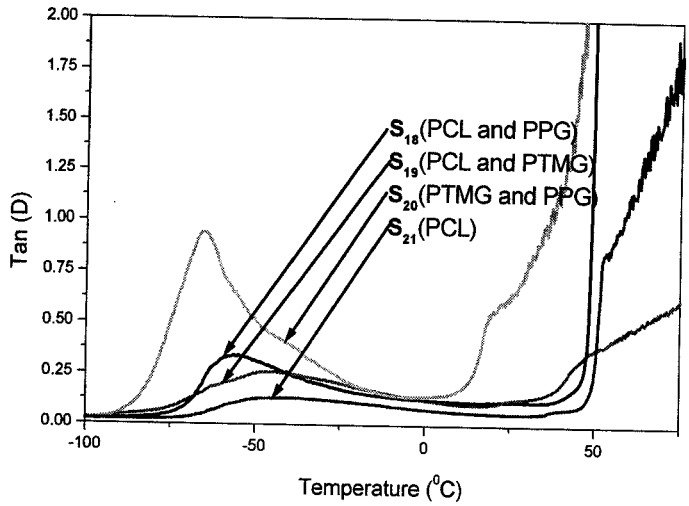

Figure 5.11: Tan (delta) results of SPU ($S_{18} - S_{21}$)

The temperature associated with the peak magnitude of tan (δ) is defined as the glass transition temperature, (T_g), and its height and shape provide information about the degree of order and freedom of molecular mobility of soft segment. In addition crystallization behavior of the polymers can be described by the shape of the tan (δ) peak [163]. Since tan (delta) peaks are not sharp, therefore it is difficult to measure the exact T_g of corresponding SPU. However we could get rough idea about the T_g from tan (delta) peak (Figure 5.11). Glass transition temperature of S_{20} (PPG 3000-PTMG 2900) is lowest among the four samples which is due to their flexible and phase mixed structure. Flexible structures increase the chain mobility that will bring down the T_g. Tan (δ) value for this sample is higher than the other samples which indicates the soft hand feeling or better tactile properties which is suitable for textile applications. The loss tan (δ) is unclear for S_{21} due to the strong interaction by ester groups which will cause the segmental mobility difficult at glass transition temperature. Higher inter-chain

interactions and crystallization (WAXD and DSC results) loosen its elasticity as a result of low tan (δ) [125] for this sample (S_{21}). Thermodynamic incompatibility between the soft and hard segments was become more distinct which implies that the material is more phase separated [135]. Tan (δ) value was increased and glass transition temperature was decreased, when PPG 3000 (S_{18}) or PTMG 2900 (S_{19}) was used along with PCL 3000 soft segment as mixed block due to the increasing chain flexibility and to some extent phase mixing which would make the segmental mobility easier. Tan (δ) value of S_{19} is lower than that of S_{18}. In sample S_{19}, both PCL 3000 and PTMG phase are crystallizable in pure state, therefore form crystalline structure in the resulted SPU (S_{19}). The increase of soft segment crystallites probably would restrict the chain mobility as a result of lower Tan (δ).

5.1.6 Influence of MWNT on Thermo-mechanical Properties of SPU

The concentrations of MWNTs have dominant influence on the thermomechanical properties of the polyurethanes. The storage modulus of polymer was decreased rapidly whereas the tan δ goes through a maximum when the polymer is heated through the glass transition temperature. The storage moduli of various SPUs are shown in Figure 5.12. Gradual decreases of E' in the temperature range between the glass transition temperatures (T_g) could be observed. The modulus changes with temperature as the molecular motions within the polymer changes. The storage modulus was increased with increasing MWNT content in the polymer matrix. This behavior is due to the increase in the exfoliation of the nano tubes in SPU matrix. Since the interfacial area between nano tubes and SPU was increased with the extent of exfoliation. The larger the interfacial area between the nano tubes and the SPU, the stronger would hinder the movement of

polymer chains as a result of higher storage modulus. The properties of polymers composite would depend on a number of factors; the interfacial adhesion between matrix and nano tubes is one of the important factor. The increase of storage modulus with increasing MWNT content signifies the well dispersion of nano tubes in the polymer matrix. The functionalized MWNT would make a strong adhesion with polymer matrix which will make better reinforcing filler effect. The storage modulus of MWNT-SPU was increased with nano tubes content by the stiffening effect of nano tubes. In addition, the presence of MWNT also enables the polymer matrix to sustain a high modulus value to higher temperature. The storage modulus value was increased with increasing the MWNT content in the polymer matrix (Figure 5.12). Therefore the presence of carbon nano tubes enables the polymer matrix to sustain a high modulus with increasing temperature.

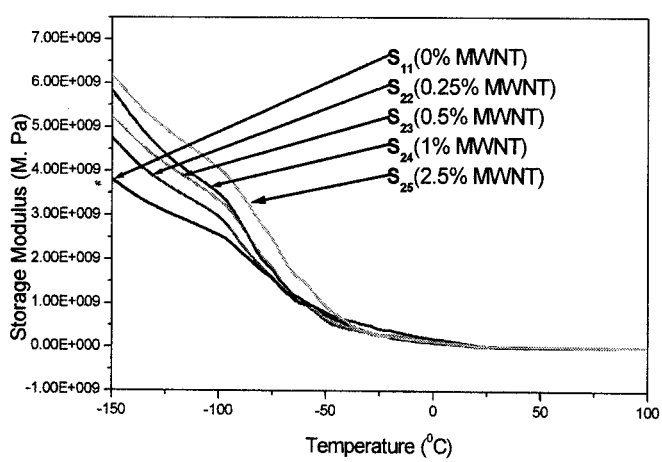

Figure 5.12: Storage modulus of SPU (S_{11}, $S_{22} - S_{25}$)

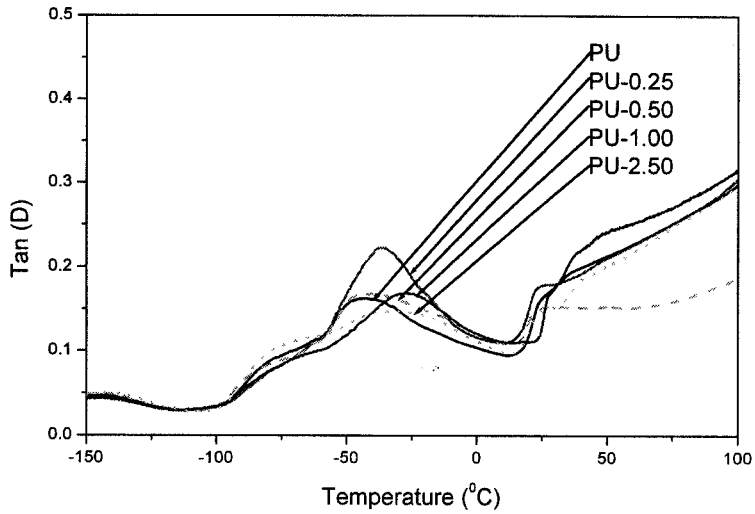

Figure 5.13: Tan (delta) of SPU (S_{11}, $S_{22} - S_{25}$)

Figure 5.13 shows the tanδ peaks of MWNT containing SPU samples. Its height and shape would provide information about freedom of molecular mobility of polymer chains. The peaks were moved to a slightly higher temperature with increasing nano tube content which shows that the T_g of the composite is raised by the addition of the nano tubes [164]. This fact implies that the nano tubes hindered the movement of the polymer molecules. Therefore the MWNT not only influence the crystalline region (DSC results) but also the amorphous region. In other words, nano tubes hinder the segmental motion of the SPU chains. One possible explanation for this difference is that the kinetics of the glass transition temperatures was altered with the presence of nano tubes. MWNT is able to impart stiffness to the polymer matrix. The tanδ peak was broadened significantly with 2.5 wt% of MWNT which indicates that the nano tubes could effectively act as reinforcing filler because of their much larger surface area and stronger interaction with the polymer chains. The improvement in the interfacial

adhesion is also suggested by the decreases in the $(\tan\delta)_{max}$ value with increasing MWNT content in the polymer matrix [148]. The diffraction peak of SPU at 2.5 wt% of MWNT broadened which indicates that the crystallization in 2.5 wt% of MWNT in SPU became slightly difficult. Therefore, this result supports the result from DSC. Tan (δ) value was suddenly increased with 0.25 wt% of MWNT content, higher loss tangent value means the material is viscous, this result is bit strange which is not easily understandable. One possible reason may be little amount of nano particles would help to increase the mobility of polymer chains which results in a more rapid overall transition. This explanation may be a plausible explanation for a shift in tan (δ).

5.2 TENSILE PROPERTIES OF SPU

In this study, soft segment crystal melting point (T_{ms}) was considered as transition temperature for shape memory testing. Some SPUs have no T_{ms} (S_6, S_9, and $S_{14} - S_{17}$) and another two SPUs ($S_7 - S_8$) have low T_{ms}. Because of machine lower temperature restriction, we could not able to carry out shape memory testing for the above SPUs. For these samples, we carried out the uni-axial tensile testing which is presented in Table 5.2. From the tensile results of the ***influence of block length of hydrophilic block length***, we can see that, SPU without hydrophilic segment is tougher than the other samples that may be due to the strong hydrogen bonding (Figure 4.1) in the polymer matrix. That will provide greater order in the hard-segment domains which will increase the cohesion between the hard and soft domain. With the introduction of low molecular weight hydrophilic block such as PEG - 200, both the modulus and strain at maximum load were decreased. Tensile strength and elongation at break are dependent on the combined

effects of hard and soft segments or more precisely the overall morphology of the copolymer [64]. Decrease of modulus was due to the breaking of H-bonds which makes molecules more mobile. On the other hand physical cross linking made by the rigid diphenylmethylene moites contributes high elongation at break for S_9 as compared with S_6. The effective physical cross-link junctions break for S_6 due to the plasticization effect by low molecular weight of PEG molecules. It can be seen from the tensile results of S_7 and S_8 that the elongation at breaks was increased with increasing block length of PEG segment. A large elongation at break is often sign of the greater extent of phase separation [58] (DSC and DMA results). A more effective network structure that restricts the amount of chain slippage and molecular relaxation occurs for these copolymers. These latter effects would prevent the chains from becoming highly aligned or extended during stretching. Therefore, when an external force was imposed on these SPUs, the soft phase would be deformed preferentially. The soft-segment domain with less dissolve hard segment shows a lower modulus and a higher elongation at break. The elongation at break is highest for S_8 having PEG-3400, due to the higher block length PEG which posses greater chain flexibility.

Tensile properties of SPUs for the ***influence of hydroxyl and/or carboxyl*** unit ($S_{14} - S_{17}$) are presented Table 5.2. Tensile strength and elongation are dependent on the effect of hard and soft segment or more precisely the overall morphology of the copolymer. Percent strain at maximum load was increased abruptly when PEG 3400 (S_{14}) was introduced in the polymer backbone as compared to the sample without any hydrophilic groups (S_{17}). The flexibility of the PEG 3400 segment is the reasons which will increase the chain mobility. Modulus on the other hand was decreased with PEG 3400. Dramatic

drop in tensile modulus of PEG 3400 containing SPU is a result of increasing flexibility of the polymer chains and dissolution of hard segment by PEG 3400 segment which increases the mobility of hard segment. Ionic group has strong influence on modulus and elongation. Modulus increases significantly when DMPA was used, and there was slightly decrease of percent strain at maximum load. This may be due to the presence of carboxylic group which causes strong interaction (discussed in 4.1 sections) between the polymer chains which will form an entangled and interconnected network structure that will prevent the chain slippage during loading, hence higher modulus and lower elongation. The modulus of SPU with PEG 3400 and DMPA (S_{16}) was in between S_{14} and S_{15}, due to the presence of DMPA which increases the modulus due to strong interaction. On the other hand PEG 3400 increases the chain flexibility. The modulus of sample S_{16} is lower than that of S_{17}. The presence of PEG 3400 segment causes chain mobility, on the other hand DMPA would restrict the chain mobility, and in this duel effect, PEG 3400's role is prominent in this case.

Table 5.2: Tensile results of SPUs

Samples	Load at maximum load		%strain at maximum load		Modulus	
	(cN)	CV (%)	(%)	CV (%)	(MPa)	CV (%)
S_6	294.2	12.5	284.5	11.5	7.65	8.3
S_7	216.1	10.4	456.3	12.4	6.87	9.5
S_8	637.0	8.5	860.7	9.6	6.83	7.8
S_9	796.0	11.0	411.0	7.3	13.60	5.5
S_{14}	159.7	12.1	999.8	5.3	1.912	9.6
S_{15}	693.8	9.4	187.5	11.1	90.210	1.7
S_{16}	57.7	8.6	343.8	12.4	2.141	11.0
S_{17}	1474.3	11.9	237	13.2	10.057	6.1

5.3 SHAPE MEMORY EFFECTS OF SPU

5.3.1 Influence of Hard Segment on Shape Memory Effect of SPU

The cyclic testing results of SPUs and their shape memory properties are reported in Figure 5.14-5.19 for the influence of hard segment. From the stress-strain curve at temperature of T_{ms} + 20 °C, we can see that stress was increased with increasing percentage of hard segment content in the polymer. Increase of stress with increasing hard segments may be due to the reinforcing effect of hard domain in the soft matrix which increases the cohesion between hard and soft segment. In all cases we carried out the cyclic testing at strain, ε_m = 30 % and 50 % for sample S_2. Sample S_1 even cannot elongate beyond 15 % at T_{ms}+20 °C, which is due to the fact that the rigid diphenylmethylene moiety coupled with hydrogen bonding and dipole-dipole interaction makes the SPU very difficult to stretch as higher percentage of hard segment is incorporated [58]. In addition physical cross-linking made by the rigid diphenylmethylene moieties also contributes to the higher stress with the increase of hard segment. Therefore, we could not able to carry out the cyclic testing at 30 % of strain for S_1. $S_2 - S_5$ were heated at T_{ms} + 20 °C for 10 min in order to make sure that all crystal melting occurred, then elongated at rubbery plateau T_k (T_{ms} + 20 °C) to strain at 30 % (ε_m) at a constant elongation rate of 10 mm min^{-1}. While maintaining the strain ε_m, samples was cooled down to a temperature T_l (T_{ms} – 15 °C) for 15 min and unloaded. Upon removing of constrains at T_l small recovery of strain ε_u occurs. The sample was subsequently heated to T_k in 10 min, and stayed at that temperature for the next 15 min, allowing recovery of strain. This completes one thermomechanical cycles leaving a residual strain, ε_p, where the next cycle would start. This phenomenon may be explained

as entanglement decoupling of molecular chains in the imperfect crystalline part in the first loading [55]. The overall stress-strain curves are almost the same form after the second cycle. Therefore, if the material is used after several cycles of mechanical testing, we can assume certain constant deformation properties under the cyclic deformation. From the cyclic testing results, we cannot find much difference in the recovery ratio however shape fixity is reasonably low with higher hard segment content polyurethane such as S_2. Since the slope of stress-strain curve during cooling represents the elastic modulus of glassy state, the increase of ε_u with increasing soft segment content is caused by the increase of soft segment crystallization. During heating and standing at temperature of T_{ms} + 20 °C under no load, the oriented and crystallized polymer segments are melted and randomized, and the original shape was recovered via a mechanism similar to the entropy elasticity of crosslinked rubbers [59].

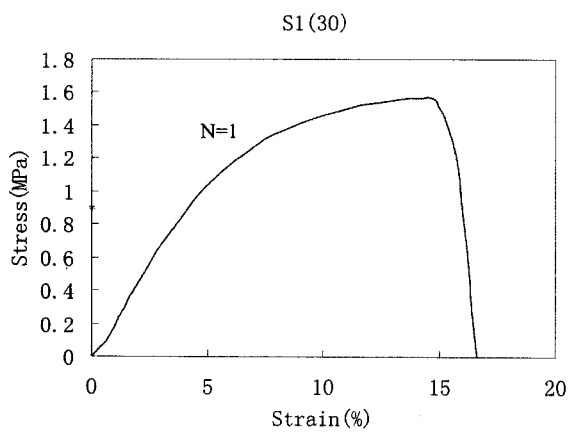

Figure 5.14: Cyclic tensile testing of S_1 (58.7% HS)

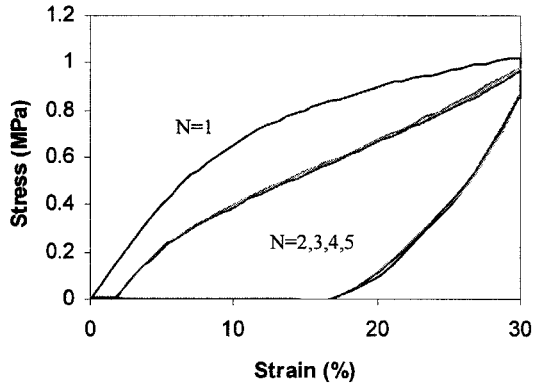

Figure 5.15: Cyclic tensile testing of S_2 (47.9% HS)

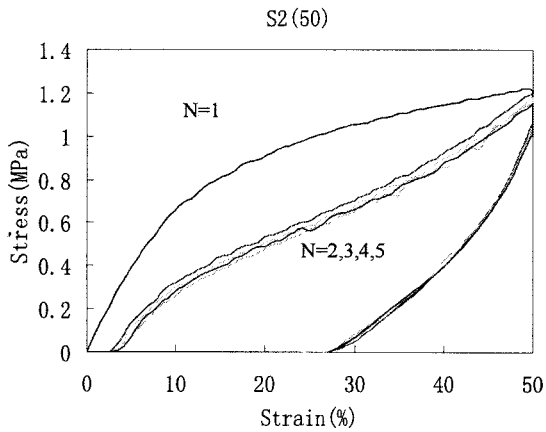

Figure 5.16: Cyclic tensile testing result of S_2 (47.9% HS)

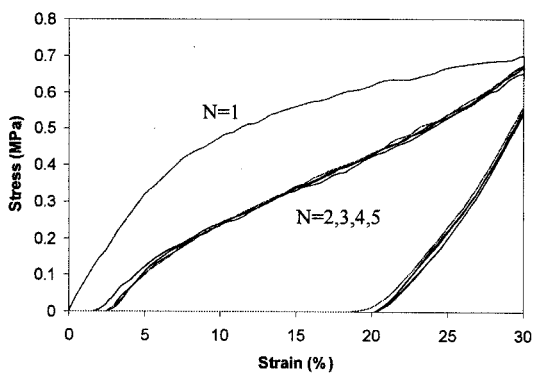

Figure 5.17: Cyclic tensile testing of S_3 (37.5% HS)

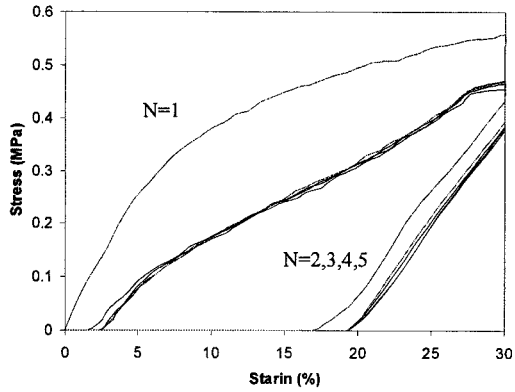

Figure 5.18: Cyclic tensile testing of S_4 (31% HS)

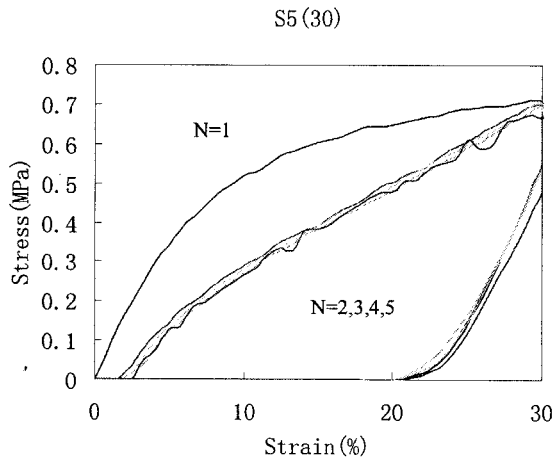

Figure 5.19: Cyclic tensile testing of S_5 (Without PEG)

5.3.2 Influence of Hydrophilic Segment Content on Shape Memory Effect of SPU

In order to clarify the shape memory behavior of SPUs on the influences of hydrophilic segment content, constant strain tests during thermal cycles were carried out. The stress-strain curves were obtained by the cyclic tensile test at maximum strain, ε_m = 50 % at constant temperature T_{ms} + 20 °C. The results under the cyclic loading and unloading are shown in Figure 5.20 – 5.23. Stress-strain curves at T_{ms} + 20 °C follows the same trends as with tensile storage modulus of all four samples as shown in Figure 5.6. When stress

is applied to the SPU, soft segment will be preferentially extended to the stress direction rather than hard segment due to the fact that hard segment is close to glassy state and soft segment is rubbery at above T_{ms} [61]. Stress was decreased with increasing of PEG 3400 content. This phenomenon may be explained by the fact that the micro-Brownian motion of the soft segments is achieved at temperature above T_{ms} due to the presence of flexible PEG 3400 segment [55]. In the cyclic testing results shown in Figure 5.20-5.23, N represents the number of cycles. In all cases, a residual strain, ε_p left after first cycle, where the next cycle would start, this is due to the entanglement decoupling of molecular chains in the imperfect crystalline part occurs in first loading [55]. The overall stress-strain curves are almost the same form after the second cycle. Therefore, if the material is used after several cycles of theromechanical cyclic testing, we can assume certain constant deformation properties under cyclic deformation. In all cases, we can see that ε_u does not change under cyclic deformation and is almost equal to ε_m, which means the excellent shape fixity. However, ε_p is different for different samples. Therefore the recovery property of the deformed specimen depends strongly on the crystalline structure, cross linking imposed by hard segment etc. Strain was recovered by hardening due to the orientation of molecular chains and crystallization progresses. From Figure 5.20 and Figure 5.23 we can see that sample S_{10} and S_{13} have excellent recovery effect due to the two different reasons. As the PEG content in the S_{10} decreases to 5 wt%, the hard segment in the SPU increases which will increase the interaction between polymer chains or impose physical cross linking that will enhance the shape recovery properties. On the other hand, in case of S_{13} having higher order structure, shape is recovered due to recrystallization of soft segment which frozen the micro-

Brownian motion of soft segment and consequently good shape recovery. With increasing PEG 3400 content shape recovery was little bit decreased (Figure 5.21-5.22) due to breaking of physical cross linking imposed by hard segment. Therefore the polymer chains could not back to its original position after removal of stress and during heating.

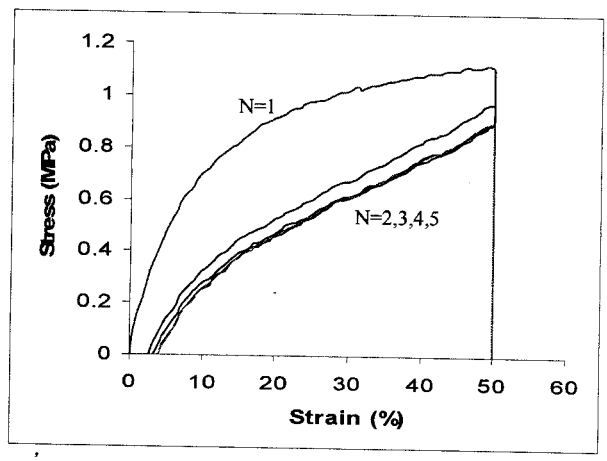

Figure 5.20: Cyclic shape memory result of S_{10} (5% PEG)

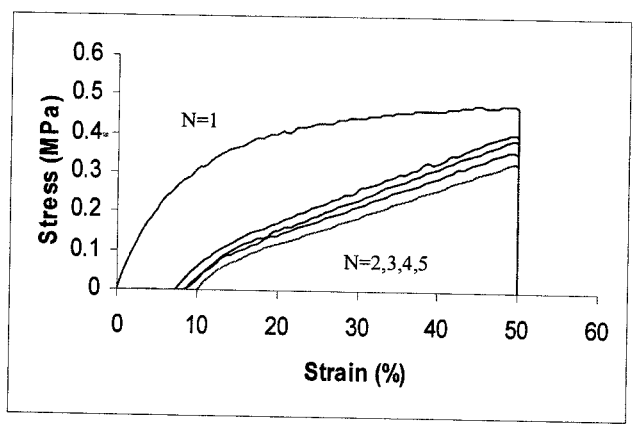

Figure 5.21: Cyclic shape memory result of sample S_{11} (10% PEG)

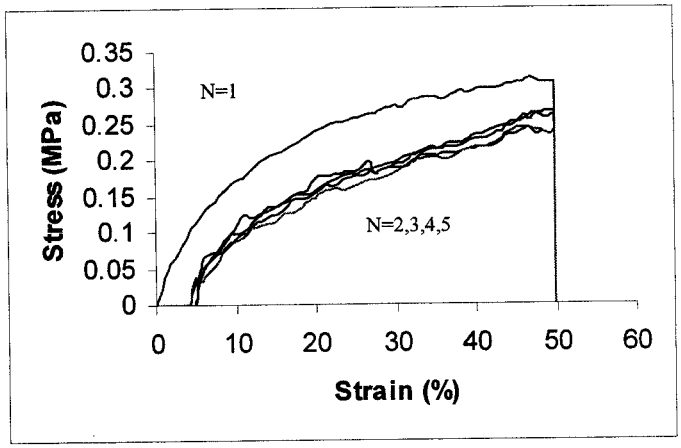

Figure 5.22: Cyclic shape memory result of S_{12} (15% PEG)

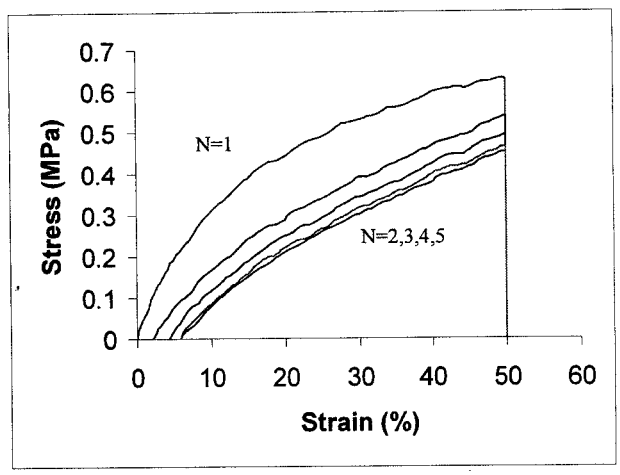

Figure 5.23: Cyclic shape memory result of S_{13} (Without PEG)

5.3.3 Influence of MWNT Content on Shape Memory Effect of SPU

The results of cyclic tensile tests to characterize the shape memory effect of SPUs for the influence of MWNT content are shown in Figure 5.21 and 5.24-5.27. When the deformation is applied to the physical crosslinked SPU, soft segment having low modulus will be extended in the first stage of deformation. As the strain increases, stress will be transferred to the hard domain. When the stress is transferred to the hard domain, the chain slippage between the hard segments will be increased [55]. The presence of MWNT will prevent the chain slippage. That's why stress was increased with increasing

MWNT content in the SPU matrix. The capability of composite interface to transfer elastic deformation depends to a great extent upon the interfacial stiffness and static adhesion strength [165-166]. A high interfacial stiffness will be corresponds to a high composite modulus. Uniform dispersion of the nano particles in the polymer matrix is absolutely necessary for obtaining the reinforcing effect. From the figure we can see that the value of ε_p and the difference in the shape of the first and second curves of the thermomechanical test were decreased as the content of MWNT increases in the SPU. The cyclic deformation properties of the material were changed depending on entanglement decoupling of molecular chains, orientation of molecular chains and hardening due to crystallization [55]. All the SPU samples show same percent of shape retention (fixity). Shape of the SPU is well preserved as judged by the shape retention result [55]. The deformation of the chain is restricted at below T_{ms} as a result of good shape fixity. In contrast, original shape is recovered at above T_{ms} which is due to the strong interactions among the polymer chains and MWNT, and recrystallization. The recoverability of the MWNT-SPU would depend on the presence and content of MWNT. The nano particles are forced to store internal elastic strain energy during loading and freezing. On the basis of this mechanism, the generation of large recoverable strain will be restricted, which would impart higher force levels. The stored elastic strain energy by the nano particles can be released during the recovery cycle. The release of the stored elastic strain energy in the nano particles would result in a more rapid and ultimately more powerful recovery of the polymer-MWNT composite [165]. Shape recovery was better for the ones with 2.5 wt% of MWNT (Figure 5.27) because of the interaction of MWNT and polymer chains. The deformed shape would be recovered by hardening due

to the orientation of molecular chains and crystallization progresses which depends strongly on the crystalline structure, cross linking imposed by hard segment etc. The higher MWNT content which will act as filler in the polymer matrix helps for quick recovery. From the heat of fusion of DSC results, we can see that in all cases amount of crystalline structure are nearly same. Higher amount of MWNT in the polymer matrix will act as molecular cross linker which will enhance the shape recovery.

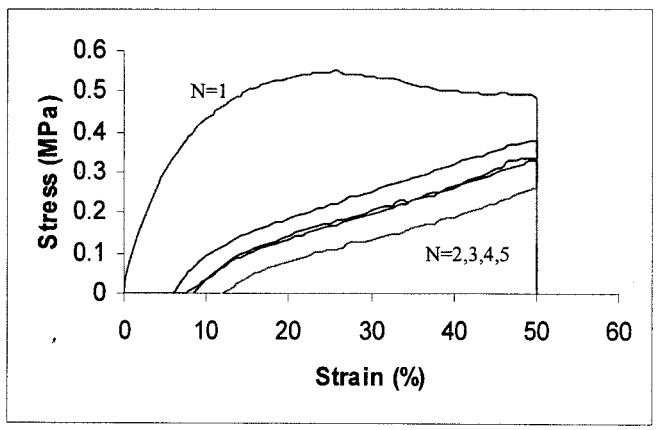

Figure 5.24: Cyclic shape memory result of sample S_{22} (0.25% MWNT)

The MWNTs will interact with the polymer chains, therefore, hinder their mobility, resulting in the increase of glass transition temperature which can be attributed to the higher degree of spontaneous recovery (rubbery elasticity) of the polymer chains at a higher temperature. At the same temperature, the storage modulus was increased with increasing MWNT content in the polymer matrix. This difference is attributed to the visco-elastic response of the SPU materials. However, a lower temperature in the glassy state is needed for the pre-deformation stress to reach zero and the shape fixity to occur. Upon subsequent heating, the stress will begin to recover. The results herein were

provided a foundation for understanding the recovery behavior of SPUs and SPU nano-composites as a function of MWNT content.

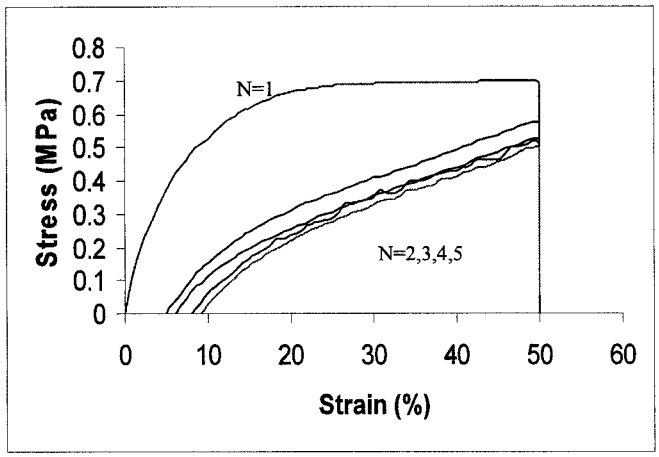

Figure 5.25: Cyclic shape memory result of S_{23} (0.5% MWNT)

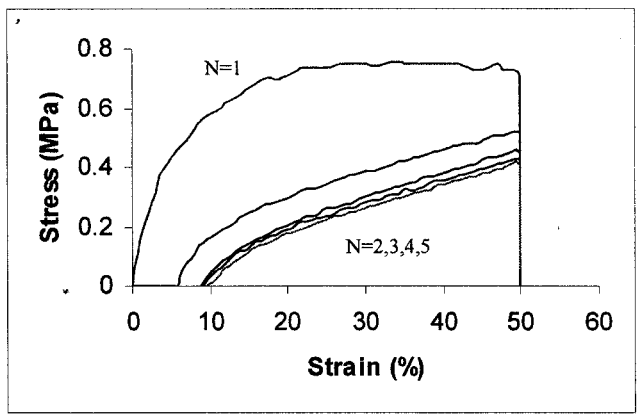

Figure 5.26: Cyclic shape memory result of S_{24} (1% MWNT)

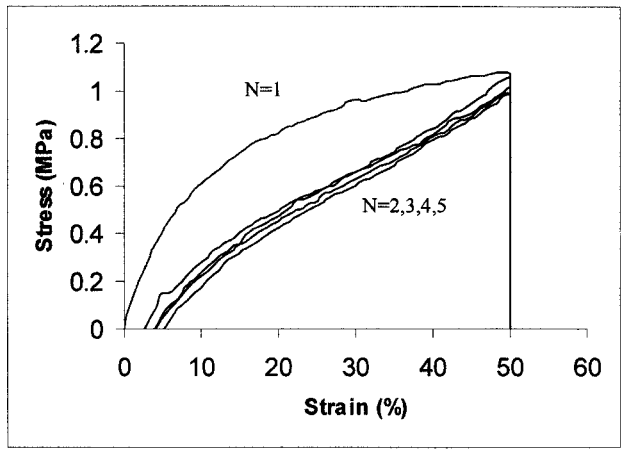

Figure 5.27: Cyclic shape memory result of sample S_{25} (2.5% MWNT)

To achieve shape memory effects, the polymer must have an optimal degree of chemical cross-linking in order to form a "memorable" network or must contain a finite fraction of order crystalline regions which will serve as physical crosslinks [3]. It is the molecular-scale ordering of polymer chains that will produce the shape memory effect. The mechanism of shape memory in polymer networks is based on the temporary storage of low conformational entropy states in molecular chains between cross-linking nodes. The low state of conformational entropy can be stored by either deforming at low stresses above the soft segment crystal melting temperature and then cooling under constraint, or by deforming at relatively large stress at low temperature. For either cycle, heating above the soft segment crystal melting temperature would result in the recovery of the stored strain via an increase in the network free volume, chain rearrangement, and recovery of a stable high entropy state in the polymer. The crystallites acted as physical crosslinks which fixes the extended shape of the SPU. Shape recovery were increased with increasing MWNT content in SPU which is due to the strong interactions among the hard segments and MWNT in the polymer matrix, as the MWNT interact with

polymer as shown by TEM image (chapter 4). Due their long nano size dimensions, MWNT will cause chain entanglement (physical cross linking) in the molecular level where SPU copolymer can make strong interaction among polymer chains to restore the polymer chains back to the original shape.

Sample S_{18} – S_{20} are too soft at T_{ms} + 20 °C, therefore the stress is too low at that temperature, and it was difficult to carry out the shape memory testing. Stress for S_{19} is higher among four samples and its shape memory testing results are shown in Figure 5.28.

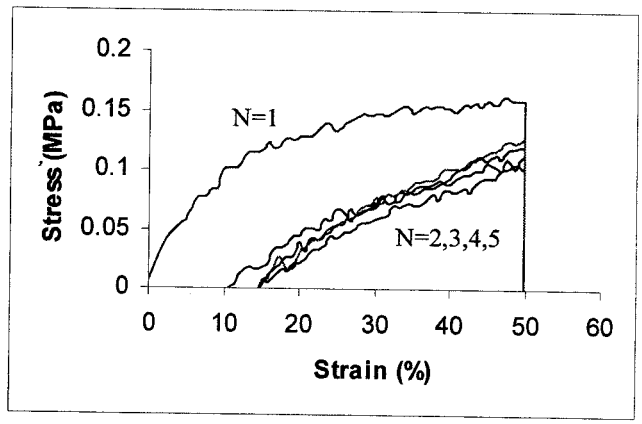

Figure 5.28: Cyclic Shape Memory Result of S_{19} (PCL and PTMG)

5.4 SUMMARY OF MECHANICAL AND THERMOMECHANICAL PROPERTIES OF SPU

There are strong influences of segmental structures on viscoelastic and tensile properties of SPU. PCL 2000 based SPUs are tough due to strong interaction between the polymer chains which was possessed by ester groups. As the hard segment content in SPU increases, tensile storage modulus was also increased due to the strong allophanate

interaction by excess of hard segment content. Ionic interaction by DMPA, and MWNT increases the glass transition temperature, storage modulus, and tensile strength. The increase of glass transition temperature by DMPA would be due to the strong ionic interaction by carboxylic groups which will reduce the polymer backbone mobility. In contrast, with the increase of PEG block length of soft segment, the glass transition temperature was decreased due to the increasing flexibility to the polymer matrix. The low glass transition temperature is related to the T_g of the soft-segment phase. Tanδ values were increased with increasing PEG block lengths and content of PEG which signifies the increasing softness or improved tactile properties. Higher Tan (delta) value indicates the greater mobility of the polymer chains due to the presence of flexible hydrophilic segments which is associated with higher energy when the polymer chains are subjected to deformation. Increased amount of crystallinity by reducing phase mixing and stronger inter-chain interaction of ester group would cause higher glassy state modulus of PCL 3000 based segmented polyurethanes. Flexible polyol segment such as PTMG 2900 or PPG 3000 along with PCL 3000 will cause phase mixing of SPU which would decrease the glass transition temperature of mixed block of SPU. The thermomechnical properties of MWNT reinforced SPU depend on the interfacial adhesion between the MWNT and polymer matrix. The tensile storage modulus was increased with increasing MWNT content in the SPU. The increase of storage modulus with increasing MWNT content signifies the well dispersion of nano tubes in the polymer matrix. Presence of MWNT content increases the glass transition temperature of SPU due to the increasing polymer chains stiffness which would hinder the segmental mobility.

Tensile strength and elongation at break are dependent on the combined effects of hard and soft segments or more precisely the overall morphology of the copolymer. The introduction of low molecular weight hydrophilic block such as PEG – 200 will decrease the modulus. Decrease of modulus with PEG 200 molecules is due to the breaking of hydrogen bonding which will make the polymer chains more mobile. In contrast, modulus was increased significantly when DMPA was introduced in the SPU backbone due to the presence of carboxylic groups which would cause strong interaction between the polymer chains. These entangled and interconnected network structures would prevent the chain slippage during loading as a result of higher modulus and lower elongation.

Shape memory properties of the SPUs have been improved by increasing micro-crystalline structures or by physical corss-linking between the polymer chains. The recovery properties of the deformed specimens depend strongly on the crystalline structure, or cross linking imposed by hard segment. Shape is recovered due to recrystallization of soft segment which frozen the micro-Brownian motion of soft segment and consequently good shape recovery. With increasing the PEG 3400 content in SPU, the shape recovery was decreased due to the breaking of physical cross linking imposed by hard segments. Therefore, the polymer chains could not be able to return to its original position after removal of forces. Strain was recovered by hardening due to orientation of molecular chains and crystallization progresses. The shape recoverability of the MWNT containing SPU would depend on the content of MWNT. The shape recovery property of MWNT containing SPU was increased due to the strong interactions among the polymer chains and MWNT, and recrystallization of soft

segments. The nano particles are forced to store internal elastic strain energy during loading and freezing. The store energy was released during recovery process. Therefore, shape recovery effect was increased with increasing MWNT content in the SPU matrix.

CHAPTER 6

WATER VAPOR TRANSPORT PROPERTIES AND FREE VOLUME OF SPU

This chapter presents the water vapor transport properties of all SPU samples. Six factors on water vapor transport properties have been considered. These are influence of hard segment, block length of hydrophilic segment, content of hydrophilic segment, hydrophilic and/or carboxylic group, mixed polyol block and multi wall carbon nano tube. Finally, free volume was measured by PALS of four selected SPUs, and their water vapor permeability was correlated with free volume data.

6.1 WATER VAPOR TRANSPORT PROPERTIES OF SPU

As we know that water vapor transport through nonporous membrane occurs by sorption – diffusion - desorption, therefore the sorption data are important for characterization of mass transfer properties. Here, we characterized mass transfer properties of the SPUs by equilibrium sorption, dynamic sorption and water vapor permeability measurements.

6.1.1 EQUILIBRIUM AND DYNAMIC SORPTION OF SPU

6.1.1.1 Influence of Hard Segment on Sorption of SPU

The equilibrium sorption data of SPUs at different temperatures are given in Table 6.1. Figure 6.1 shows the influence of hard segment on dynamic sorption. At soft segment

crystal melting point, dynamic sorption was influenced by the quantity of soft domain present in the SPU matrix. The equilibrium sorption was increased linearly with increasing temperature (Table 6.1). When the temperature reaches the crystal melting temperature there are significant change of water sorption of SPUs. The increase of water sorption before crystal melting was due to the increase of free volume. From the DMTA results we observed that the T_g of $S_1 - S_5$ is from (-39) – (-50) °C, therefore the T_g of the polymer is well below the experimental temperature. The polymer will be in a rubbery state in the experimental temperature range that will increase the chain mobility which will allows easier penetration of the water vapor molecules [59]. The crystal melting would increase the chain mobility in the soft segment region which will provide more gaps for water vapor molecule. With increasing hard segment content in the segmented polyurethane the sorption was decreased due to the decrease of free volume. The hard segments act as reinforcing filler which would be preventing the segmental mobility of the polymer chains. As the hard segment content was increased, the percentage crystallinity also decreases, that's the reason for decrease equilibrium sorption at crystal melting temperature with increasing hard domain in the polymer. Another interesting observation can be seen that, the sample S_4 and S_5 have nearly the same amount of HS, however the equilibrium sorption for S_4 (having PEG-200 component) is higher than that of the sample S_5 (without PEG-200). Therefore, the introduction of polar groups in the polymer chains could attract more water molecule.

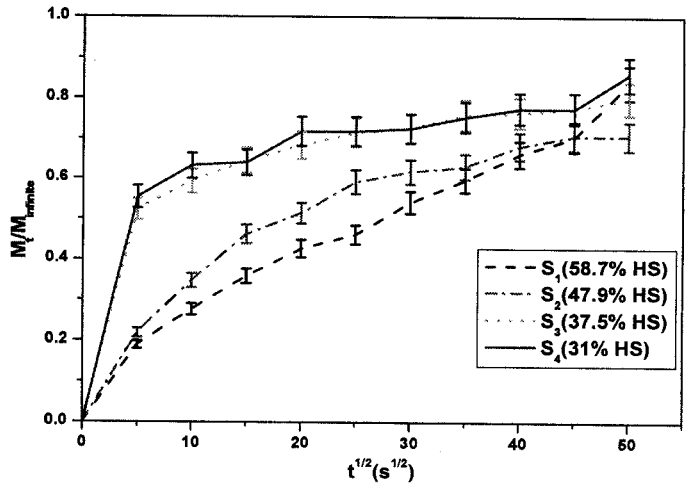

Figure 6.1: Dynamic sorption of S_1 – S_4 at 45 °C

6.1.1.2 Influence of Hydrophilic Block Length on Sorption of SPU

The equilibrium sorption data for SPU for the influence of hydrophilic segment block length are presented in Table 6.1. From the Table 6.1, it can be seen that the SPU without PEG i.e. S_9 has very low equilibrium water sorption as compared to other SPUs due to the presence of hydrophobic hard domain which will prevent water sorption. For this sample, the increase of sorption with increasing temperature is not significant as compared to the other samples. The hard segment acts as reinforcing filler in soft matrix which will prevent the increase of free volume. With the increase of block length of PEG, sorption was increased with temperature due to the two reasons. First of all with higher block length of PEG, there are an increased number of polar groups which can attract water molecules. The second reason for higher water sorption is due to the increase of free volume. As the block length of PEG was increased, the molecules are more flexible, therefore with increase of temperature, the free volume will also increase

abruptly which will provide more paths for water vapor molecules. The dynamic sorption and equilibrium sorption for sample S_8 at various temperatures are shown in Figure 6.2 and 6.3 respectively. From the WAXD and DSC data we found that in all SPUs there are little crystalline structure (except S_9), therefore in all cases the increase of sorption with the increase of temperature is due to the presence of hydrophilic component and increase of free volume. Again, from the dynamic sorption result it can be seen that, at the beginning, the curves seem to show a slight sigmoidal shape which indicates the non-Fickian sorption trend [167].

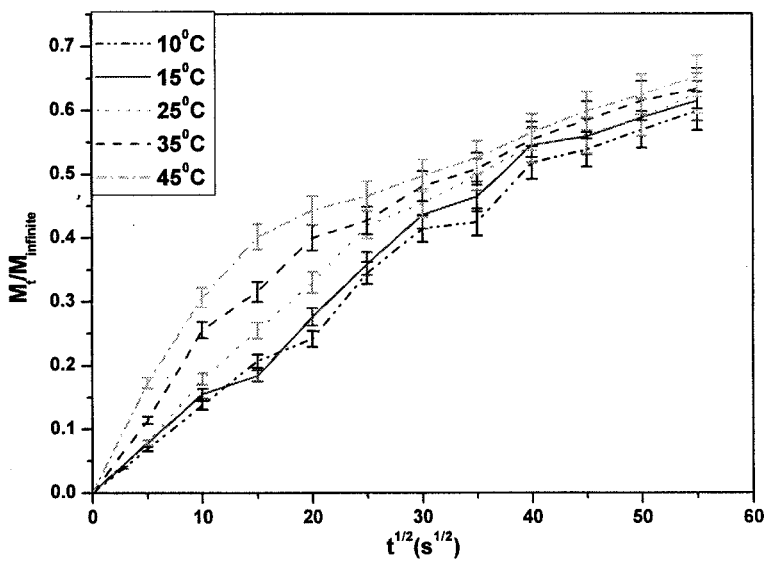

Figure 6.2: Dynamic sorption of S_8 (PEG-3400)

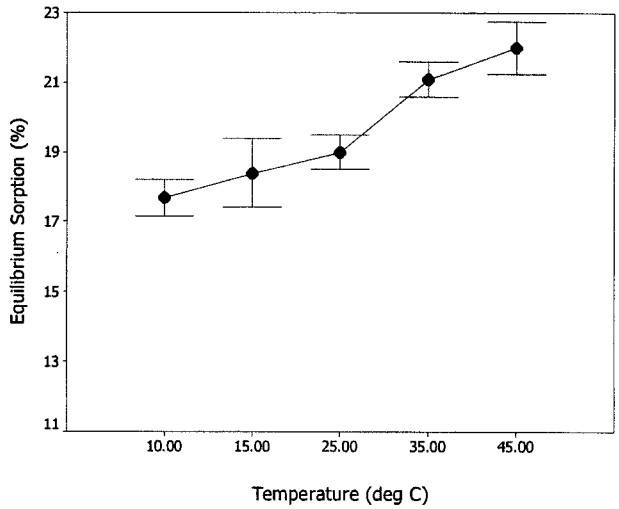

Figure 6.3: Equilibrium sorption of S_8 (PEG-3400)

6.1.1.3 Influence of Hydrophilic Segment Content on Sorption of SPU

The equilibrium sorption as a function of temperature for the influence of hydrophilic segment contents are shown in Figure 6.4 and the results are tabulated in Table 6.1. Experimental result shows that water sorption was increased with increasing PEG 3400 content in polymer backbone due to the increasing hydrophilicity. Water sorption was again enhanced with increasing temperature. Once the water molecules was absorbed by the polymer chains which could increases the chain flexibility with increasing temperature due to plasticization effect of water molecules and polymer chains that will provide more space for water molecules. In addition, increasing temperature increases the free volume which would also enhance the sorption. Equilibrium sorption was further enhanced in the soft segment crystal melting temperature which would cause discontinuous density changes inside the membrane that will provide more gaps for water molecules. Interestingly, for the samples with 10 wt% of PEG 3400 (S_{11}) and 15 wt% of PEG 3400 (S_{12}), desorption occurred above 25 °C. This desorption could be

explained by the lower critical sorption temperature phenomenon for PEG 3400 chain [88].

Table 6.1: Equilibrium sorption (g/g %) data of SPUs

Sample	10 °C		15 °C		25 °C		35 °C		45 °C	
	ES	CV%	ES	CV%	ES	CV%	ES	CV%	ES	CV%
S_1	0.95	2.4	0.98	1.8	1.15	2.3	1.18	3.2	2.3	1.6
S_2	0.96	1.5	1.06	2.1	1.08	2.5	1.31	0.5	2.5	1.1
S_3	1.17	2.8	1.36	3.5	1.44	1.2	1.51	1.5	8.2	0.8
S_4	1.18	2.5	1.24	1.8	1.36	0.9	1.71	0.5	8.6	0.4
S_5	0.48	1.5	0.49	1.1	0.58	1.6	0.82	1.7	6.50	1.2
S_6	3.76	1.6	4.60	1.9	5.40	2.2	6.00	1.9	6.50	1.1
S_7	12.3	1.0	13.7	0.8	15.58	2.5	16.95	1.1	18.40	0.8
S_8	17.69	1.5	18.40	1.7	19.20	2.1	21.10	1.7	22.00	1.2
S_9	1.23	1.1	1.50	1.0	2.10	1.8	2.50	0.8	3.60	2.1
S_{10}	7.23	2.1	8.5	1.7	9.15	1.5	10.40	1.2	11.20	1.8
S_{11}	17.65	0.9	18.50	1.3	22.10	1.0	20.45	1.4	19.15	1.5
S_{12}	18.9	1.2	20.22	1.1	24.10	1.7	30.63	2.1	22.25	2.6
S_{13}	1.67	1.6	2.10	0.8	3.50	1.8	4.50	1.2	4.95	1.5
S_{14}	6.5	2.7	7.25	1.8	8.18	1.6	9.12	1.3	10.19	1.7
S_{15}	3.26	0.4	3.81	0.9	4.15	0.7	4.70	1.1	5.15	0.5
S_{16}	4.75	0.4	5.28	0.6	5.60	0.5	5.95	0.8	6.35	0.8
S_{17}	1.61	2.4	1.96	2.3	2.15	1.9	2.80	3.2	3.87	0.8
S_{18}	13.18	2.7	14.57	1.7	16.25	2.1	17.15	0.8	18.39	1.5
S_{19}	12.44	1.7	13.1	1.3	13.55	0.7	14.15	1.5	15.87	1.8
S_{20}	20.17	2.3	21.50	1.5	22.85	1.2	24.69	0.8	25.85	1.5
S_{21}	6.72	2.5	7.18	1.7	8.30	1.2	8.88	2.1	9.35	1.6
S_{22}	17.80	1.8	18.64	1.1	23.28	1.5	21.20	0.8	20.67	1.3
S_{23}	17.50	1.1	18.40	1.7	22.50	2.0	20.68	1.6	19.50	1.2
S_{24}	16.88	1.5	17.50	1.0	21.35	2.5	21.75	1.7	22.15	1.9
S_{25}	16.50	1.8	17.15	1.5	20.85	2.1	21.28	1.8	21.95	1.0

ES – equilibrium sorption data, CV% – coefficient of variation of measurements

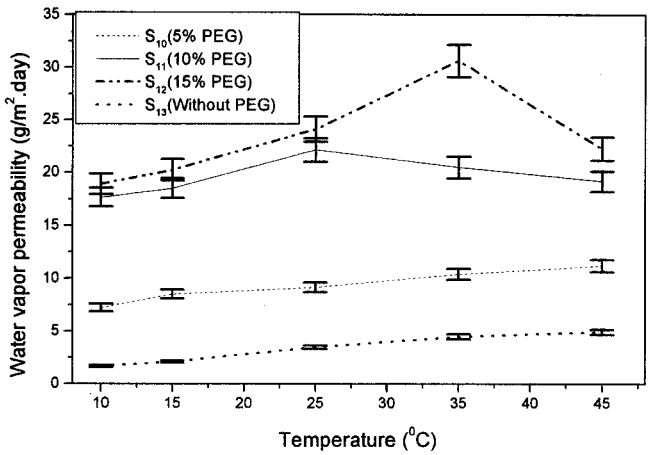

Figure 6.4: Equilibrium sorption of SPU (S_{10}-S_{13})

6.1.1.4 Influence of Hydrophilic and/or Carboxylic Unit on Sorption of SPU

Equilibrium sorption data for the influence of hydrophilic and/or carboxylic unit content in SPUs are presented in Table 6.1. Sorption of SPU without any hydrophilic/functional (S_{17}) group is low regardless of temperature. Since there are no hydrophilic groups, therefore in this case some water molecule can be only absorbed by amorphous region of the polymers. There is abrupt increase of sorption for SPU with PEG 3400 due the presence of more hydrophilic group which could easily absorb the water vapor molecules. Increase of polar groups will increase the affinity of the membrane with water vapor molecules. This phenomenon indicates that the solubility of water molecules to polyurethanes was increased when PEG 3400 was introduced in the polymer backbone. The high value of equilibrium sorption therefore is attributed to the reduction in intermolecular density of the polymer due to the chain flexibility restriction. The sorption of SPU with DMPA (S_{15}) is lower than that of sample with PEG 3400, however higher than the S_{17}. This fact is probably due to the presence of carboxyl

groups which causes strong interaction between the polymer chains, and few carboxyl groups are free which could absorb water molecules. The sorption of S_{16} (containing both PEG 3400 and DMPA) is in between the S_{14} and S_{15} however higher than the S_{17}. The sorption of all SPU increases with increasing temperature that may be due to the fact that some of the intermolecular interactions between the polymer chains may be weakened or broken. This results in the polymer matrix being more flexible in nature which would provide more paths for water molecules.

6.1.1.5 Influence of Mixed Polyol Block on Sorption of SPU

Absorptivity of all SPUs was influenced by the mixed polyol block due to the difference of microstructure. Table 6.1 shows that, water sorption of S_{20} was highest among four samples. The equilibrium sorption of this sample was influenced by the presence of hydrophilic segment i.e. PEG 3400 and almost amorphous loose structure which would provide more space for water vapor molecules. Water sorption for all samples was enhanced with increasing temperature. Once water molecules were absorbed by the polymer chains which could increase the chain mobility with increasing temperature due to plasticization effect of water molecules and polymer chains which would provide more space for water molecules in the polymer membranes. In addition, increasing temperature will increase the free volume which will also enhance the equilibrium sorption.

The sorption of S_{21} is lowest among the four SPUs, due to the presence of ester groups which will cause strong inter-chain interaction that hinders the equilibrium sorption. Sorption of PCL 3000 based SPU was increased when PPG 3000 or PTMG 2900 was

used along with PCL 3000 segment due to the increasing chain mobility. When the experimental temperature reached soft segment crystal melting point which will cause discontinuous density changes inside the membrane, sorption was further enhanced.

6.1.1.6 Influence of MWNT Content on Sorption of SPU

From Table 6.1, we can see that presence of impermeable MWNT at 1 and 2.5 wt% concentration in SPU matrix reduces the equilibrium water sorption. The increase of the mean free path of the water molecules to pass through the matrix of SPU-MWNT seems to be the reasons of reduced water sorption [147]. In fact, the hydrophilicity/ hydrophobicity characteristics of the polymer membrane are the major parameter determining the preferential sorption. In all cases water sorption was increased with increasing temperature due to increase of free volume. There were significant changes of sorption at T_{ms}. The increase of water sorption of S_{22} above T_{ms} was higher than the other SPUs, since the amount of crystalline structure content in the S_{22} was little higher than the other samples, therefore the crystal melting provides more space for water molecule of S_{22}. The desorption phenomena of sample S_{11}, S_{22}, S_{23} above 35 °C could be explained by the lower critical sorption temperature phenomenon for PEG 3400 chain [88].

6.1.2 WATER VAPOR PERMEABILITY (WVP) OF SPU

6.1.2.1 Influence of Hard Segment on WVP of SPU

Water vapor permeability for the influences of hard segments are presented in Table 6.2 and shown in Figure 6.5. From the WVP data we can see that, with the decrease in HS

content in the polyurethane (S_1 - S_4) the mass transfer was increased due to the increase of flexibility in the polymer chains. The decrease of mass transfer with increasing hard segment domain is due to the reduction in soft segment mobility because of increasing phase mixing between hard and soft segment [169]. The increase in hard segment contents will produce greater intersegment mixing which in turn, will increase the membrane density. A higher intersegment mixing and membrane density will always induce lower water vapor permeability. With the introduction of hydrophilic component in the polymer backbone the water vapor permeability was also increased. There are two reasons for this happening; first of all, PEG would increase the flexibility in the polymer chains which will increase the free volume. Therefore the water molecules will pass through the membrane easily. Secondly, introduction of PEG component would increase the hydrophilicity in the polymer which will also enhance the water vapor permeability. From the principle of mass transfer through the non-porous membrane, we know that there are three steps, sorption-diffusions-desorption. Water vapor on the high-pressure side of the membrane is dissolved in the membrane material, and then diffuses down a concentration gradient to the low pressure side of the membrane where the vapor would be disrobed. PEG molecule helps to absorb more water molecules. Again from the Table 6.2, we can see that, there are significant changes of WVP at 45 °C, because crystal melting occurs at this temperature which would provide more paths for water molecule to pass through the membrane. This phenomenon (Figure 6.6) follows the same trend as with increase of percentage of crystallinity with increasing amount of PCL (Figure 4.18) in the SPUs. The mobility of the PCL segments is enhanced by soft segment crystal

melting, the mobility of the closely linked PEG 200 segments is also increased which will make path through which water vapor molecules could easily pass [170].

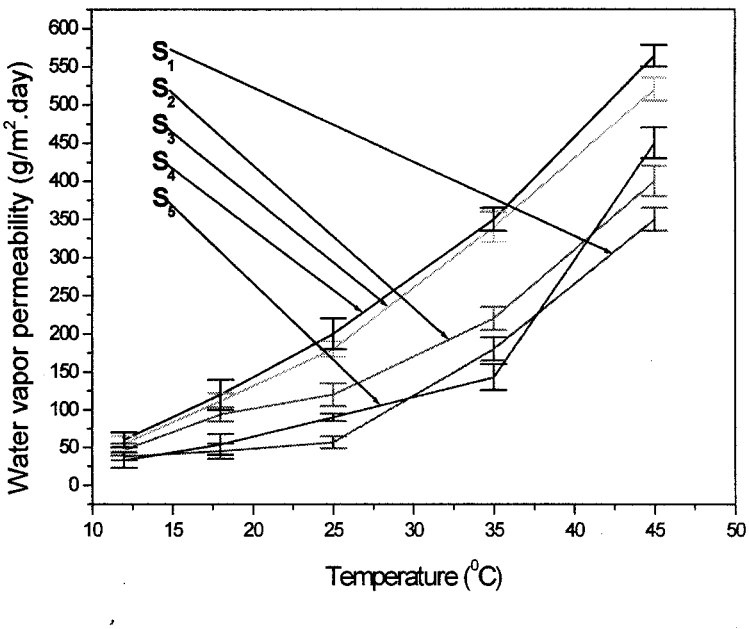

Figure 6.5: Water vapor permeability of SPU ($S_1 - S_5$)

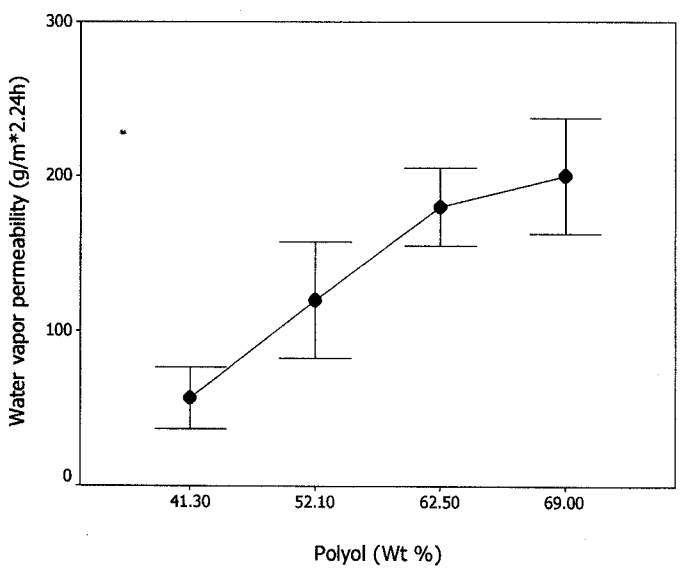

Figure 6.6: Effect of polyol content on WVP at 45 °C

The Log (WVP) versus temperature plot of S_4 is shown in Figure 6.7. The figure shows the perfect fit of Arrhenius relationship.

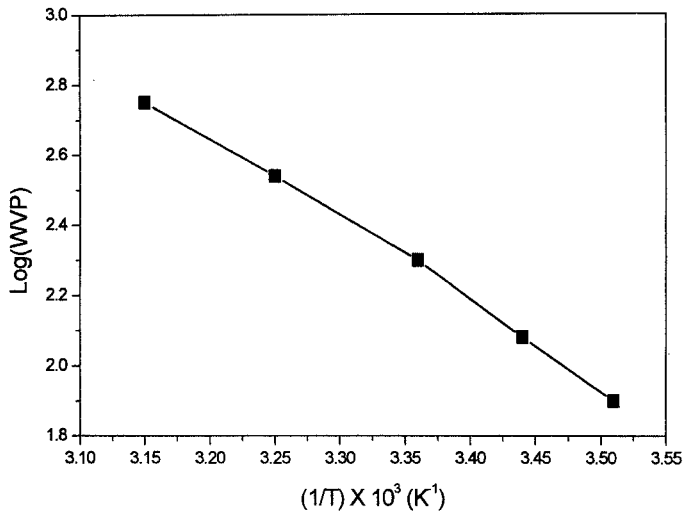

Figure 6.7: Arrhenius plot for sample S_4 (31% HS)

It is evident from the Figure 6.7 that the slope of the linear curves was increased with increase in temperature which indicates that the permeability process is temperature dependent. This follows the Arrhenius relationships for permeation as:

$$P = P_0 \exp^{-Ep/RT} \text{ ----------(6.1)}$$

Where, E_p is the activation energy required to create opening between the polymer chains to permit penetrant molecules to pass. E_p is the function of inter- and intrachain forces [76]. The activation energy can be considered as the energy to "loosen" the polymer structure which is related to the change in thermal expansion. An increase in

temperature will provide energy to increase segmental mobility which will increase the penetrant diffusion rate.

6.1.2.2 Influence of Hydrophilic Block Length on WVP of SPU

The WVP of SPUs for the influences of hydrophilic block length follows the same trend (Figure 6.8) with the equilibrium sorption results. The permeability of small molecule through the nonporous polymer membrane was enhanced when their solubility and diffusivity in polymer increases [171]. From the DMTA data we observed that the T_g of all polymers are well below the experimental temperature, therefore the fractional free volume will increase with temperature according to the equation 6.2 which will provide more path for water vapor molecule to pass through the membrane.

$$FFV = f_g + (\alpha_1 - \alpha_2)(T - T_g) \text{ ------(6.2)}$$

where α_1 and α_2 are thermal expansion coefficients in the rubbery and glassy states, respectively, f_g fractional free volume at T_g which is constant (0.025) and T is the experimental temperature. The increase of free volume in the polymer, and the micro-Brownian motion of the soft segment obviously will increase the intermolecular gap large enough to allow water vapor molecule to pass through the membrane [172]. With increasing the block length of PEG component in polymer, the WVP was also increased due to the increase of flexibility of the polymer chains and increase of hydrophilicity. The increase of hydrophilicity and chain flexibility increases the interaction between water molecules and polymer chain segments. On the other hand longer polymer chains

of PEG originate larger polymer network holes that would also enhance the water vapor permeability.

The Log (WVF) versus temperature plot of sample S_8 was shown in Figure 6.9. Figure 6.9 shows the perfect fit of Arrhenius relationship. It is evident from the Figure 6.9, that the slope of the linear curve was increased with increase in temperature which indicates that the permeability process is temperature dependent.

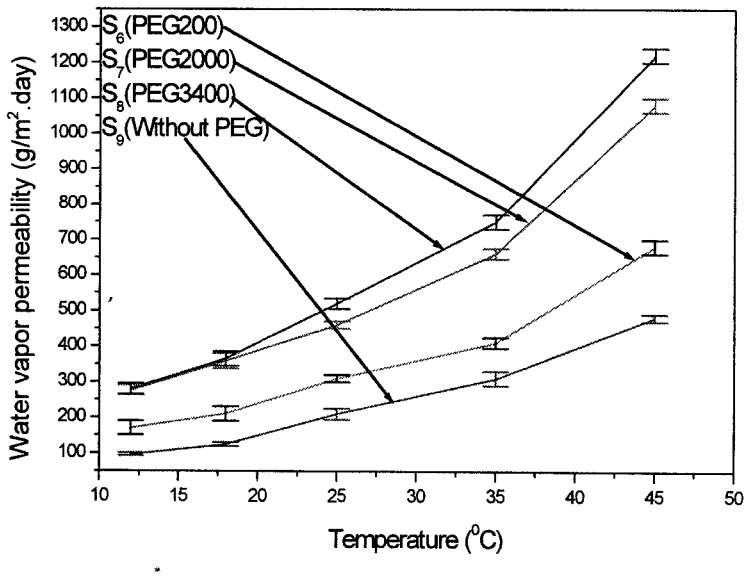

Figure 6.8: WVF results of SPUs (S_6 –S_9)

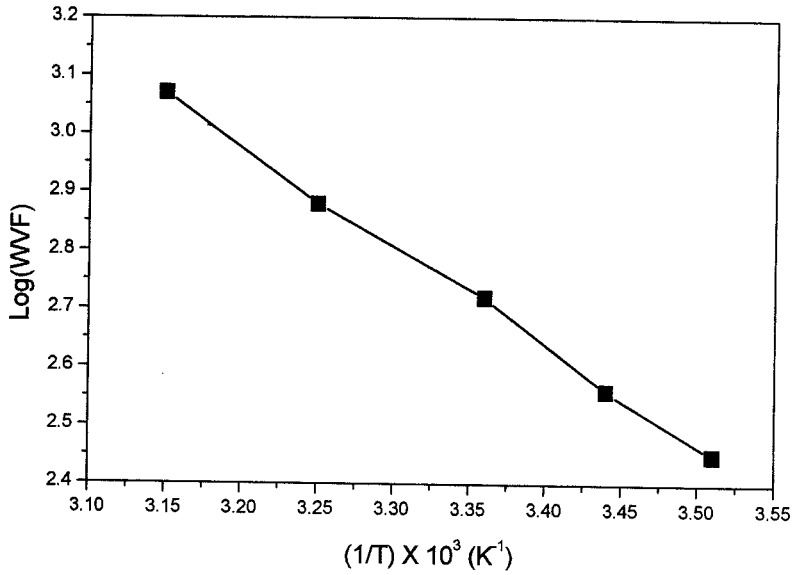

Figure 6.9: Arrhenius plot of sample S_8 (PEG 3400)

6.1.2.3 Influence of Hydrophilic Segment Content on WVP of SPU

Water Vapor permeability data of SPUs for the influences of hydrophilic segment content are presented in Table 6.2 and Figure 6.10-6.11. From the DMTA results we observed that glass transition temperature (T_g) of all samples is well below the experimental temperature. Above T_g expansion of the soft segment in a larger volume occurred which results in an expansion of non-physical voids that would permit the water vapor molecules to transmitted through the polymer films easily. Water vapor permeability of SPUs was also the function of the content of hydrophilic groups at fixed temperature (Figure 6.11). The permeability was further enhanced at the soft segment crystal melting temperature. High molecular weight hydrophilic segments (PEG 3400) enhance the permeability due to the increase of the hydrophilicity which will increase

the interactions between water vapor molecules and polymer chains. Longer polymer chains of PEG would originate larger polymer holes, and their chain flexibility may be additional reasons for increasing WVP with increasing PEG 3400 content in the polymer membranes [149]. The crystal melting point temperature of S_{12} (15 wt% PEG 3400 content) was shifted to the higher temperature. However the WVP of S_{12} below the soft segment crystal melting temperature is still higher than the other samples which may be due to increase of PEG 3400 content that increases the hydrophilicity as a result of increase of WVP. There is sharp change of WVP between 35 to 45 °C due to soft segment crystal melting for S_{12}. In contrast WVP results varies inversely proportional to the thickness of nonporous membrane as shown in Figure 6.12.

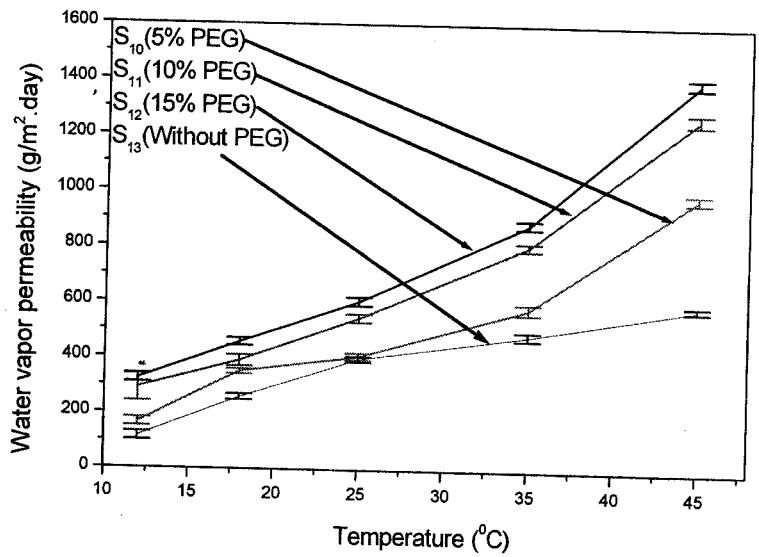

Figure 6.10: WVP of SPU ($S_{10} - S_{13}$)

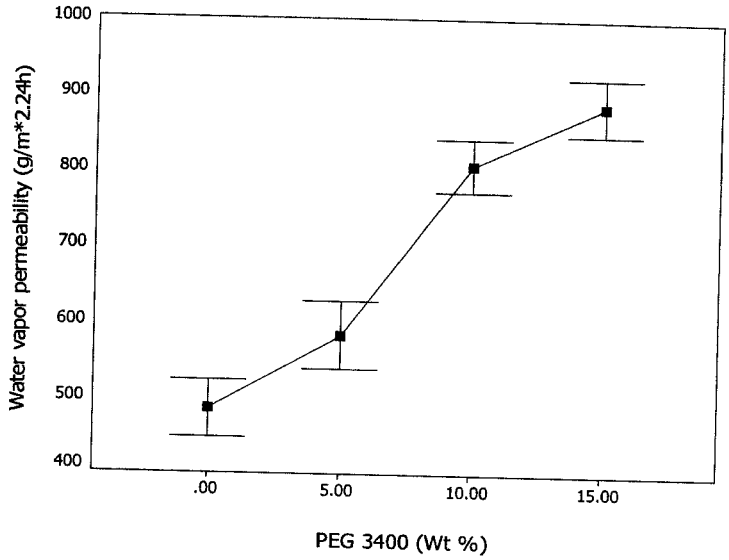

Figure 6.11: Influence of PEG content in WVP at 35 °C

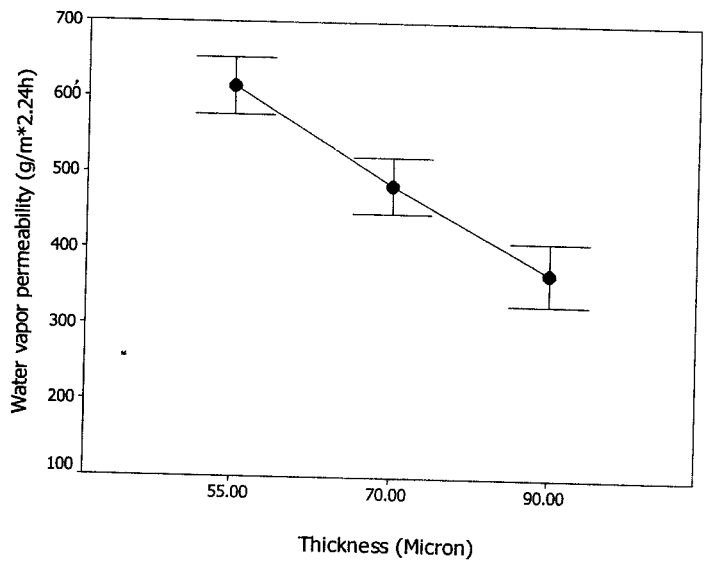

Figure 6.12: Thickness dependence WVP results of S_{13} (Without PEG)

6.1.2.4 Influence of Hydrophilic and/or Carboxylic Unit Content on WVP of SPU

Temperature dependent water vapor permeability of polyurethanes for the influences of hydrophilic and/or carboxylic unit content is shown in Figure 6.13 and data are presented in Table 6.2. WVP result plays the similar trend as equilibrium sorption. From the DMTA results, glass transition temperatures for all samples (except S_{15}) were well below the experimental temperature, therefore all the SPUs exist in the rubbery stage in the experimental temperature which would increase the free volume as a result of increases of the permeability. However, the presence PEG 3400 or DMPA unit significantly enhances or hinders the permeability, because of the increase or decrease of mobility of soft segment respectively. There are abrupt changes of permeability for the SPU with PEG 3400 that may be due to the three fold reasons: first of all presence of PEG segment increases the flexibility of polymer chains which would lead to an increase of the free volume. Secondly the increase of hydrophilicity which would increase the solubility of water vapors molecules. Finally longer polymer chains of PEG 3400 will originate larger polymer network holes that will also enhance the water vapor permeability [149]. The permeability of membrane with DMPA (S_{15}) is low as compared with S_{14} (PEG 3400) due to the presence of strong ionic interaction (discussed in section 4.1) which will act as physical crosslinks that would prevent the passage of water vapor molecules. Permeability of the membrane with both PEG 3400 and DMPA (S_{16}) unit is in between the S_{14} and S_{15} as expected. SPU without any hydrophilic or carboxyl groups has higher permeability than the sample (S_{15}) containing carboxylic groups. The change of permeability also depends on the interaction of water vapor molecules and polymer.

SPU containing carboxylic group causes strong interaction of polymer and water vapor molecules which reduces the permeability. The increase of the physical cross-linking imposed by carboxylic groups, usually results in decrease of membrane permeability. Since the existence of cross-linking network would restrict the mobility of the molecular chains. This result is contradictory to the equilibrium sorption: may be in this case water molecules are strongly bound by the carboxylic group by hydrogen bonding and prevent the diffusion. The glass transition temperature of this SPU (S_{15}) is higher than the other SPU which will prevent the segmental motion of the polymer chains that would prevent the increase of free volume. Therefore, it could be concluded that the effect of diffusivity plays a dominant role in determining the water vapor permeability SPU membranes.

Table 6.2: Water Vapor Permeability ($g/m^2.24h$) data of SPU

Sample	12 °C		18 °C		25 °C		35 °C		45 °C	
	WVP	CV%	WVP	CV%	WVP	CV%	WVP	CV%	WVP	CV%
S_1	38	7.0	45	5.6	57	4.4	130	3.9	350	2.5
S_2	47	5.3	94	4.1	120	3.2	220	2.6	400	2.1
S_3	55	5.5	112	3.4	180	2.5	340	2.2	520	1.8
S_4	60	2.7	120	5.8	200	5.2	350	2.2	564	0.9
S_5	33	4.5	54	3.7	90	2.5	143	1.7	450	2.6
S_6	170	3.2	210	2.1	310	1.3	410	2.1	680	1.5
S_7	276	1.9	359	1.4	460	1.1	660	1.2	1080	1.2
S_8	280	2.7	365	1.2	520	1.9	750	2.3	1220	1.1
S_9	96	3.8	124	5.3	210	3.2	310	2.6	480	2.7
S_{10}	165	2.6	351	3.2	408	2.9	582	3.5	985	1.6
S_{11}	290	3.6	390	1.9	545	2.1	806	1.1	1270	0.8
S_{12}	324	1.6	457	3.8	605	1.1	885	2.3	1399	1.5
S_{13}	115	2.3	258	1.4	398	2.3	485	2.8	590	1.1
S_{14}	156	1.9	191	0.9	285	3.7	450	3.2	625	2.1
S_{15}	30	2.7	45	1.7	68	2.5	106	2.7	149	0.8
S_{16}	66	1.3	119	2.6	147	1.2	228	1.5	325	1.6
S_{17}	45	2.8	113	1.5	163	1.8	291	0.8	385	1.9
S_{18}	215	3.7	290	0.7	420	3.9	511	2.5	850	0.6
S_{19}	124	2.1	310	1.1	488	1.2	605	1.2	955	1.8
S_{20}	367	1.1	465	1.5	615	2.5	900	2.5	1450	2.3
S_{21}	115	4.7	155	4.5	272	0.8	337	1.8	405	2.8
S_{22}	296	2.1	408	2.3	552	2.3	846	0.9	1285	1.1
S_{23}	295	1.6	404	1.8	547	1.5	820	2.1	1277	0.9
S_{24}	285	1.1	365	2.5	530	2.7	795	1.7	1265	2.2
S_{25}	266	2.8	349	0.9	518	0.5	781	2.8	1248	1.5

WVP – water vapor permeability, CV% – coefficient of variation percent of measurements

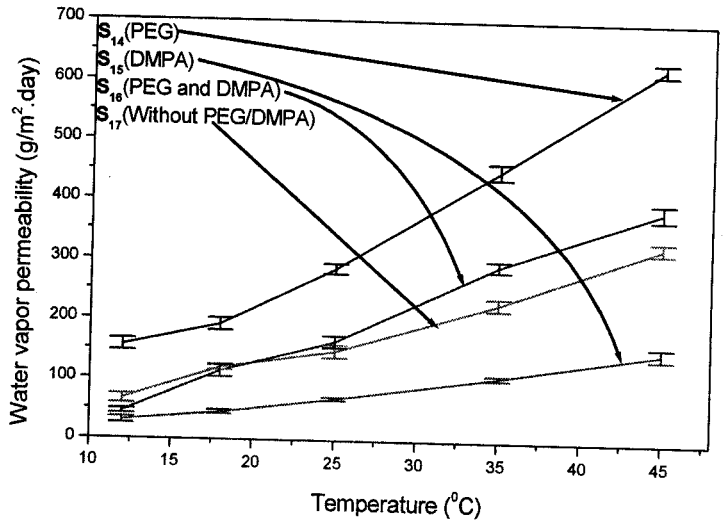

Figure 6.13: Water vapor permeability of SPUs (S_{14} –S_{17})

6.1.2.5 Influence of Mixed Polyol Block on WVP of SPU

The water vapor permeability (WVP) result shows the same trends with equilibrium water sorption behavior of the corresponding SPU for the influence of mixed soft segment block. From DMTA results we observed that the glass transition temperature of all SPU samples are well below the experimental temperature, therefore the fractional free volume will increase with increasing temperature [172] at experimental temperature according to the equation (6.2) which would provide more paths for water molecule to pass through the membrane. In addition the increase of WVP with increasing temperature is due to the higher energy in the membrane segment at higher temperature. Some of intermolecular interactions among the individual segments within the polymer may be weaken or broken at higher temperature. This results in the polymer matrix being more fluids in nature which will enhance the permeability [173]. Water vapor permeability of S_{20} (PPG 3000-PTMG 2900) is best among the four SPUs (Table 6.2 and

Figure 6.14) regardless of temperature. The presence of flexible PPG and PTMG segment in the polymer backbone and their phase mixing in the resulted SPUs will increase the chain mobility that was the reasons for higher water vapor permeability of S_{20}. The low crystallinity and flexible structure will give a loose amorphous [84] structure through which water vapor molecules could easily pass. The WVP was further enhanced when the experimental temperature reached the soft segment crystal melting point (T_{ms}). At and above T_{ms}, WVP was confluenced by chain flexibility, hydrophilicity, and soft segment crystal melting temperature which causes discontinuous density changes inside the membranes. Due to their combined effects, the WVP was increased abruptly. The WVP of S_{21} (PCL 3000) is lowest among four SPUs due to the presence of ester groups which increases the inter-chain interaction and prevents the water molecules to pass through the membrane. The percent crystallinity of this sample is highest among the four samples; therefore, the combination of stiff character of polymer chains and high content of crystallinity in the soft segments may probably create a polymeric "molecular sieve", as with the glassy polymer [174] as a result of lower permeability. For this sample the increase of WVP with increasing temperature is due to the increasing free volume according to the equation (6.2). The soft segment crystal melting temperature for this sample is higher than the experimental temperature (DSC results) which would not influence the WVP. When PPG 3000 (S_{18}) or PTMG 2900 (S_{19}) was used as mixed block along with PCL 3000, the permeability of resulted SPU was increased significantly due to the enhanced chain flexibility as compared to SPU containing only PCL 3000 segment. Once the experimental temperature reaches about 19 °C, the crystal melting of PTMG 2900 phase which would further enhance the

permeability. However, the T_{ms} of other phase i.e. PCL 3000 phase would not be influence the WVP as it is higher than the experimental temperature. The micro-Brownian motion of soft segment at crystal melting point temperature (T_{ms}) obviously increases the intermolecular gap large enough to allow water vapor molecule to pass through the membrane [172].

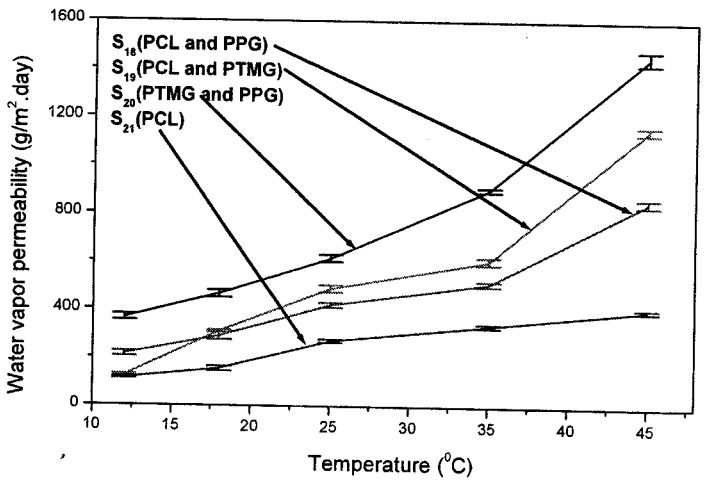

Figure 6.14: WVP of SPUs ($S_{18} - S_{21}$)

6.1.2.6 Influence of MWNT on WVP of SPU

The MWNT-SPU is a multiphase system in which the coexistence of phases with different permeabilities can cause complex transport phenomena. In fact, SPU itself can be considered as a two-phase of soft segment-hard segment rich phase system. The permeability through hard segment is poor. The permeation of small molecules through polymer is enhanced when their solubility and diffusivity in polymer increases. The presence of MWNT content may be expected to cause a decrease of permeability due to more tortuous path for the diffusing molecules that must pass through impermeable nano particles. The SPU with 0.25 and 0.50 wt% of MWNT content has no significant

influence on the permeability (Table 6.2). In contrast, the permeability of membrane with 0.25 wt% of MWNT increases slightly above the T_{ms} (Table 6.2) due to the presence of more crystalline structure and their melting enhances the permeability. Crystal melting is able to completely plasticize the polymer chain due to presence of water molecules which will lead to a high mobility of polymer chains. 2.5 wt% of MWNT content will give raise to a lower permeability due to the increases of stiffness of the polymer chains that would prevent the passage of water molecules.

6.1.2.7 Comparison of Low and Improved Permeability

From experimental results we observed that the WVP results depend on type of polyol, hydrophilicity, soft segment crystal melting point temperature. Due to their combined influence some of sample shows abrupt change of WVP (Figure 6.15) depending on the composition. Figure' 6.15 shows a comparison of poor permeability and high permeability results. However, few samples show smart water vapor permeability results at soft segment crystal melting point temperature as shown in Figure 6.16.

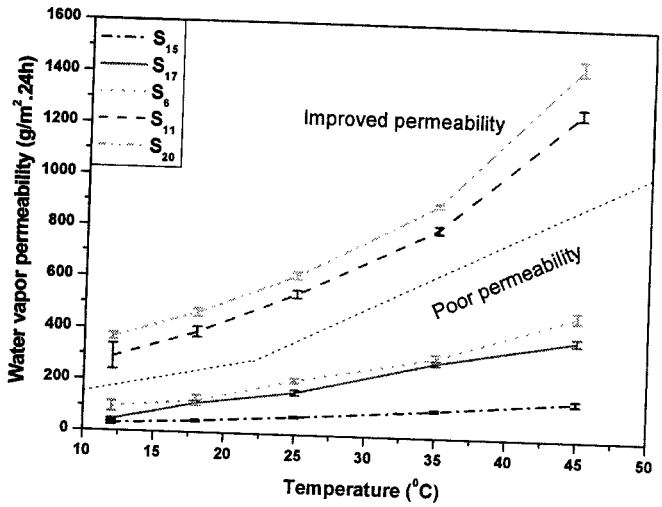

Figure 6.15: Comparison of High Permeable Membrane over Poor Permeability

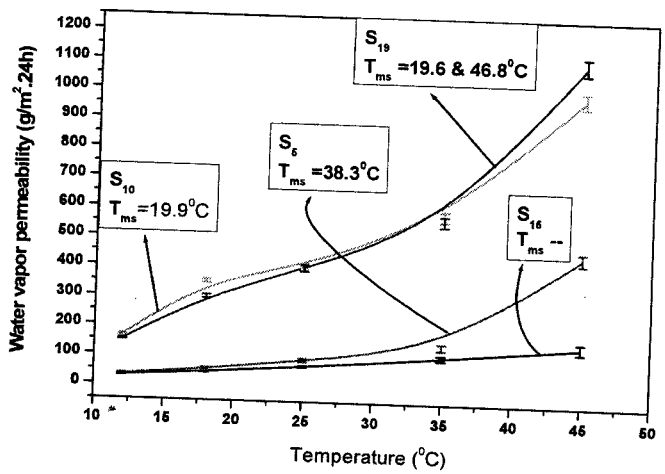

Figure 6.16: Smart WVP at Soft Segment Crystal Melting Point

6.2 FREE VOLUME AND WATER VAPOR PERMEABILITY OF SPU

PALS has emerged as an unique and potent probe for detecting the free volume properties of polymers in recent years [175-177]. The shortest lived component (τ_1) and the intermediate component (τ_2) are attributed to the self-annihilation of para-

positronium (*p*-Ps) and the positron annihilation, respectively. The longest-lived component (τ_3) results from the pick-off annihilation of ortho-positronium (*o*-Ps) in the free volume sites [178]. The *o*-Ps lifetime (τ_3) is the measures of size of free volume site in polymers (the greater τ_3, the larger the size), and intensities (I_3) is indicative of the number concentration of free volume sites in polymers [176].

6.2.1 o-Ps Lifetime and Intensity Properties of SPU

The results for PALS free volume parameters of *o*-Ps lifetime (τ_3) and intensities as a function of temperature are shown in Figure 6.17-6.20.

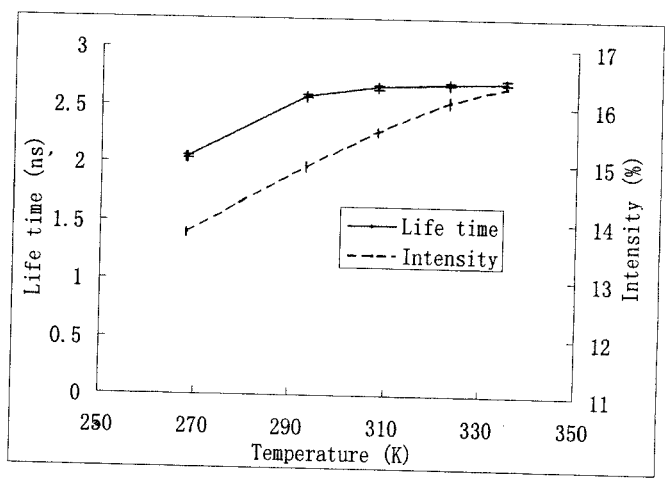

Figure 6.17: o-Ps and intensity of S_{10}

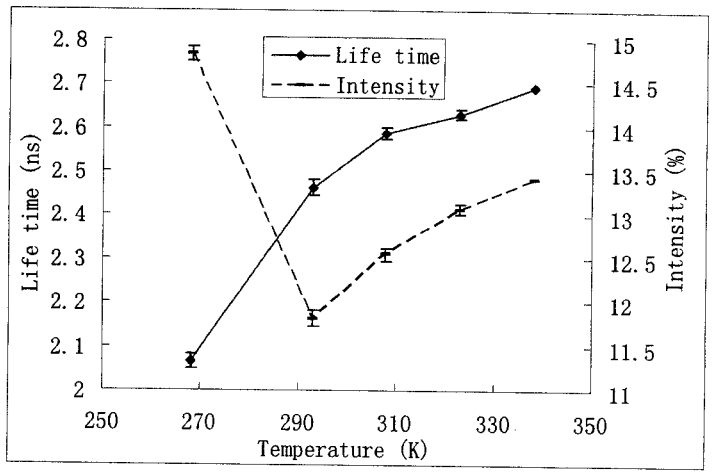

Figure 6.18: o-Ps and intensity of S_{11}

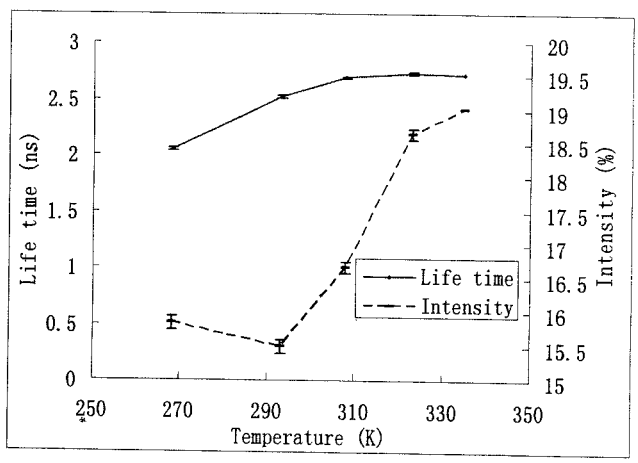

Figure 6.19: o-Ps and intensity of S_{19}

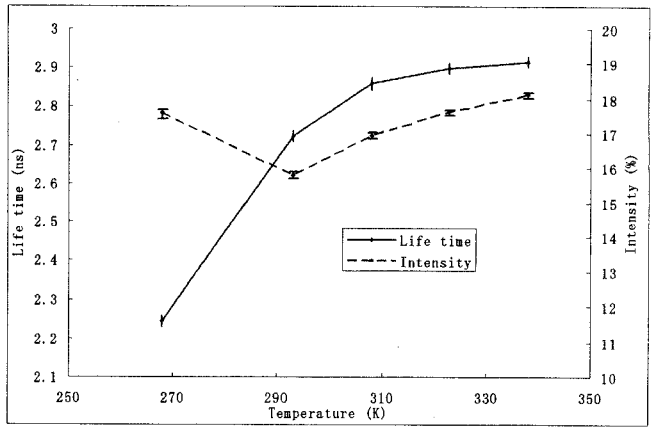

Figure 6.20: o-Ps life and intensity of S_{20}

From Figure 6.17-6.20, we can see that o-Ps lifetimes were increased linearly with increasing temperature because of the thermal expansion of the free volume hole size as a function of temperature. However, the absolute values of o-Ps lifetime for four samples at specific temperature are different. Sample with higher PEG 3400 contain, the free volume was increased due to the longer PEG 3400 which will increase the chain flexibility and make larger hole in the membranes. The degree of phase separation also influences the free volume [179] in the SPU. As shown in TEM image (Figure 4.12), for sample S_{19}, hard segment, crystalline region and soft segment phase are coexisted and this would not increase the free volume significantly as expected. But in S_{20} (Figure 4.13), little amount of crystalline regions are dispersed in soft-soft and soft-hard segment phase mixed matrix. The increase of free volume would be abrupt in this case, and PALS data confirm the fact. The S_{11} (Figure 4.11) has better phase separated structure than S_{19} as a result of higher free volume. Since their compositions are different, therefore the selection of soft segment is important which will influence the morphology of membrane and membrane functionality such water vapor permeability.

6.2.2 Free Volume Radius of SPUs

The radius of free volume is shown in Figure 6.21. The effect of different soft segment on water vapor permeability is mainly attributed to the free volume. Free volume hole sizes are different for four samples, this could be explained by interactions between the polymer chains, packing of polymer chains due to the different composition. Even for the same hard and soft segment element but different quantity of flexible hydrophilic segment (PEG 3400) the free volume hole size will be also affected. SPU with higher PEG block (S_{11}) has higher free volume hole size than SPU (S_{10}) having lower PEG segment content. This can be explained in terms of flexibility of the polymer chains which was imposed by PEG segment. S_{20} has highest free volume hole size among four samples, due to their loose and almost amorphous structure. On the other hand S_{19} has lowest free volume hole size among the four selected SPUs. Presence of ester groups causes strong interactions between the polymer chains which would restrict the movement of soft segments. This may be the suitable explanation for the trend of water vapor permeability and free volume hole size for all four selected SPUs. The obvious change of I_3 can be observed in the melting temperature range of SPU. The temperature dependency of o-Ps intensity, I_3, composed of two segments [180] for S_{11} and S_{20}, and three segments for S_{19}. Intensity was decreased from 268 K to room temperature for these samples, and above room temperature intensity increases significantly. The meeting point is soft segment crystal melting point which is about 20 °C, and this result supports the DSC results. In case of S_{19} the second meeting point is interpreted as second soft segment crystal melting point which is about 320 K (47 °C), and supports the DSC results as well. However, in case of S_{10}, no obvious transition point was observed

in PALS experiment that may be due to their lower percent crystalline structure, and most importantly their strong hydrogen bonding between the molecular chains (Figure 4.2) which would prevent the change of o-Ps intensity at soft segment crystal melting point temperature.

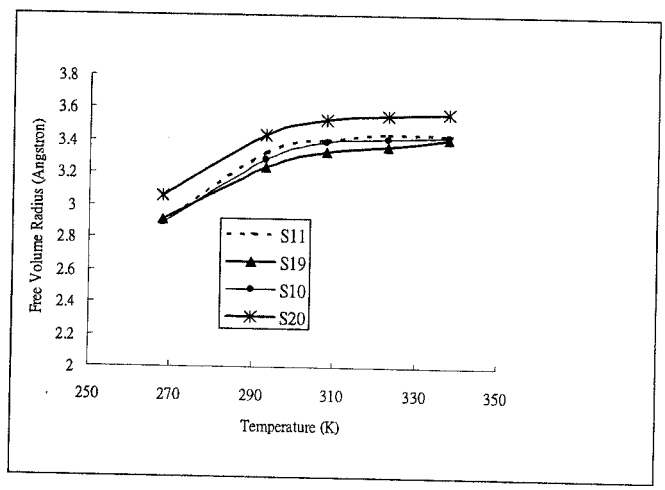

Figure 6.21: Free volume radius

6.2.3 Free Volume and Water Vapor Permeability of SPU

Figure 6.22 shows the WVP of all four SPU samples. The water vapor permeability in dense membrane is the measure of the effective mobility of the penetrant in the polymer matrix. When the size of free volume is comparable with water vapor molecule, its diffusion would be restricted. On the other hands, if the free volume hole size is large enough as compared to the water vapor molecules, it will diffuse through the membrane with a large diffusion constant. This could provide an explanation, why the water vapor permeation increases as a function of free volume hole size [179]. The effect of different soft segment on water vapor permeability is mainly attributed to the free volume. From

the Figure 6.22, we can see that S_{20} has much higher WVP than that of other three samples which is attributed to its much higher free volume. The flexibility and loose packing of soft segment result in increase of the concentration of free volume holes which would capable of supporting water vapor permeability in soft segment region. As expected, free volume has a direct correlation with the water vapor permeability: a large hole of free volume is required for greater gas permeability [181]. The structural changes that cause the change in the free volume will also effect the polymer-water vapor molecules interactions.

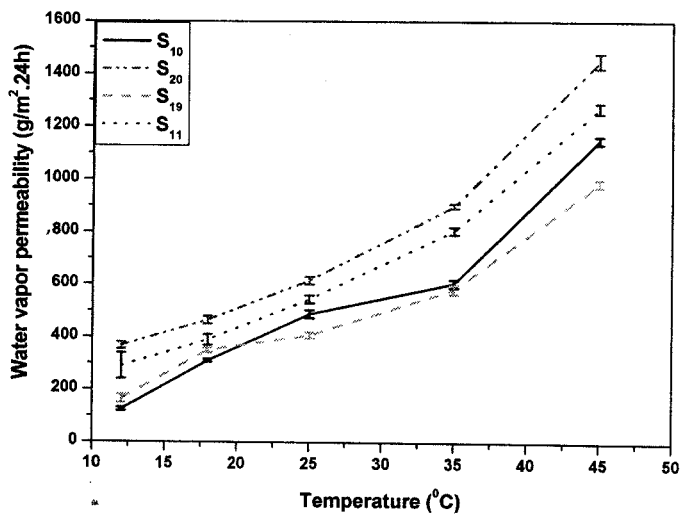

Figure 6.22: Water vapor permeability results of SPU

The effect of chemical compositions on water vapor permeabilities are due to the free volume and the nature of chain packing. The water vapor permeability in these SPU membranes with hydrophilic soft segment would be controlled by not only the free volume but also hydrophilicity of the polymer. As for example, S_{11} contain higher PEG 3400 content than S_{10} that imparting its membrane a higher level of hydrophilicity to a

higher WVP. The water vapor permeability of sample S_{19} is comparatively low as compared with other three samples, in this case strong interactions of polymer chains occur due to the presence of ester groups in PCL 3000 segment which will prevent the increase of free volume as a result of lower WVP. Another factor which will decrease the free volume and subsequently WVP of S_{19} is entanglement of hard, soft and crystal regions as shown in TEM image (Figure 4.12). Above the soft segment crystal melting temperature free volume was increased significantly due to the discontinuous density changes inside the membrane which will enhance the water vapor permeability of dense membrane. However, in case of S_{19}, the primary soft segment crystal point temperature is 46.8 °C which would not influence the WVP as the WVP testing temperature range is 12 – 45 °C.

6.3 SUMMARY OF WATER VAPOR TRANSPORT PROPERTIES AND FREE VOLUME OF SPU

In summary, water vapor transport property of SPU depends on type and content of soft segment, molecular weight and content of hydrophilic segments. Sorption was decreased with increasing hard segment content due to their hydrophobic nature. In contrast, sorption was increases with increasing soft segment content in the SPU matrix due to the chain flexibility possessed by soft segment. Soft segment crystal melting will cause discontinuous density changes inside the SPU membrane which will provide more paths for water vapor molecules. Equilibrium sorption was also increased with increasing block length of hydrophilic segment and content of hydrophilic segment. The sorption was increased with increasing hydrophilic block length due to the increasing hydrophilicity of polymer chains which could attract more water molecules. The

presence of flexible hydrophilic segment also increases the chain flexibility between the polymer chains which will provide more gaps for water molecules. With the increasing hydrophilic segment content in the SPU, desorption would occur at higher temperature (above 35 °C). This desorption phenomena could be explained by the lower critical sorption temperature phenomenon of hydrophilic segment (PEG 3400). Presence of DMPA unit in the polymer backbone decreases the sorption properties of SPU. Presence of carboxylic groups causes strong ionic interaction between the polymer chains which is the reasons for decrease of equilibrium sorption. Mixed block SPU based on PTMG 2900 and PPG 3000 polyol has higher equilibrium sorption among the all SPUs due to their loose and nearly amorphous structure. The sorption of PCL 3000 based SPUs was increased when PPG 3000 or PTMG 2900 was used along with PCL 3000 segment. In contrast with the increase of MWNT content in the SPU the equilibrium sorption was decreased due to the increasing stiffness between the polymer chains.

The influence of different factors on water vapor permeability follows the same trends with equilibrium sorption of SPU. Water vapor permeability of SPUs have been improved with increasing soft segment content in the polymer backbone or in other way with decreasing of hard segment content in SPU. The increase of hard segment will cause greater intersegment mixing which in turns will increase the membrane density. Higher intersegment mixing and density would always decrease the water vapor permeability of SPU membranes. WVP was increased with increasing hydrophilic block length and hydrophilic segment content. High molecular weight hydrophilic segment (PEG 3400) would enhance the permeability due to the increase of the hydrophilicity which will increase the interaction between water vapor molecules and polymer chains.

The longer polymer chain of hydrophilic segment would originate larger polymer network holes that will also enhance the water vapor permeability. The soft segment crystal melting causes discontinuous density changes inside the membranes which would provide more paths for the water vapor molecules to pass through the membranes. In contrast presence of carboxylic group (DMPA) in SPU backbone will decrease the water vapor permeability of SPU due to the strong ionic interaction which would act as physical crosslinks that would prevent the passage of water vapor molecules. Mixed polyol block SPU based on PPG and PTMG posses higher water vapor permeability due to their loose and nearly amorphous structure. The presence of flexible PPG and PTMG segments in the polymer backbone and their phase mixing structure will increase the chain mobility that will enhance the WVP of SPU. Water vapor permeability of SPU membrane having low quantity (0.25 wt%) of MWNT would increase slightly in the room temperature range due to the more order structure which was melted in this temperature range, and enhances the permeability. However water vapor permeability of SPU having 2.5 wt% of MWNT decreases due to the increase of stiffness of polymer chains.

Free volume of polymer depends on the morphology of polymers. PALS results revealed that the free volume of polymers could be improved by using the flexible soft segment in the polymer backbone. The flexibility and loose packing of soft segment would increase the concentration of free volume holes which are capable of supporting the water vapor permeability through the soft segment region. The degree of phase separation would also influence the free volume of SPUs. The free volume was not influenced significantly when the crystal structure, soft and hard segments were coexisted. Therefore the

selection of soft segment is important which will influence morphology of the polymer. The variation of morphological structure would affect the free volume as well as water vapor permeability. Therefore, water vapor permeability of SPUs would be controlled by segmental architecture, increasing hydrophilicity and free volume.

CHAPTER 7

COATING OF FABRICS WITH SPU AND POTENTIAL APPLICATIONS OF SPU

Selected SPUs have been applied to the cotton fabrics. This chapter includes evaluation of the coated fabrics by scanning electron microscopy (SEM), water pressure head measurements (waterproofness), tensile strength measurements and water vapor permeability measurements. Finally, UV blocking of multi wall carbon nano tube containing SPU coated fabrics have been presented in this chapter.

7.1 FABRIC SURFACE OBSERVATIONS

Observations of the uncoated fabrics (Figure 7.1) by SEM revealed that the surfaces are porous. In contrast, inter filamental gaps are filled up by polymer after coating (Figure 7.2 – Figure 7.4). The nonporous SPU layer is formed continuously over the surface of the coated fabrics. Presence of nonporous SPU layer suggested that the water vapor permeability of coated fabrics originated from the properties of SPU itself. Therefore the chemical structure of SPU would play major roles in the breathability of coated fabrics. The mobility of SPU chains above its glass transition and soft segment crystal melting point temperatures are important parameters in determining the water vapor permeability of coated fabrics.

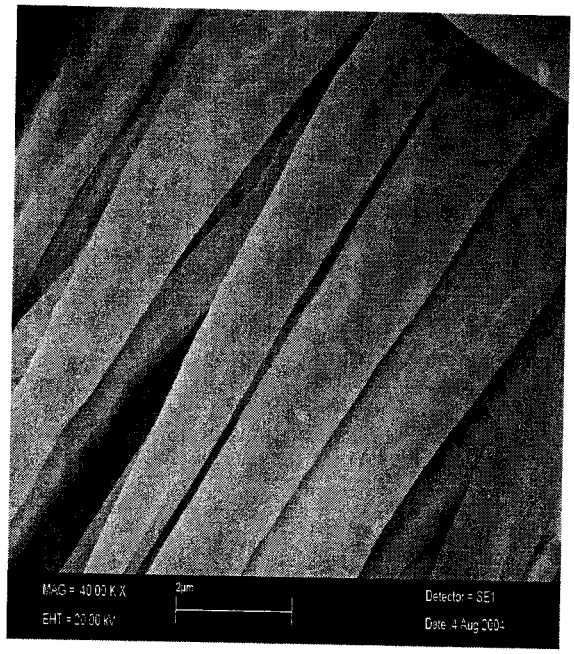

Figure 7.1: SEM image of uncoated fabric

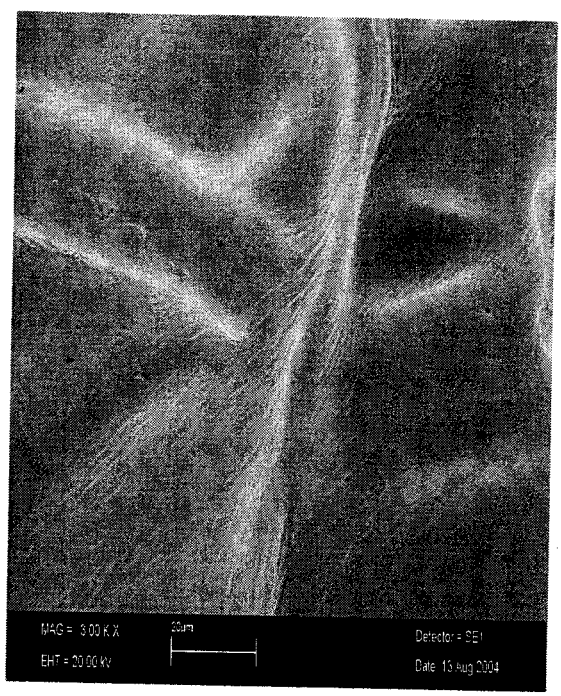

Figure 7.2: SEM image of coated fabric with PTMG-PEG10

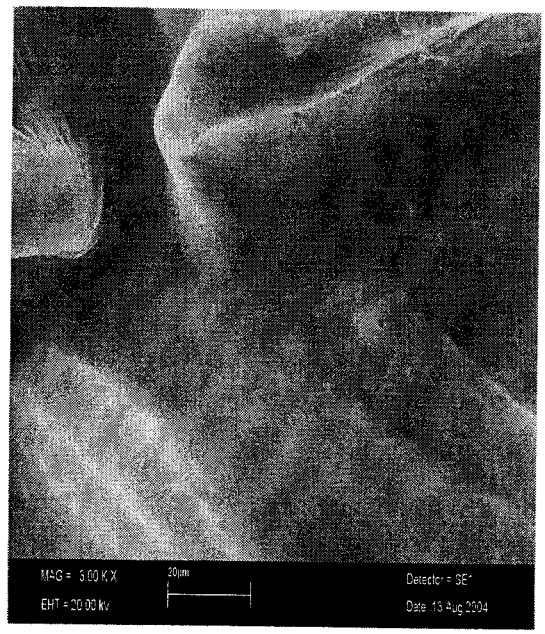

Figure 7.3: SEM image of coated fabric with 0.25 % of MWNT content SPU

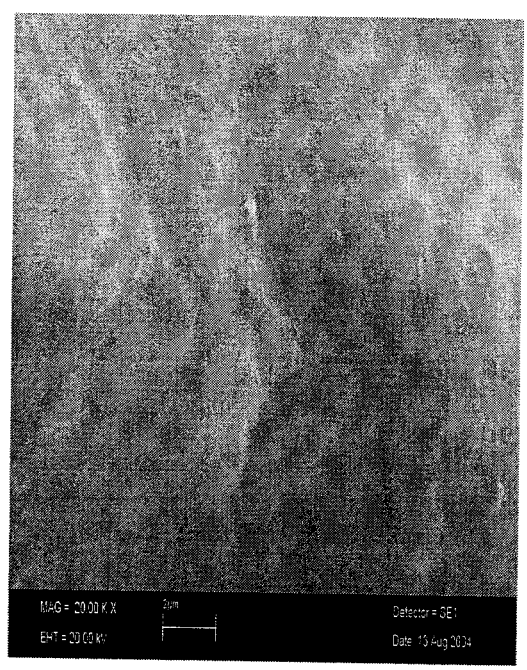

Figure 7.4: SEM image of coated fabric with 2.5 % of MWNT content SPU

7.2 WATER VAPOR PERMEABILITY OF FABRICS

The water vapor permeability (WVP) data for uncoated and coated fabrics with SPU (without MWNT) are shown in Figure 7.5 and 7.6 and results are tabulated in Table 7.1. From the Table 7.1 and Figure 7.5, we can see that in all cases WVP increases with temperature due to the two fold reasons. Firstly, as the temperature increases the difference between saturation vapor pressure of water inside cup and surroundings is also increased which would increase the permeability. Second reason is the polymer morphological changes with increasing temperature. In all cases first factor remaining constant, therefore the difference of water vapor permeability for different coated samples at a particular temperature is due to the change in polymer morphological structure.

Although in all cases we have carried out the experiment at 70 % relative humidity, for one sample (F-PCL-PEG10) we carried out WVP testing at 35 °C with different relative humidity. With the increasing relative humidity in the surrounding, the difference of saturation water vapor pressure between cup and surrounding was decreased which prevent the water vapor molecules to release to the surrounding from the outer surface of the coated fabrics as a result of decrease of WVP with increasing relative humidity of testing condition (Figure 7.6).

As the SEM pictures show thin layer of polymeric films on the coated fabric, therefore the polymer structure plays major role in the permeability of coated fabric. The permeation of small molecules through polymer membrane is enhanced when their solubility and diffusivity in the polymer increases (Figure 7.5). In this study we used

PTMG 2900 and PCL 3000 based SPU which contained hydrophilic segment (PEG 3400) of 10 and 15 wt%. From the Table 7.1 and Figure 7.6, we can see that WVP of PTMG 2900 SPU coated fabrics are higher than that PCL 3000 based SPU coated fabrics. The reason is due to the loose amorphous structure of PTMG 2900 based [84] SPU which would help to transport the water vapor molecules easily. These results follow the same trends with polymer membrane (discussed in chapter 6). In all cases WVP increases steadily with temperature due to deformation of polymer structure (Figure 7.7) which provides more gaps for water vapor molecules to transport through the polymer film. When the hydrophilic segment content in the SPUs was increased, WVP also increases as the water vapor permeability occurred in the nonporous membrane by the molecular mechanism i.e. sorption-diffusion-desorption. More hydrophilic group would enhance the sorption of polymer membrane [149]. Once the water vapor molecules were absorbed by the polymer membrane, they will diffuse across the membrane and come to the other side of membrane. Finally, they would be release to the environment due to the concentration differences.

Table 7.1: Water Vapor Permeability ($g/m^2.24h$) data of SPU Coated and Uncoated Fabrics

	12 °C		18 °C		25 °C		35 °C		45 °C	
Sample	WVP	CV	WVP	CV	WVP	CV	WVP	CV	WVP	CV
F_0	880	3.7	1587	1.7	2125	0.6	2751	0.9	3701	0.2
F-PTMG-PEG10	715	1.3	990	0.9	1735	0.9	2117	0.8	3086	0.7
F-PTMG-PEG15	750	2.7	1079	1.8	1851	1.1	2271	0.9	3215	0.3
F-PCL-PEG10	455	2.2	848	2.2	1572	1.3	1760	1.5	2625	0.8
F-0.25CNT	700	1.2	1015	1.5	1760	1.7	2150	0.7	3105	0.4
F-1.00CNT	690	1.5	970	2.1	1700	1.2	2090	0.7	3000	0.6
F-2.50CNT	660	1.5	930	2.9	1650	1.1	2011	1.4	2980	1.3

WVP – water vapor permeability, CV – coefficient of variation percent of measurements.

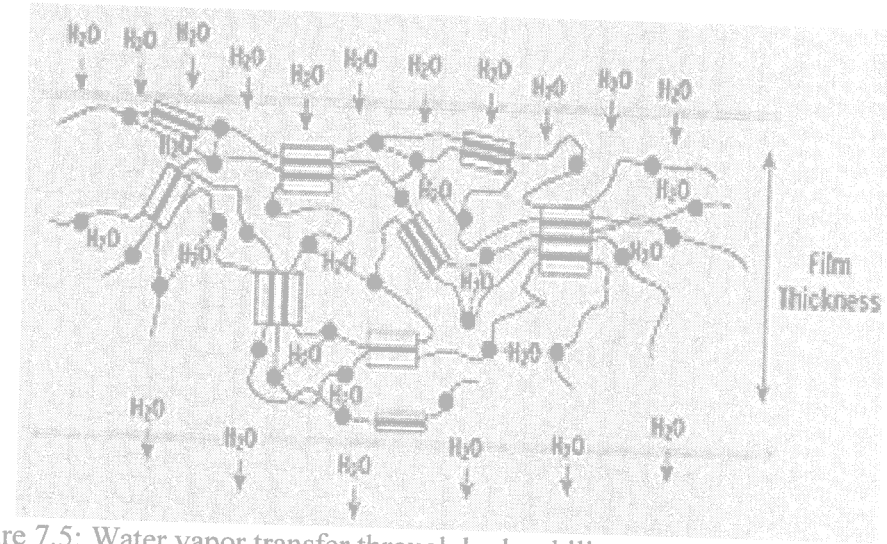

Figure 7.5: Water vapor transfer through hydrophilic membranes (Adapted with permission from Johnson L, and Samms J, *J. Coated Fabrics*, 27 (July), (1997), 48 © Technolmic Publishing Co. Inc [19])

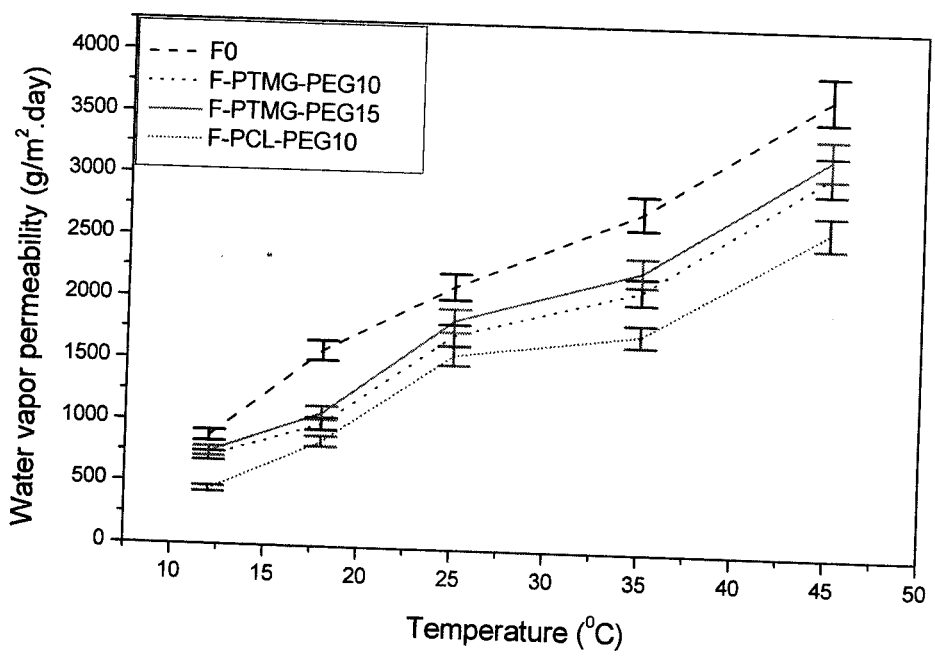

Figure 7.6: Water vapor permeability of coated and uncoated fabrics

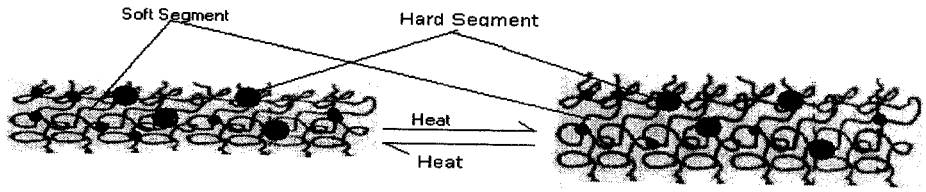

Figure 7.7: Deformation of shape memory polyurethane (SMPUs) network structure by heat

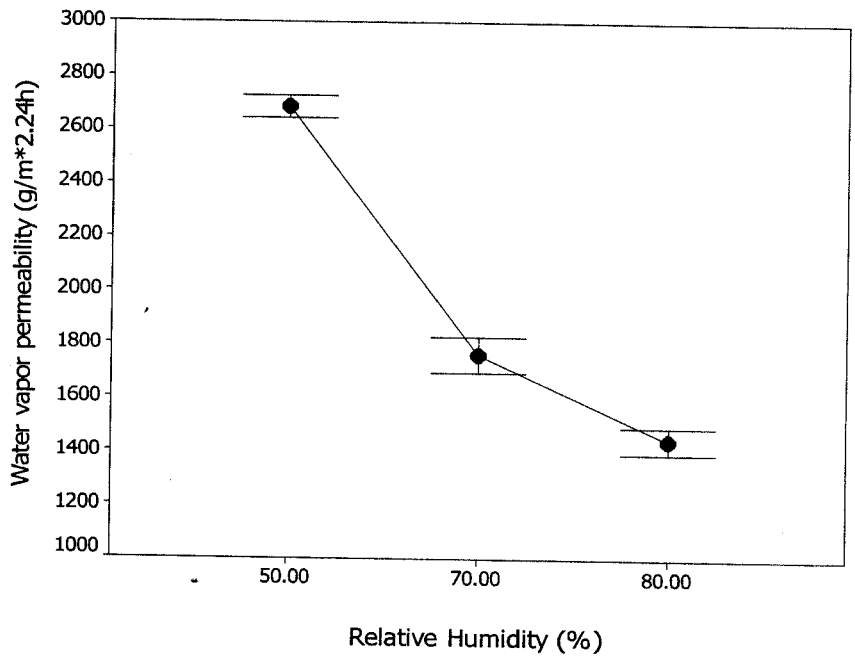

Figure 7.8: Influence of relative humidity on water vapor permeability at 35°C (sample F-PCL-PEG10)

Figure 7.8 shows the water vapor permeability of MWNT containing SPU coated fabrics. Since the differences between the experimental data are small, therefore for clarity, we fixed the water vapor permeability results of F-2.5CNT, others point are shifted each other by value of 50. The presence of MWNT content might be expected to cause decreases of water permeability due to more tortuous path for the diffusing molecules

that must pass through impermeable nano particles. Interestingly, the permeability of coated fabrics with 0.25 wt% of MWNT was increased slightly (Figure 7.7 and Table 7.1) above the T_{ms} due to the presence of more crystalline structure (DSC results) and their melting enhances the permeability. Crystal melting would be able to completely plasticize the polymer chain due to the presence of water molecules which will lead to a high mobility of polymer chains. At 2.5 wt% of MWNT content, coated fabrics give to a lower permeability due to the increase of stiffness of the polymer chains which will prevent the passage of water molecules. The water vapor permeability curve is steep from 18 to 25 °C because of the soft segment crystal melting (20 – 23 °C) which enhances the permeability. Experimental results revealed that there was about 20 % reduction of water vapor permeability of coated fabrics as compared with uncoated fabrics at all temperature, except in 18 °C, where the reduction of WVP is about 35 %. Low permeability at lower temperature (12 – 18 °C) is significant, it keeps the wearer warm by preventing the escape of body heat and/or water vapor losses.

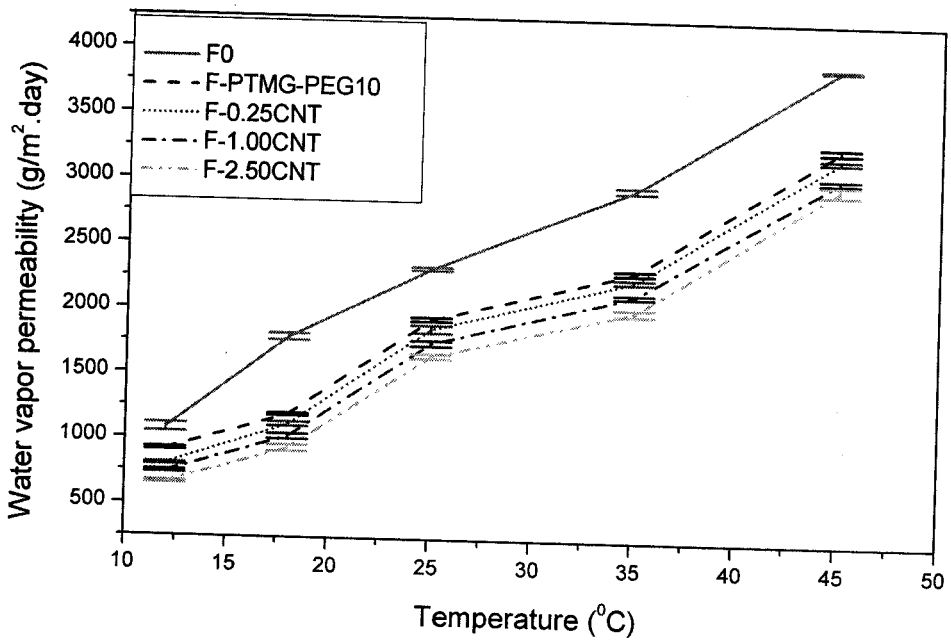

Figure 7.9: Water vapor permeability results of coated and control fabric

7.3 TENSILE PROPERTIES OF FABRICS

The tensile strength of coated fabrics is the manifestation of visco-elastic nature of polymer, and the interaction of polymer and filaments of the coated fabrics. In general, the application of coatings would tend to increase the tensile strength of coated fabrics. The longitudinal tension applied to the fabric during coating which stretches the warp thread yarn system and increases its parallelism. The yarns were become "locked" in place by the coating materials. Therefore, the warp yarns are essentially in plane to any longitudinally applied stress which is able to support the applied load hence increases the tensile strength of coated fabrics [182]. The tensile properties of coated and uncoated fabrics are tabulated in Table 7.2. Tensile strength in both warp and weft directions increase for the coated fabrics. The base fabrics are porous which allows sufficient

penetration of polymer to achieve some chemical and mechanical adhesion between the filaments. Coated fabric is a composite of SPU and fabrics, and the final tensile properties of the coated fabrics are function of the base fabrics and the polymeric materials. Tensile strength of the fabrics coated with PTMG 2900 based SPU is higher than that of the fabric coated with PCL 3000 based SPU due to the strong interaction of PTMG-PEG polymer and filaments. Strength of the coated fabrics with the SPU containing higher PEG content (PTMG-PEG15) is higher than that of the fabric coated with lower PEG content (PTMG-PEG10) due to the increase of polar groups which will increase the adhesion between the filaments. After coating, fabric becomes stiffer, which will decrease the percent strain at maximum load in both directions.

Table 7.2: Tensile Properties of Coated and Uncoated Fabrics

Samples	Load at Max. Load (N)				% Strain at Max. Load (%)			
	WP	CV (%)	WF	CV (%)	WP	CV (%)	WF	CV (%)
F_0	247.2	5.2	147.4	4.4	21.1	5.5	16.0	4.6
F-PTMG-PEG10	285.5	4.9	172.0	2.2	20.0	2.0	15.7	1.7
F-PTMG-PEG15	312.2	3.6	175.2	5.2	18.5	4.7	14.1	1.6
F-PCL-PEG10	271.4	2.8	174.0	4.7	17.4	2.1	12.9	4.7

7.4 WATERPROFNESS RESULTS OF FABRICS

Water penetration resistance (Table 7.3) is 0 mbar for uncoated fabrics due to its porous structure which is unable to prevent water head pressure. Higher water penetration pressure was obtained for fabrics coated with PTMG 2900 based SPU due to strong adhesion of polymer with fabrics. Water penetration resistance was further enhanced with SPU containing higher amount of PEG in the polymer backbone which can increase

the adhesion between the filaments, therefore, make more compact polymer-filaments structure. On the other hand, water resistance pressure is lowest for the fabrics coated with PCL 3000 based SPU due to its hydrophobic nature which causes less bond formation with the cotton fibre and SPU. Therefore the polymer only exists on the surface of the fabric.

Table 7.3: Hydrostatic head of coated and uncoated samples

Sample code	Hydrostatic Pressure (mbar)
F_0	0
F-PTMG-PEG10	17.5
F-PTMG-PEG15	24.5
F-PCL-PEG10	12.5

7.5 UV PROPERTIES OF FABRICS

The UV light fallen on fabric was divided into three parts according to the resulting light distribution: reflection, absorption, and transmission (Figure 7.8). In order to make the fabric protecting from UV light, the fabric must not allow transmitting any UV rays through the fabrics. This could be possible by reflection and/or absorption. The UV absorption of coated fabric without MWNT containing SPU was revealed a UPF rating of 46 (< +50), very good according to the Australian/New Zealand Standard. This UPF results is a very good protection due to bit of absorption as compared to a low UPF rating of 5.6 which is classified as non ratable for uncoated fabrics (Table 7.5). From Figure 7.9, we can see that UV transmission of coated fabrics containing MWNT is

almost zero which indicates that the MWNT containing coated fabrics would be capable to protect the wearer from UVA as well as UVB rays.

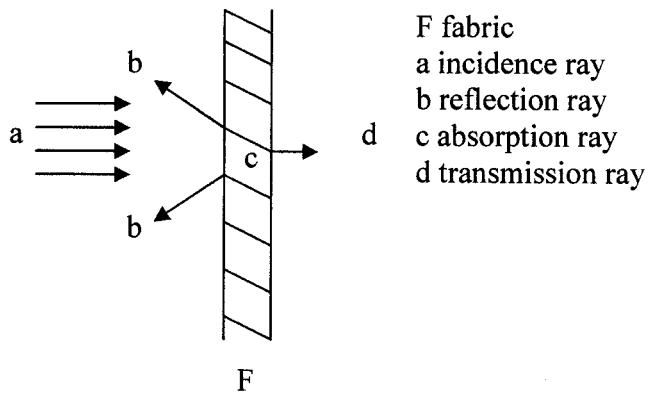

Figure 7.10: Fabric-UV interactions

UPF rating of coated fabric containing 1.00 wt% of MWNT is 174 and for coated fabric containing 2.5 wt% of MWNT is 421. Very high UPF rating for carbon nanotube containing SPU coating is obviously due to the UV-shielding characteristics of MWNT. Absorption of UV-rays was increased with increasing MWNT contain in the SPU. The UV-absorption property is a natural attributes of MWNT which can be explained by the solid band theory. Due to the extra-ordinary strength of the carbon-carbon bond, the small atomic diameter of the carbon atom and the availability of the free π-electrons in the graphite configuration, carbon nano tubes exhibit a number of remarkable electronic characteristics which are summarized in Table 7.4 [183]. For application in microelectronics, the most interesting features are the ballistic (scattering free) and spin conserving transport of the electrons along the nano tubes. The ability to have metallic as well as semi conducting behavior and the access to the energy gap would depend on

the diameter of the nano tubes. Carbon nano tube is a kind of semiconductor having diameter of 10 -50 nm with a large band gap (10~50 eV) and

Table 7.4: Some important electrical characteristics of Carbon Naotubes

Electrical Conductivity	Metallic or semi-conducting
Electrical Transport	Ballistic, no scattering
Energy gap (semicond.)	E_g [eV] = 1/d [nm]
Maximum current density	~10^{10} A/cm^2
Thermal conductivity	6000 W/(km)

optically active nanostructures [183-185]. When MWNT is illuminated by light with energy higher than its band gaps (i.e., with wavelength shorter than the absorption edges), the electrons will absorb the energy of the photons and be excited to cross the band gaps, therefore will produce the pairs of electrons and holes. Electrons and holes are injected from opposite contacts into a single nano tube molecule [184]. The ambipolar domains, where electrons and holes current were overlap which will form a microscopic light emitter within the carbon nanotube. The photocurrent shows resonances whose energies are in agreement with the energies of exciton states of semiconducting nano tubes of the appropriate diameter. The photo current is maximized for photons polarized along the direction of the carbon nano tubes [186]. These excited electrons quinces: either coming with other holes or electrons, or being captured by the absorbents surrounding of MWNT which initiates reduction and oxidation reactions. The former explains how the UV-protector of MWNT were functions, whereas the latter reveals the mechanism of MWNT as a light catalyzer [137].

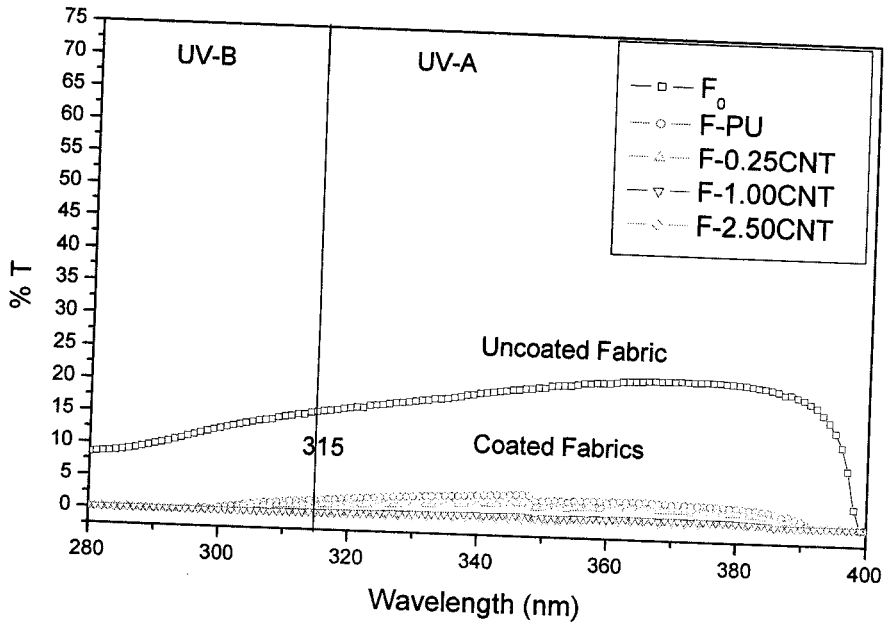

Figure 7.11: UV blocking results of coated and uncoated fabric

Table 7.5: UV properties of treated and untreated fabrics

Samples	Mean Transmission (%)		Calculated UPF	UPF Rating
	UVA	UVB		
F_0	18.523	13.112	5.600	Non-rateable
F-PU	2.590	0.940	46.128	Very good (<50+)
F-0.25CNT	1.709	0.709	61.919	Excellent (50+)
F-1.00CNT	0.550	0.196	173.987	Excellent (50+)
F-2.50CNT	0.291	0.105	421.198	Excellent (50+)

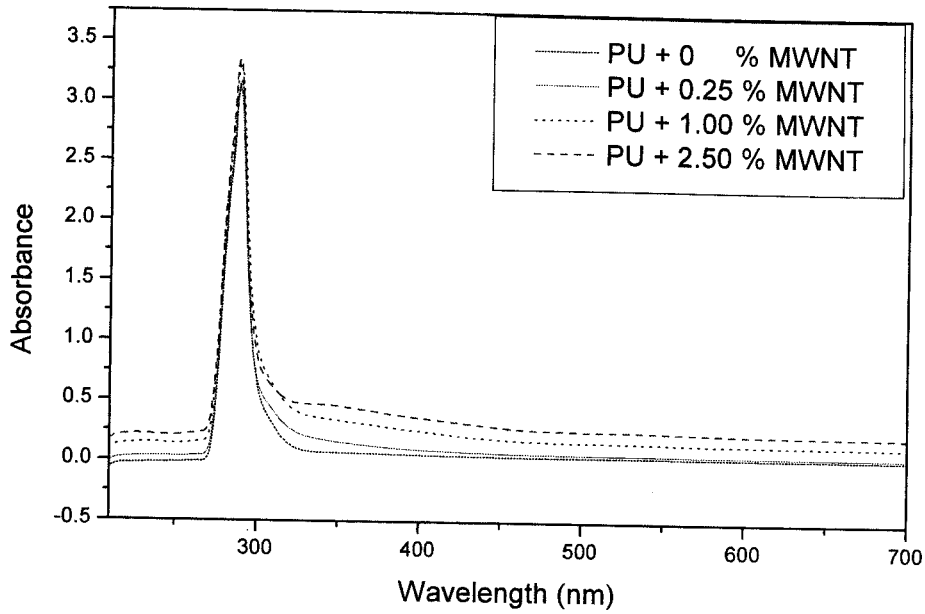

Figure 7.12: UV-vis spectra of PU and MWNT content PU solution in DMF

The UV absorption capability of MWNTs could also be proved by UV-vis spetrophotometric analysis. Figure 7.10 shows the UV-vis spectra of polyurethane solutions as function of MWNT content. For sake of the comparison, the UV-vis spectrum of pure polyurethane solution is also shown in the above figure. The result indicates that there are increases of the absorption in the UV range of 200 – 700 with the increasing of MWNT content in SPU.

7.6 POTENTIAL APPLICATIONS OF SPU IN TEXTILE FIELD

Water- and windproof garments which are permeable to perspirations have been on the market for over 20 years. These breathable and therefore functional clothings gaining more market segments in apparel wear. The range would include the high-tech garments for professional athletes as well as casual wear. Highly sophisticate high-tech

membranes are used to produce laminates which are then treated by the clothing industry to make high-tech garments for special professional groups like firemen, postmen or the military. Besides the adhesion, other important specifications that would be fulfilled by the laminates are soft hand, high water vapor permeability etc. The materials have to be extremely water- and windproof and very high breathability. Several characteristics make the segmented polyurethane especially suited for use in the breathable textile industry. Their flexibility, especially at low temperatures, will yield a soft hand. The materials maintain good barrier properties while providing high breathability, a combination of attributes are required by the outdoor and performance sportswear industries.

In coating and laminating field, the term hydrophilic (water-loving) is synonymous with polymer formulation which exhibits a high rate of molecular diffusion of water vapor. These polymer coatings and laminated films are amongst the latest developments in waterproof and breathable fabrics which are used in foul-weather clothing and other diverse applications.

Hydrophilic segmented polyurethanes have three main applications in breathable fabric technology: First, their major contribution is as a complete nonporous coating on a suitable base fabric. Secondly, solid polyurethane layers can be applied to microporous films and coatings to seal the surface pores. This process is often carried out to improve the certain inherent deficiencies of microporous polyurethane and PTFE membranes laminates. The pore sealing of polyurethane layer reduces the likelihood of contamination by a number of agencies, including particulate and air-borne dirt,

pesticide residues, insect repellents, sun tan lotions, salts (marine environments), skin exudates, and detergents and surfactants used for laundering or dry cleaning. All of these contaminants have been suspected of lowering the breathability of the microporous film laminates or coatings. Thirdly, hydrophilic polyurethanes could be used as adhesives to laminate different types of breathable membrane to face fabrics, and optionally to liner fabrics. The use of hydrophilic adhesives layer minimizes the loss in breathability of the membrane which will inevitably occur in the laminating process.

Mechanical properties of the coated and laminated fabrics are also important from application point of view. SPU could be tailor made by the combination of hydrophobic and hydrophilic polyols with diisocyanate components to produce optimum moisture vapor transmission properties without the loss of other physical properties. Hydrophilicity of poly(ethylene oxide)-based polyurethanes can be varied, either by increasing the overall content (% w/w) of the hydrophilic component or by altering the length of the hydrophilic segments. The role that the hydrophobic segment plays to hold the neighboring polymer chains together is critical. Monolithic hydrophilic coatings can be applied by conventional coating techniques on a suitable base fabrics, and they can be less expensive than laminated or micro-porous films. Each of these systems has specific advantages and disadvantages in addition to the differences in cost. The laminated and micro-porous films have poor adhesion to the textile substrates as compared to hydrophilic coatings. On the other hand, the hydrophilic films have lower water vapor permeability (WVP) as compared to micro-porous film laminates. Other advantages of hydrophilic coatings/laminating are: 1) The price of the polymer is lower, the process is

simpler, and production speeds are higher, 2) Having no holes, hydrophilic coatings is less sensitive to possible deterioration.

7.7 SUMMARY OF COATING OF FABRICS

In summary, thin layer of polymer film was formed on the coated fabric surface which signifies that the water vapor permeability of coated fabric originated from the properties of polymer itself. Therefore, the WVP of coated fabrics depends on the polyol structure used during polymer synthesis. The WVP result follows the same trends with original membranes permeability. The mobility of polymer chains above its glass transition temperature and soft segment crystal melting temperature are important in determining the water vapor permeability of SPU coated fabrics. PTMG based SPU coated fabrics have higher permeability than PCL based SPU coated fabrics. The water vapor permeability of coated fabrics was increased with increasing hydrophilic segment content in the SPU backbone. Increasing hydrophilicity of the polymer backbone attracts more water vapor molecules by polymer membranes which enhances the permeability of coated fabrics. The WVP of SPU coated fabrics was decreased with increasing relative humidity. With the increasing of the relative humidity, the difference of saturation vapor pressure between the cup and surrounding was decreased which would prevent the water vapor molecules to release. Water penetration pressure of 24.5 mbar was achieved after coating as compared to the zero for uncoated fabrics. Tensile strength of coated fabrics in both directions was increased due to the increase of interaction between the polymer and filaments. The tensile strength of coated fabrics with PTMG 2900 based SPU is higher than that of the fabrics coated with PCL 3000 based SPU due to the strong interaction between the polymer and filaments.

Introduction of MWNT in SPU would improve the UV blocking properties of coated fabrics. With only 1 wt % of MWNT content in SPU, UV protection factor of 121 was achieved as compared to the 5.6 for uncoated fabrics. Experimental results revealed that UV transmission of SPU-MWNT coated fabrics was almost zero. Therefore, the MWNT containing SPU coated fabrics are capable to protect the wearer from UVA rays as well as UVB rays. The UV absorptivity of MWNT-SPU solutions was also increased with increasing MWNT content in the polymer solution which signifies that the MWNT containing SPU solutions were capable to absorb the UV rays. Water vapor permeability of coated fabrics with SPU having 2.5 wt % of MWNT decreases slightly due to the increasing stiffness of polymer chains.

CHAPTER 8

CONCLUSIONS AND SUGGESTIONS FOR FUTURE WORK

8.1 CONCLUSIONS

Segmented polyurethanes (SPU) with well defined architectures were synthesized and their structure, shape memory and water vapor transport properties were investigated in this study. From the experimental results and discussion, we could make general conclusions that the microstructures, thermo-mechanical properties and shape memory effect of segmented polyurethanes would be altered by segmental architecture. Water vapor transport (WVT) properties of shape memory segmented polyurethanes were confluenced by the polyol structure, soft segment crystal melting, and hydrophilicity. Therefore, the water vapor permeability of SPU could be improved by the molecular structure design prior to polymer synthesis.

This dissertation makes a number of significant and original contributions in the area of development of water vapor permeable shape memory segmented polyurethane for breathable textiles. Six unique factors on microstructure, shape memory and water vapor transport properties of SPUs have been studied systematically in this project. Selected polymers were applied to the cotton fabric, and their water vapor permeability properties have been studied accordingly. UV-blocking of MWNT containing SPU coated fabrics were also evaluated. The conclusions of this study are summarized in the following sections:

8.1.1 Influence of Hard Segment on Structure, Shape Memory Effect and WVT of SPU

The influence of hard segment on structure, shape memory and water vapor transport properties of PCL-2000 based polyurethanes were investigated. From the experimental results and discussions, following conclusions could be drawn:

- Soft segments form crystalline structure in this kind of polyurethane. The percent crystallinity of PCL 2000 based SPU increases with increasing soft segment (PCL-2000) content which signifies the soft segment crystallization in SPU. On the other hand presence of hard segment hinders the soft segment crystallization due to their reinforcing filler effect. However, 100% hard segment could also form the crystalline structure. In SPU, these hard segments could not form crystalline structure as these are scattered in the soft matrix and their chains lengths are shorter than the soft segment.
- The heat of fusion of PCL 2000 based SPU was increased with decreasing hard segment content in the polymer due to the presence of more order structure. Soft segment crystal melting temperature (T_{ms}) was shifted to the higher value with decreasing hard segment content in the SPU. DSC cooling curves did not show any exothermic peaks due to the presence of hard segment, and strong interaction of polymer chains by ester groups. The mobility of soft segment depressed by the interaction of ester groups and hard segments which prevents the crystallization of soft segment in DSC cooling cycles.
- Tensile storage modulus was increased with increasing hard segment content in SPU due to the increase of cohesion between the polymer chains. The glass

transition temperature was also increased with increasing hard segment content due to strong allophanate interactions by excess hard segment content. In contrast, Tan (delta) value was increased with increasing soft segment content in the polymer backbone.

- The stress at T_{ms} + 20 °C was increased with increasing hard segment content in the SPU. The reinforcing effect of hard segment in the soft domain region increases the cohesion between the polymer chains as a result of higher tensile strength. The soft segment crystallinity plays major role in shape fixity. The deformation would be only limited in the soft segment matrix at high temperature, T_{ms}+20 °C, after crystal melting. The deformed shape is fixed by recrystallization on cooling steps.
- Hard segment would provide the mechanical strength and integrity to the membrane, whereas the water vapor transport properties depend on content of hydrophilic group and soft segment content. The equilibrium sorption as well as water vapor permeability was increased after soft segment crystal melting. Discontinuous density changes occurred at soft segment crystal temperatures which will increase the chain mobility in the soft segment region. Higher chain mobility and lower density of SPU membranes will provide more gaps for water vapor molecules. As the hard segment content in SPU was increased the equilibrium sorption as well as water vapor permeability was decreased. The decrease of water vapor transport properties with increasing hard segment is due to the reduction of soft segment mobility.

8.1.2 Influence of Block Length of Hydrophilic Segment on Structure and WVT of SPU

From the results of the influence of block length of hydrophilic segment on structure and water vapor transport properties of PTMG-2000 based segmented SPU, following conclusion could be drawn:

- PTMG 2000 based SPU shows strong hydrogen bonded carbonyl stretching due to the interaction between hard and soft segments. Introduction of PEG 200 would break hydrogen bonding as shown in FTIR spectra. SPU without PEG is completely amorphous in nature, although pure polyol has about 26 % of crystalline structure. Crystalline structure would be formed in the SPU with the introduction of PEG in the polymer matrix. The PEG segment would increase the flexibility between the polymer chains which helps for soft segment crystallization.
- No endothermic peaks were observed for the PTMG 2000 based SPU which signifies the amorphous structure. Introduction of PEG segment in the SPU backbone enhances the soft segment crystallization. However, the percent crystallinity hence the heat of fusion would depend on molecular weight of PEG. The SPU with PEG 2000 has higher heat of fusion due to the better intermolecular packing of polymer chains. The heat of fusion was decreased with PEG 200 due to the plasticization effect of PEG 200 which would hinder the crystallization of soft segment. The percent crystallinity or heat of fusion was decreased with PEG 3400 segment due to the chain entanglement possessed by

PEG 3400. Therefore, the polymer molecules must undergo a considerable degree of motion in order to enhance the soft segment crystallization process.

- Introduction of PEG in the polymer matrix will help to form phase-separated structure which would depend on the molecular weight of PEG. Phase separation for SPU without PEG and with PEG –200 is not clear. Best phase separated structure was observed with PEG-2000 which is comparable to the polyol (PTMG 2000) molecular weight. Further increase of molecular weight of hydrophilic segment (PEG 3400) will increase phase mixing due to the chain entanglement. The glass transition temperature was decreased with increasing block length of PEG segment due to the increasing flexibility of polymer chains. The tan (delta) value was increased with increasing block length of PEG segment which signifies increasing the softness or improved tactile properties.
- The equilibrium sorption as well as water vapor permeability was increased with increasing block length of hydrophilic segment. The higher block length of PEG will increase the number of polar groups in polymer backbone which could attract more water vapor molecules. Another reason of increasing water vapor transport properties with higher block length of PEG is due to the increase of free volume. Higher block length of PEG would increase the chain flexibility of polymer chains which will provide more paths for water vapor molecules to pass through the nonporous membranes. The water vapor permeability of SPU would be further enhanced by soft segment crystal melting. The increase of free volume with temperature and the micro-Brownian motion of the soft segment obviously

increase the intermolecular gaps large enough to allow water vapor molecules to pass through the membranes.

8.1.3 Influence of Hydrophilic Segment Content on Structure, Shape Memory Effect and WVT of SPU

The influences of hydrophilic segment content on structure, shape memory and water vapor transport properties of PTMG 2900 based SPUs were studied. The experimental findings are summarized as follow:

- From the FTIR spectra, it was observed that polymers could become gradually more intra- or interconnected for PTMG 2900 based SPU with 5 and 10 wt % of PEG 3400. This is flexible enough to allow perfect topographical position of hard and soft segment for interaction. Further increase of PEG 3400 content will loosen the interactions due to the unstable and distortion of interactions.
- Micro crystallites are present in SPUs which were detected by WAXD and DSC measurements. Percent crystallinity of SPU without PEG 3400 is higher than that of SPUs with PEG 3400, may be due to the better phase separated structure of SPU without PEG 3400. Introduction of 5 wt% of PEG 3400 would increase the phase mixing which will decrease the order structure of soft segment. The little amount (5 wt%) of PEG 3400 would hinder the crystallization process of soft segment. The arrangements of soft segment during crystallization are restricted by chain entanglement with 5 wt% of PEG 3400. Further increase of PEG 3400 content (10 and 15 wt%), the percent crystallinity was increased probably due to the increase of phase separation. With 15 wt% of PEG 3400 content, soft segment crystal melting

point was shifted to higher values. The SPU with higher PEG 3400 content may be some order structure would be formed by crystalline PEG 3400 segment. The PEG 3400 segment crystallization increases the overall crystallinity of the resulted SPU which would shift the T_{ms} to higher value.

- Dynamic mechanical thermal properties of SPUs were also influenced by content of PEG 3400. The glassy state tensile storage modulus of SPU with 15 wt% of PEG 3400 was increased. The higher glassy state modulus with higher PEG 3400 content is due to the chain flexibility possessed by PEG segment. The SPU without PEG 3400 shows a T_g lower than that of SPUs with PEG 3400 due to an increase in the soft segment crystallites. Tan (δ) peak is unclear for the SPU with 5 wt% of PEG 3400 content due to the increase of interactions between the polymer chains. Tan (delta) value was increased with increasing PEG 3400 content in the polymer backbone due to the greater mobility possessed by PEG segment.
- The stress at T_{ms} + 20 ° C was decreased with increasing PEG 3400 segment content in the SPU. The micro-Brownian motion of soft segment which is achieved above T_{ms} is the reasons for decrease of stress. The shape recovery property of the deformed specimen depends strongly on the crystalline structure, or interaction between the polymer chains. As the content of crystalline structure was increased or PEG content was decreased better shape recovery was observed. Recrystallization of soft segment will freeze the micro-Brownian motion of soft segment, and consequently lead to good shape recovery properties.
- Water vapor transport properties of SPUs were influenced by both hydrophilic group content as well as soft segment crystal melting in the room temperature range.

The equilibrium sorption was increased with increasing hydrophilic segment content in the SPU backbone due to the increasing hydrophilicity. Equilibrium sorption was further increased above soft segment crystal melting point temperature which will cause discontinuous density changes inside the membranes. Desorption occurred above 35 °C for SPU with 10 or 15 wt% of PEG due to the lower critical sorption phenomena of PEG 3400 chains. The water vapor permeability of SPUs are also the function of PEG 3400 content at specific temperature. The WVP was increased with increasing hydrophilic segment content in the polymer backbone which will increase the interaction between the polymer chains and water vapor molecules. Soft segment crystal melting was enhanced the water vapor permeability of SPU. The soft segment crystal melting results in an expansion of non-physical voids which will permit the water vapor molecules to transport through the membranes.

8.1.4 Influence of Hydrophilic and/or Carboxylic Unit on Structure and WVT of SPU

From the experimental results of the influence of PEG 3400 and/or DMPA unit on structure and water vapor transport properties of PPG 1000 based SPU, we could draw the following conclusions:

- From FTIR spectra, SPU could be more intra and interconnected through dipole-dipole interaction, hydrogen bonding as the DMPA unit is introduced in the polymer backbone of PPG 1000 based SPU. In contrast PEG 3400 would break the hydrogen bonding between the polymer chains.

- All the SPUs are amorphous in nature as detected by WAXD and DSC. Lower molecular weight of soft segment and strong interaction between the polymer chains will cause phase mixing between the soft and hard segments. The PPG 1000 has relatively shorter chain length and the interaction between the hard and soft segment is relatively strong which will make the microphase separation difficult. Therefore, soft and hard segments do not aggregate mutually, and can not form crystal structure.
- Introduction of small amount of DMPA unit in the segmented polyurethane would lead to a substantial increase in its glass transition temperature, tensile strength and storage modulus. In contrast, small amount of PEG 3400 in the SPU backbone decreases the T_g, tensile strength and storage modulus. The increase of tensile storage modulus with DMPA unit is due to the presence of ionic interaction possessed by carboxyl groups. Glass transition temperature was decreased with the introduction of PEG 3400 segment in the polymer backbone due to the chain flexibility possessed by PEG segment.
- Water vapor transport properties were not only influenced by amorphous region, but also by the interaction between the polymer chains. Water vapor permeability was drastically decreased with the introduction of small amount of DMPA unit in the polymer backbone. Presence of DMPA unit in the polymer backbone increases the interaction between the polymer chains that will make the situation difficult for water vapor molecules to pass through the membranes. In contrast, PEG 3400 enhances the sorption as well as water vapor permeability. The WVP as well as equilibrium sorption was increased in the presence of PEG 3400

segment due to the increasing hydrophlicity and increasing chain flexibility. The higher polymer chain mobility will provide more paths for water vapor molecules to pass through the nonporous membranes.

8.1.5 Influence of Mixed Polyol Block on Structure and WVT of SPU

PCL 3000, PPG 3000 and PTMG 2900 polyols were used to investigate the influence of mixed polyol on structure and water vapor transport properties of SPUs. The experimental findings are summarized as follow:

- SPU with PCL 3000 based soft segment shows strong inter-chain interaction as detected by FTIR. The interactions were loosened by using PPG 3000 or PTMG 2900 along with PCL 3000 soft segment. An ester group has much stronger interaction than an ether group which is the reasons for decreasing absorption spectra in the hydrogen bonded NH region. Soft-soft segment phase mixing would weaken the inter-chain interaction.
- WAXD and DSC results confirmed that if the pure soft segment is crystallizable, then it could be able to form crystalline structure in the resulted SPU separately in mixed soft segment block SPU. The presence of noncrystalline polyol such as PPG 3000 segment hinders the crystallization of PCL 3000 segment. The soft-soft segment phase mixing will make the situation difficult for ordering of crystallizable soft segment. The shape and position of exothermic as well as endothermic peaks have been altered with mixed block SPU due to the soft-soft segment phase mixing. The endothermic peaks were divided into two parts for

SPU having same quantity of PCL 3000 and PTMG 2900. Both phases form crystalline structure in the resulted SPU that's the reason for this phenomenon.

- Dynamic mechanical thermal properties were also influenced by selection of soft segment block. PCL 3000 based SPU would enable the polymer matrix to sustain a high modulus value to higher temperature. The highest loss tangent was obtained with mixed block SPU of PTMG 2900 and PPG 3000 due to their loose flexible and nearly amorphous structure which suggests the importance of the combination of mixed soft segment block. Glassy state modulus of PTMG 2900-PPG 3000 mixed block SPU was increased due to the increasing chain flexibility of polymer chains. PCL 3000 based SPU has lower tan (delta) value due to the increasing interaction between the polymer chains. In contrast tan (delta) value was increased and glass transition temperature was decreased when PPG 3000 or PTMG 2900 was used along with PCL 3000 segment. The increasing polymer chain flexibility and to some extent phase mixing will make the segmental motion of polymer chains easier as a result of higher tan (delta) value and lower glass transition temperature.
- The behavior of water vapor transport properties in SPU membranes could be interpreted on the basis of the chemical nature of soft segment in the SPU backbone, changes in crystallinity, hydrophilicity and T_g of SPU. SPU with mixed polyol, containing PTMG 2900 and PPG 3000 performed best with water sorption as well as water vapor permeability. The presence of flexible PPG 3000 and PTMG 2900 segment in the SPU backbone, and their phase mixed structure increase the chain mobility which will enhance the water vapor permeability.

Soft segment crystal melting in the experimental temperature range would enhance the permeability due to increasing chain mobility and discontinuous density changes inside the membrane. The micro-Brownian motion of soft segment at crystal melting point will obviously increase the intermolecular gaps large enough to allow water vapor molecules to pass through the membranes easily.

8.1.6 Influence of MWNT on Structure, Shape Memory effect and WVT of SPU

When functionalized multi wall carbon nano tubes (MWNT) was reinforced in the PTMG 2900 based SPU matrix, they were effectively exfoliated in SPU matrix. Their structure, shape memory and mass transfer properties were affected by content MWNT content in the SPU matrix.

- MWNTs were entrapped by the SPU at low concentration such as 0.25 wt% which was detected by SEM and Raman spectra studies. TEM and WAXD results show the interaction of MWNT and SPU. The FTIR absorbency of MWNT containing SPU was increased as the MWNT has higher IR absorbance capability. Uniform dispersion of functionalized MWNTs was observed in the SPU matrix which was detected by TEM image.
- The soft segment crsytallinity was slightly increased with 0.25 wt% of MWNT due to the crystallization by nano particles. Further increase of MWNT in SPU matrix would hinder the crystallization process of soft segment. Higher MWNT content will act as filler in polymer matrix which would suppress the mobility of soft segment as a result of decrease of soft segments crystallinity.

- The modulus and hardness were enhanced by reinforcing effect of functionalized MWNT. The tensile storage modulus was increased with increasing MWNT content in the SPU. The increase of tensile storage modulus with increasing MWNT content signifies the well dispersion of MWNT in the polymer matrix. Glass transition temperature was increased with increasing MWNT content in SPU which suggests that MWNT not only influence the crystalline region but also the amorphous region of SPU. The presence of MWNT content in the SPU would hinder the segmental mobility of the polymer chains as a result of higher glass transition temperature.
- Experimental results revealed that the formation of network structure for a polymer was important to exhibit the typical shape-memory effect. The soft segment will freely absorb external stress by unfolding or extending their molecular chains. On the other hand, hard segment together with MWNT in the polymer matrix would help to recover deformed shape. As the MWNT in the polyurethane was increased the higher shape recovery effect was observed. Nano particles will help to store internal elastic energy during loading and shape fixing. The stored elastic strain energy by nano particles would be released during heating process of shape memory testing as a result of higher recovery effect.
- Equilibrium sorptions were decreased for the SPU having 1 or 2.5 wt% of MWNT. The increase of the mean free paths of the water molecules to pass through the SPU/MWNT matrix seems the cause of decrease of water sorption. Soft segment crystal melting would enhance the water vapor transport properties of membrane. Above soft segment crystal melting point temperature, water vapor

permeability of SPU with 0.25 wt% of MWNT was increased slightly as compared to the pristine SPU membrane. Further increase of MWNT would hinder the water vapor permeability due to the polymer chain stiffening effect posses by nano particles.

8.1.7 Free Volume and Water Vapor Permeability of SPU

The free volume of SPU membranes was measured by PALS. The free volume data were correlated with water vapor permeability results. The conclusions for free volume and WVP results are as follow:

- The free volume and water vapor permeability of dense SPU membranes were varies with temperature. TEM and PALS study revealed that the phase separation of polymer influences the free volume of SPUs. TEM image shows that the hard segment, soft segment and crystal regions are coexisted in PTMG 2900-PCL 3000 based SPU. Due to the phase mixed structure, the free volume of this sample did not increase significantly. The radius of free volume was influenced by type of soft segment in the SPU. The interaction and packing of polymer chains are the reason for the variation of free volume. PTMG 2900-PPG 3000 based SPU possessed higher free volume radius due to their loose and nearly amorphous structure which will increase the free volume.
- Direct correlation was observed among the polymer morphology, water vapor permeability and free volume results. Morphology, hence the fractional free volume of SPU would depend on polymer chain flexibility. Water vapor permeability was increased as the fractional free volume increases. The concept of bi-soft segment SPU used in this work signifies the selections and tailoring of structure and

functional properties (here WVP) in segmented polyurethane copolymer membrane. Experimental results revealed that the water vapor permeability can be controlled by free volume which would depend on the chemical composition of SPU, and hydrophilicity of membranes. The flexibility and loose packing of soft segment would result in increase of the concentration of free volume holes which are capable of supporting water vapor permeability in the soft segment regions.

8.1.8 Coated Fabrics Evaluations

Selected SPUs and MWNT containing SPUs were applied to the cotton fabrics. From the experimental findings following conclusions could be drawn:

- SEM micrographs shows nonporous SPU film layers formed continuously over the surface of the coated fabrics. The presence of nonporous SPU layers suggested that the water vapor permeability of coated fabrics were originated from the properties of SPU itself. Water pressure resistance value of 24.5 mbar was achieved for coated fabric with PTMG 2900 based SPU containing 15 wt% of PEG 3400 as compared to "0" for uncoated fabrics. Coated fabrics also maintained good water vapor permeability thus confirmed the physiological comfort to the wearer. The WVP of SPU coated fabric was increased with increasing hydrophilic segment content in the SPU. Coated fabrics with PCL based SPU has lower water vapor permeability as compared with PTMG based SPU coated fabrics. These results follow the same trends with original membrane permeability.
- MWNT reinforced SPU coated fabrics shows excellent UV blocking. With only 1 wt% of MWNT in the SPU, the UV protection factor (UPF) was about 125 (according to the Australian/New Zealand standard). This results is of excellent

UPF rating (>+50) as compared to the uncoated fabric having UPF of 5.6 which is non ratable. UV transmissions through the MWNT containing SPU coated fabrics were almost zero. Therefore, the MWNT containing coated fabrics are capable to protect the wearer from UVA rays and well as UVB rays. The high UV absorption capability of MWNT containing SPU was explained by solid band theory. The water vapor permeability of MWNT containing SPU fabrics depends on the quantity of MWNT in the SPU matrix. Coated fabric with low (0.25 wt%) MWNT content of SPU did not influence the WVP. However, WVP of 2.5 wt% of MWNT containing SPU coated fabrics was decreased little bit due to the stiffening effect of polymer chains possessed by MWNT.

8.2 SUGGESTIONS FOR FUTURE WORK

This study presented development of temperature stimulating shape memory nonporous segmented polyurethanes membrane with improved water vapor permeability and soft segment crystal melting temperature in the room temperature range. Such nonporous membrane would be applicable to develop smart breathable textiles by laminating solid nonporous membrane instead of microporous membrane on a suitable base fabric which would have lower water vapor permeability at lower temperature and significant increase of water vapor permeability with increasing temperature. This "flexible barrier function" will enable the garments to intelligently adjust its insulating properties in response to temperature changes which will assure optimum comfort regardless of environmental temperature. Systematic study on structure and water vapor transport properties presented in this study throws lights to the polymer chemist to develop smart

polyurethane membrane by molecular design from the wide range of raw materials available for polyurethane synthesis.

It should be no surprise to anyone who has completed a thesis that the experiment could be improved through further iterations. The contributions described in this dissertation can be summarized as the development of temperature sensitive breathable shape memory segmented polyurethane membrane. These contributions have been demonstrated with real world examples which have potential application in smart breathable textiles and medical applications. With these contributions there are wide ranges of future possibilities for new research and applications that may be used in scientific and commercial settings. The areas require further study:

8.2.1 Increasing Percent Crystallinity and Engender Smartness of WVP

The percent crystallinity of SPU having room temperature range soft segment crystal melting points was about 15 %. Therefore, there is scope to increase the percent crystallinity by molecular design which will engender the smartness of WVP in the soft segment crystal melting range. Crystal structure would act as barrier properties of film, WVP below the T_{ms} would be low and abrupt change of WVP would occur above T_{ms}, and this property would be applicable in smart garment.

8.2.2 Film Thickness

The film thickness for WVP testing of the present study was about 90 micron which would not be suitable for textile lamination. Suitable methods must be developed for thinner and uniform film surface. Since, the permeability is inversely proportional to the

film thickness. Therefore, the permeability of membrane prepared from our SPU having thickness of 20 – 30 micron (suitable for lamination) would be few times higher than the presented value in this thesis.

8.2.3 Model Setup

From the experimental results, we found that there are certain changes of water vapor permeability of SPU at soft segment crystal melting point temperature. The T_{ms} was also used as transition point for shape memory effect measurements. Therefore, there are scope for the systematic study of shape memory properties and water vapor permeability, and set up a model for better understanding of the switch temperature for water vapor permeability and shape recovery temperature.

8.2.4 MWNT-SMPU Characterization

Carbon nano tubes (CNT) are attracting considerable attention due to their unique physical, mechanical, and chemical properties, including high Young' s modulus and strength, thermal and electrical conductivity, thermal stability, high specific surface area, and many others as reported in literatures. Therefore, the other properties such as conductivity, antibacterial properties of MWNT-SPU coated fabrics should be investigated. MWNT-SPU supposed to exhibit the surface properties of polymers, as well as electrical conductivity of carbon frame which could provide new possibility for advanced textiles applications.

8.2.5 Evaluations of SPU and MWNT-SPU Coated Fabrics

Although few selected SPUs were applied to cotton fabrics, and their water vapor permeability properties were measured. However, other properties of coated/laminated fabrics such as abrasion resistance, tear resistance, flexibility etc should be evaluated in order to take the product in reality. Washing resistance for coated fabrics and delamination of laminated fabrics should also be evaluated accordingly. Segmented polyurethanes should be applied to synthetic textile matrix as well.

LIST OF ABBREVIATIONS

BWF	Breathable waterproof fabrics
1,4-BDO	1,4-butane diol
CNT	Carbon nano tube
DMPA	Dimethyl amino propionic acid
DMTA	Dynamic mechanical thermal analysis
DSC	Differential scanning calorimetry
DTG	Derivative thermogravimetry
ES	Equilibrium sorption
FFV	Fractional free volume
FTIR	Fourier transforms infrared
H-bonded	Hydrogen bonded
HDF	High density fabrics
HDI	Hexamethylene diisocyanate
HS	Hard segment
mbar	Milli bar
4,4'-MDI	4,4'-diphenylmethane diisocyanate
MWNT	Multi wall carbon nano tube
MWNT-SPU	Multi wall carbon nano tube reinforced SPU
NOL	Naval ordnance laboratory
PALS	Positron annihilation lifetime spectra
PBA	Polybutilene adipate
PCL	Polycaprolactone diol

PCL2000	Polycaprolactone diol with molecular weight 2000 g mol^{-1}
PEG	Polyethylene glycol
PEO	Polyethylene oxide
PPG	Polypropylene glycol
PPO	Polypropylene oxide
PTFE	Polytetrafluroethylene
PTMG	Poly(tetramethylene glycol)
PU	Polyurethane
RuO_4	Ruthenium tetraoxide
SEM	Scanning electron microscopy
SMA	Shape memory alloy
SMP	Shape memory polymer
SMPU	Shape memory polyurethane
SPU	Segmented polyurethane
SWNT	Single wall carbon nano tube
TEM	Transmission electron microscopy
TGA	Thermo-gravimetry analysis
TMP	Trimethylol propane
UPF	UV protection factor
WAXD	Wide angle X-ray diffraction
WBF	Waterproof breathable fabrics
WVF	Water vapor flux
WVP	Water vapor permeability

LIST OF SYMBOLS

Symbol	Definition	Unit
A	Test area of water vapor permeability testing	m^2
d	Distance between the parallel planes in the crystallites	nm
D_w	Equilibrium sorption	%
δ	Phase angle	°
ΔH	Heat of fusion	Cal
E'	Storage modulus	MPa
E"	Loss modulus	MPa
ε_m	Strain	%
ε_p	Strain recovery	%
ε_u	Strain retention	%
G	Equilibrium water sorption	%
h	Thickness of membrane	mm
I_3	o-Ps intensity	%
J	Rate of transport of permeant	kg $\mu m/m^2$
λ	Wavelength of X-ray radiation	Å
M_∞	Fractional weight gain at equilibrium	g/g
M_n	Number average molecular weight	g mol^{-1}
M_t	Fractional weight gain at time t	g/g
M_w	Weight average molecular weight	g mol^{-1}
P	Permeability	$g/m^2.24h$

p_1	External partial pressure of the vapor on the high pressure sides of the membrane	Pa
p_2	External partial pressure of the vapor on the low pressure sides of the membrane	Pa
S	Sorptivity	g/g
t	Time	s
T	Absolute temperature	K
T_a	Temperature of ambient	°C
T_g	Glass transition temperature	°C
T_m	Melting point temperature	°C
T_{ms}	Soft segment crystal melting temperature	°C
T_x	Transformation temperature	°C
T_s	Temperature of skin	°C
θ	Incidence angle of X-ray	°
τ_3	o-Ps lifetime	ns
v	Specific volume of polymer	cm^3/g
v_f	Free volume	cm^3/g
V_f	Total free volume	cm^3/g
v_m	Free volume of penetrant molecules	cm^3/g
v_p	Equivalent molecular volume	cm^3/g
χ	Degree of crystallinity	--

REFERENCES

1. Srinivasan AV, and McFarland DM, *Shape Memory Alloys* in Smart Structures, Cambridge University Press, p 26-72, (2001).
2. Lendlein A and Kelch S, *Shape-memory polym*er, Angew Chem Int Ed, **41**, 2034-2057, (2002).
3. Irie M, *Shape memory polym*er, in *Shape memory materials*, Edited by Otsuka K and Wayman CM, Cambridge University Press, 203-219, (1998)
4. Mondal S, Hu JL, Yang Z, Liu Y and Szeto YS, *Shape memory polyurethane for smart garment*, Res J Text & Appar, **6** (2), 75-83, (Nov 2002).
5. Lomax GR, *Intelligent polyurethane for interactive clothing*, Text Asia, Sept, 39 – 50, (2001).
6. EU Patent No 83305387.9 (date of filing 14.09.83), *Moisture-permeable waterproof fabric*, J Coated Fabric, **14**, 148-164, (1985).
7. Shishoo RL, *Technology for comfort*, Textile Asia, **19** (6), 93-110, (1998).
8. Sen AK, *Coated Textiles: Principle and Applications*, Tech Ed Damewood J, Technomic Publishing Co., USA, p 133-154, (2001).
9. Holmes DA, *Performance characteristics of waterproof breathable fabrics*, J Coated Fabrics, **29** (4), 306-316, (2000).
10. Kubin I, *Functional and fashion coating for apparel*, Melliand Inter, **7** (June), 134-138, (2001).
11. Kramar L, *Recent and future trends for high performance fabrics providing brethability and waterproofness*, J Coated Fabrics, **28** (October), 107-115, (1998).

12. Lomax GR, *Hydrophilic polyurethane coatings*, J Coated Fabrics, **20** (October), 88-107, (1990).

13. Roey MV, *Water-resistant breathable fabrics*, J Coated fabrics, **21**(Jul.), 21-31, (1991).

14. Gottwald L, *Water vapor permeable PUR membranes for weatherproof laminates*, J Coated Fabrics, **25** (Jan.), 169-175, (1996).

15. Tsujita Y, *The Physical Chemistry of Membranes* in Membrane Science and Technology, Edited by Osada Y, and Nakagawa T, Marcel Dekker, Inc, New York, p 3-58, (1992).

16. Baker WR, *Membrane Technology and Applications*, McGraw-Hill, New York, p 1-86, (2000).

17. Strathmann H, *Synthetic Membrane and Their Preparation* in Handbook of Industrial Membrane Technology, Edited by Porter M C, Noyes Publications, New Jersey, p 1-60, (1989).

18. Mooney CL and Schwartz P, *Effect of salt spray on the rate of water vapor transmission in microporous fabric*, Text Res J, **55** (8), 449-452, (1985).

19. Johnson L and Samms J, *Thermoplastic Polyurethane Technologies for the Textile Industry*, J Coated Fabrics, **27** (July), 48-62, (1997).

20. Lomax GR, *Design of waterproof, water-vapor-permeable fabrics*, J Coated Fabric, **15** (July), 40-66, (1985).

21. Cussler EL, *Diffusion: Mass Transfer in Fluid Systems*, (Cambridge University Press, Cambridge), 1st Ed., Chap 15 (1997).

22. Bannwart AC and Bontemps A, *condensation of vapor with incondensables –an improved gas-phase film model accounting for the effect of mass-transfer on film thickness*, Inter J Heat & Mass Transf, **33** (7), 1465-1474, (1990).

23. Wirpsza Z, *Polyurethanes: Chemistry, Technology and Applications*, Ellis Horwood, New York, p 11-82 and 95-137, (1993).

24. Dieterich D, Grigat E and Hahn W, *Chemical and Physical-Chemical Principles of Polyurethane Chemistry*, Polyurethane Handbook, Edited by Oertel G, Hanser Publisher, New York, p 6-41, (1985).

25. Lamba NMK, Woodhouse KS and Cooper SL, *Polyurethanes in biomedical applications*, CRC Press, Boca Raton, p 43-89, (1998).

26. *Chemistry and Technology of Polyurethanes*, Chap 1, Vilar Polyurethanes, http://www.poliuretanos.com.br/, (Viewed on 11th July, 2005).

27. Chu B, Gao T, Li Y, Wang J, Desper CR and Byrne CA, *Microphase separation kinetics in segmented polyurethanes: effects of soft segment length and structure*, Macromolecules, **25**, 5724-5729, (1992).

28. Hu W and Koberstein JT, *The effect of thermal annealing on the thermal properties and molecular weight of a soft segmented polyurethane copolymer*, J Polym Sci, Part B: Polym Phys, **32**, 437-446, (1994).

29. Takahashi T, Hayashi N and Hayashi S, *Structure and properties of shape-memory polyurethane block copolymers*, J Appl Polym Sci, **60** (7), 1061-1069. (1996).

30. Leibler L, *Theory of microphase separation in block copolymers*, Macromolecules, **13**, 1602-1617, (1980).

31. Dai L, *Phase separation of polyisoprene-polyacetylene copolymers*, Synthetic Metals, **84**, 957-960, (1997).

32. Qipeng G and Zhenhai L, *Phase behavior of polymer blends*, J Ther Analy & Calorimetry, **59**, 101-120, (2000).

33. Altena FW and Smolders CA, *Calculation of liquid-liquid phase separation in a ternary system of a polymer in a mixture of a solvent and a nonsolvent*, Macromolecules, **15**, 1491-1497, (1982).

34. Alig I, Jenninger W and Schawe JEK, *Curing kinetics of phase separating thermosets studied by DSC, TMDSC and dielectric relaxation spectroscopy*, Thermochimica Acta, **330**, 167-174, (1999).

35. Velankar S and Cooper SL, *Microphase separation and rheological properties of polyurethane melts. 2. effect of block incompatibility on the microstructure*, Macromolecules, **33**, 382-394, (2000).

36. Lee HK, Kim JY, Kim YD, Shin JY and Kim SC, *Liquid-liquid phase separation in a ternary system of segmented polyurethane/dimethylformamide/water: effect of hard segment content*, Polymer, **42**, 3893-3900, (2001).

37. Murgasova R, Brantley EL, Hercules DM and Nefzger H, *Characterization of polyester-polyurethane soft and hard blocks by a combination of MALDI, SEC, and chemical degradation*, Macromolecules, **35**, 8338-8345, (2002).

38. Leung LM and Koberstein JT, *DSC annealing study of microphase separation and multiple endothermic behavior in polyether-based polyurethane block copolymers*, Macromolecules, **19**, 706-713, (1986).

39. Li W, Ryan AJ and Meier IK, *Morphology devlopment via reaction-induced phase separation in flexible polyurethane foam,* Macromolecules, **35**, 5034-5042, (2002).

40. Yontz DJ and Hsu SL, *A mass spectrometry analysis of hard segment length distribution in polyurethanes*, Macromolecules, **33**, 8415-8420, (2000).

41. Sung CSP, Hu CB and Wu CS, *Properties of segmented poly(urethaneureas) based on 2,4-toluene diisocyanate, 1. thermal transitions, X-ray studies, and comparison with segmented poly(urethanes)*, Macromolecules, **13**, 111-116, (1980).

42. Li C, Goodman SL, Albrecht RM and Cooper SL, *Morphology of segmented polybutadiene-polyurethane elastomers*, Macromolecules, **21**, 2367-2375, (1988).

43. Jeong HM, Kim BK and Choi YJ, *Synthesis and properties of thermotropic liquid crystalline polyurethane elastomers*, Polymer, **41**, 1849-1855, (2000).

44. Wang CB and Cooper SL, *Morphology and properties of segmented polyether polyurethaneureas*, Macromolecules, **16**, 775-786, (1983).

45. Delpech MC and Coutinho FMB, *Waterbrone anionic polyurethanes and poly(urethane-urea)s: influence of the chain extender on mechanical and adhesive properties*, Polym Test, **19**, 939-952, (2000).

46. Delpech MC and Coutinho FMB, *Some properties of films cast from polyurethane aqueous dispersions of polyether-based anionomer extended with hydrazine*, Polym Test, **15**, 103-113, (1996).

47. Tao HJ, Meuse CW, Yang X, MacKnight WJ and Hsu SL, *A spectroscopic analysis of phase separation behavior of polyurethane in restricted geometry: chain rigidity effects*, Macromolecules, **27**, 7146-7151, (1994).

48. Velankar S and Cooper SL, *Microphase separation and rheological properties of polyurethane melts. 1. effect of block length*, Macromolecules, **31**, 9181-9192, (1998).

49. Desai S, Thakore IM, Sarawade BD and Devi S, *Effect of polyols and diisocyanates on thermo-mechanical and morphological properties of polyurethanes*, Europ Polym J, **36**, 711-725, (2000).

50. Kim BK, Lee SY, Lee JS, Baek YJC, Lee JO and Xu M, *Polyurethane ionomers having shape memory effects*, Polymer, **39** (13), 2803-2808, (1998).

51. Funakuba H, Shape *Memory Alloys*, Vol. 1, Gordon and Breach Publisher, New York, Chap 3, (1987).

52. Feninat FE, laroche G, Fiset M and Mantovani D, *Shape memory materials for biomedical applications*, Adv Engg Mater, **4** (3), 91-104, (2002).

53. Thrasher MA, Shahin AR, Meckl PH and Jones JD, *Thermal cycling of shape memory alloy wires using semiconductor heat pump modules*, Proceeding first European conference on smart structures and materials, Glasgow, 12-14 May 1992, Edited by Culshaw B, Gardiner P T and McDonach A, 197-200, (1992).

54. Okano T and Kikuchi A, *Intelligent biointerface: remote control for hydrophilic-hydrophobic property of the material surfaces by temperature*, Proceeding of the third international conference on intelligent materials, Third European

conference on smart structures and materials, Lyon, France, 3-5 June 1996, Edited by Gobin P F and Tatibouët J, 34-41, (1996).

55. Tobushi H, Hashimoto T, Hayashi S and Yamada E, *Thermomechanical constitutive modeling in shape memory polymer of polyurethane series*, J Intell Mater Syst & Struct, **8** (8), 711-718, (1997).

56. Li F, Hou J, Zhu W, Zhang X, Xu M, Luo X, Ma D and Kim BK, *Studies on thermally stimulated shape memory effect of segmented polyurethanes*, J Appl Polym Sci, **64** (8), 1511-1516, (1997).

57. Li F, Hou J, Zhu W, Zhang X, Xu M, Luo X, Ma D and Kim BK, *Crystallinity and morphology of segmented polyurethanes with different soft-segment length,* J Appl Polym Sci, **62** (4), 631-638, (1996).

58. Kim BK, Shin YJ, Cho SM and Jeong HM, *Shape-memory behavior of segmented polyurethanes with an amorphous reversible phase: the effect of block length and content*, J Polym Sci: Part B, Polym Phys, **38**, 2652-2657, (2000).

59. Kim BK, Lee SY and Xu M, *Polyurethanes having shape memory effects*, Polymer, **37** (26), 5718-5793, (1996).

60. Lee HY, Jeong HM, Lee JS and Kim BK, *Study on the shape memory polyamides. Synthesis and thermomechanical properties of polycaprolactone-polyamide block copolymer*, Polym J, **32**, 23-28, (2000).

61. Lee BS, Chun BC, Chung YC, Sul Li and Cho JW, *Structure and thermomechanical properties of polyurethane block copolymers with shape memory effect*, Macromolecules, **34**, 6431-6437, (2001).

62. Lin JR and Chen LW, *Study on shape-memory behavior of polyether-based polyurethanes. I influence of the hard-segment content*, J. Appl. Polym. Sci., **69** (8), 1563-1574, (1998).

63. Lin JR and Chen LW, *Shape-memorized crosslinked ester-type polyurethane and its mechanical viscoelastic model*, J. Appl. Polym. Sci., **73**, 1305-1319, (1999).

64. Yilgor I and Yilgor E, *Hydrophilic polyurethaneurea membranes: influence of soft block composition on the water vapor permeability rates*, Polymer, **40**, 5575-5581, (1999).

65. Osada Y and Nakagawa T, *Membrane Science and Technology*, Marcel Dekker, Inc, Chap 7, (1990).

66. Balik CM, *On the extraction of diffusion coefficients from gravimetric data of small molecules by polymer thin films*, Macromolecules, **29**, 3025-3029, (1996).

67. Kamaruddin H and Koros WJ, *Some observations about the application of Fick's first law for membrane separation of multicomponent mixtures*, J. Membr. Sci., **135**, 147-159, (1997).

68. Meares P, *The physical chemistry of transport and separation by membranes*. In Membrane Separation process, Elsevier, New York, Chap. 1, (1976).

69. Cranks J, *The mathematics of diffusion*, Clarendon: Oxford, 2nd Ed., p 48, 248, (1975).

70. Crank J and Park GS, *Methods of diffusion measurement, in: Diffusion in polymers*, Academic press, London and New York, NY, Chap. 1, (1968).

71. Aitken A and Barrer RM, *Transport and solubility of paraffin in rubber*, Trans Faraday Soc, **51**, 116-130, (1955).

72. Cohen MH and Turnbull D, *Molecular transport in liquid and glasses*, J Chem Phys, **31**, 1164-1169, (1960).

73. Vrentas JS and Duda JL, *Diffusion in polymer-solvent system II A predictive theory for the dependence of diffusion coefficients on temperature, concentration and molecular weight*, J Polym Sci: Polym Phys Ed, **15**, 417-439, (1977).

74. Meares P, *The influence of penetrant concentration on the diffusion and permeation of small molecules in polymers above glass transition temperature*, Eur Polym J, **29**, 237-243, (1993).

75. Mulder M, *Transport in membranes. Basic principles of membrane technology*, in Dordrecht: Kluwer, Chap 6, 198-280, (1991).

76. Gupta T and Adhikari B, *Diffusion Behavior of hexane in diamine chain-extended hydroxyterminated polybutadiene based polyurethanes*, J Appl Polym Sci, **86** (1), 90-97, (2002).

77. Chen CX, Han BB, Li JD, Shang TG, Zou J and Jiang WJ, *A new model on the diffusion of small molecule penetrants in dense polymer membranes*, J Membr Sci, **187**, 109-118, (2001).

78. Yen MS and Cheng KL, *The effect of soft segments on the physical properties and water vapor permeability of H_{12}MDI-PU cast films*, J Appl Polym Sci, **52**, 1707-1717, (1994).

79. Jonquieres A, Clement R and Lochon P, *Permeability of block copolymers to vapors and liquid*, Prog. Polym. Sci., **27**, 1803-1877, (2002).

80. Kanapitas A, Pissis P, Ribeles JLG, Pradas MM, Privalko E and Privalko V, *Molecular mobility and hydration properties of segmented polyurethanes with*

varying structure of soft- and hard-chain segments, J Appl Polym Sci, **71**, 1209-1221, (1999).

81. Huang LS, Chao MS and Lai JY, *Diffusion of ethanol and water through PU membranes*, Eur Polym J, **34** (3/4), 449-454, (1998).

82. Ponangi R, Pintauro PN and Kee DD, *Free volume analysis of organic vapor diffusion in polyurethane membranes*, J Membr Sci, **178**, 151-164, (2000).

83. Schneider N, Dusablon L, Snell E and Prosser R, *Water vapor transport in structurally varied polyurethanes*, J Macromol Phys, **B3**, 623-644, (1969).

84. Hsieh K, Tsai C and Tseng S, *Vapor and gas permeability of polyurethane membranes. Part I. Structure-property relationship*, J Membr Sci, **49**, 341-350, (1990).

85. Petrik S, Hadobas F, Simek L and Bohdanecky M, *Sorption of water-vapor by hydrophilic polyurethane-ureas*, J Appl Polym Sci, **47** (4), 677-684, (1993)

86. Tsunoda M and Kobayashi T, *Preparation of a polyurethane film having high water vapor-permeability and its physicochemical properties*, Nippon Kagaku Kaishi, **11**, 761-766, (1998).

87. Jeong HM, Ahn BK and Kim BK, *Temperature sensitive water vapor permeability and shape memory effect of polyurethane with crystalline reversible phase and hydrophilic segments*, Polym Int, **49**, 1714-1721, (2000).

88. Jeong MH, Ahn KB, Cho MS and Kim KB, *Water vapor permeability of shape memory polyurethane with amorphous reversible phase*, J Polym Sci, Part B: Polym Phys, **38**, 3009-3017, (2000).

89. Hsieh HK, Tsai CC and Chang MD, *Vapor and gas permeability of polyurethane membranes. Part II. Effect of functional groups*, J Membr Sci, **56**, 279-287, (1991).

90. Rutkowska M and Eisenberg A, *Ionomeric blends. IV. Miscibility of urethane elastomers with styrene-styrene sulfonic acid copolymer*, J Appl Polym Sci, **29** (3), 755-762, (1984).

91. Hsieh KH and Chou LM, *Interpenetrating polymer networks of polyurethane and polystyrene ionomers*, J Appl Polym Sci, **38** (4), 645-654, (1989).

92. Valentová H, Nedbal J, Ilavský M and Pissis P, *Dynamic mechanical and water sorption behavior of ordered polyurethanes*, J Non-crystalline Solids, **307-310**, 304-310, (2002).

93. Bharadwaj V, Somani K and Kansara S, *The effect of chain length of polyethylene glycol on properties of castor oil based polyurethane elastomers*, J Macrom Sci –Pure and Appl Chem, **39** (1-2), 115-127, (2002).

94. Chen CT, Eaton RF, Chang YJ and Tobolsky AV, *Synthesis, characterization, and permeation properties of polyether-based polyurethanes*, J Appl Polym Sci, **16**, 2105-2114, (1972).

95. Green RJ, Corneillie S, Davies MC, Roberts CJ, Schach E, Tendler SBJ and Williams PM, *Investigation of the hydration kinetics of novel poly (ethylene oxide) containing polyurethanes*, Langmuir, **16**, 2744-2750, (2000).

96. Schneider N, Langlois D and Byrne C, *The effect of water on the glass transition behavior of hydrophilic polyurethanes*, Polym Mater Sci, Engg, **69**, 249-250, (1993).

97. Hayashi S, Ishikawa N and Giordano C, *High moisture permeability polyurethane for textile application*, J Coated Fabrics, **23** (7), 74-83, (1993).

98. Chen W, Zhu C and Gu X, *Thermosetting polyurethanes with water-swollen and shape memory properties*, J. Appl. Polym. Sci., **84**, 1504-1512, (2002).

99. Rinzler AG, Hafner JH, Nikolaev P, Lou L, Kim SG, Tomanek D, Colbert DT and Smalley RE, *Unraveling Nanotubes: Field Emission from an Atomic Wire*, Science, **269** (5230), 1550-1553, (1995).

100. Biro LP, Mark GI, Koos AA, Nagy JB and Lambin P, *Coiled carbon nanotube structures with supraunitary nonhexagonal to hexagonal ring ratio*, Physical Rev. B, **66** (16), Art. No 165405 (2002).

101. Kiang CH, *Electron irradiation induced dimensional change in bismuth filled carbon nanotubes,* Carbon, **38** (11-12), 1699-1701, (2000).

102. Liu S, Tang X, Mastai Y, Felner I and Gedanken A, *Preparation and characterization of iron-encapsulating carbon nanotubes and nanoparticles*, J Mater Chem, **10** (12), 2502-2506, (2000).

103. Prados C, Crespo P, Gonalez JM, Hernando A, Macro JF, Gancedo R, Grobert N, Terrones M, Walton RM and Kroto HW, *Magnetic and hysteretic properties of Fe-filled nanotubes*, IEEE Transactions on Magnetics, **37** (4), 2117-2119, (2001).

104. Andrews R, Jacques D, Rao AM, Derbyshire F, Qian D, Fan X, Dickey EC and Chen J, *Continuous production of aligned carbon nanotubes: a step closer to commercial realization*, Chem Phys Lett, **303** (5-6), 467-474, (1999).

105. Han JH, Yoo JE and Lee CJ, *Low temperature synthesis of carbon nanotubes by thermal chemical vapor deposition using co-catalyst*, J Korean Phys Soc, **39** (Suppl S Dec), S116-S119, (2001).

106. Puretzky AA, Geohegan DB, Fan X and Pennycook SJ, *Dynamics of single-wall carbon nanotube synthesis by laser vaporization*, Appl Phys, A: Mater Sci & Proc, **70** (2), 153-160, (2000).

107. Tang YH, Zheng YF, Lee CS, Wang N, Lee ST and Sham TK, *Carbon monoxide-assisted growth of carbon nanotubes*, Chem Phys Lett, **342** (3-4), 259-264, (2001).

108. Che G, Lakshmi BB, Martin CR and Fisher ER, *Chemical vapor deposition based synthesis of carbon nanotubes and nanofibers using a template method*, Chem. Mater., **10** (1), 260-267, (1998).

109. Subramoney S, *Fundamental and technological aspects of carbon nanotubes, on Nanoscale Materials*, Edited by Liz-Marzán, and Kamat PV, Kluwer Academic Publishers, London, p 455-474, (2003).

110. Grady BP, Pompeo F, Shambaugh RL and Resasco DE, *Nucleation of polypropylene crystallization by single-walled carbon nanotubes*, J Phys Chem, **B 106** (23), 5852-5858, (2002).

111. Werner P, Altstadt V, Jaskulka R, Jacobs O, Sandler JKW, Shaffer MSP and Windle AH, *Tribological behaviour of carbon-nanofibre-reinforced poly(ether ether ketone)*, Wear, **257** (9-10), 1006-1014, (2004).

112. Pan ZW, Xie SS, Lu L, Cheng BH, Sun LF, Zhou WY, Wang G and Zhang DL, *Tensile tests of ropes of very long aligned multiwall carbon nanotubes*, Appl. Phys. Lett., 74 (1999) 3152-3154, (1999).

113. Sun Y, Wilson SR and Schuster DI, *High dissolution and strong light emission of carbon nanotubes in aromatic amine solvents*, J American Chem Soc, **123** (22), 5348-5349, (2001).

114. Safadi B, Andrews R and Grulke EA, *Multiwalled carbon nanotube polymer composites: synthesis and characterization of thin films*, J Appl Polym Sci, **84**, 2660-2669, (2002).

115. Ajayan PM, *Carbon Nanotubes*, in Nanostructured Material and Nanotechnology, Edited by Nalwa HS, Academic Press, New York, p 329-360, (2002).

116. Zhou SX, Wu LM, Sun J and Shen WD, *Effect of nanosilica on the properties of polyester-based polyurethane*, J Appl Polym Sci, **88** (1), 189-193, (2003).

117. Chen XC, Wu LM, Zhou SX and You B, *In situ polymerization and characterization of polyester-based polyurethane/nano-silica composites*, Polym Inter, **52** (6), 993-998, (2003).

118. Tien YI and Wei KH, *The effect of nano-sized silicate layers from maontmorillonite on glass transition, dynamic mechanical, and thermal degradation properties of segmented polyurethane*, J Appl Polym Sci, **86**, 1741-1748, (2002).

119. Gall K, Dunn ML, Liu Y, Finch D, Lake M and Munshi NA, *Shape memory polymer nanocomposites*, Acta Materialia, **50**, 5115-5126, (2002).

120. Gore WL, *Relaxed working in any weather*, Bekleidung-Wear, **51** (20), (1999), 22.

121. Ward D, *World's leading companies reveal their strategies for success*, Tech. Text. Inter., **11** (7), (Sept. 2002), 9-10.

122. *Precious nanoparticles*, Textile Month, Issue 1, p 31, (2005).

123. Krishnan S, *Technology of breathable coatings*, J Coated Fabrics, **22** (Jul.), 71-74, (1992).

124. Goldsmith J, *Water-based polyurethanes*, J Coated Fabrics, **18** (July), 12-25, (1998).

125. Mitov Z and Kumacheva E, *Convection-induced patterns in phase-separating polymeric fluids*, Physical Rev Lett, **81** (16), 3427-3430, (1998).

126. Smrčková MD and Dušek K, *Process and states during polymer film formation by simultaneous crosslinking and solvent evaporation*, J Mater Sci, **37**, 4733-4741, (2002).

127. Haas DE and Birnie DP III, *Evaluation of thermocapillary driving forces in the development of striations during the spin coating process*, J Mater Sci, **37**, 2109-2116, (2002).

128. Strawhecker KE and Kumar SK, Douglas JF, and Karim A, *The critical role of solvent evaporation on the roughness of spin-cast polymer films*, Macromolecules, **34**, 4669-4672, (2001).

129. Zhang X, Li H, Zhao B, Shen J, Gao Z and Li X, *Ordered self-organizing films of an amphiphilic polymer by slow evaporation of organic solvents*, Macromolecules, **30**, 1633-1636, (1997).

130. Ray B, Elhasri S, Thierry A, Marie P and Guenet JM, *Solvent-induced crystallization of syndiotactic polystyrene: thermodynamics and morphology*, Macromolecule, **35**, 9730-9736, (2002).

131. Kim YD, Kim JY, Lee HK and Kim SC, *A new modeling of asymmetric membrane formation in rapid mass transfer system*, J Membr Sci, **190**, 69-77, (2001).

132. Mwaura JK, Thomsen DL III, Phely-Bobin T, Taher M, Theodoropulos S and Papadimitrakopoulos F, *Luminescent rare-earth multiplayer chelates from segmented poly(urethane ureas)*, J Am Chem Soc, **122**, 2647-2648, (2000).

133. Gu J, Bullwinkel MD and Campbell GA, *Solvent concentration measurement for spin coating*, J Appl Polym Sci, **57**, 717-725, (1995).

134. Huang YJ, Chu CJ and Dong JP, *Effects of chemical structure of polyurethane-based low-profile additives on the miscibility, curing behavior, volume shrinkage, glass transition temperature, and mechanical properties for styrene/unsaturated polyester/low-profile additive ternary systems. I: miscibility, curing behavior, and volume shrinkage*, J Appl Polym Sci, **78**, 543-557, (2000).

135. Ramani R and Ranganathaiah C, *Free-volume microprobe study of iodine diffusion in polymers*, Polym Inter, **50**, 237-248, (2001).

136. Nakanishi H, Wang SJ and Jean YC, in *Positron Annihilation Studies of Fluids*, Sharma SC (ed), Singapore, World Scientific Publisher, p 292, (1988).

137. Yang H, Zhu S and Pan N, *Studying the Mechanisms of Titanium Dioxide as Ultraviolet-Blocking Additive for Films and Fabrics by an Improved Scheme*, J Appl Polym Sci, **92**, 3201-3210, (2004).

138. Harjunalanen T and Lahtinen M, *The effect of altered reaction conditions on the properties of anionic poly(urethane-urea) dispersions and films cast from the dispersions*, Euro Polym J, Article in Press, (2003).

139. Yen FS and Hong JL, *Hydrogen-bond interactions between ester and urethane linkages in small model compounds and polyurethanes*, Macromolecules, **30** (25), 7927-7938, (1997).

140. McKiernan RL, Heintz AM, Hsu SL, Atkins EDT, Penelle J and Gido SP, *Influence of hydrogen bonding on the crystallization behavior of semicrystalline polyurethane*, Macromolecules, **35**, 6970-6974, (2002).

141. Seymour RW, Estes GM and Cooper SL, *Infrared studies segmented polyurethane elastomers. I. hydrogen bonding*, Macromolecules, **3** (5), 579-583, (1970).

142. Teo LS, Chen CY and Kuo JF, *Fourier transform infrared spectroscopy study on effect of temperature on hydrogen bonding in amine-containg polyurethanes and poly(urethane-urea)s*, Macromolecules, **30**, 1793-1799, (1997).

143. Yang JH, Chun BC, Chung YC and Cho JH, *Comparison of thermal/mechanical properties and shape memory effect of polyurethane block-copolymer with planer or bent shape of hard segment*, Polymer, **44**, 3251-3258, (2003).

144. Lee CJ, Kim DW, Lee TJ, Choi YC, Park YS, Kim WS, Lee YH, Choi WB, Lee NS, Kim JM, Choi YG and Yu SC, *Synthesis of uniformly distributed carbon*

nanotubes on a large area of Si substrates by thermal chemical vapor deposition, Appl Phys Lett, **75** (12), 1721-1723, (1999).

145. Lan PN, Corneillie S, Schacht E, Davies M and Shard A, *Synthesis and characterization of segmented polyurethanes based on amphiphilic polyether diols*, Biomaterials, **17**, 2273-2280, (1996).

146. Jin Z, Pramoda KP, Xu G and Goh SH, *Dynamic mechanical behavior of melt-processed multi-walled carbon nanotube/poly(methyl methacrylate) composite*, Chem Phys Lett, **337**, 43-47, (2001).

147. Kim BK, Seo JW and Jeong HM, *Morphology and properties of waterborne polyurethane/clay nanocomposites*, Europ Polym J, **39**, 85-91, (2003).

148. Goh HW, Goh SH, Hu GQ, Pramoda KP and Zhang WD, *Dynamic mechanical behavior of in situ functionalized multi-walled carbon nanotube/phenoxy resin composite*, Chem Phys Lett, **373**, 277-283, (2003).

149. Hu JL and Mondal S, *Structural characterization and mass transfer properties of segmented polyurethane: influence of block length of hydrophilic segments*, Polym Inter, **54** (5), 764-771.

150. Jr. Billmeyer WF, *Textbook of Polymer Sci*, John Wiley & Sons, Singapore, p 229-290, (2000).

151. Miller JA, Lin SB, Hwang KKS, Wu KS, Gibson PE and Cooper SL, *Properties of polyether polyurethane block copolymers-effects of hard segment length distribution*, Macromolecules, **18** (1), 32-44, (1985)

152. Young RJ and Lovell PA, *Introduction to Polymers*, 2nd ed., Chaman & Hall, London, 1991.

153. Zhou O, Fleming RM, Murphy DW, Chen CH, Haddon RC, Ramirez AP and Glarum SH, *Defects in carbon nanostructures*, Science, **263** (5154), 1744-1747, (1994).

154. Orchon S and Orchon SE, *Development of single component, solventless, moisture-cured polyurethane coatings*, J. Coated Fabrics, **17** (July), 50-67 (1987).

155. Stepanski H and Nebe V, *Polyurethane adhesives for textiles*, J Coated Fabrics, **27** (Jul.), 27-39, (1997).

156. Schmelzer GH, *Polyurethane for flexible surface coatings and adhesives*, J Coated Fabrics, **17** (Jan.), 167-182, (1988).

157. Omoto M, Umeda K and Hidai T, *Polyether-based flexible polyurethane foam for flame lamination*, J Coated Fabrics, **19** (Apr.), 231-240, (1990).

158. Lomax GR, *Hydrophilic polyurethane*, International Dyer, **175** (9), p 22,32, (1990).

159. Oertel WR and Brentin PR, *Thermoplastic polyurethane for coated fabrics*, J Coated Fabrics, **22** (Oct.), 150-160, (1992).

160. Wang LT and Hsieh HT, *Effect of polyol structure and molecular weight on the thermal stability of segmented poly(urethaneureas)*, Polym Degrad & Stab, **55** (1), 95-102, (1997).

161. Grassie N and Zulfiqar M, *Thermal degradation of polyurethane from 1,4-butanediol and methylene bis(4-phenyl isocyanate)*, J Polym Sci, Part A: Polym Chem, **16** (7), 1563-1574, (1978).

162. Bilbao R, Mastral JF, Ceamanos J and Aldea ME, *Kinetics of the thermal decomposition of polyurethane foams in nitrogen and air atmosphere*, J Analytical & Appl Pyrol, **37**, 69-82, (1996).

163. Son TW, Lee DW and Lim SK, *Thermal and phase behavior of polyurethane based on chain extender, 2,2-bis-[4-(2-hydroxyethoxy)phenyl]propane*, Polym J, **31** (7), 563-568, (1999).

164. Guo H, Sreekumar TV, Liu T, Minus M, and Kumar S, *Structure and properties of polyacrylonitrile/single wall carbon nanotube composite films*, Polymer, **46** (9), 3001 – 3005, (2005).

165. Zhang M, Zeng H, Zhang L, Lin G and Li RKY, *Fracture characteristics of discontinuous carbon fiber-reinforced PPS and PESC composites*, Polym Polym Comp, **1**, 357 – 365, (1993)

166. Wu CL, Zhang MQ, Rong MZ and Friedrich K, *Tensile performance improvement of low nanoparticles filled-polypropylene composites*, Comp Sci & Tech, **62**, 1327 – 1340, (2002).

167. Desai S, Thakore IM and Devi S, *Effect of crosslink density on transport of industrial solvents through polyether based polyurethanes*, Polym Inter, **47**, 172-178, (1998).

168. Chen TK, Tien YI and Wei KH, *Synthesis and characterization of novel segmented polyurethane/clay nanocomposites*, Polymer, **41**, 1345-1353, (2000).

169. Elabd YA, Sloan JM and Barbari TA, *Diffusion of acetonitrile in conformational isomers of an H_{12}MDI polyurethane*, Polymer, **41**, 2203-2212, (2000).

170. Hayashi S, Ishikawa N and Giordano C, in *Polyurethane World Congress Proceedings*, Technomic, Lancaster, P 400, (1993).

171. Van Krevelen DW, *Properties of Polymers*, 3rd Ed., Elsevier, New York, p 535-583 (1990).

172. Hu JL, Zeng YM and Yan HJ, *Influence of processing conditions on the microstructure and properties of shape memory polyurethane membranes*, Text Res J, **73** (2), 172-178, (2003).

173. Rzeszutek K and Chow A, *Transport of organic dyes through ether-type polyurethane membrane*, Talanta, **49**, 757-771, (1999).

174. Stern SA, Mi Y, Yamamoto H and Clair AKS, *Structure/permeability relationships of polyimide membranes. Application to the separation of gas mixtures*, J Polym Sci, Part B: Polym Phys, **27** (9), 1887-1909, (1989)

175. Wang B, Zhang M, Zhang JM, He CQ, Dai YQ, Wang SJ and Ma DZ, *Compositional and temperature dependence of free volume in segmented copolymer PET/PEO studied by positron annihilation lifetime measurement*, Phys Lett, **A 262** (2-3), 195 – 205, (1999).

176. Hsieh TT, Tiu C and Simon GP, *Miscibility and free volume behaviour of a number of polymer blends containing only thermotropic liquid crystalline polymers*, Polymer, **41** (12), 4737 – 4742, (2000).

177. Robertson JE, Ward TC and Hill AJ, *Thermal, mechanical, physical, and transport properties of blends of novel oligomer and thermoplastic polysulfone*, Polymer, **41** (16), 6251 – 6262, (2000).

178. Zhou Q, Zhang L, Zhang M, Wang B and Wang S, *Miscibility, free volume behavior and properties of blends from cellulose acetate and castror oil-based polyurethane*, Polymer, **44**, 1733 – 1739, (2003).

179. Wang ZF, Wang B, Yang YR and Hu CP, *Correlations between gas permeation and free-volume hole properties of polyurethane membranes*, Europ Polym J, **39**, 2345-2349, (2003)

180. Abdel-Hady EE and Mohamed HFM, *Microstructure changes of poly(vinyl chloride) investigated by positron annihilation techniques*, Polym Deg & Stab, **77** (3), 449-456, (2002).

181. Wang ZF, Wang B, Qi N, Ding XM and Hu JL, *Free volume and water vapor permeability properties in polyurethane membranes studied by positrons*, Mater Chem and Phys, 88, 212-216, (2004).

182. Wilkinson CL, *A review of industrial coated fabric substrates*, J Coated Fabrics, **26** (Jul), 45-64, (1996).

183. Hoenlein W, Kreupl F, Duesberg GS, Graham AP, Liebau M, Seidel RV and Unger E, *Carbon Nanotube Applications in Microelectronics*, IEEE Trans. On Component and Pack Tech, **27** (4) 629-633, (2004).

184. Freitag M, Chen J, Tersoff J, Tsang JC, Fu Q, Liu J and Avouris P, *Mobile Ambipolar Domain in Carbon-Nanotube Infrared Emitters*, Phys Rev Lett, **93** (7), Article No. 076803-1 (4 pages), (2004).

185. Bachilo SM, Strano MS, Kittrell C, Hauge RH, Smattey RE and Weisman RB, *Structure-Assigned Optical Spectra of Single-Walled Carbon Nanotubes*, Science, **298**, 2361-2365, (2002).

186. Freitag M, Martin Y, Misewich JA, Martel R and Avouris PH, *Photoconductivity of Single Carbon Nanotubes*, Nano Lett, **3** (8), 1067-1071, (Aug 2003).